Dielectric Studies of Nanostructures and Directed Self-assembled Nanomaterials in Nematic Liquid Crystals

by

Rajratan Basu

A Dissertation
Submitted to the Faculty
of the

WORCESTER POLYTECHNIC INSTITUTE

In partial fulfillment of the requirements for the
Degree of Doctor of Philosophy
in
Physics
by

Rajratan Basu

March 30, 2010

APPROVED:

Germano Iannacchione

Germano S. Iannacchione, Head of Physics, WPI, PhD Advisor.

P.K. Aravind

P.K. Aravind, Professor of Physics, WPI.

Jianyu Liang, Assistant Professor of Mechanical Engineering, WPI.

ABSTRACT

Self-assembly of nanomaterials over macroscopic dimensions and development of novel nano-electromechanical systems (NEMS) hold great promise for numerous nanotech applications. However, it has always been a great challenge to find a *general route* for controlled self-assembly of nanomaterials and generating electromechanical response at the nanoscale level. This work indicates that self-organized anisotropic nematic *liquid crystals* (LC) can be exploited for nanotemplating purposes to pattern *carbon nanotubes* (CNTs) and *Quantum dots* (QDs) over a macroscopic dimension. The pattern formed by the CNTs or QDs can be controlled by applying external electric and magnetic fields, developing novel *nano-electromechanical* and *nano-magnetomechanical* systems.

Self-organizing nematic liquid crystals (LC) impart their orientational order onto dispersed carbon nanotubes (CNTs) and obtain CNT-self-assembly on a macroscopic dimension. The nanotubes-long axis, being coupled to the nematic director, enables orientational manipulation via the LC nematic reorientation. Electric field induced director rotation of a nematic LC+CNT system is of potential interest due to its possible application as a nano-electromechanical system. Electric field and temperature dependence of dielectric properties of an LC+CNT composite system have been investigated to understand the principles governing CNT-assembly mediated by the LC. In the LC+CNT nematic phase, the dielectric relaxation on removing the applied field follows a single exponential decay, exhibiting a faster decay response than the pure LC above a threshold field. Due to a strong LC-CNT anchoring energy and structural symmetry matching, CNT long axis follows the director field, possessing enhanced dielectric anisotropy of the LC media. This strong anchoring energy stabilizes local *pseudo-nematic* domains, resulting in nonzero dielectric anisotropy in the isotropic LC phase. These anisotropic domains respond to external electric fields and show intrinsic frequency response. The presence of these domains makes the isotropic phase electric field-responsive, giving rise to a large dielectric hysteresis effect. These polarized domains maintain local directors, and do not relax back to the original state on switching the field off, showing non-volatile electromechanical memory effect.

Assembling quantum dots (QDs) into nanoscale configurations over macroscopic dimensions is an important goal to realizing their electro-optical potential. In this work, we present a detailed study of a pentylcyanobiphenyl liquid crystal (LC) and a CdS QD colloidal dispersion by probing the dielectric property $\bar{\varepsilon}$ and relaxation as a function of an applied ac-electric field E_{ac}. In principle, dispersing QDs in a nematic LC medium can direct the dots to align in nearly one-dimensional chain-like structures along the nematic director and these assemblies of QDs can be directed by external electric fields. In a uniform planar aligned cell, the Fréedericksz switching of the LC+QDs appears as a two-step process with the same initial switching field as the bulk but with the final $\bar{\varepsilon}$ value larger than that for an aligned bulk LC. The relaxation of $\bar{\varepsilon}$ immediately following the removal of E_{ac} follows a single-exponential decay to its original value that is slower than the bulk but becomes progressively faster with increasing E_{ac}, eventually saturating. These results suggest that the arrangement of the QDs is mediated by the LC.

TABLE OF CONTENTS

Chapter **Page**

1. INTRODUCTION 1–10

1.1 Introduction to Dielectric Spectroscopy 1
1.2 Dielectric measurement technique 4
1.3 Introduction to the samples used in experiments 6
1.3.1 Liquid Crystals 6
1.3.2 Carbon Nanotubes 7
1.3.3 Quantum Dots 9

2. DIELECTRIC RESPONSE FOR DIFFERENT CARBON STRUCTURES ..11–18

2.1 Introduction 11
2.2 Dielectric measurement technique 12
2.3 Sample preparation for experiments 12
2.4 Results, discussions, and conclusions 13

3. DIELECTRIC RESPONSE OF MULTIWALL CARBON NANOTUBES AS A FUNCTION OF AC FIELDS 19–29

3.1 Introduction 19
3.2 Experimental procedures 21
3.3 Sample preparation for experiments 22
3.4 Results 23
3.5 Discussion and conclusions 26

4. CARBON NANOTUBE DISPERSED LIQUID CRYSTAL- A NANO ELECTROMECHANICAL SYSTEM 30–38

4.1 Introduction 30
4.2 Experiments 31
4.3 Results, analysis, and conclusions 33

Chapter **Page**

5. DIELECTRIC HYSTERESIS, RELAXATION DYNAMICS, AND NON-VOLATILE MEMORY EFFECTS IN CARON NANOTUBE DISPERSED LIQUID CRYSTAL 39–55

5.1 Introduction 39
5.2 Experiments 41
5.3 Results and analysis 43
5.4 Conclusions 54

6. NEMATIC ANCHORING ON CARBON NANOTUBES 56–63

6.1 Introduction 56
6.2 Experimental procedures and sample preparation 57
6.3 Results and interpretations.....58

7. ORIENTATIONAL COUPLING ENHANCEMENT IN CARBON NANOTUBE DISPERSED LIQUID CRYSTAL 64–73

7.1 Introduction.....64
7.2 Experiments 66
7.3 Results and interpretations.....67

8. DIRECTED SELF-ASSEMBLY OF QUANTUM DOTS IN A NEMATIC LIQUID CRYSTAL 74–84

8.1 Introduction.....74
8.2 Experiments 76
8.3 Results and interpretations.....76

9. ISOTROPIC TO NEMATIC PHASE TRANSITION IN CARBON NANOTUBE DISPERSED LIQUID CRYSTALDIRECTED 85–93

9.1 Introduction 85
9.2 Experimental procedures and sample preparation 88
9.3 Results and interpretations.....90

10. GENERAL CONCLUSIONS AND FUTURE DIRECTION 94–98

10.1 Introduction 94

10.2 Back ground and summery of my work 95
10.3 My proposed research directions 96
10.4 Conclusions.....97

11. JOURNAL ARTICLES 99

LIST OF FIGURES

Figure **Page**

1.1 Mechanisms of polarization. 3

1.2 Debye relaxation: frequency dependence of $\varepsilon'(\omega)$ and $\varepsilon''(\omega)$ for a relaxation process. 3

1.3 Cole-Cole diagram displaying a semi-circle for Debye equations for ε^* 4

1.4 Dielectric spectrometer in Order-Disorder Phenomena Laboratory, WPI. 5

1.5 Liquid crystal phases; (a) Nematic, (b) Smectic-*A*, and (c) Smectic-*C* 6

1.6 3D model of three types (zigzag, chiral, and armchair) of single-walled carbon nanotubes (taken from Wikipedia). 8

2.1 The electric field intensity dependence of $\varepsilon'(\omega)$ and $\varepsilon''(\omega)$ for the amorphous carbon sample. Upper panel legend lists the applied field factor $\boldsymbol{e}_R$. In $\varepsilon''(\omega)$, the low-frequency mode is denoted by 1 while the high-frequency mode is denoted by 2. 13

2.2 Dielectric Spectrum of Diamond; frequency dependence of real part (ε', hollow blue circles) and imaginary part (ε'', red solid circles) of dielectric constant at temperature, and $\boldsymbol{e}_R = 1$. 14

2.3 The electric field intensity dependence of $\varepsilon'(\omega)$ and $\varepsilon''(\omega)$ for the SWNT sample (in units of 1000). Upper panel legend lists the applied field factor $\boldsymbol{e}_R$. For $\varepsilon''(\omega)$, the low-frequency mode is denoted by 1 and the high-frequency mode is denoted by 2. 15

2.4 The electric field intensity dependence of $\varepsilon'(\omega)$ and $\varepsilon''(\omega)$ for the SWNT sample (in units of 1000). Upper panel legend lists the applied field factor $\boldsymbol{e}_R$. For $\varepsilon''(\omega)$, the low-frequency mode is denoted by 1 and the high-frequency mode is denoted by 2. 16

2.5 Cole-Cole plots of $\varepsilon''(\omega)$ versus $\varepsilon'(\omega)$ for the SWNT (top), MWNT (middle), and amorphous glass AG (bottom) carbon samples at $\boldsymbol{e}_R$=2. Note that the upper two panels are in units of 1000. The arrows indicate the direction of increasing frequency and the labels denote the mode. 25

3.1 The ac-electric fields E_{rot} and E_{ac} in the complex rotating-frame of the dielectric measurement. The field E_{rot}, along the real axis, is in phase and at the same frequency as the measurement, hence 'static' in complex rotating-frame. Being at a different

frequency than the measurement, E_{ac} acts as an ac-field in the complex rotating-frame. The field E is the resultant field and, at any time, the sample experiences the real component. 20

3.2 The frequency and E_{ac} (shown by field factor $\boldsymbol{e}_{AC}$; star = 1, diamond = 2, triangle = 3, circle = 4, and square = 5) dependence of dielectric storage ε' (top panel) and loss ε'' (bottom panel) of MWCNT sample for three values of E_{rot} (or $\boldsymbol{e}_R$). 24

3.3 **(a)** Relaxation frequency of mode-1 (f_1) as a function of E_{rot} (or $\boldsymbol{e}_R$). Note the initial linear dependence with zero intercept and the apparent saturation for $\boldsymbol{e}_R > 5$.
(b) Relaxation frequency of mode-2 (f_2) and dispersion strength ($\Delta\varepsilon_2''$, peak magnitude of ε'') of mode-2 as a function of E_{ac} (or $\boldsymbol{e}_{AC}$) for $\boldsymbol{e}_R$ =1 25

3.4 Effective capacitors (C) between the layers hooked up in series with the effective resistors (R) of the walls 26

3.5 The dielectric ac-conductivity σ_{ac} of MWCNT sample as a function of frequency. **(a)** For constant $\boldsymbol{e}_R$ and varying $\boldsymbol{e}_{AC}$; star = 1, diamond = 2, triangle = 3, circle = 4, and square = 5. **(b)** For constant $\boldsymbol{e}_{AC}$ and varying $\boldsymbol{e}_R$; star = 1, diamond = 2, triangle = 3, circle = 4, and square = 5 27

3.6 The dielectric spectrum of the MWCNT sample for $\boldsymbol{e}_R = 1$ and $\boldsymbol{e}_{AC} = 0$, open circles are the data and the solid lines are fits to a Debye relaxation form.
Mode-1 and 2 are labeled in the figure where $\Delta\varepsilon_1$ and $\Delta\varepsilon_2$ are the real dielectric strengths, respectively 28

4.1 Helical surface anchoring of LC molecule on CNT wall 31

4.2 (**a**) Schematic diagram of alignment of LC molecules in a homogeneous cell without electric field; (**b**) Schematic diagram of alignment of LC molecules in a homogeneous cell with field 32

4.3 (**a**) Schematic diagram of alignment coupling of LC+CNT in a homogeneous cell without electric field; (**b**) Schematic diagram of alignment of coupling of LC+CNT in a homogeneous cell with field 32

4.4 (**a**) Dynamic response of the average dielectric constant $\bar{\varepsilon}$ for the LC+CNT system in the nematic phase (T = 25°C) after E_{ac} = 0; the inset (same main graph axes) represents the same relaxation in log-time scale to show the single exponential decay. Lines represent the fitting according to a single exponential decay function, see text for details; (**b**) Dynamic response of the average dielectric constant $\bar{\varepsilon}$ for LC+CNT system in the isotropic phase (T = 45°C) after E_{ac} = 0. The legends in both the panels represent the magnitude of E_{ac} (kV/m, 1MHz) 33

4.5 (**a**) Field-saturated dielectric constant, $\bar{\varepsilon}_{max}$ ($\bar{\varepsilon}$ at t = 0) as a function E_{ac} in the nematic phase (T = 25°C). Lines represent guide to the eye; **(b)** Field-saturated dielectric constant, $\bar{\varepsilon}_{max}$ ($\bar{\varepsilon}$ at t = 0) as a function E_{ac} in the isotropic phase (T = 45°C).....35

4.6 Fitting parameters according to a single-exponential decay ($f(t) = \bar{\varepsilon}_1 e^{(-t/\tau)} + \bar{\varepsilon}_0$) function for pure 5CB and 5CB+MWCNT system. Lines represent guide to the eye 36

4.7 Schematic of permanent orientation of pseudo-nematic domains on application of electric field in isotropic LC+CNT mixture.....37

5.1 Schematic diagram of symmetry matching; Dotted cylinder shows the cylindrical symmetry of uniaxial nematic phase; the small cylinder shows the cylindrical confinement of a CNT 40

5.2 (**a**) Field annealing hysteresis cycles, $\bar{\varepsilon}$ vs. E, for 5CB (top 2 panels) and 5CB+MWCNT (bottom 4 panels) in the nematic phase (T = 25°C). (**b**) The area under the hysteresis loop as a function number of cycle for 5CB and 5CB+MWCNT.....44

5.3 Dynamic response of the average dielectric constant $\bar{\varepsilon}$ for 5CB+MWCNT as a function of time and E_{ac} (1 MHz) in the nematic phase (T = 25°C) after E_{ac} goes off.....45

5.4 Field-saturated dielectric constant, $\bar{\varepsilon}_{max}$ ($\bar{\varepsilon}$ at t = 0) as a function of E_{ac} for 5CB and 5CB+MWCNT in the nematic phase (T = 25°C). Lines represent guide to the eye 46

5.5 (**a**) Relaxation dynamic response of $\bar{\varepsilon}$ in logarithmic time scale. The legend represents the magnitude of E_{ac} (1 MHz) in kV/m; (**b**), (**c**), (**d**) Fitting parameters according to a single-exponential decay ($f(t) = \bar{\varepsilon}_1 e^{(-t/\tau)} + \bar{\varepsilon}_0$) function for 5CB and 5CB+MWCNT system. Lines represent guide to the eye.....48

5.6 (**a**) Dynamic response of the average dielectric constant $\bar{\varepsilon}$ for 5CB+MWCNT as a function of time and E_{ac} (1 MHz) in the isotropic phase (T = 37°C) after E_{ac} goes off; (**b**) Field-saturated dielectric constant, $\bar{\varepsilon}_{max}$ ($\bar{\varepsilon}$ at t = 0) as a function of E_{ac} for 5CB and 5CB+MWCNT in the isotropic phase (T = 37°C). Lines represent guide to the eye 50

5.7 Schematic diagram of presence of field-responsive anisotropic pseudo-nematic domains in the isotropic media. Dashed rectangles represent the LC-CNT pseudo-nematic domains 51

5.8 Normalized average dielectric constant $\bar{\varepsilon}$ for 5CB and 5CB+MWCNT as a function of temperature shift, $\Delta T_{IN} = T - T_{IN}$.....53

6.1 (**a**) The average dielectric constant $\bar{\varepsilon}$ as a function of applied ac voltage for 5CB and 5CB+CNT in the nematic phase (T = 23°C); (**b**) The average dielectric constant $\bar{\varepsilon}$ as a function of applied ac voltage for 5CB and 5CB+CNT in the isotropic phase (T = 45°C) 58

6.2 Imaginary part of $\varepsilon_\perp$ (top panel) and $\varepsilon_\parallel$ (bottom panel) for 5CB and 5CB+MWCNT in the nematic phase (T = 23°C).....60

6.3 Schematic diagrams; **(a)** presence of field-responsive anisotropic pseudo-nematic domains due to LC (ellipsoidal) –CNT (cylindrical) interaction in the isotropic media; **(b)** a model for a four-electrode LC cell for writing and erasing memory 60

6.4 Dielectric hysteresis for 5CB and 5CB+CNT. The arrows show the cycling direction of the applied ac voltage 61

7.1 **(a)** The dielectric constant $\bar{\varepsilon}$ as a function of applied ac voltage for 5CB and 5CB+CNT in the nematic phase (T = 25°C) at frequency 1 kHz; $\Delta\varepsilon_{LC}$ = +10.5 and $\Delta\varepsilon_{LC+CNT}$ = +13.8; **(b)** The dielectric constant $\bar{\varepsilon}$ as a function of applied ac voltage for 5CB and 5CB+CNT in the nematic phase (T = 25°C) at frequency 100 kHz; $\Delta\varepsilon_{LC}$ = +10.1 and $\Delta\varepsilon_{LC+CNT}$ = +11.2 67

7.2 **(a)** The dielectric anisotropy $\Delta\varepsilon$ as a function of frequency for 5CB and 5CB+CNT in the nematic phase (T = 25°C); **(b)** The dielectric anisotropy $\Delta\varepsilon$ as a function of frequency for 5CB and 5CB+CNT in isotropic phase (T = 42°C).....68

7.3 Schematic diagrams; **(a)** the presence of a CNT (cylindrical) in an nematic LC media and formation of the local short range orientational order by LC molecules on the surface of the CNT due to the LC-CNT anchoring energy (π–π stacking). The thin arrow represents the long-range nematic director and the thick arrow on the CNT represents the short range local director; **(b)** the isotropic phase of LC; **(c)** the presence of a CNT (cylindrical) in an isotropic LC media and formation of the local short range orientational order by LC molecules.....69

7.4 The splay elastic constant K_{11} (in pico Newton) as a function of applied frequency for 5CB and 5CB+CNT in the nematic phase (T = 25°C). K_{11} has been extracted from the formula $V_{th} = \pi\sqrt{(K_{11}/\varepsilon_o\Delta\varepsilon)}$. 70

8.1 Dynamic response of the average dielectric constant $\bar{\varepsilon}$ for the 5CB+CdS system in the nematic phase (T = 25°C) after E_{ac} = 0; the inset (same main graph axes) represents the same relaxation in log-time scale to show the single exponential decay. The legend represents the magnitude of E_{ac} (1 MHz) in kV/m 77

8.2 (**a**) Field-saturated dielectric constant, $\bar{\varepsilon}_{max}$ ($\bar{\varepsilon}$ at t = 0) as a function E_{ac} for pure 5CB and 5CB+CdS in the nematic phase (T = 25°C). The downward arrow indicates the intermediate step for 5CB+CdS. Lines represent guide to the eye; (**b**) Field-saturated dielectric constant, $\bar{\varepsilon}_{max}$ ($\bar{\varepsilon}$ at t = 0) as a function E_{ac} for pure 5CB and 5CB+CdS in the isotropic phase (T = 45°C) 79

8.3 Fitting parameters according to a single-exponential decay (f(t) = $\bar{\varepsilon}_1 e^{(-t/\tau)} + \bar{\varepsilon}_0$) function for pure 5CB and 5CB+CdS system. Lines represent guide to the eye.....80

8.4 Schematic diagrams; (**a**) Dotted cylinder shows the cylindrical symmetry of uniaxial nematic phase; the small cylinder shows the cylindrical confinement of self-assembled QDs aggregation; (**b**) Electrode-surface-induced homogeneous alignment of nematic LC molecules (ellipsoidal), and QD self-assembly (spherical) in the nematic matrix; (**c**) Electric field induced homeotropic alignment of nematic LC molecules, and homeotropically directed one-dimensional QD arrays 82

9.1 Cartoons of (a) one carbon nanotube structure, (b) one 5CB liquid crystal molecule. The diagram of the MWCNT and 5CB are shown approximately to scale. Black spheres are carbon atoms and white spheres are hydrogen atoms. 87

9.2 Normalized average dielectric constant $\bar{\varepsilon}$ for pure 5CB and 5CB+MWCNTs as a function of temperature shift, ΔT_{IN}. The legend shows the concentrations of dispersed MWCNTs in weight % in 5CB. The absolutes values of T_{IN} for all concentrations are shown in Fig. 8.4a.....88

9.3 Excess specific heat ΔC_p for pure 5CB and 5CB+MWCNTs as a function of temperature shift, ΔT_{IN}. The legend shows the concentrations of dispersed MWCNTs in weight % in 5CB. The absolutes values of T_{IN} for all concentrations are shown in Fig. 8.4a.....89

9.4 (a) The transition temperature, T_{IN}, as a function of MWCNTs concentration and comparison between the two techniques used for the measurements, (b) AC- enthalpy (right) and imaginary enthalpy (left) as a function of MWCNTs concentration, for details see text, (c) The normalized dielectric constant, $\bar{\varepsilon}$, as a function of MWCNTs concentration at the starting temperature, 302 K (left) and absolute dielectric constant in the deep isotropic phase (315 K) as a function of MWCNTs concentration (right).....90

CHAPTER 1

INTRODUCTION

1.1 Introduction to dielectric spectroscopy

Materials that do not electrically conduct but have the ability to store the electric charges as electric energy are known as dielectrics. Dielectric spectroscopy measures the dielectric properties of a medium as a function of frequency. Dielectric constant is determined by the molecular polarizability and structural arrangement of molecules. This is essentially a measure of a charge-free sample's response to an applied electric field. The built up polarization in a dielectric medium following the sudden application of a direct dc electric field takes a finite time interval before the polarization attains its maximum value. This phenomenon is described by the general term *dielectric relaxation*. However, there are a number of different dielectric relaxation mechanisms, connected to the way a particular medium reacts to the applied field. Each mechanism is characterized by fixed frequency, which is the reciprocal of the characteristic time of the relaxation process. In general, dielectric mechanisms can be divided into relaxation and resonance processes. The most common, starting from high frequencies, are [1]:

Electronic polarization: This resonant process occurs in a neutral atom when the electric field displaces the electron density relative to the nucleus it surrounds. This displacement occurs due to the equilibrium between restoration and electric forces.

Atomic polarization: Atomic polarization is observed when the electronic cloud is deformed under the force of the applied field, so that the negative and positive charges are formed. This is a resonant process.

Dipole relaxation: This originates from permanent and induced dipoles aligning to an electric field. Their orientation polarization is disturbed by thermal noise (which mis-

aligns the dipole vectors from the direction of the field), and the time needed for dipoles to relax is determined by the intrinsic frequencies of the dipoles. In liquids, the local viscosity determines the intrinsic time response of the dipoles. This two fact make dipole relaxation heavily dependent on temperature and chemical surrounding.

Space charge relaxation: Space charge relaxation comprises ionic conductivity and interfacial and space charge relaxation. Ionic conductivity predominates at low frequencies and introduces only losses to the system. Interfacial relaxation occurs when charge carriers are trapped at interfaces of heterogeneous systems.

When a dc field is applied to a polar dielectric the polarization builds up from zero to a final value according to an exponential law,

$$P(t) = P_{\infty}(1 - e^{-\frac{t}{\tau}}) \tag{1.1}$$

where $P(t)$ is the polarization at time t and τ is called the relaxation time and P_{∞} is the built up polarization at time $t = \infty$. Based on this fundamental idea it can be shown [2] that under an alternating electric field the real component (in phase) of dielectric constant can be written as,

$$\varepsilon' = \varepsilon_{\infty} + \frac{\Delta\varepsilon}{1 + (\omega\tau)^2} \tag{1.2}$$

and the imaginary component ($\pi/2$ out of phase) of the dielectric constant can be written as,

$$\varepsilon'' = \frac{\Delta\varepsilon}{1 + (\omega\tau)^2}(\omega\tau) \tag{1.3}$$

where ω is sweeping frequency and $\Delta\varepsilon = \varepsilon_0 - \varepsilon_{\infty}$ is the dielectric relaxation strength for a single relaxation process. Here, ε_{∞} is the dielectric constant at infinite frequency, ε_0 is the static dielectric constant. Equations (1.2) and (1.3) are known as Debye dipole relaxation, and the complex dielectric constant of a dielectric material is expressed as,

$$\varepsilon^*(\omega) = \varepsilon' - j\varepsilon''. \tag{1.4}$$

The real part of the dielectric constant $\varepsilon'(\omega)$ is associated with the storage of the electric field energy while the imaginary part $\varepsilon''(\omega)$ corresponds to the dissipation of energy through a relaxation process.

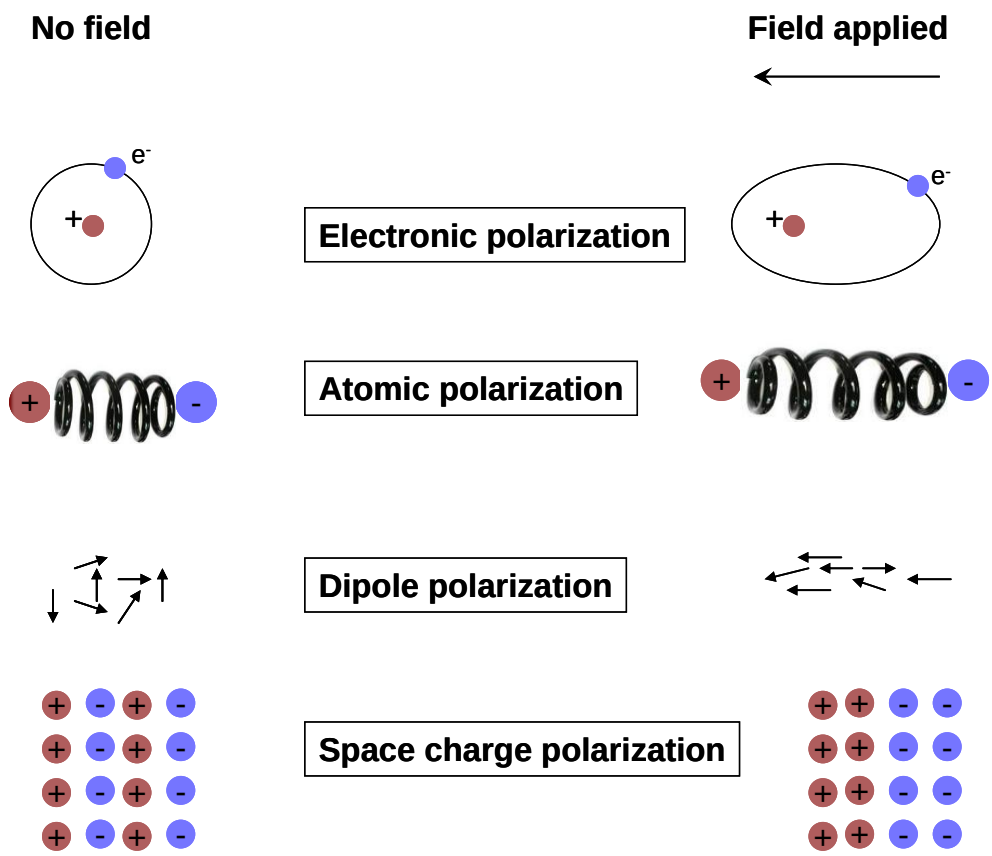

Figure 1.1: *Mechanisms of polarization.*

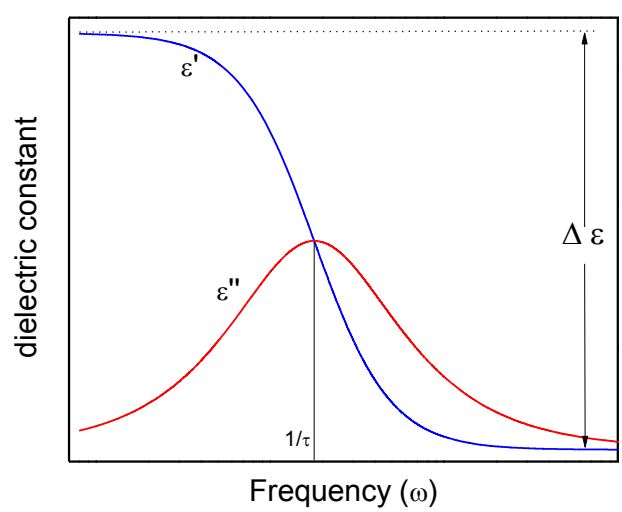

Figure 1.2: *Debye relaxation: frequency dependence of ε'(ω) and ε''(ω) for a relaxation process.*

Cole and Cole [3] showed that in a material exhibiting Debye relaxation a plot of $\varepsilon''(\omega)$ vs. $\varepsilon'(\omega)$, each point corresponding to a particular frequency, yields a semi-circle. The Debye equation can be written as,

$$(\varepsilon' - \frac{\varepsilon_0 + \varepsilon_\infty}{2})^2 + (\varepsilon'')^2 = (\frac{\Delta\varepsilon}{2})^2 \tag{1.5}$$

which is the equation of a circle with radius ($\Delta\varepsilon/2$) and having its centre at $(\frac{\varepsilon_0 + \varepsilon_\infty}{2}, 0)$.

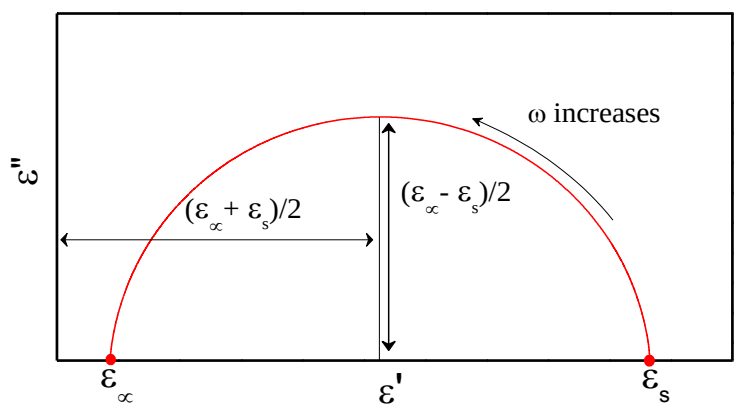

Figure 1.3: *Cole-Cole diagram displaying a semi-circle for Debye equations for ε^*.*

1.2 Dielectric measurement technique:

The dielectric constant ε^* for any dielectric sample can be defined by the ratio of the sample filled capacitor to the empty cell capacitor. So, capacitance measurement is one way to get dielectric constant. For our experiments, by using an ac-capacitance bridge technique [4,5,6], the real $\varepsilon'(\omega)$ and imaginary $\varepsilon''(\omega)$ part of the complex dielectric constant are determined as a function of frequency and the amplitude of the applied ac-electric probing field. The capacitive cell consists of a parallel-plate configuration,

housed in a temperature controlled bath. Comparison between the empty and sample filled capacitor allows for an absolute measurement of $\varepsilon^*(\omega)$.

The experiment begins by balancing the ac-bridge at some reference frequency. A frequency scan is then performed from this point while the off-balance 'in-phase' and 'out-of-phase' signals are acquired by a digital lock-in amplifier (*Stanford Research Systems SR830 DSP*). The off-balance voltage signal is converted to the equivalent change in capacitance by a simple multiplicative conversion factor and converted to the dielectric constant by dividing by the empty cell capacitance. Finally, the absolute real and imaginary parts of complex dielectric constant are determined by adding or subtracting (depending on whether the frequency scan moved to higher or lower frequencies relative to the reference frequency) the converted off-balance signal to that directly measured at the reference frequency. The dielectric constant can be studied as a function of probing ac field strength. But, because of the capacitive bridge technique, the actual magnitude E_{rot} across the sample is not known (only the driving voltage can be controlled). However, the factor by which E_{rot} increases is known if measured in units of that produced by the lowest voltage (denoted as E^0_{rot} for 1 V applied), this field is labeled $\boldsymbol{e}_R = E_{rot}/E^0_{rot}$. So, $\boldsymbol{e}_R$ represents the factor by which E_{rot} increases from its lowest value to higher values.

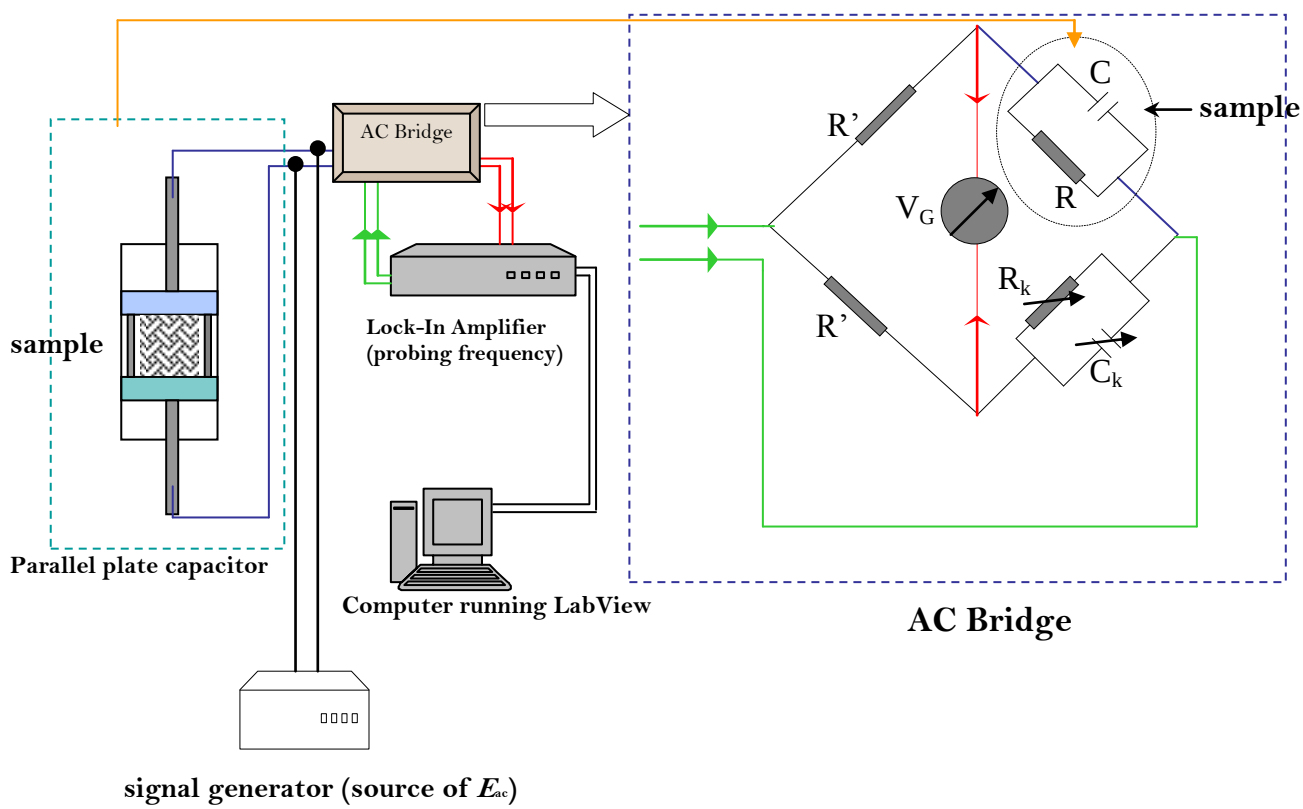

Figure 1.4: *Dielectric spectrometer in Order-Disorder Phenomena Laboratory, WPI.*

1.3 Introduction to the samples used in experiments

1.3.1 Liquid Crystals

Liquid crystals are substances that exhibit a phase of matter that has properties between those of a conventional liquid, and those of a solid crystal. For instance, a liquid crystal (LC) may flow like a liquid, but have the molecules in the liquid arranged and/or oriented in a crystal-like way. There are many different types of LC phases, which can be distinguished based on their different optical properties (such as birefringence). When viewed under a microscope using a polarized light source, different liquid crystal phases will appear to have a distinct texture. The contrasting areas in the texture each correspond to a domain where the LC molecules are oriented in a different direction. Within a domain, however, the molecules are well ordered [[7]].

Liquid crystals are usually classified as either lyotropic or thermotropic. Lyotropic LCs are obtained usually as a mixture of different substances, e.g., liquid crystal molecules and solvent, with the most common systems being mixtures of water and amphiphilic molecules (molecules that posses a hydrophilic and a hydrophobic part). The variable that controls the existence of the liquid crystalline phase in these systems is the amount of solvent, i.e. the concentration of the sample. Lyotropic LCs are of great interest in biological studies. The term 'thermotropic' arises from the fact that this class of liquid crystals shows different phases as temperature changes. They are the most widely studied, and used in applications. Another classification is based on the phases and symmetries that mesogens display. Several tens of thousands of mesogens are known to show one or more mesomorphic phases. Although there are many mesomorphic phases corresponding to different degrees of order and symmetries, most materials exhibit only a few of them.

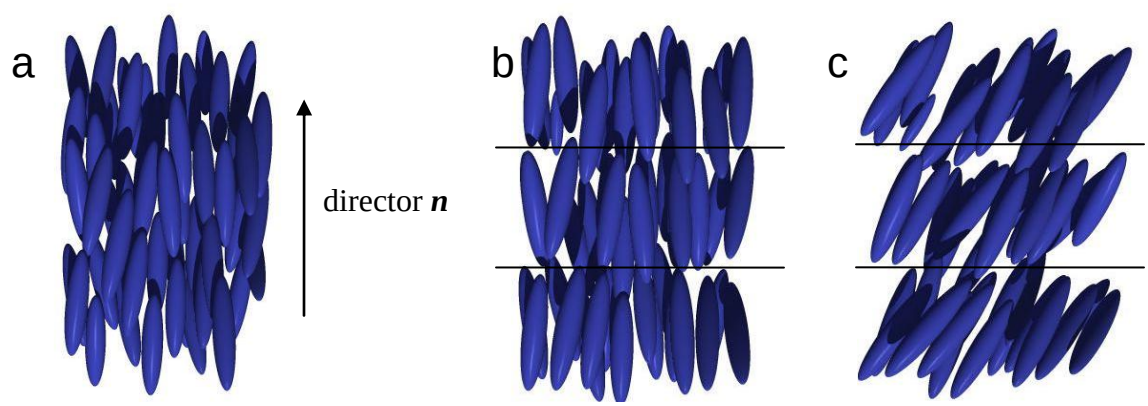

Figure 1.5: *Liquid crystal phases;* (a) *Nematic,* (b) *Smectic-A, and* (c) *Smectic-C*

Nematic Phase: The nematic liquid crystal phase is characterized by molecules that have no positional order but tend to point in the same direction (along the director). Molecules align parallel to each other, i.e., long-range orientational order. Center of mass positions of each molecule are completely random, i.e., no long-range positional order.

Smectic Phase: The smectic state is another distinct mesophase of liquid crystal substances. Molecules in this phase show a degree of translational order not present in the nematic. In the smectic state, the molecules maintain the general orientational order of nematics, but also tend to align themselves in layers or planes. Motion is restricted to within these planes, and separate planes are observed to flow past each other. The increased order means that the smectic state is more "solid-like" than the nematic. Many compounds are observed to form more than one type of smectic phase.

In the smectic-*A* mesophase, the director is perpendicular to the smectic plane, and there is no particular positional order in the layer. Similarly, the smectic-*B* mesophase orients with the director perpendicular to the smectic plane, but the molecules are arranged into a network of hexagons within the layer. In the smectic-*C* mesophase, molecules are arranged as in the smectic-*A* mesophase, but the director is at a constant tilt angle measured normally to the smectic plane.

As in the nematic, the smectic-*C* mesophase has a chiral state designated *C**. Consistent with the smectic-*C*, the director makes a tilt angle with respect to the smectic layer. The difference is that this angle rotates from layer to layer forming a helix. In other words, the director of the smectic-*C** mesophase is not parallel or perpendicular to the layers, and it rotates from one layer to the next. Notice the twist of the director, represented by the green arrows, in each layer in the following diagram.

Other relevant properties will be discussed in Chapter 3, 4, and 5.

1.3.2 Carbon Nanotubes

Carbon nanotubes (CNTs) are allotropes of carbon with a nanostructure that can have a length-to-diameter ratio greater than 10,000,000 and as high as 40,000,000. These cylindrical carbon molecules have novel properties that make them potentially useful in many applications in nanotechnology, electronics, optics and other fields of materials science, as well as potential uses in architectural fields. They exhibit extraordinary strength and unique electrical properties, and are efficient conductors of heat. Their final usage, however, may be limited by their potential toxicity [8].

Nanotubes are members of the fullerene structural family, which also includes the spherical buckyballs. The cylindrical nanotube usually has at least one end capped with a hemisphere of the buckyball structure. Their name is derived from their size, since the diameter of a nanotube is in the order of a few nanometers (approximately 1/50,000th of

the width of a human hair), while they can be up to several millimeters in length (as of 2008). Nanotubes are categorized as single-walled nanotubes (SWNTs) and multi-walled nanotubes (MWNTs) [8].

Individual carbon nanotubes can conduct electricity better than copper, possess higher tensile strength than steel, and conduct heat better than diamond. In electronic applications, carbon nanotubes can possess higher mobilities than single crystal silicon. All this in a material that is over 10,000 times thinner than a human hair. There are multiple forms of carbon nanotubes, varying in diameter, length, and in the tendency of the nanotubes to form ropes and bundles of tubes. Some forms of carbon nanotubes are metallic and highly conducting; other forms are semiconducting, and can form the basis of electronic switches [9].
Properties of CNTs [9,10]:

1. High Electrical Conductivity: Carbon nanotubes are the best conductors of electricity of any organic molecule ever discovered with a current carrying capacity per unit area that is 100X greater than copper.

2. Electron mobility: Carbon nanotube transistors can have a mobility that is 70 times higher than silicon.

3. High thermal conductivity: The thermal conductivity along the carbon nanotube is twice that of diamond (which was the best thermal conductor until the discovery of CNTs).

4. Tremendous mechanical strength**:** The tensile strength of carbon nanotubes is 100X greater than steel, but CNTs are less dense than aluminum. Nanotubes are the stiffest, strongest, and toughest molecule known.

Applications for CNTs [9]:

1. Electronics: one of the more amazing attributes of carbon nanotubes is that they can form films that are highly electrically conductive, but almost completely transparent. Electron mobility: Carbon nanotube transistors can have a mobility that is 70 times higher than silicon.

2. Structural Composites: High performance carbon fibers are used in structural composites in a wide range of applications including aerospace, automotives, and sporting equipment.

3. Conductive Composites: Carbon nanotubes blend well with plastics, and can impart reasonable conductivity at modest loadings.

4. Energy: Carbon nanotubes have the intrinsic characteristics desired for material used as electrodes in batteries, capacitors, and fuel cells.

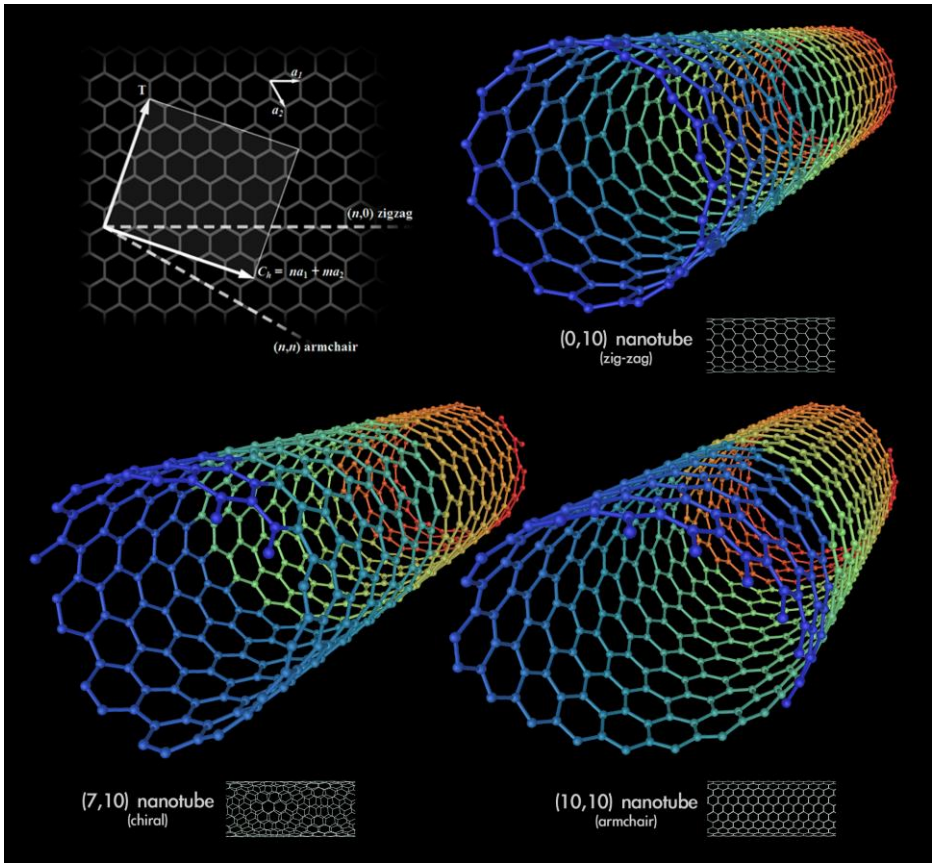

Figure 1.6: *3D model of three types (zigzag, chiral, and armchair) of single-walled carbon nanotubes.*[8]

1.3.3 Quantum Dots

A quantum dot is a semiconductor whose excitons are confined in all three spatial dimensions. As a result, they have properties that are between those of bulk semiconductors and those of discrete molecules. Researchers have studied quantum dots in transistors, solar cells, LEDs, and diode lasers. They have also investigated quantum dots as agents for medical imaging and hope to use them as qubits. In an unconfined (bulk) semiconductor, an electron-hole pair is typically bound within a characteristic length called the Bohr exciton radius. If the electron and hole are constrained further, then the semiconductor's properties change. This effect is a form of quantum confinement, and it is a key feature in many emerging electronic structures [11].

An immediate optical feature of colloidal quantum dots is their coloration. While the material which makes up a quantum dot defines its intrinsic energy signature, the

quantum confined size of the nanocrystal is more significant at energies near the band gap. Thus quantum dots of the same material, but with different sizes, can emit light of different colors. The physical reason is quantum confinement effect [[11]].

The larger the dot, the redder (lower energy) its fluorescence spectrum. Conversely, smaller dots emit bluer (higher energy) light. The coloration is directly related to the energy levels of the quantum dot. Quantitatively speaking, the bandgap energy that determines the energy (and hence color) of the fluoresced light is inversely proportional to the square of the size of the quantum dot. Larger quantum dots have more energy levels which are more closely spaced. This allows the quantum dot to absorb photons containing less energy, i.e. those closer to the red end of the spectrum. Recent articles in nanotechnology and other journals have begun to suggest that the shape of the quantum dot may well also be a factor in the coloration, but as yet not enough information has become available. Furthermore it was shown recently that the lifetime of fluorescence is determined by the size. Larger dots have more closely spaced energy levels in which the electron-hole pair can be trapped. Therefore, electron-hole pairs in larger dots live longer and thus these large dots show a larger lifetime [[11]].

As with any crystalline semiconductor, a quantum dot's electronic wave functions extend over the crystal lattice. Similar to a molecule, a quantum dot has both a quantized energy spectrum and a quantized density of electronic states near the band edge [[11]].

Reference

[1] Wikipedia (http://en.wikipedia.org/wiki/Dielectric_spectroscopy)
[2] Gorur G. Raju, *Dielectrics in Electric Fields* (Dekker, New York, 2003), page 100.
[3] K. S. Cole and R. H. Cole, *J. Chem. Phys.* **9**, 345 (1941); *and* K. S. Cole and R. H. Cole, *J. Chem. Phys.* **9**, 345 (1941) 10, 98 (1942).
[4] S. Pilla, J. A. Hamida, and N. S. Sullivan, *Rev of Sci. Instrum.* **70** 4055 (1999)
[5] S.C. Bera, S. Chattopadhyay, *Measurement* **33**, 3 (2003)
[6] M. C. Foote and A. C Anderson, *Rev of Sci. Instrum.* **58**, 130, (1987)
[7] Wikipedia (http://en.wikipedia.org/wiki/Liquid_crystal)
[8] Wikipedia (http://en.wikipedia.org/wiki/Carbon_nanotube)
[9] Unidym: Carbon for electronics (http://www.unidym.com)
[10] M. S. Dresselhaus, *Phil. Trans. R. Soc. Lond. A* **362**, 2065 (2002)
[11] Wikipedia (http://en.wikipedia.org/wiki/Quantum_dot)

CHAPTER 2

DIELECTRIC RESPONSE OF DIFFERENT CARBON STRUCTURES

2.1 Introduction

Carbon is an element of great technical importance and interest to industry and science. For our experiment, carbon has been chosen for probing the local structural dependence on dielectric spectra as pure carbon occurs as several different allotropes, or structures, that differ only in the arrangement of the atoms. High-resolution isothermal dielectric spectroscopy is reported as a function of frequency up to 10^5 Hz and electric field E_{rot} on four carbon allotropes; amorphous glass, diamond, multi-wall nanotubes (MWNT), and single-wall nanotubes (SWNT). The diamond spectra are featureless while the glass, MWNT, and SWNT samples exhibit two modes. A common low-frequency mode, likely due to surface space charges, is observed at ~16 Hz that decreases in dispersion strength and increases in frequency linearly with increasing E_{rot}. A higher-frequency mode, different for each sample, is also observed having a dispersion strength and frequency independent of E_{rot}.

The complex dielectric constant $\varepsilon^* = \varepsilon' - i\varepsilon''$ of a material is determined by the molecular polarizability and structural arrangement. This is essentially a measure of a charge-free sample's response to an applied electric field. The real part of the dielectric constant $\varepsilon'(\omega)$ is associated with the storage of the electric field energy while the imaginary part $\varepsilon''(\omega)$ corresponds to the dissipation of energy through a relaxation process. Typically, relaxations below 100 Hz are due to normal conduction while those between 100 and 10^5 Hz are associated reorientation of permanent and/or induced molecular dipoles in the material. Molecular interactions play an important role in such relaxation processes. Changes in the structural arrangement of the molecules can also

induce large changes in the dielectric spectra, leading to its use in the study of phase transitions [1]. Dielectric spectroscopy can provide detailed information on dynamic modes, such as segmental mobility of the molecules, or vibrational modes of a solid.

2.2 Dielectric measurement technique

We use an ac-capacitance bridge technique, discussed in chapter 1, to measure the isothermal dielectric spectra from 1 to 10^5 Hz of four different carbon structures; amorphous glass, crystalline diamond, single-wall nanotubes (SWNT), and multi-wall nanotubes (MWNT). In addition, the electric field dependence was probed by increasing the magnitude of the ac-electric field used in the capacitive measurement. The real and imaginary parts of the complex dielectric constant are determined from the in-phase and ($\pi/2$) out-of-phase off-balance signal of the bridge. Because of the experimental arrangement, the actual magnitude of E_{rot} across the sample is not known (only the driving voltage was controlled). However, the factor by which E_{rot} increases is known if measured in units of that produced by the lowest voltage (denoted as E^0_{rot} for 1 V applied), this normalized field is labeled $\boldsymbol{e}_R = E_{rot}/E^0_{rot}$. The capacitive cell consists of a parallel-plate configuration, 1 cm across and 100 μm thick using a Kapton spacer, housed in a temperature controlled bath. Comparison between the empty and sample filled capacitor allows for an absolute measurement of $\varepsilon^*(\omega, \boldsymbol{e}_R)$.

2.3 Sample preparation for experiments

All carbon samples were of powder form. The glass sample consisted of spherical particles 2 – 12 μm in diameter and 99.95% pure. The diamond sample was of natural mono-crystalline form approximately 1 μm in size and 99.9% pure. These powders were obtained from Aldrich and used after degassing under vacuum at 100 ^oC. The MWNT sample contains nanotubes 10 – 100 nm in diameter and 1 – 5 μm in length. The SWNT sample contains nanotubes ~ 1.3 nm in diameter and 0.5 – 50 μm in length. Both carbon nanotube samples were received from Prof. Saion Sinha and used without further processing.

The same amount by mass of each sample was loaded into the capacitor cell. The orientation of CNTs was completely random as was the distribution of the diamond and amorphous powders, thus only the average dielectric constant was determined. For consistency, the same thermal history was applied to each sample and all measurements reported here were performed at a fixed temperature of 328 K (55 ^oC) with a stability of ±0.005 ^oC. Temperature dependent experiments on all samples from 300 to 350 K reveal essentially identical spectra indicating that, at least, volatile impurities, which may have been adsorbed onto the carbon, do not play a significant role.

2.4 Results, discussions, and conclusions

The dielectric spectra for the diamond powder sample reveal no features over the entire frequency range studied. An increase in ε' and ε'' is seen below 10 Hz and is attributed to the onset of normal static conduction. Given the static nature observed, a detailed electric field dependence study was not carried out on diamond. For powders of glass, diamond, MWNT, and SWNT carbon, the dielectric spectra exhibits two prominent features, clearly seen in Figs. 2.1, 2.2, 2.3, and 2.4, respectively. A low-frequency feature (denoted mode-1), between 16 to 80 Hz and common to these three samples, is observed to decrease in dispersion strength (peak magnitude of ε'') and shift to higher frequencies linearly with increasing $\boldsymbol{e}_R$. The characteristics of mode-1 suggests that it is related to space charge polarization, which may involve several mechanisms of charge built up at the particle surface or electrode-sample interface [2]. Table I gives the result of a linear regression of the mode-1 peak frequency as a function of $\boldsymbol{e}_R$.

A higher-frequency feature (mode-2) is observed for the glass, MWNT, and SWNT samples whose peak frequency occurs at 63, 1.9, and 0.6 kHz, respectively, independent of $\boldsymbol{e}_R$. In addition, the magnitude of the mode-2 dispersion peak is also independent of $\boldsymbol{e}_R$ and exhibits markedly different appearance for the glass than for either of the nanotube samples. The behavior of this mode is consistent with orientational polarization of molecular permanent and/or induced dipoles in the different samples.

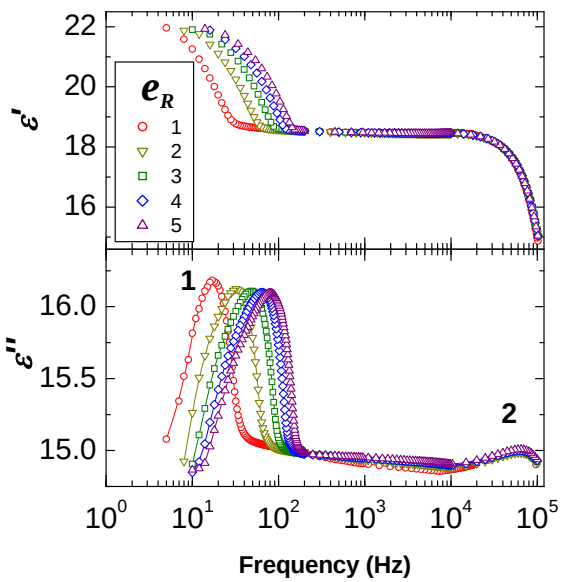

Figure 2.1: *The electric field intensity dependence of $\varepsilon'(\omega)$ and $\varepsilon''(\omega)$ for the amorphous carbon sample. Upper panel legend lists the applied field factor $\boldsymbol{e}_R$. In $\varepsilon''(\omega)$, the low-frequency mode is denoted by 1 while the high-frequency mode is denoted by 2.*

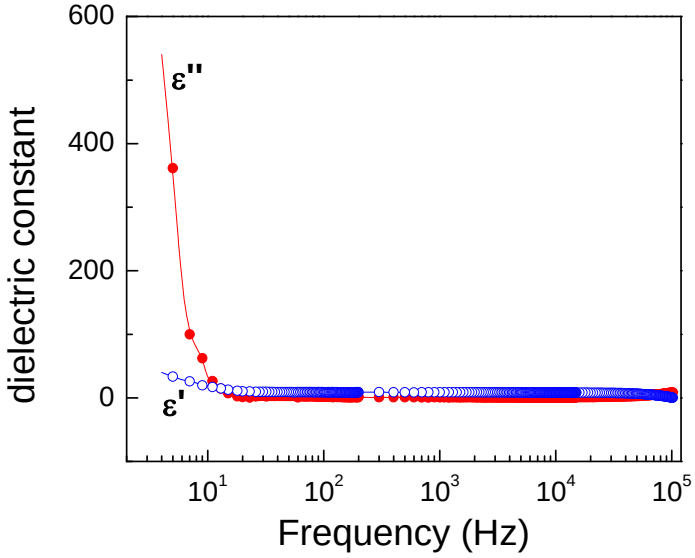

Figure 2.2: *Dielectric Spectrum of Diamond; frequency dependence of real part* (ε', *hollow blue circles*) *and imaginary part* (ε'', *red solid circles*) *of dielectric constant at room temperature, and* $\boldsymbol{e}_R = 1$.

To further illuminate the nature of the observed spectra, a "Cole-Cole" construction [3,4] is performed for the glass, MWNT, and SWNT samples. In making this construction, the complex dielectric constant is written as, $\varepsilon^* = \varepsilon_\infty + \Delta\varepsilon(1 + i\omega\tau)^{-\beta} - \alpha\, i(\sigma_0/\omega\varepsilon_{\mathrm{vac}})$, where $\Delta\varepsilon = \varepsilon_\infty - \varepsilon_0$ is the dielectric strength. Here, ε_∞ is the dielectric constant of the material at infinite frequency, ε_0 is the static dielectric constant, ω is the frequency, τ is the relaxation time constant, and β is the fitting factor (where normally $0 < \beta < 1$). The last term describes electronic conduction where α is the conduction factor, σ_0 is the static conductivity, and ε_{vac} is the vacuum permittivity. For $\alpha = 0$, i.e. negligible conduction, this relation yields the Cole-Davidson form [5] while setting $\beta = \alpha = 1$ results in the Debye dispersion relation with a static conductivity [6,7]. For $\beta = 1$ and $\alpha = 0$, a plot of the same scaled units of $\varepsilon''(\omega)$ versus $\varepsilon'(\omega)$ (a Cole-Cole plot) would reveal a semicircle for a single, well-defined, relaxation process whose diameter is $\Delta\varepsilon$.

However, dc-conductivity, resulting in a divergence of $\varepsilon''(\omega \to 0)$, or a distribution of relaxation times ($\beta < 1$) will lead to distortions of the semicircle [8,9]. Figure 2.5 shows a Cole-Cole plot for the glass, MWNT, and SWNT carbon samples at the same $\boldsymbol{e}_R$ revealing two well-separated features for each sample. Clearly, Fig. 2.5 indicates that mode-2 for the glass sample does not represent a typical relaxation process while mode-2 for the MWNT and SWNT samples are similar to each other, though at different frequencies, and represent a single, well-defined, relaxation process.

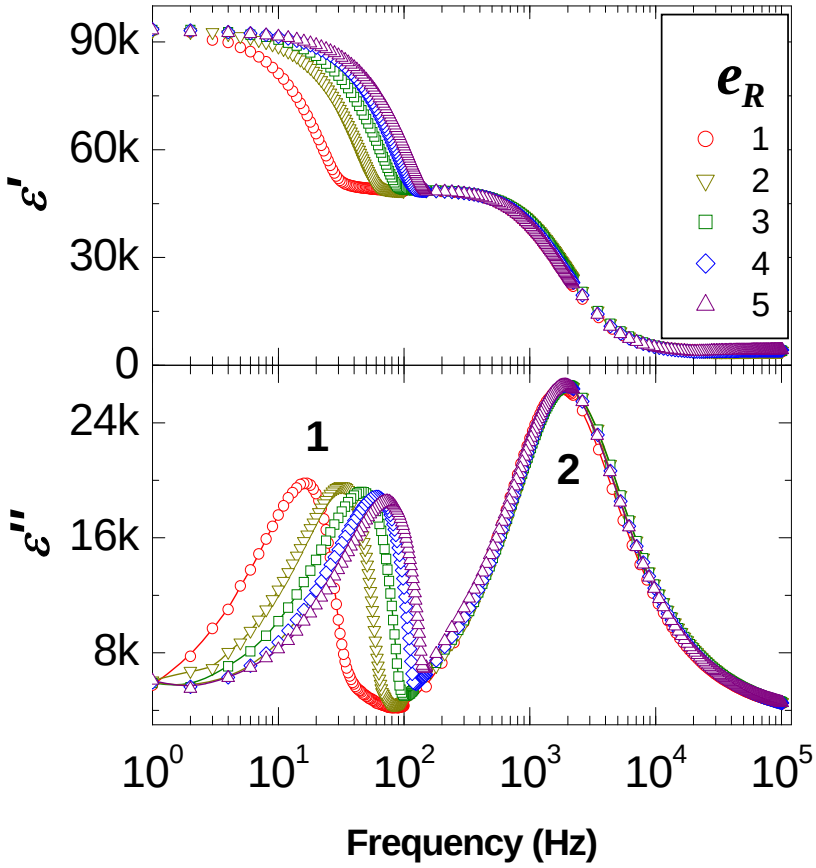

Figure 2.3: *The electric field intensity dependence of ε'(ω) and ε''(ω) for the SWNT sample (in units of 1000). Upper panel legend lists the applied field factor* $\boldsymbol{e}_R$. *For ε''(ω), the low-frequency mode is denoted by 1 and the high-frequency mode is denoted by 2.*

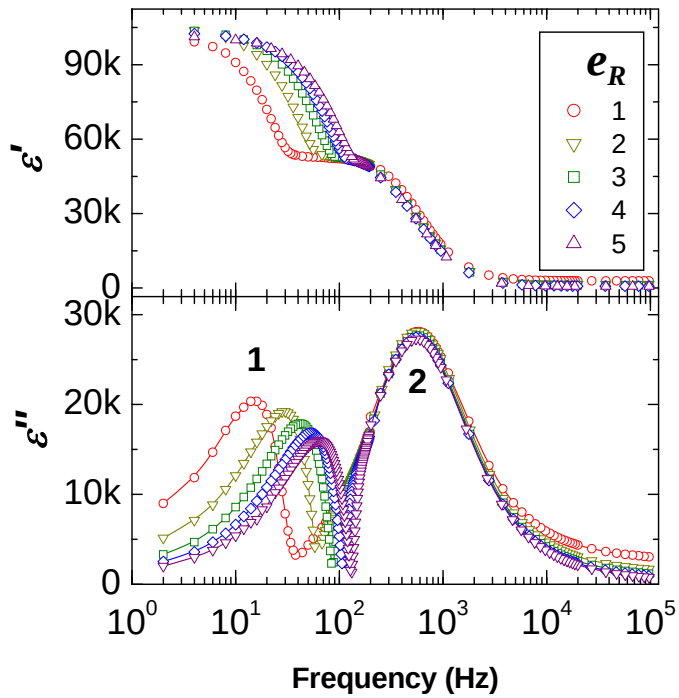

Figure 2.4: *The electric field intensity dependence of $\varepsilon'(\omega)$ and $\varepsilon''(\omega)$ for the SWNT sample (in units of 1000). Upper panel legend lists the applied field factor $\mathbf{e}_R$. For $\varepsilon''(\omega)$, the low-frequency mode is denoted by 1 and the high-frequency mode is denoted by 2.*

Quantity	***m*** **(*Hz*)**	***b*** **(*Hz*)**	**R**	$\sqrt{(\chi^2/N)}$ **(*Hz*)**
f_1(AG)	15.8 ± 0.1	0.8 ± 0.4	0.99992	0.282
f_1(MWNT)	14.2 ± 0.2	2.6 ± 0.7	0.99963	0.548
f_1(SWNT)	12.4 ± 0.6	3.6 ± 2.0	0.99636	1.483

Table I: *Results of a linear fit to the mode-1 peak frequency f_1 as a function of electric field $\mathbf{e}_R$. The slope m and intercept b (in the appropriate units) are given along with the regression coefficient R and the square-root of χ^2 per point. Note that all fits contain the same number of points (N = 5) and so, the R and $\sqrt{(\chi^2/N)}$ can be quantitatively compared among each set.*

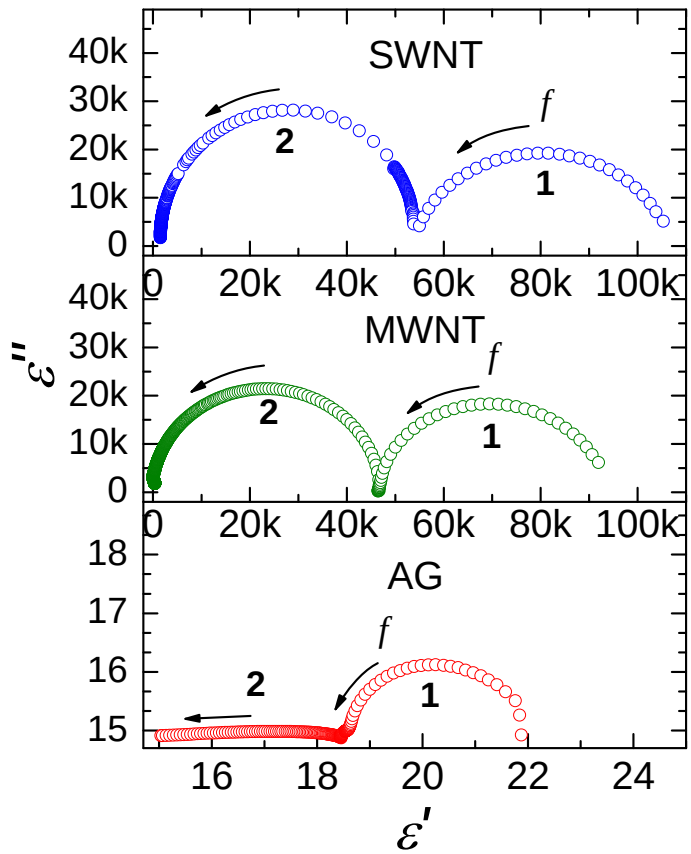

Figure 2.5: *Cole-Cole plots of $\varepsilon''(\omega)$ versus $\varepsilon'(\omega)$ for the SWNT (top), MWNT (middle), and amorphous glass AG (bottom) carbon samples at $\boldsymbol{e}_R$=2. Note that the upper two panels are in units of 1000. The arrows indicate the direction of increasing frequency and the labels denote the mode.*

In summary, the local molecular structures of carbon allotropes have a strong effect on their dielectric spectra up to 10^5 Hz. Given the static and featureless spectra for the diamond sample under identical experimental conditions, the two features in the spectra of the other carbon powders are intrinsic to their particular form and nature. For the glass, MWNT, and SWNT samples, the ac-electric field $\boldsymbol{e}_R$ plays an important role in linearly changing the dispersion strength and peak position of mode-1 but does not affect the higher frequency mode-2. All samples are powders of comparable grain size, but the diamond is an insulator while the glass is a conductor and the MWNT and SWNT are potentially conductors depending on their chirality, which is not known in our samples.

Thus, mode-1 is consistent with the build up of space-charges within the sample+cell, likely at the grain surfaces, if the nanotubes are conducting.

The mode-2 observed for the MWNT and SWNT appears as a single well-defined relaxation process, possibly due to orientational dynamics of permanent and/or induced dipoles, in the graphene layers. The mode observed in the glass sample is of different character and likely related to the amorphous powder containing a range of carbon structures, some of which are nanotubes. The higher frequency of mode-2 in the MWNT compared to that in SWNT may be due to "capacitor-like" structure of the multiple graphene walls and so, coupling of the polarization between layers. These results clearly indicate that the local structure plays a crucial role for mode-2 while mode-1 appears to be dictated by surfaces and the conducting nature of the samples.

Reference:

[1] J. Leys, G. Sinha, C. Glorieux, and J. Thoen, *Phys. Rev. E* **71**, 051709 (2005).

[2] G. G. Raju, *Dielectrics in Electric Fields*, Marcel Dicker, Inc. (New York, 2003)

[3] K. S. Cole and R. H. Cole, *J. Chem. Phys*. **9**, 345 (1941); *and* K. S. Cole and R. H. Cole, *J. Chem. Phys.* **10**, 98 (1942).

[4] Y.-Z. Wei and S. Sridhar, *J. Chem. Phys.* **4**, 99 (1993).

[5] D. W. Davidson and R. H. Cole, *J. Chem. Phys.* **19**, 1484 (1951).

[6] Y. Wei and S. Sridhar, *J. Chem. Phys.* **92**, 923 (1990).

[7] Y. Wei, P. Chiana, and S. Sridhar, *J. Chem. Phys.* **96**, 4569 (1992).

[8] W. Haase and S. Wrobel (eds), *Relaxation Phenomena*, Springer (Verlag, Berlin, Heidelberg, New York 2003).

[9] F. Kremer and A. Schonhals, *Broadband Dielectric Spectroscopy*, Springer (Verlag, Berlin, Heidelberg, New York 2003).

CHAPTER 3

ELECTRIC FIELD DRIVEN DIPOLE ORIENTATION DYNAMICS IN MULTIWALL CARBON NANOTUBES

3.1 Introduction

The complex dielectric constant (ε^*) is reported for multi-wall carbon nanotubes (MWCNTs) up to 10^5 Hz as a function of ac-electric field amplitude E_{rot} (in-phase and same frequency as the measurement) and E_{ac} (different phase and fixed frequency with respect to the measurement). A slow relaxation process (mode-1) is observed that increases in peak frequency with increasing E_{rot} but is independent of E_{ac}. A fast relaxation process (mode-2) is also observed that is independent of E_{rot} and shifts to higher frequency with increasing E_{ac} (opposite to that of mode-1). An ac-conductivity analysis of MWCNT reveals insights on how E_{rot} and E_{ac} influence the dissipation.

The dielectric storage and loss properties are of especial interest to researchers and engineers as these two parameters, among others, provide insight to CNTs and their suitability for electronic applications. In recent years, a CNT dispersion in an anisotropic liquid media (such as a liquid crystal) has gained interest for inducing parallel alignment of CNTs and ac-field induced orientation manipulation for use as switches at the nano scale level [1,2,3]. In these kinds of applications, it is important to know the dynamic dielectric modes of CNTs as well as their behavior under an applied ac-electric field. Dielectric spectroscopy of CNTs can reveal insights on those dynamic modes of potential interests as a function of ac field intensity.

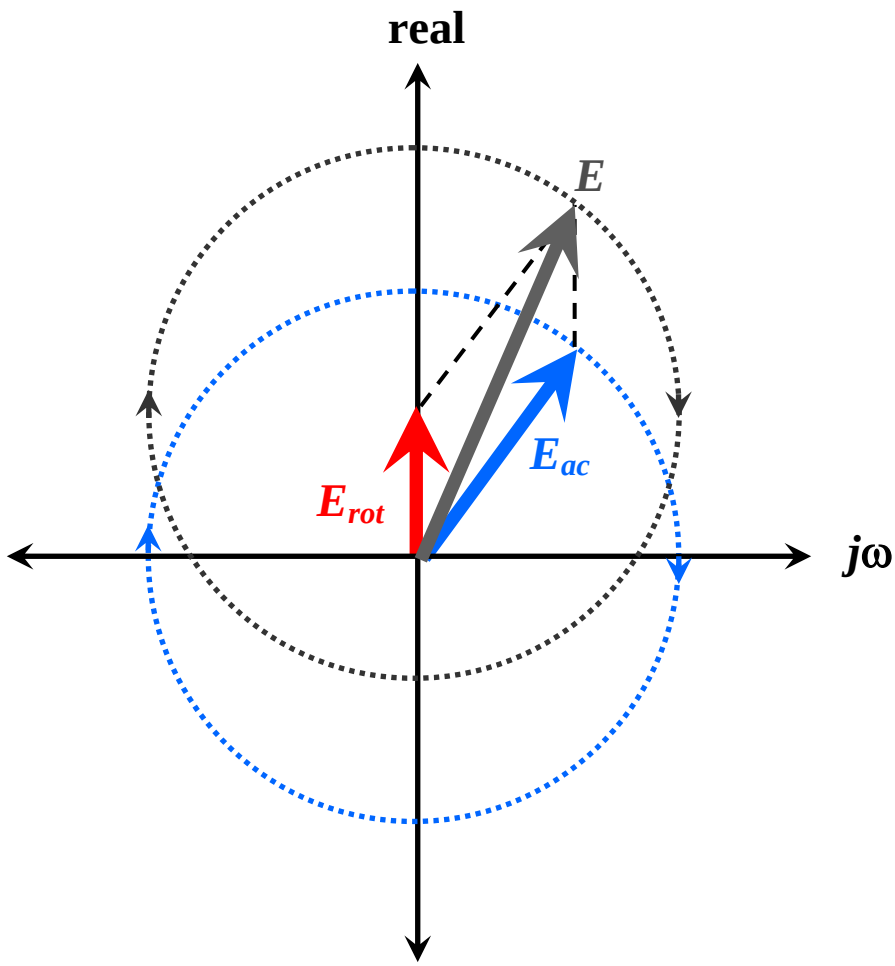

Figure 3.1: *The ac-electric fields* $\boldsymbol{E}_{rot}$ *and* $\boldsymbol{E}_{ac}$ *in the complex rotating-frame of the dielectric measurement. The field* $\boldsymbol{E}_{rot}$*, along the real axis, is in phase and at the same frequency as the measurement, hence 'static' in complex rotating-frame. Being at a different frequency than the measurement,* $\boldsymbol{E}_{ac}$ *acts as an ac-field in the complex rotating-frame. The field* $\boldsymbol{E}$ *is the resultant field and, at any time, the sample experiences the real component.*

Aggregated CNTs shows unique dielectric spectra [4] and the relaxation mechanisms are found to distort on application of electric fields. However, the experimental application of an external ac-electric field can be complicated. For example, the probing field, $E_{\mathrm{rot}}(\omega)$, in a capacitive measurement, is in phase and at the same frequency as the measurement of the complex dielectric constant, $\varepsilon^*(\omega) = \varepsilon' - i\varepsilon''$. Thus, in the complex *rotating-frame* of the measurement, E_{rot} can be considered a 'static' field. Conversely, the applied ac-electric field may be at a fixed frequency ω' with respect to the ac-capacitive measurement frequency ω, *i.e.* ω' = constant > ω. This field $E_{\mathrm{ac}}(\omega')$ is

an oscillating field in the complex rotating-frame of the measurement. Figure 3.1 illustrates the phasor diagram of these two electric fields.

In this chapter, the focus is to understand the dielectric response of CNTs with respect to applied ac-electric fields. The dielectric storage $\varepsilon'(\omega)$ and loss $\varepsilon''(\omega)$ of a multiwall carbon nanotube (MWCNT) sample are reported as a function of amplitude of both E_{rot} (ω) and E_{ac} $(\omega' = 203$ kHz) over the frequency range $1 \leq \omega \leq 10^5$ Hz. The results demonstrate how E_{ac} and E_{ac} polarize the curved graphene layers in MWCNT sample. The dielectric spectra reveal two relaxation modes; a slow mode below 100 Hz that is likely attributed to space-charge polarization at the electrode-nanotube interface, and a fast mode in the kHz range that is discussed in terms of reorientation polarization of permanent and/or induced electric dipoles.

3.2 Experimental procedures

A homebuilt ac-capacitance bridge technique [5,6,7], discussed in chapter 1, operating with a probing field E_{rot} (ω), is used to measure $\varepsilon'(\omega)$ and $\varepsilon''(\omega)$ as a function of frequency and magnitude of E_{rot} and E_{ac}. The capacitive cell consists of a parallel-plate configuration, 1 cm across with a 100 μm gap using a Kapton spacer, housed in a temperature controlled bath. The real and imaginary parts of the complex dielectric constant are determined from the in-phase and (π/2) out-of-phase off-balance signal of the bridge. Comparison between the empty and sample filled capacitor allows for an absolute measurement of $\varepsilon^*(\omega, E_{rot}, E_{ac})$. The probing ac-field E_{rot} (ω) is applied across the sample through the capacitive bridge and is adjusted by increasing the probing voltage. Because of this technique, the actual magnitude of E_{rot} across the sample is not known (only the driving voltage across the bridge was controlled). However, the factor that E_{rot} increases is known if measured in units of that produced by the lowest voltage (denoted as E^0_{rot} for 1 V amplitude applied probing voltage), this factor is labeled $\boldsymbol{e}_R = E_{rot}/E^0_{rot}$. To apply and vary the $E_{ac}(\omega')$ field, a second signal generator, independent of the capacitance bridge, is applied directly across the parallel capacitor plates parallel to the bridge. The presence of E_{ac} can be visualized as measurement of dielectric constant in presence of an ac bias field that is independent of the measurement technique. The frequency of E_{ac} is a constant 203 kHz, which is well above the maximum frequency range (100 kHz) of the lock-in-amplifier used to detect the off-balance signal and avoids interference. For consistency, the magnitude of E_{ac} is also labeled $\boldsymbol{e}_{AC} = E_{ac}/E^0_{ac}$ where E^0_{ac} is that produced using 1 V amplitude output. These quantities $\boldsymbol{e}_R$ and $\boldsymbol{e}_{AC}$ are the factors that the actual electric field magnitudes increase from their lowest to higher values.

The MWCNT sample, received from Prof. Sinha, was used without further processing. The MWCNT sample used is polydisperse containing nanotubes 10 – 100 nm in diameter and 1 – 5 μm in length. Roughly 80 vol % of the capacitive cell was occupied

by MWCNT sample. The sample was filled into the capacitive cell by drop-cast evaporation, thus the orientation of the nanotubes are random between the plates. The measurements reported here are of the *average* complex dielectric constant $\varepsilon^*(\omega) = (\varepsilon_{\|} + 2\varepsilon_{\perp})/3$, where $\varepsilon_{\|}$ and $\varepsilon_{\perp}$ are the complex dielectric constants parallel and perpendicular to the nanotube long-axis, respectively.

We use an ac-capacitance bridge technique, discussed in chapter 1, to measure the isothermal dielectric spectra from 1 to 10^5 Hz of four different carbon structures; amorphous glass, crystalline diamond, single-wall nanotubes (SWNT), and multi-wall nanotubes (MWNT). In addition, the electric field dependence was probed by increasing the magnitude of the ac-electric field used in the capacitive measurement. The real and imaginary parts of the complex dielectric constant are determined from the in-phase and ($\pi/2$) out-of-phase off-balance signal of the bridge. Because of the experimental arrangement, the actual magnitude of E_{rot} across the sample is not known (only the driving voltage was controlled). However, the factor by which E_{rot} increases is known if measured in units of that produced by the lowest voltage (denoted as E^0_{rot} for 1 V applied), this normalized field is labeled $\boldsymbol{e}_{\mathrm{R}} = E_{\mathrm{rot}}/E^0_{\mathrm{rot}}$. The capacitive cell consists of a parallel-plate configuration, 1 cm across and 100 μm thick using a Kapton spacer, housed in a temperature controlled bath. Comparison between the empty and sample filled capacitor allows for an absolute measurement of $\varepsilon*(\omega, \boldsymbol{e}_{\mathrm{R}})$.

3.3 Sample preparation for experiments

All carbon samples were of powder form. The glass sample consisted of spherical particles 2 – 12 μm in diameter and 99.95% pure. The diamond sample was of natural mono-crystalline form approximately 1 μm in size and 99.9% pure. These powders were obtained from Aldrich and used after degassing under vacuum at 100 ^{o}C. The MWNT sample contains nanotubes 10 – 100 nm in diameter and 1 – 5 μm in length. The SWNT sample contains nanotubes ~ 1.3 nm in diameter and 0.5 – 50 μm in length. Both carbon nanotube samples were received from Prof. Saion Sinha and used without further processing.

The same amount by mass of each sample was loaded into the capacitor cell. The orientation of CNTs was completely random as was the distribution of the diamond and amorphous powders, thus only the average dielectric constant was determined. For consistency, the same thermal history was applied to each sample and all measurements reported here were performed at a fixed temperature of 328 K (55 ^{o}C) with a stability of ±0.005 ^{o}C. Temperature dependent experiments on all samples from 300 to 350 K reveal essentially identical spectra indicating that, at least, volatile impurities, which may have been adsorbed onto the carbon, do not play a significant role.

3.4 Results

The dielectric spectra of the MWCNT sample exhibit two well-distinguished dynamic modes in the frequency range studied. See Figure 3.2. The slow mode is likely due to space charge polarization at the electrode-nanotubes interface (denoted mode-1) and the faster mode is likely due to orientational polarization of permanent and/or induced dipoles (denoted mode-2) either of the nanotubes themselves or within the multiple graphene layers. Mode-1 is strongly coupled to E_{rot} while mode-2 is independent of E_{rot} as seen in Fig. 3.2 of the dielectric spectra. The spectra reveal opposite behavior with the application of E_{ac}. Here, the relaxation frequency increases while the strength (peak height of ε'' for mode-2, $\Delta\varepsilon_2''$) decreases for mode-2 as E_{ac} increases. Mode-1 is independent of E_{ac}.

Since, mode-1 is likely to originate from space charge polarization; it may involve several mechanisms of space charge accumulation at the electrode-nanotubes interface. However, all such processes for powder dielectric samples generally occur at low frequency, typically below 100 Hz [8] and depend strongly on the surface conductivity of the sample and cell [21]. The probing field E_{rot} is static in the rotating frame. Thus, this effectively DC field couples strongly to charge conduction and so to the relaxation mode-1 as the frequency is varied across this low-frequency range. Figure 3.3a indicates that the relaxation frequency of mode-1 (f_1) increases linearly for $0 \leq \boldsymbol{e}_R \leq 3$. For $\boldsymbol{e}_R > 3$, f_1 appears to begin saturating, reaching approximately $f_1^{max} \sim 75$ Hz for $\boldsymbol{e}_R > 5$. The behavior of f_1 is consistent with conduction of finite space charges built up at the electrode-nanotubes (and perhaps nanotube-nanotube) interfaces. To strengthen this interpretation, f_1 extrapolates to zero as $\boldsymbol{e}_R = 0$, further indicating that mode-1 is associated with a charge conduction mechanism that vanishes as field strength goes to zero. However, the second electric field E_{ac} was applied at a much higher fixed frequency and so should not affect mode-1 as is observed.

It is expected that the magnitude of the probing field in an ac-capacitance bridge method (E_{rot}) should not affect the orientational relaxation of permanent or induced dipoles [9,10,11]. Thus, it is expected that mode-2, being associated with a dipole relaxation process, should be independent of E_{rot} as seen in Fig. 3.2 for constant $\boldsymbol{e}_{AC}$. The frequency and strength dependence of mode-2 on E_{ac} suggests a different insight into the relaxation mechanism. Figure 3.3b illustrates that above a threshold ($\boldsymbol{e}_{AC} \approx 1$ where both E_{rot} and E_{ac} are approximately of equal magnitude), f_2 increases linearly while $\Delta\varepsilon_2''$ decreases linearly with increasing E_{ac}.

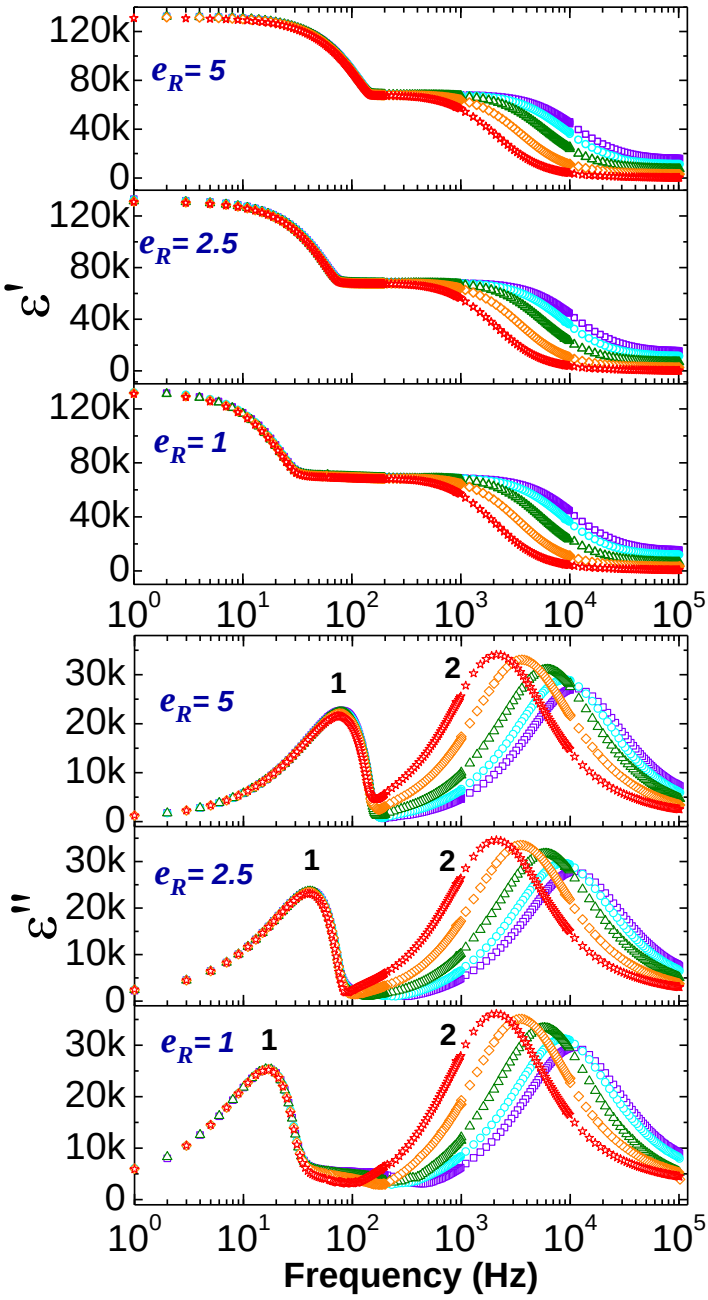

Figure 3.2: *The frequency and E_{ac} (shown by field factor $\boldsymbol{e}_{AC}$; star = 1, diamond = 2, triangle = 3, circle = 4, and square = 5) dependence of dielectric storage ε′ (top panel) and loss ε″ (bottom panel) of MWCNT sample for three values of E_{rot} (or $\boldsymbol{e}_R$).*

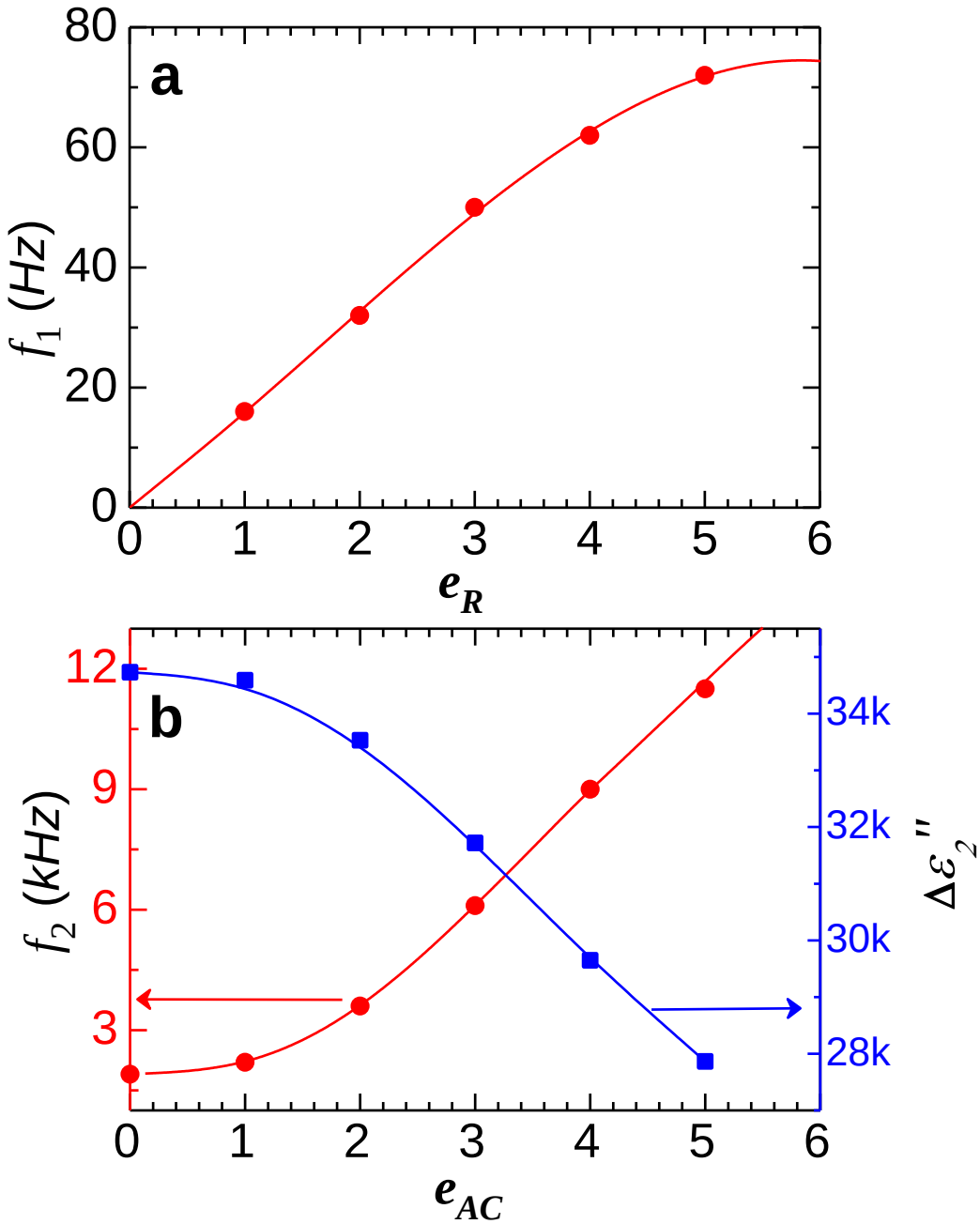

Figure 3.3: (a) *Relaxation frequency of mode-1 (f_1) as a function of E_{rot} (or $\boldsymbol{e}_R$). Note the initial linear dependence with zero intercept and the apparent saturation for $\boldsymbol{e}_R > 5$.*
(b) *Relaxation frequency of mode-2 (f_2) and dispersion strength ($\Delta\varepsilon_2''$, peak magnitude of ε'') of mode-2 as a function of E_{ac} (or $\boldsymbol{e}_{AC}$) for $\boldsymbol{e}_R = 1$. Lines are guide-to-the-eye.*

3.5 Discussions and conclusions

The observed behavior of mode-2 with E_{ac} may be explained by the following simple model that suggests a unique relaxation mechanism. The multiple graphene layers of an MWCNT can be visualized as an effective capacitor (C) between the layers in series with an effective resistor (R) of the carbon wall. See Figure 3.4. The applied field E_{ac} generates a voltage difference $V = E_{ac}d$ between the inner and outer graphene layers of an MWCNT, where d is the average distance between graphene layers. The natural frequency of this analogous RC circuit is given by $\omega_0 = 2\pi f_2 = 1/RC$. The equivalent effective capacitor C for multiple graphene walls is approximately given by $C = (V/Q + V/Q + \ldots n^{th}\ layer)^{-1} = Q/(nV)$; where n is the number of walls and Q is the charge on the each curved graphene layer. Substituting gives $\omega_0 = Vn/RQ = E_{ac}(dn/RQ)$, a linear dependence of ω_0 with increasing E_{ac} (once E_{ac} is sufficiently above the effect of E_{rot}) with all other factors being constant for a given sample. This simple model appears to describe well the observed amplitude dependence of the relaxation frequency of mode-2.

The ac-conductivity is related to the dielectric properties by $\sigma_{ac} = \omega\varepsilon''\varepsilon_0$ [12] and represents the sum contributions from all dissipative mechanisms. Figure 3.5 shows the MWCNT sample ac-conductivity frequency dependence and reveals the two modes seen in the actual dielectric spectra. The slow and fast modes are observed with a $\sigma_{ac}(\omega)$ for mode-1 typical of charge conduction while that for mode-2 reminiscent of that for induced polarization (perhaps related to that between the graphene layers within a nanotube). For frequencies at or above 50 kHz, σ_{ac} exhibits a slow increase above the plateau associated with mode-2 that may be a signature of a mode observed by K. Ahmad *et all.* [12] at ~ 10^7 Hz for the highest volume concentration of MWCNT in alumina.

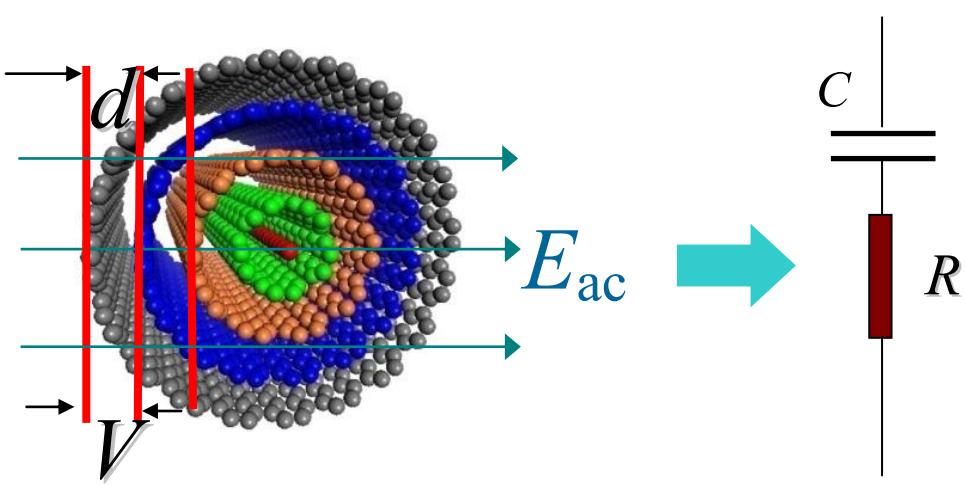

Figure 3.4: *Effective capacitors* (C) *between the layers hooked up in series with the effective resistors* (R) *of the walls.*

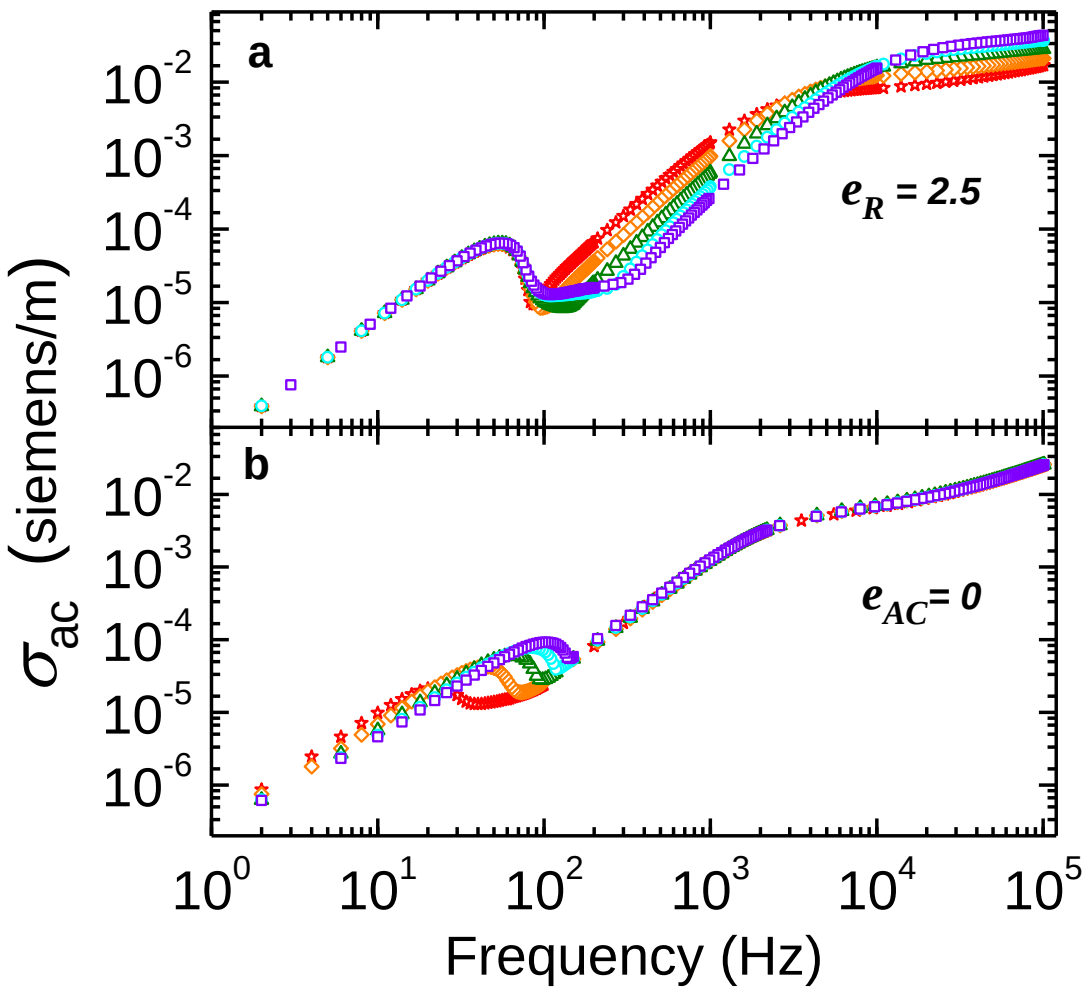

Figure 3.5: *The dielectric ac-conductivity σ_{ac} of MWCNT sample as a function of frequency.* **(a)** *For constant $\boldsymbol{e}_R$ and varying $\boldsymbol{e}_{AC}$; star = 1, diamond = 2, triangle = 3, circle = 4, and square = 5.* **(b)** *For constant $\boldsymbol{e}_{AC}$ and varying $\boldsymbol{e}_R$; star = 1, diamond = 2, triangle = 3, circle = 4, and square = 5.*

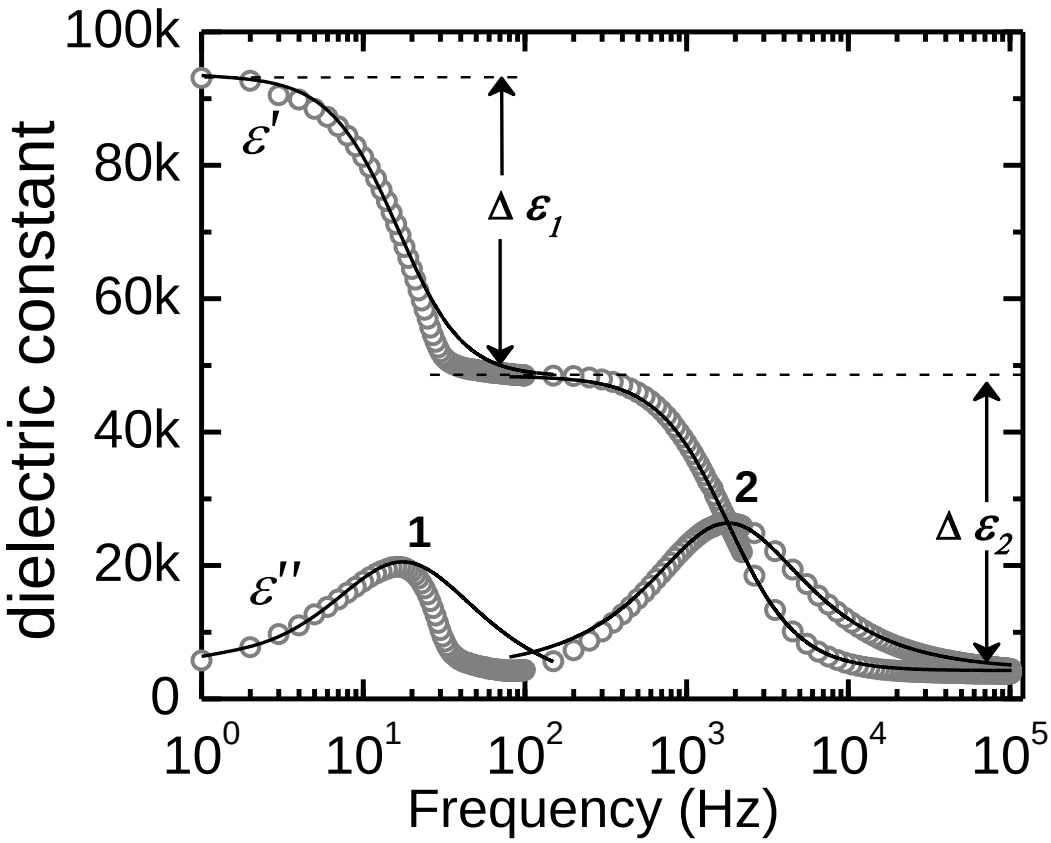

Figure 3.6: *The dielectric spectrum of the MWCNT sample for* $\boldsymbol{e}_R = 1$ *and* $\boldsymbol{e}_{AC} = 0$*, open circles are the data and the solid lines are fits to a Debye relaxation form. Mode-1 and 2 are labeled in the figure where* $\Delta\varepsilon_1$ *and* $\Delta\varepsilon_2$ *are the real dielectric strengths, respectively.*

A Debye relaxation analysis has been performed on the observed dielectric spectra. A Debye relaxation can be expressed as $\varepsilon^* = \left(\varepsilon_\infty + \frac{\Delta\varepsilon}{1+(\omega\tau)^2}\right) - i\left(\frac{\Delta\varepsilon\omega\tau}{1+(\omega\tau)^2}\right)$; where τ is the relaxation time constant and $\Delta\varepsilon = \varepsilon_0 - \varepsilon_\infty$ is the dielectric relaxation strength (the difference between the static and infinite frequency dielectric constant) for a single relaxation process. Figure 3.6 shows such a fit and indicates mode-2 is quite consistent with this form without any additional fitting factor. This confirms that mode-2 is related to a polarization process where charge migration does not play an important role. Clearly, mode-1 is asymmetric and not a Debye relaxation.

In summary, these results clearly reveal that this nano scale system can be perturbed by applying ac-electric fields in two different ways; E_{rot} and E_{ac}. The observed electric field dependence of the spectra reveals the polarization mechanism within the graphene layers of MWCNT. A simple theoretical model can explain the observed frequency shift of mode-2 with E_{ac}: capacitor-resistor-like structure of the multiple graphene walls. This model accounts for the coupling of the polarization between multiple graphene layers in MWCNT. The extracted dielectric ac-conductivity increases by four orders of magnitude for increasing frequencies up to 100 kHz and suggests a way to tune the suitable value of conductivity of a MWCNT for a given application.

Reference:

[1] Michael D. Lynch and David L. Patrick, *Nano Letters* **2**, 1197 (2002).

[2] I. Dierking, G. Scalia and P. Morales, *J. Appl. Phys.* **97**, 044309 (2005).

[3] Seok Jin Jeong, K. Ah Park, S. H. Jeong, H. J. Jeong, K. H. An, C. W. Nah, D. Pribat, S. H. Lee, and Y. Hee Lee, Sr., *Nano Letters* **7**, 2178 (2007).

[4] R. Basu and G. Iannacchione, *Appl. Phys. Lett.* **92**, 052906 (2008).

[5] S. Pilla, J. A. Hamida, and N. S. Sullivan, *Rev. of Sci. Instrum.* **70**, 4055 (1999).

[6] S.C. Bera, S. Chattopadhyay, Measurement **33**, 3 (2003).

[7] M. C. Foote and A. C Anderson, *Rev. of Sci. Instrum.* **58**, 130 (1987).

[8] Gorur G. Raju, *Dielectrics in Electric Fields* (Dekker, New York, 2003).

[9] *Relaxation Phenomena*, edited by W. Haase and S. Wrobel (Springer, New York, 2003).

[10] F. Kremer and A. Schonhals, *Broadband Dielectric Spectroscopy*, (Springer, New York, 2003).

[11] N. E. Hill, W. E. Vaughan, A. H. Price and M. Davies, *Dielectric Properties and Molecular Behavior*, (Van Nostrand Reinhold Co., London, 1969).

[12] *Dielectric Materials and Applications*, edited by A. R. Von Hippel, (Chapman & Hall, Ltd., London, 1954).

CHAPTER 4

CARBON NANOTUBE DISPERSED LIQUID CRYSTAL-A NANO ELECTROMECHANICAL SYSTEM

4.1 Introduction

Electric field induced director orientation of a nematic liquid crystal (LC) + carbon nanotube (CNT) system reveals insights on switching behavior for this anisotropic composite. Once the field goes off, the LC+CNT system relaxes back to the original orientation through a mechanical rotation, revealing the intrinsic dynamics. LC molecules and CNTs cooperatively form local *pseudo-nematic* domains in the isotropic phase due to strong LC-CNT interactions. These field-responsive anisotropic domains do not relax back to the original orientation on switching of the field off; which could find potential applications in memory devices.

Carbon nanotubes (CNTs) dispersed nematic liquid crystal (LC) represents a versatile functional composite that has gained interest in recent years for inducing parallel alignment of CNTs and improving electro-optic effect of LCs [1,2,3,4,5,6]. This LC+CNT system is a unique assemblage of an anisotropic dispersion (CNTs) in an anisotropic media (LC). This makes it an attractive anisotropic physical system to study the electric field induced switching behavior and nano-dynamic response of LC and CNTs. After a field induced *director* (average direction of LC molecules) orientation of the nematic LC+CNT system [1,2,3], the LC molecules, as well as the CNTs dynamically reorient back into their original orientation on turning the electric field off, revealing the intrinsic dynamics. However, the reorientation and relaxation mechanisms of CNTs are strongly influenced by the surrounding LC media, such as nematic phase or isotropic phase. In this letter, we report the dynamic response of the average dielectric constant ($\bar{\varepsilon}$) for multiwall carbon nanotubes (MWCNTs) dispersed in 4-cyano-4′-pentylbiphenyl (5CB) LC as a function of applied ac-field in both the nematic and isotropic phases.

4.2 Experiments

A small amount (0.005 wt %) of MWCNT sample (containing nanotubes < 8 nm in diameter and 0.5-2 μm in length) was dispersed in 5CB ($T_{nematic\text{-}isotropic}$ = 35°C) and the mixture was ultrasonicated for 5 hours to reduce the bundling tendency of CNTs. Strong interaction with a binding energy of about -2eV between LC-CNT [4,7] makes the long axes of CNTs follow the nematic LC director [1,2,3]. After ultrasonication, the mixture was filled into a cell (5 mm × 5 mm indium tin oxide (ITO) coated area and 20 μm spacing) by capillary action, housed in a temperature controlled bath. Surface treatment inside the LC cell imposes the planar alignment to the nematic director, see Figure 4.2. Empty LC cells [8] were measured first in order to extract the absolute $\bar{\varepsilon}$. The relaxation dynamics also depend on cell configuration; for comparisons, the same type of cells was used for both pure 5CB and 5CB+MWCNT.

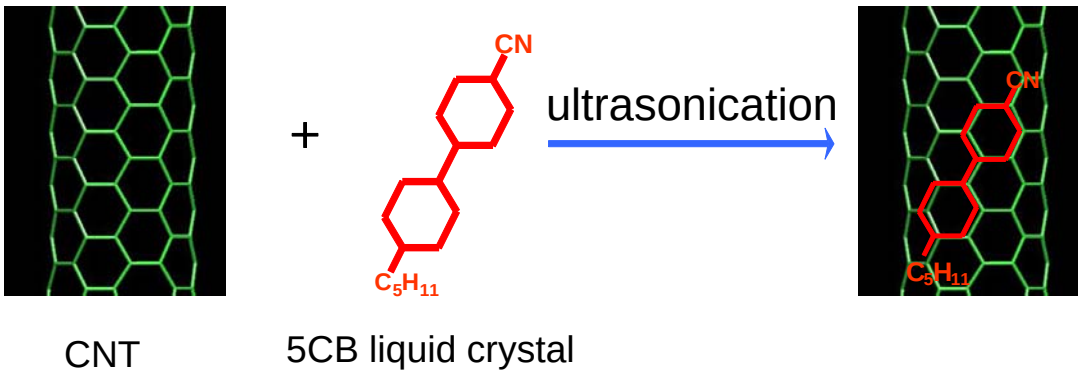

Figure 4.1: *Helical surface anchoring of LC molecule on CNT wall.*

After the LC+CNT sample was loaded into the cell, an external ac electric field pulse, E_{ac} (1 MHz) of 30 seconds duration was applied across the cell at magnitudes ranging from 0 - 250 kV/m. The reason for applying the ac field (not dc) is to avoid the affect of ion migration on the dielectric relaxation measurements. Once E_{ac} was turned off (at t = 0 sec), isothermal average dielectric ($\bar{\varepsilon}$) measurements were carried in the nematic (T = 25° C) and isotropic (T = 45° C) phases as a function of time. See Fig. 4.4. The dielectric measurements were performed by the ac capacitance bridge technique [9,10,11], operating with a probing field far below the reorientation threshold field and at 100 kHz frequency. The LC 5CB does not exhibit any tumbling mode [12] and MWCNTs show no space charge or dipole orientation dynamics at this probing frequency [13]. Thus, the observed dynamics should be driven mainly by a mechanical relaxation mechanism of the director after E_{ac} is switched off.

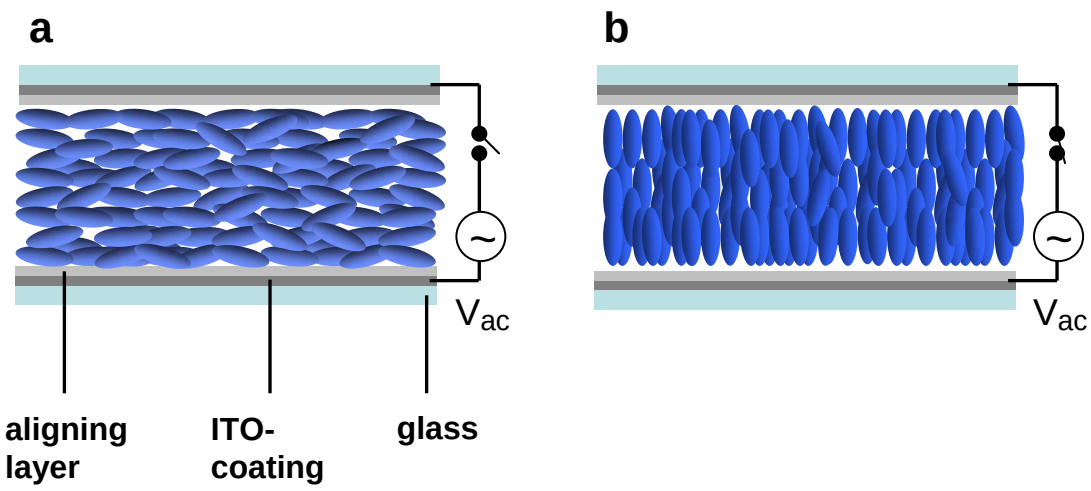

Figure 4.2: (**a**) *Schematic diagram of alignment of LC molecules in a homogeneous cell without electric field;* (**b**) *Schematic diagram of alignment of LC molecules in a homogeneous cell with field.*

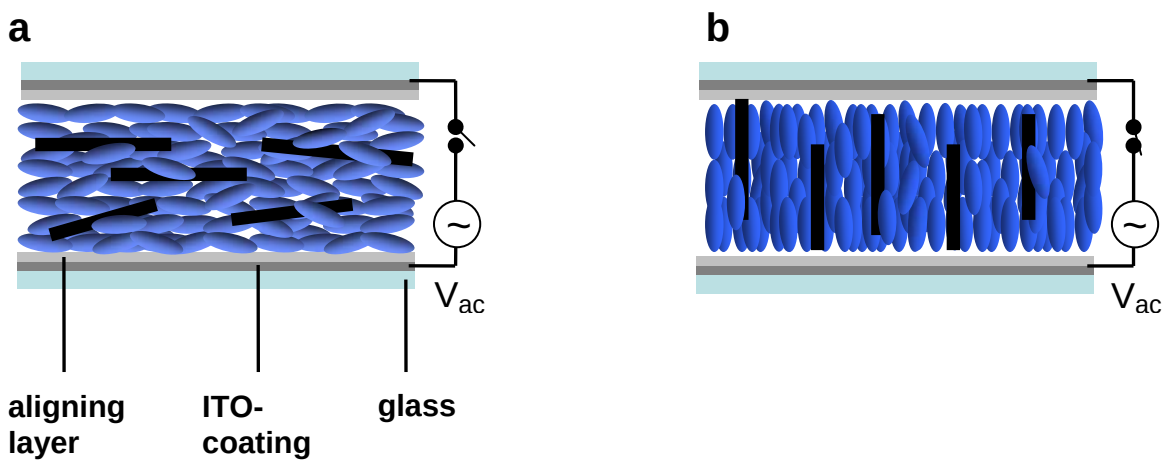

Figure 4.3: (**a**) *Schematic diagram of alignment coupling of LC+CNT in a homogeneous cell without electric field;* (**b**) *Schematic diagram of alignment of coupling of LC+CNT in a homogeneous cell with field.*

4.3 Results, analysis, and conclusions

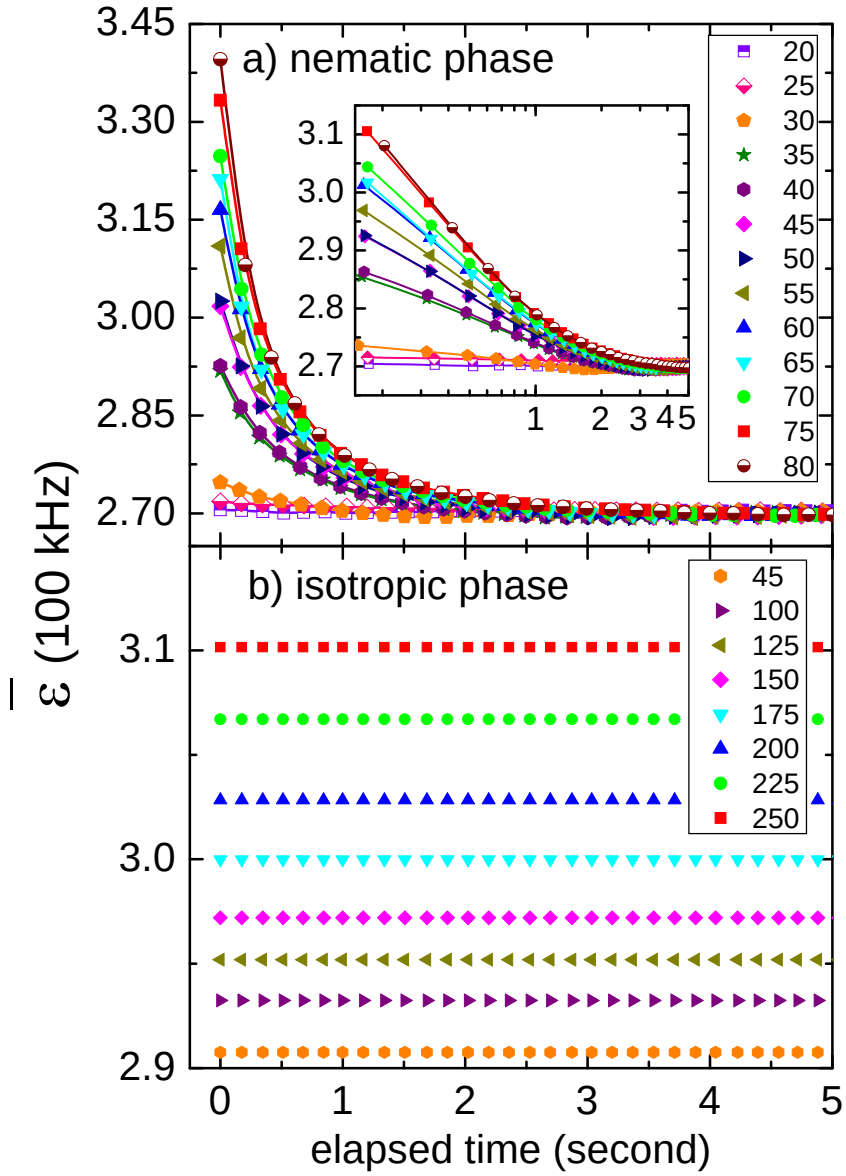

Figure 4.4: (**a**) *Dynamic response of the average dielectric constant* $\bar{\varepsilon}$ *for the LC+CNT system in the nematic phase (T = 25°C) after* E_{ac} *= 0; the inset (same main graph axes) represents the same relaxation in log-time scale to show the single exponential decay. Lines represent the fitting according to a single exponential decay function, see text for details;* (**b**) *Dynamic response of the average dielectric constant* $\bar{\varepsilon}$ *for LC+CNT system in the isotropic phase (T = 45°C) after* E_{ac} *= 0. The legends in both the panels represent the magnitude of* E_{ac} *(kV/m, 1MHz).*

Figure 4.4 shows the average complex dielectric constant, $\bar{\varepsilon}$ (100kHz) as a function of time after E_{ac} was tuned off for 5CB+MWCNT sample. In the nematic phase (T = 25° C), CNTs and LC molecules cooperatively relax back to the planar orientation after the field goes off, clearly seen in Fig. 4.4a. Field induced director orientation occurs when the torques, due to the external electric field, overcome the elastic interactions between LC molecules and, through surface coupling, the CNT long axis follows the director orientation. See Fig. 4.3. Soon after the field goes off, these restoring forces, between the planar surface state and LC director, drive the system back to the original orientation through a mechanical rotation. The field-saturated dielectric constant, $\bar{\varepsilon}_{max}$ ($\bar{\varepsilon}$ at t = 0, from Fig 4.5a) for each relaxation is plotted as a function of E_{ac} in Fig. 2a and is directly associated with the director orientation. The value of $\bar{\varepsilon}_{max}$ starts to increase above E_{ac} = 20 kV/m for both pure 5CB and 5CB+MWCNT samples, confirming the director reorientation from planar to homeotropic, but, $\bar{\varepsilon}_{max}$ saturates at a higher field for the composite sample than pure 5CB. See Fig. 4.5a. This is probably due to the higher aspect ratio of CNTs that require higher fields to fully reorient.

A dramatic change in the field induced orientation mechanism has been observed in the isotropic phase (T = 45° C). Due to the absence of elastic interactions in the isotropic phase, the LC molecules no longer form long range orientation order. So, it is expected to have no field induced director reorientation for pure 5CB, as also experimentally observed in Fig. 4.5b. But, the composite shows an increment in $\bar{\varepsilon}$ on application of electric field which does not relax back over time on switching the field off, as seen in Fig. 4.4b. Even though there are no long-range nematic interactions in the isotropic phase, the coupling between LC-CNT [4,7] still exists. Due to this coupling, the CNT induces local short-range orientation order of LC surrounding the CNT, which can be visualized as presence of isolated *pseudo-nematic* domains in an isotropic media. See Fig. 4.7. These local anisotropic *pseudo-nematic* domains are also field responsive and can be reoriented on application of E_{ac}. But, after the field goes off, there is no restoring force in the isotropic LC media to mechanically torque these domains back into the original orientation. Fig. 4.5b depicts that in the isotropic phase there is no sharp threshold field to start the reorientation and $\bar{\varepsilon}_{max}$ does not seem to saturate in the field range studied. The field induced reorientations of these anisotropic domains can only be erased by slowly cooling the system down to the nematic phase and then heating it up again to the isotropic phase.

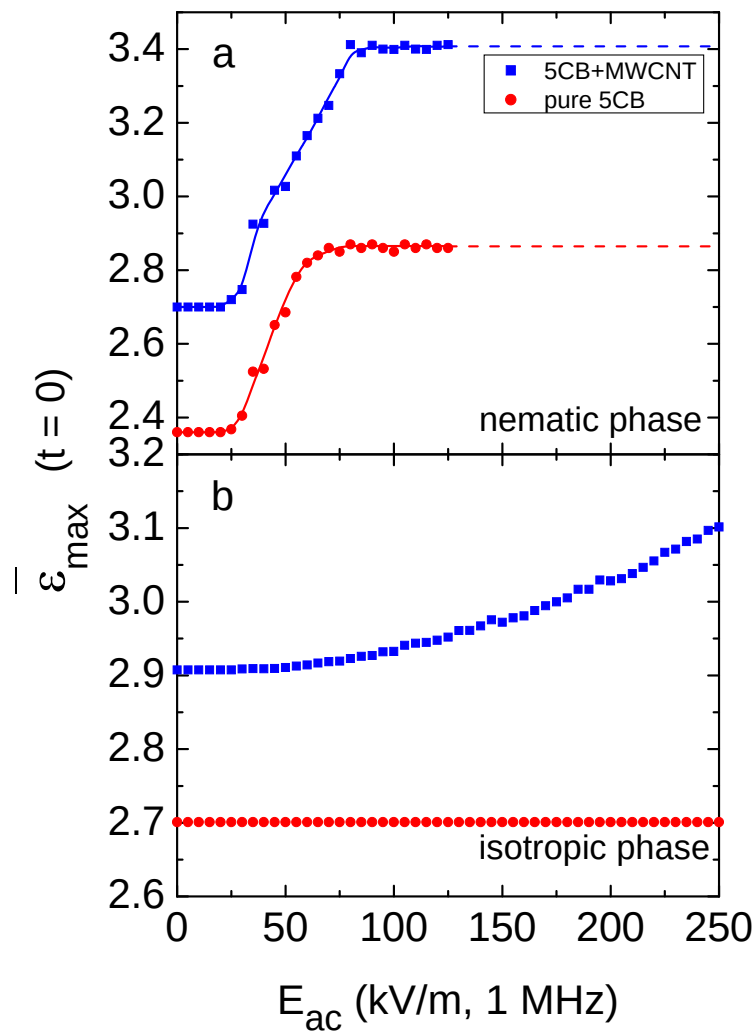

Figure 4.5: **(a)** *Field-saturated dielectric constant,* $\bar{\varepsilon}_{max}$ *(* $\bar{\varepsilon}$ *at t = 0) as a function* E_{ac} *in the nematic phase (T = 25°C). Lines represent guide to the eye;* **(b)** *Field-saturated dielectric constant,* $\bar{\varepsilon}_{max}$ *(* $\bar{\varepsilon}$ *at t = 0) as a function* E_{ac} *in the isotropic phase (T = 45°C).*

Dielectric relaxation curves for 5CB and 5CB+MWCNT composite were fitted according to a single exponential decay function $f(t) = \bar{\varepsilon}_1 e^{(-t/\tau)} + \bar{\varepsilon}_0$ with a typical regression coefficient of R = 0.9996. Here, τ is the relaxation decay time, and $\bar{\varepsilon}_1 + \bar{\varepsilon}_0 = \bar{\varepsilon}_{max}$. The inset in Fig. 4.4a shows the linear dependency of $\bar{\varepsilon}$ at small t with logarithmic time scale. The values for the three fitting parameters, τ, $\bar{\varepsilon}_0$ and $\bar{\varepsilon}_1$ as a

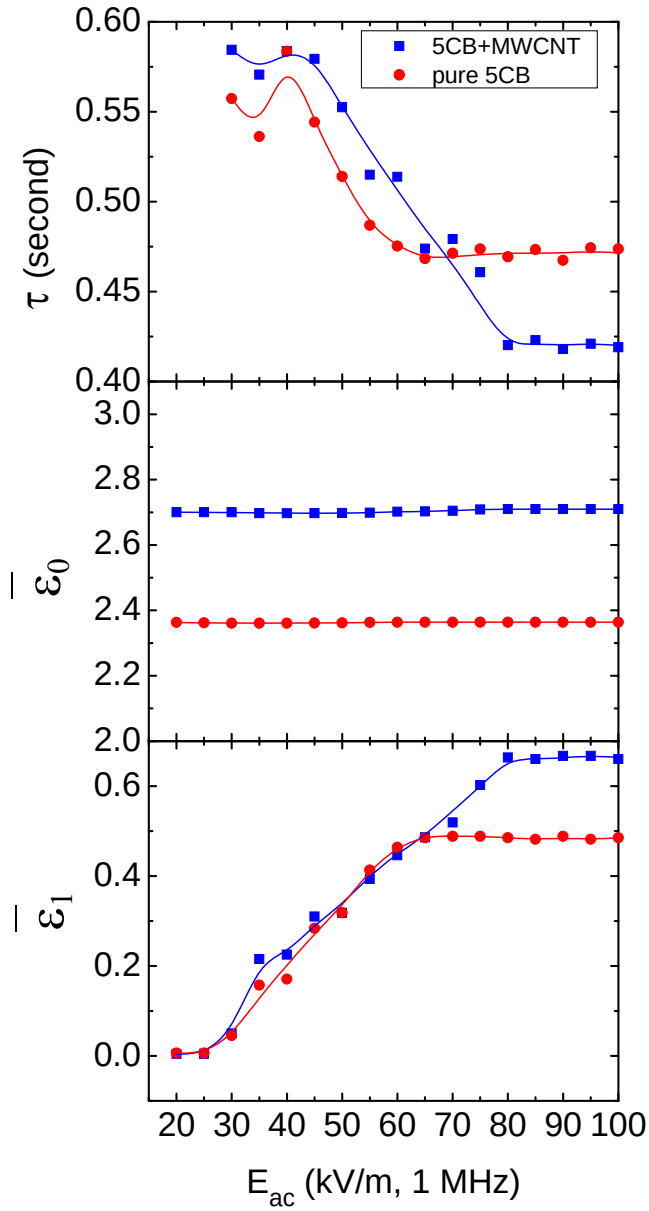

Figure 4.6: *Fitting parameters according to a single-exponential decay* ($f(t) = \bar{\varepsilon}_1 e^{(-t/\tau)} + \bar{\varepsilon}_0$) *function for pure 5CB and 5CB+MWCNT system. Lines represent guide to the eye.*

function of E_{ac} are shown in Fig. 4.6. Generally, the relaxation time decreases as E_{ac} increases and, for the composite, saturates at a higher field than that of pure 5CB, which is consistent with the behaviors of $\bar{\varepsilon}_{max}$ shown in Fig. 4.5a. For E_{ac} larger than the saturation point, the composite system relaxes back faster than pure 5CB as seen in Fig. 4.6. It is possible that the dispersed CNTs attract ions present in the LC media [4], which

may influence this result. The presence of ions would slow down the elastic-force driven mechanical relaxation of the nematic domains. The presence of CNTs would lower the free ion concentration and allow the composite system relax faster. If true, this could be an interesting application for image stabilization in LC displays.

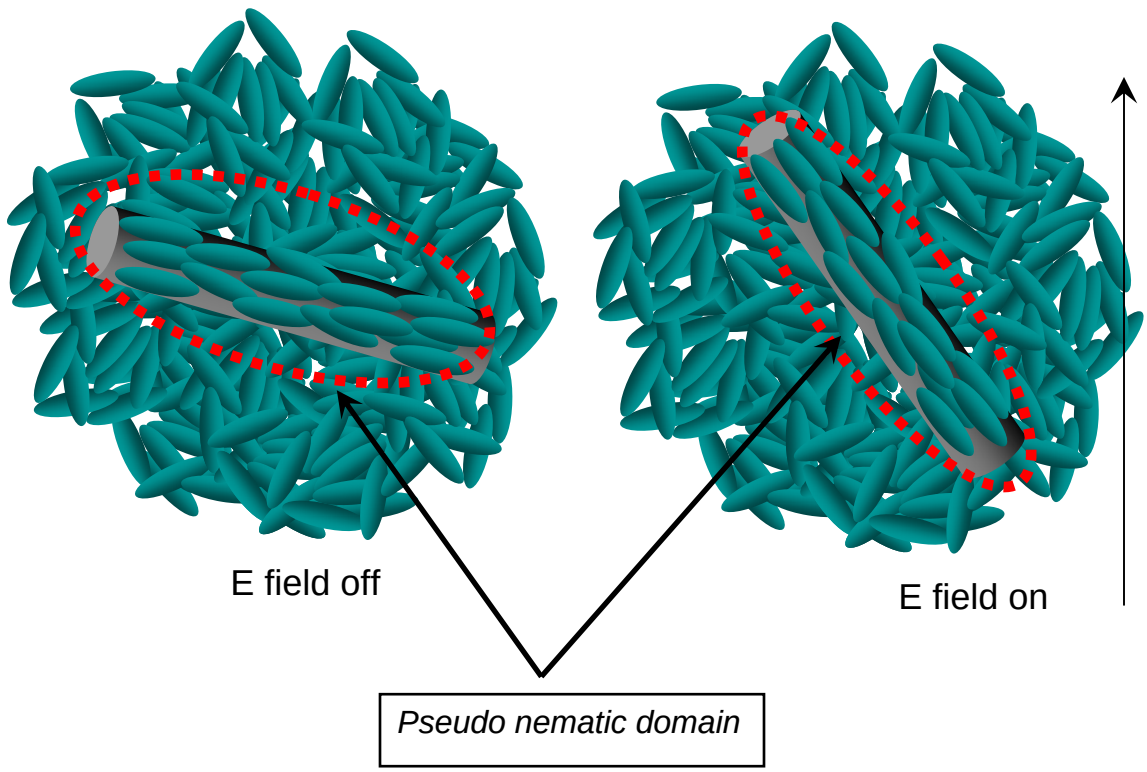

Figure 4.7: *Schematic of permanent orientation of pseudo-nematic domains on application of electric field in isotropic LC+CNT mixture.*

In summary, the nano-dynamics of LC+CNT system has been studied to understand the stability of these systems. In the nematic phase, the composite system results in an improvement in relaxation decay time for larger E_{ac}, which might be an application for LC display technology. The presence of local anisotropic *pseudo-nematic* domains in the isotropic phase in the system demonstrates a promising field induced storage memory device application. This versatile nano-scale electro-mechanical system might reveal interesting individual molecular dynamics of LC and CNTs in high frequency (GHz) dielectric measurements. Future work involves field-induced frequency dependent dielectric studies for different CNT concentrations in LC media for both the nematic and isotropic phases.

Reference:

[1] Michael D. Lynch and David L. Patrick, *Nano Letters* **2** 1197 (2002).

[2] I. Dierking, G. Scalia and P. Morales, *J. Appl. Phys.* **97**, 044309 (2005).

[3] I. Dierking, G. Scalia, P. Morales, and D. LeClere, *Adv. Mater.* **16**, 865 (2004).

[4] In-Su Baik, S. Y. Jeon, S. H. Lee, K. A. Park, S. H. Jeong, K. H. An, and Y. H. Lee, *Appl. Phys. Lett.* **87**, 263110 (2005).

[5] P. V. Kamat, K. G. Thomas, S. Barazzouk, G. Girishkumar, K. Vinodgopal, and D. Meisel, *J. Am. Chem. Soc.* **126**, 10757 (2004).

[6] Joette M. Russell, Soojin Oh, Issac LaRue, Otto Zhou, and Edward T. Samulski, *Thin Solid Films* **509**, 53 (2006).

[7] Kyung Ah Park, Seung Mi Lee, Seung Hee Lee, and Young Hee Lee, *J. Phys. Chem. C* **111**, 1620 (2007).

[8] Empty LC cells (*LC2-20.0, homogeneous anti-parallel rubbed with* 1° *pre-tilt*) are commercially available from *Instec Research Instrumentation Technology.*

[9] S. Pilla, J. A. Hamida, and N. S. Sullivan, *Rev of Sci. Instrum.* **70**, 4055, (1999)

[10] S.C. Bera, S. Chattopadhyay, *Measurement* **33**, 3 (2003).

[11] M. C. Foote and A. C Anderson, *Rev of Sci. Instrum.* **58**, 130 (1987).

[12] F. Kremer and A. Schonhals, *Broadband Dielectric Spectroscopy* (Springer, Berlin, 2003).

[13] R. Basu and G. Iannacchione, *Appl. Phys. Lett.* **92,** 052906 (2008).

CHAPTER 5

DIELECTRIC HYSTERESIS, RELAXATION DYNAMICS, AND NON-VOLATILE MEMORY EFFECTS IN CARBON NANOTUBE DISPERSED LIQUID CRYSTAL

5.1 Introduction

Self-organizing nematic liquid crystals (LC) impart their orientational order onto dispersed carbon nanotubes (CNTs) and obtain CNT-self-assembly on a macroscopic dimension. The nanotubes-long axis, being coupled to the nematic director, enables orientational manipulation via the LC nematic reorientation. Electric field induced director rotation of a nematic LC+CNT system is of potential interest due to its possible application as a nano-electromechanical system. Electric field and temperature dependence of dielectric properties of an LC+CNT composite system have been investigated to understand the principles governing CNT-assembly mediated by the LC. In the LC+CNT nematic phase, the dielectric relaxation on removing the applied field follows a single exponential decay, exhibiting a faster decay response than the pure LC above a threshold field. The observed dielectric behaviors on field-cycling in the nematic phase for the composite indicates an electromechanical hysteresis effect of the director field due to the LC-CNT anchoring mechanism. Observations in the isotropic phase coherently combine to confirm the presence of anisotropic *pseudo-nematic* domains stabilized by the LC-CNT anchoring energy. These polarized domains maintain local directors, and respond to external fields, but, do not relax back to the original state on switching the field off, showing non-volatile memory effect.

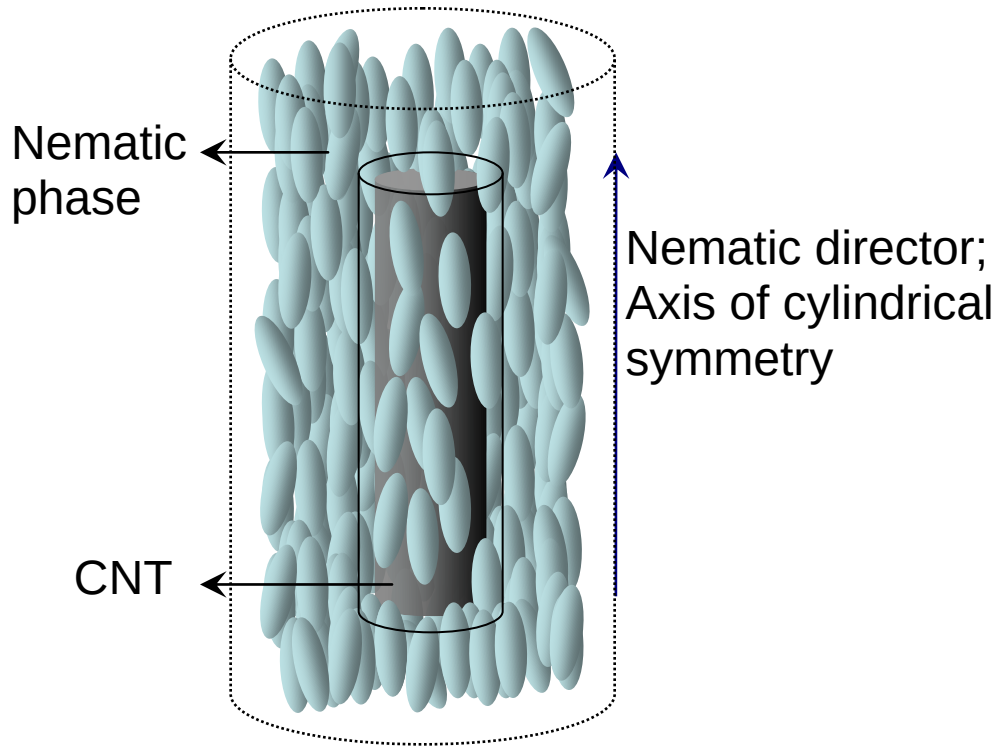

Figure 5.1: *Schematic diagram of symmetry matching; Dotted cylinder shows the cylindrical symmetry of uniaxial nematic phase; the small cylinder shows the cylindrical confinement of a CNT.*

Self-organizing nematic liquid crystal (LC) has gained interest in recent years for transferring orientational order onto suspended nanoparticles [1,2,3,4,5,6,7,8]. It has been demonstrated that inside a nematic liquid crystal matrix, the long axes of carbon nanotubes (CNTs) orient parallel to the *director field* (average direction of LC molecules) with an orientational order parameter S between 0.6 to 0.9 [1,2,7], while bulk nematic liquid crystals themselves have orientational order of $S \approx 0.6$. Recent theoretical work shows that a strong interaction, mainly due to surface anchoring with a binding energy of about –2 eV for π–π stacking between LC-CNT [4,9], is associated with the CNT alignment mechanism in the nematic state. It has also been known theoretically for some time that the distribution of orientations of the nano-size anisotropic guest particles in an anisotropic and ordered solution is along the symmetry axis of the solution [10]. An anisotropic nematic LC shows cylindrical symmetry along the director field [10,11]. Thus, the anchoring energy favors the dispersed CNT long-axis parallel to the director field, minimizing the elastic distortion of the nematic matrix, which is essential a minimization of excluded volume [10]. This is shown schematically in Fig. 5.1.

As the CNTs are much thinner than the elastic penetration length, the alignment is driven by the coupling of the unperturbed director field to the anisotropic interfacial tension of the CNTs in the nematic LC matrix [12]. Thus, the concentration of CNTs in

LC is a very important parameter for this alignment process as mono-dispersion without any agglomerates is need. The dilute suspensions are stable because well dispersed CNTs individually (not in bundles) do not perturb the director field significantly. Consequently, the nanotubes share their intrinsic properties with the LC matrix, such as electrical conductivity [2], due to the alignment with the LC molecules. Thus, comprehensive understanding of the interaction of CNTs with an LC and the principles governing their self-assembly through an LC mediated interactions is an important and active area of research. Exploiting the nematic LC for nanotemplating purposes and controlling the director by applying fields make the LC+CNT mixture an attractive anisotropic physical system to study the Fréedericksz switching through an electromechanical response at the nanoscale level. After a field-induced director rotation of the nematic in an LC+CNT [1,2,3] contained in a planar LC cell [13], the LC molecules as well as the CNTs dynamically reorient back into their original orientation on the immediate removal of the electric field, exhibiting the intrinsic relaxation dynamics. The LC media, such as nematic phase or isotropic phase, strongly influences the reorientation and relaxation mechanisms of CNTs.

In this paper, we report the dynamic response, the hysteresis effect, and the temperature dependence of the dielectric constant ($\bar{\varepsilon}$) for multiwall carbon nanotubes (MWCNTs) dispersed in 4-cyano-4'-pentylbiphenyl (5CB) LC in both the nematic and isotropic phases. The nematic phase shows dielectric anisotropy due to the anisotropic nature of the LC molecules where $\varepsilon_{\parallel}$ and $\varepsilon_{\perp}$ are the components parallel and perpendicular to the molecular long axis, respectively. For a positive dielectric anisotropic LC, $\varepsilon_{\parallel} > \varepsilon_{\perp}$, and so, the director field reorients parallel to an applied electric field. In a uniform homogeneously aligned parallel-plate cell configuration, the nematic director is aligned perpendicular to the applied electric field due to surface anchoring but the director can reorient parallel to the field if the field magnitude is above some critical threshold. This is the essence of a Fréedericksz transition and an ac-capacitive measurement of the $\bar{\varepsilon}$ will reveal $\varepsilon_{\perp}$ below and $\varepsilon_{\parallel}$ above this switching, the exact values depending on frequency. Having very high aspect ratio, CNTs also exhibit dielectric anisotropy.

5.2 Experimental Procedures

A. Materials and sample preparation

The MWCNT sample used for this experiments contains nanotubes < 8 nm in diameter and 0.5 – 2 μm in length with purity 95%, purchased from *Nanostructured & Amorphous Materials, Inc*. The well characterized LC 5CB used for this experiments has nematic to isotropic phase transition at temperature T_{NI} = 35°C. A small amount (0.005 wt %) of MWCNT sample was dispersed in 5CB and the mixture was ultrasonicated for 5

hours to reduce the bundling tendency of CNTs. Soon after ultrasonication, the mixture was degassed under vacuum at 40°C for at least two hours. The mixture then was filled into a homogeneous LC cell (5 × 5 mm^2 indium tin oxide (ITO) coated area and 20 μm spacing) by capillary action, housed in a temperature controlled bath. The typical amount of the LC filled into the cell is around 0.5 mg. The cell spacing filters out any nanotube aggregates larger than the spacing dimension. Surface treatment inside the LC cell induces the planar alignment to the nematic director [13]. Empty LC cells were measured separately first in order to extract the $\bar{\varepsilon}$. The relaxation dynamics also depend on cell configuration; for comparisons, the same type of cells was used for both pure 5CB and 5CB+MWCNT.

B. AC-capacitance bridge technique and dielectric spectrometer

The dielectric measurements were performed by the ac capacitance bridge technique [14,15,16], operating with a probing field E at 100 kHz frequency. Comparison between the empty capacitance (C_o) and sample filled cell capacitance (C_s) allows for a relative measurement of dielectric constant $\bar{\varepsilon}$ (= C_s / C_o) with respect to the empty cell. The probing field, E (100 kHz), in a capacitive measurement, is in phase and at the same frequency as the measurement of the complex dielectric constant, $\bar{\varepsilon}$(100 kHz). Thus, in the complex *rotating-frame* of the measurement, the probing field E (100 kHz) can be considered a 'static' field [17]. After the sample was freshly loaded into the cell, dielectric hysteresis experiments were performed by cycling the E (100 kHz) field magnitude ranging from 25 ↔ 250 kV/m and monitoring $\bar{\varepsilon}(E)$. The field annealing treatment trains the sample to improve the nematic ordering controlling any defects in the nematic matrix. Temperature annealing was also performed by heating the system to isotropic phase and then cooling it down to the nematic phase; but, no thermal hysteresis was observed.

After the completion of field and temperature annealing, an external ac electric field pulse, E_{ac} (1 MHz) of 30 seconds duration was applied across the cell at magnitudes ranging from 0 to 250 kV/m. The field E_{ac} (1 MHz) is independent of the capacitance bridge and measurement technique. The reason for applying the ac field (not dc) is to avoid the affect of ion migration or ionic conduction on the dielectric relaxation measurements. Once E_{ac} was turned off (at t = 0 sec), isothermal average dielectric $\bar{\varepsilon}(t)$ measurements were carried in the nematic (T = 25° C) and isotropic (T = 37° C) phases as a function of time. The magnitude of the probing field E (5 kV/m, 100 kHz) was kept far below the Freedericksz reorientation threshold field during this measurement. The LC 5CB does not exhibit any tumbling relaxation mode [18] and MWCNTs show no space charge or dipole orientation dynamics at this probing frequency, 100 kHz [16,19]. Therefore, the observed dielectric relaxation is caused mainly by a mechanical relaxation mechanism of the director on turning E_{ac} off. Temperature dependence of $\bar{\varepsilon}$ was

studied in order to understand the behavior of nematic and isotropic phase of the LC in presence of CNTs. Temperature dependence of $\bar{\varepsilon}$ provides information about isotropic to nematic phase transition and structural changes due to the anchoring energy arising from the presence of CNTs.

5.3 Results and Discussions

A. Dielectric hysteresis in the nematic phase

Figure 5.2 (a) depicts the dielectric hysteresis effects for 5CB and 5CB+MWCNT in the nematic phase (T = 25°C). The area under the hysteresis loop, which is proportional to the energy lost during the cycle, is shown in Fig. 5.2 (b). The hysteresis area for bulk 5CB decreases by a considerable amount after the first cycle and then remains constant for rest of the number of cycles performed. A vivid change in the dielectric hysteresis has been observed for the composite system. The first cycle shows the highest amount the of hysteresis loss which gradually decreases through the 2nd and 3rd cycle, reaching saturation at the 4th cycle. After the 4th cycle the hysteresis area remains the same throughout the rest of the number of annealing cycles performed. It is important to note that this dramatic change is observed due to the presence of only 0.005 wt% of MWCNTs in the nematic LC media. As an ac field is used for this annealing process, ion migration or ionic conduction has no contribution to the dielectric behavior observed, and so, the hysteresis effects observed is not caused by the residual dc effect.

The structural changes due to the application of an ac field in the LC-CNT nematic matrix result in the observed *electromechanical* hysteresis of the director field. The LC-CNT anchoring energy increases the elastic constant for bent distortion in the nematic phase, increasing the elastic energy in the LC molecules. [[20],[21]]. The increase in the elastic constant for bent distortion leads the director field to follow different paths during field cycling up and down; hence the observed electromechanical hysteresis in the LC-CNT hybrid system. The hysteresis area has been found to be increasing with increasing CNT concentration. Also, the multiple field-annealing controls LC defects [[22]] and perhaps results in a reduction of the defects in the matrix inside the cell - hence, decreasing hysteresis area with increasing cycle number for the first few cycles.

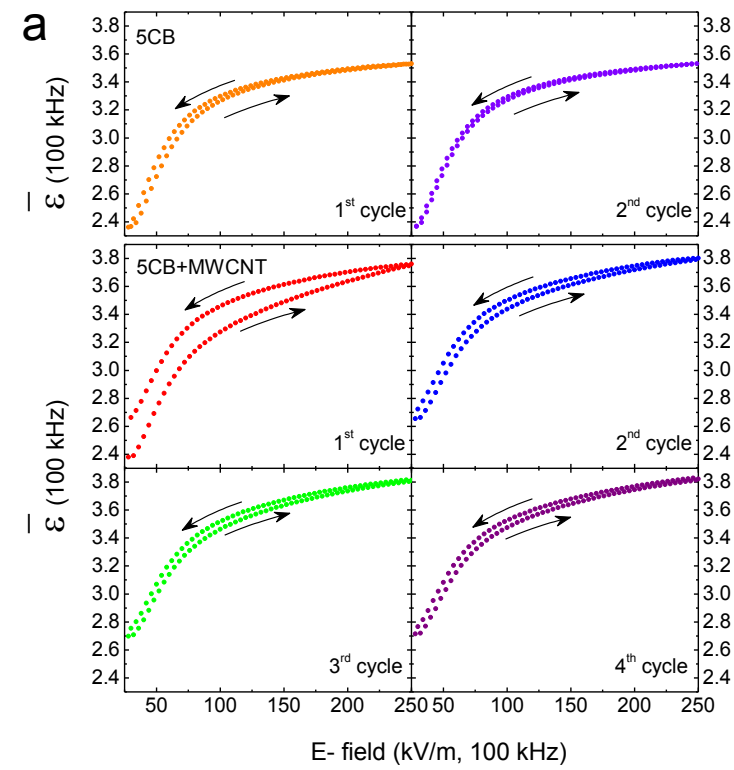

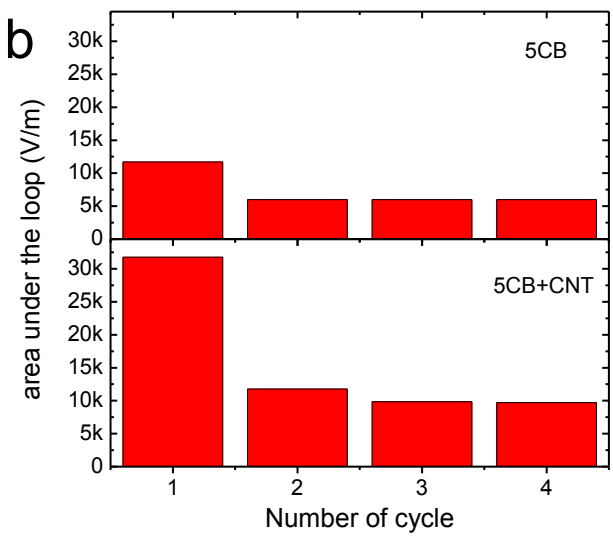

Figure 5.2: **(a)** *Field annealing hysteresis cycles,* $\bar{\varepsilon}$ *vs.* ***E****, for 5CB* (*top 2 panels*) *and 5CB+MWCNT (bottom 4 panels) in the nematic phase* ($T = 25^{o}C$). **(b)** *The area under the hysteresis loop as a function number of cycle for 5CB and 5CB+MWCNT.*

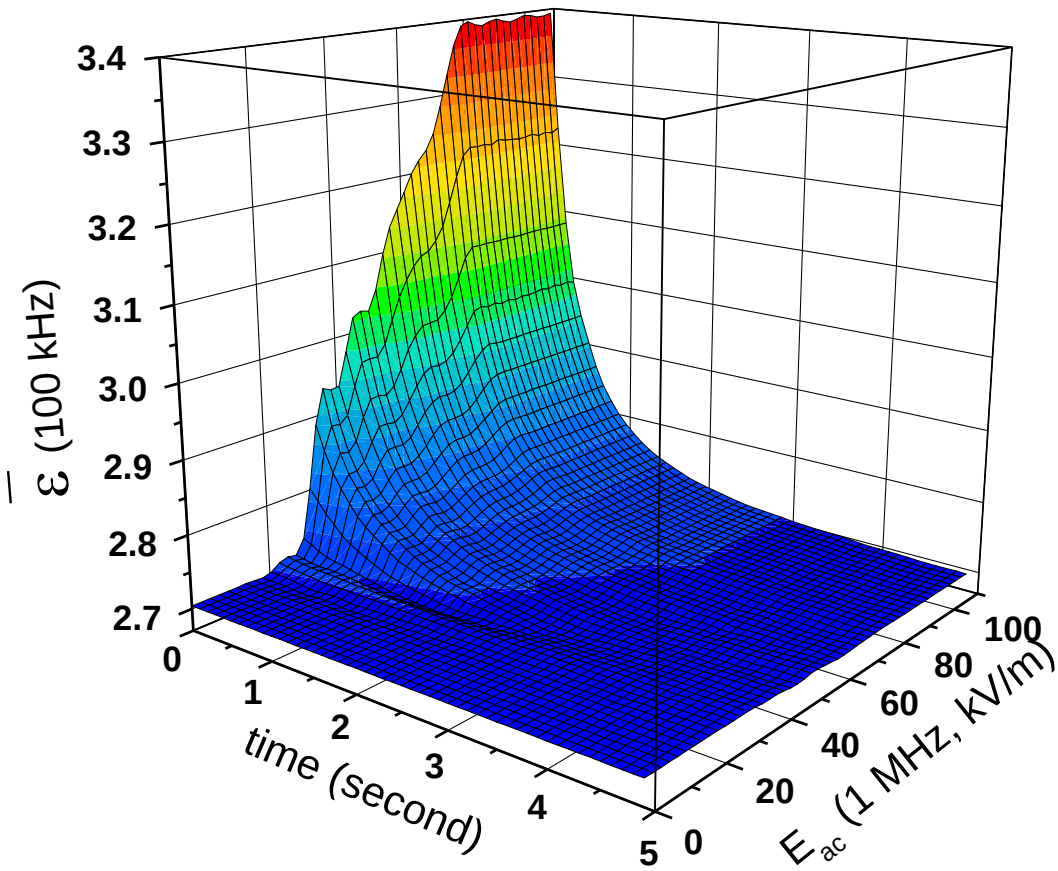

Figure 5.3*: Dynamic response of the average dielectric constant* $\bar{\varepsilon}$ *for 5CB+MWCNT as a function of time and* E_{ac} *(1 MHz) in the nematic phase (*$T = 25^{o}C$*) after* E_{ac} *goes off.*

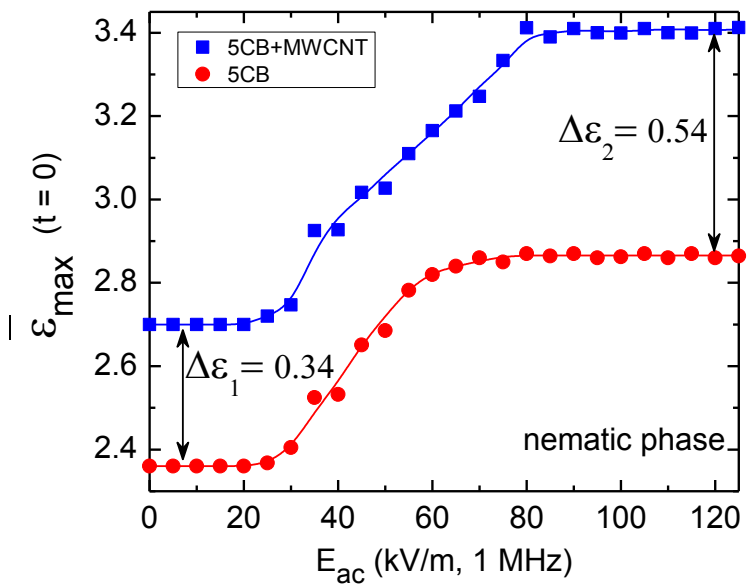

Figure 5.4: *Field-saturated dielectric constant,* $\bar{\varepsilon}_{max}$ ($\bar{\varepsilon}$ *at t = 0) as a function of* E_{ac} *for 5CB and 5CB+MWCNT in the nematic phase* ($T = 25^oC$). *Lines represent guide to the eye.*

B. Relaxation dynamics of $\bar{\varepsilon}$ in the nematic phase

The planar rubbing direction on the surface of the electrodes inside the LC cell acts as an anchoring field that induces homogeneous alignment on the first few LC layers touching the top and bottom electrodes. Then, the elastic interaction between the LC molecules makes the homogeneous alignment propagate through whole media, obtaining a planar director profile inside the cell. Being embedded in the nematic matrix CNT long axis also follows the planar director field. Electric field induced director reorientation occurs when the torques, due to the external electric field, overcome the elastic interactions between LC molecules and, through surface coupling, the CNT long axis follows the director rotation. Soon after the field goes off, these restoring forces, between the planar surface state and LC director, drive the system back to the planar configuration through a mechanical rotation.

The dielectric constant $\bar{\varepsilon}$ as a function of time and E_{ac}, after switching E_{ac} off for the 5CB+MWCNT sample in the nematic phase (T = 25° C), is shown in Fig. 5.3. The relaxation of $\bar{\varepsilon}$ follows a single-exponential decay, reaching to its original value. The field-saturated dielectric constant, $\bar{\varepsilon}_{max}$ ($\bar{\varepsilon}$ at t = 0, from Fig 3) for each relaxation is plotted as a function of E_{ac} in Fig. 4 and is directly associated with the director profile. The value of $\bar{\varepsilon}_{max}$ starts to increase above E_{ac} = 20 kV/m for both pure LC and LC+CNT samples, confirming the director reorientation from planar to homeotropic, but, $\bar{\varepsilon}_{max}$

saturates at a higher field for the composite sample than pure 5CB. See Fig. 5.4. This is probably due to the higher aspect ratio of CNTs that require higher fields to fully reorient. As mentioned earlier, because of having very high aspect ratio, CNTs also exhibit dielectric anisotropy [23] and contribute their $\varepsilon_{\perp}$ or $\varepsilon_{\parallel}$ to the system depending on a particular orientation. For the homogeneous director profile (E_{ac} < 20 kV/m in Fig. 5.4), individual CNTs being perpendicular to the measuring field, contribute their average $\varepsilon_{\perp}$ to the average dielectric constant of the system. Figure 5.4 shows that the average dielectric constant of the composite system increases by an amount $\Delta\varepsilon_1 = 0.34$. After the saturation point, when the system is fully reoriented parallel to the field, dispersed CNTs also show homeotropic alignment, contributing their average $\varepsilon_{\parallel}$ (> $\varepsilon_{\perp}$) to the system. Above the saturation (E_{ac} > 80 kV/m) point, the dielectric increment is given by $\Delta\varepsilon_2 = 0.54$. The significant dielectric difference $\Delta\varepsilon = \Delta\varepsilon_2 - \Delta\varepsilon_1 = 0.2$ due to the presence of only 0.005 wt% CNTs in LC media confirms that the dispersed CNTs follow the field-induced director rotation. If the CNTs were to stay in the LC matrix in random orientation without following the nematic director, one would expect $\Delta\varepsilon_1$ to be equal to $\Delta\varepsilon_2$. Thus, parallelly organized CNTs in the nematic matrix can be rotated (between 0° and 90°) mechanically by switching E_{ac} on and off, obtaining directed self-assembly of suspended CNTs. This directed self-assembled system can be used as a nano-electromechanical system and micro/nano switch exploiting the high electrical conductivity of CNTs along the long axis. It is important to point out that the E_{ac} driven director rotation is a much faster response than the relaxation response (decay) on switching E_{ac} off. On switching E_{ac} on and off this system acts as a *nano-oscillator* governing two different characteristic frequencies.

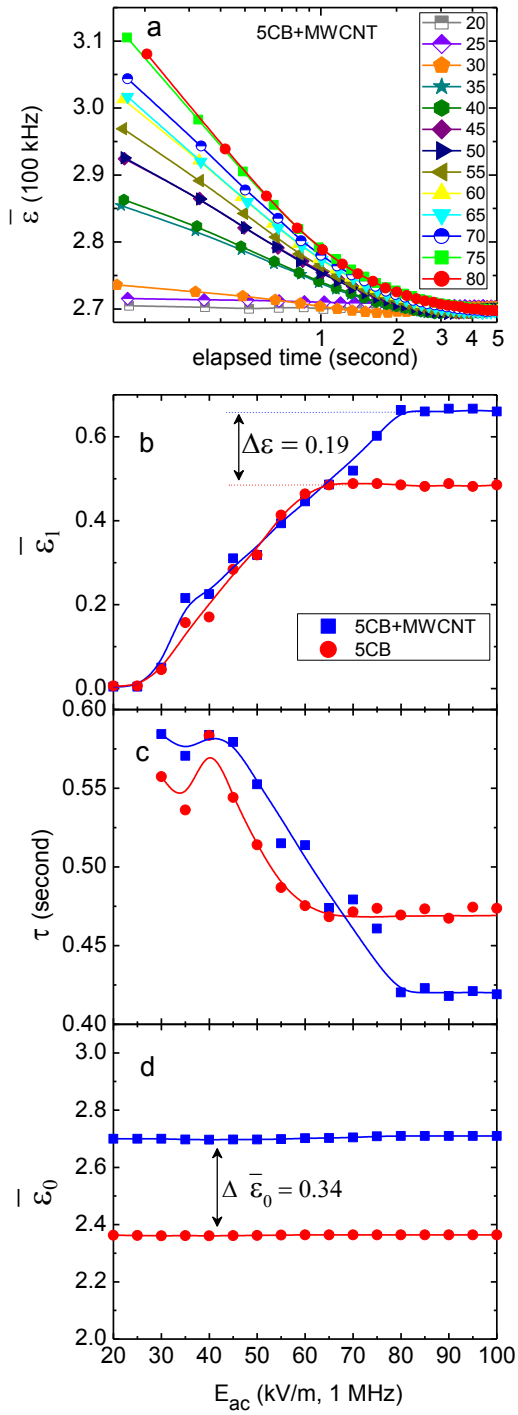

Figure 5.5: (a) *Relaxation dynamic response of* $\bar{\varepsilon}$ *in logarithmic time scale. The legend represents the magnitude of* E_{ac} *(1 MHz) in kV/m;* **(b), (c), (d)** *Fitting parameters according to a single-exponential decay* ($f(t) = \bar{\varepsilon}_1 e^{(-t/\tau)} + \bar{\varepsilon}_0$) *function for 5CB and 5CB+MWCNT system. Lines represent guide to the eye.*

Dielectric relaxation curves for 5CB and 5CB+MWCNT were fitted according to a single-exponential decay function $f(t) = \bar{\varepsilon}_1 e^{(-t/\tau)} + \bar{\varepsilon}_0$ with a typical regression coefficient of R = 0.9996. Here, τ is the relaxation decay time, $\bar{\varepsilon}_0$ is the average base dielectric constant, and $\bar{\varepsilon}_1$ is the field-induced average dielectric constant. Thus, the field-saturated average dielectric constant, $\bar{\varepsilon}_{max} = \bar{\varepsilon}_0 + \bar{\varepsilon}_1$. Figure 5a shows the linear dependency of $\bar{\varepsilon}$ with logarithmic time scale. The values for the three fitting parameters, $\bar{\varepsilon}_1$, τ, and $\bar{\varepsilon}_0$ as a function of E_{ac} are shown in Fig. 5.5 (b), (c), and (d) respectively. It is obtained from the Fig. 5.5 (b) that the difference in field-induced average dielectric constant $\bar{\varepsilon}_1$ between 5CB and 5CB+MWCNT after the saturation point is $\Delta\varepsilon = 0.19$. As expected, this value of $\Delta\varepsilon$ has been found to be very close to the value of $\Delta\varepsilon_2 - \Delta\varepsilon_1$ from Fig. 4. It is observed that the relaxation time decreases as E_{ac} increases and, for the composite, saturates at a higher field than that of pure 5CB. This is consistent with the behaviors of $\bar{\varepsilon}_{max}$ shown in Fig. 5.4. Figure 5.5 (c) depicts that, the composite system, for E_{ac} larger than the saturation point (E_{ac} > 80 kV/m) relaxes back faster than pure 5CB. Possibly, dispersed CNTs attract free ions present in the LC media [4]. The presence of ions would slow down the elastic-force driven mechanical relaxation of the nematic domains. The presence of CNTs would lower the free ion concentration allowing the composite system to relax considerably faster. The reduction of the free ion concentration results in a decrease in the rotational viscosity of the nematic media. Thus the improvement in the relaxation time is attributed to the decrease in rotational viscosity [24]. The average base dielectric constant $\bar{\varepsilon}_0$, shown in Fig. 5.5 (d), does not depend on E_{ac}. Also, as expected, the increment in average base dielectric constant $\Delta\bar{\varepsilon}_0$ is found to be equal to $\Delta\varepsilon_1$ from Fig. 4, indicating self-consistency.

C. Relaxation dynamics of $\bar{\varepsilon}$ in the isotropic phase

The same experiment was repeated in the isotropic phase (T = 37 ^{o} C) to study the relaxation dynamics. A dramatic change in the field induced orientation mechanism has been observed in this phase. See Fig. 6 (a). Due to the absence of elastic interactions in the isotropic phase, the LC molecules no longer maintain long range orientation order and act as an isotropic liquid. The isotropic phase, as expected, does not respond to an external field, as also experimentally confirmed in Fig. 5.6 (b). But, the composite shows an increment in $\bar{\varepsilon}$ on application of electric field. Interestingly, $\bar{\varepsilon}$ does not relax back over time on switching the field off, as observed in Fig. 5.6 (a). The data of $\bar{\varepsilon}$ *vs.* time were recorded for few hours (not shown in Fig. 5.6 a) and no decays in $\bar{\varepsilon}$ were observed during that period. This suggests that the hybrid system goes through some permanent structural changes each time on application of E_{ac}.

Even though there are no long-range nematic interactions in the isotropic phase, the interaction (surface anchoring) between the LC and CNT surfaces [4,7] still exists.

Due to this coupling, the CNT induces local short-range orientation order of LC molecules surrounding the CNT. Presence of few layers of LC molecules on CNT-walls

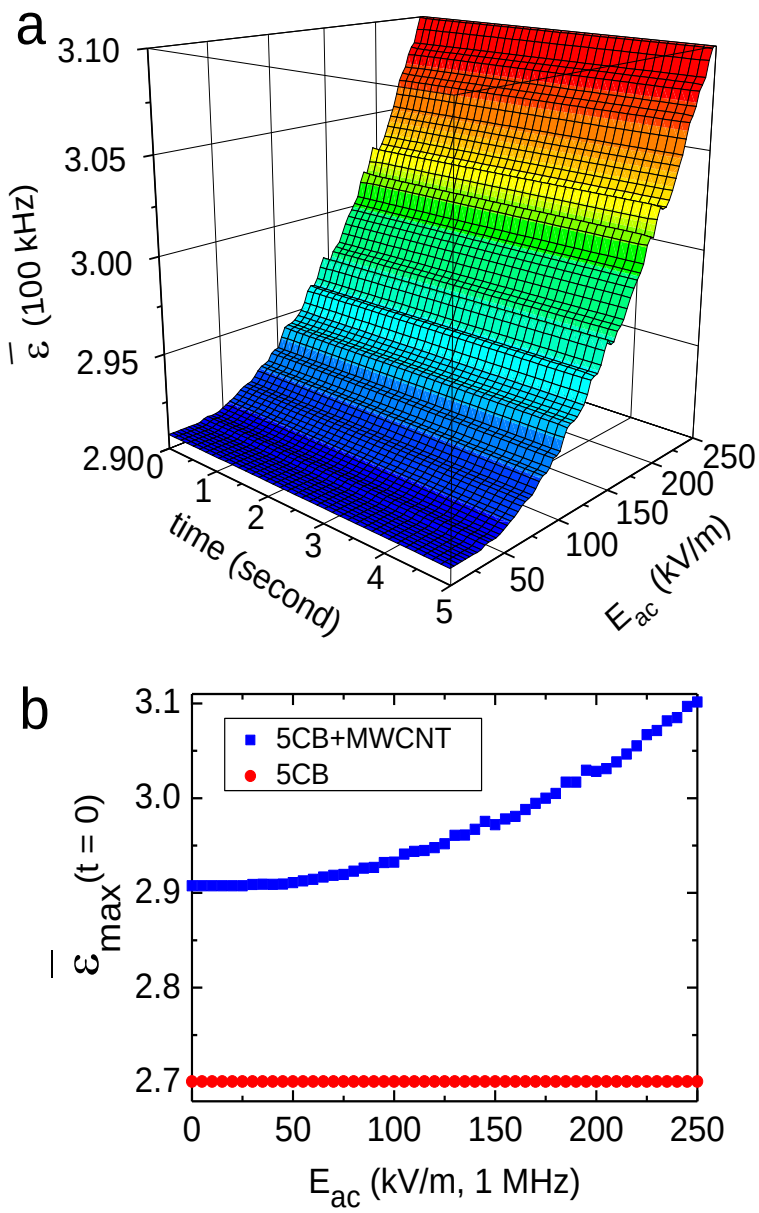

FIGURE 5.6: (a) *Dynamic response of the average dielectric constant* $\bar{\varepsilon}$ *for 5CB+MWCNT as a function of time and* E_{ac} *(1 MHz) in the isotropic phase* ($T = 37^oC$) *after* E_{ac} *goes off;* **(b)** *Field-saturated dielectric constant,* $\bar{\varepsilon}_{max}$ ($\bar{\varepsilon}$ *at* $t = 0$) *as a function of* E_{ac} *for 5CB and 5CB+MWCNT in the isotropic phase* ($T = 37^oC$)*. Lines represent guide to the eye.*

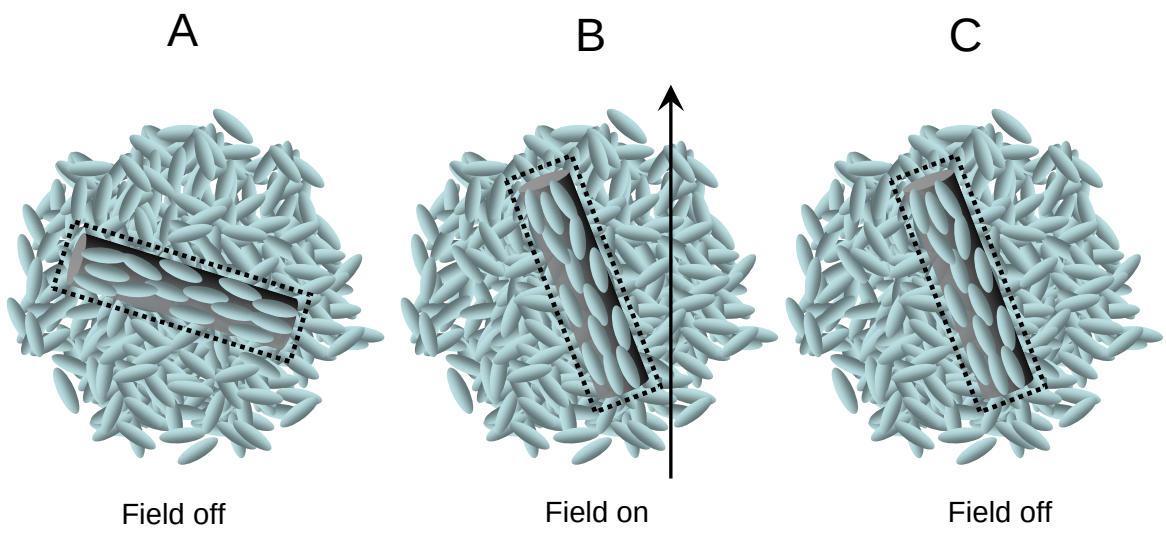

Figure 5.7: *Schematic diagram of presence of field-responsive anisotropic pseudo-nematic domains in the isotropic media. Dashed rectangles represent the LC-CNT pseudo-nematic domains.*

can be visualized as presence of isolated *pseudo-nematic* domains [21] in an isotropic media as described in Fig. 5.7. These local anisotropic *pseudo-nematic* domains have polarization and they interact with external electric fields. Thus, these field responsive domains can be rotated on application of E_{ac} without disturbing the isotropic media. But, after the field goes off, there is no restoring force in the isotropic LC media to mechanically torque these domains back into the original state. Therefore, each time higher E_{ac} is applied the system goes through some permanent local structural changes, exhibiting a non-volatile memory effect, thus, $\bar{\varepsilon}$ shown in Fig. 5.6 (a) does not decay over time. It is important to note that it is a structural memory on application of E_{ac}. Figure 5.6 (b) displays that there is no sharp threshold field to start the reorientation in the isotropic phase and $\bar{\varepsilon}_{max}$ does not seem to saturate in the field range studied. The field induced reorientations of these anisotropic domains can only be erased by slowly cooling the system down to the nematic phase and then heating it up again to the isotropic phase.

D. Temperature dependence of $\bar{\varepsilon}$ in the nematic and isotropic phase

For temperature dependent study a different cell was used in order to maintain temperature stabilization of the sample inside the cell. A droplet of each sample was sandwiched between a parallel-plate capacitor configuration, 1 cm diameter and 100 μm spacing, housed in a temperature controlled bath. Dielectric measurements were

performed at very low probing field (5kV/m) and at 100 kHz frequency. The normalized $\bar{\varepsilon}$ for 5CB and 5CB+MWCNT are shown in Fig. 5.8 as a function of temperature shift ΔT_{NI}. The temperature shift is defined as $\Delta T_{NI} = T - T_{NI}$, where T_{NI} is the nematic (N) to isotropic (I) transition temperature for each sample. The transition temperature is defined as the temperature where $\bar{\varepsilon}$ shows the first discontinuity while entering the $N+I$ phase coexistence region from isotropic phase and was determined from $\bar{\varepsilon}$ *vs.* T graphs. For 5CB T_{NI} = 35.1°C and for 5CB+MWCNT T_{NI} = 34.67°C. To compare the dielectric behaviors properly for 5CB and 5CB+MWCNT, the dielectric constants are normalized to the highest temperature (42°C) point studied. The bulk 5CB exhibits the classic temperature dependence of the dielectric constant. Above the transition temperature ($\Delta T_{NI} > 0$) the dielectric constant $\bar{\varepsilon}$ for 5CB flattens out in the isotropic phase and shows no temperature dependence at all. This indicates that the bulk 5CB, for $\Delta T_{NI} > 0$, reaches complete disorder state having order parameter, $S(T) = 0$. The inset in Fig. 5.8 presents the extracted $d\bar{\varepsilon}/dT$ in the isotropic temperature range. This shows that, $d\bar{\varepsilon}/dT = 0$ for 5CB in the isotropic phase, further indicating the complete isotropic phase of 5CB above the transition temperature.

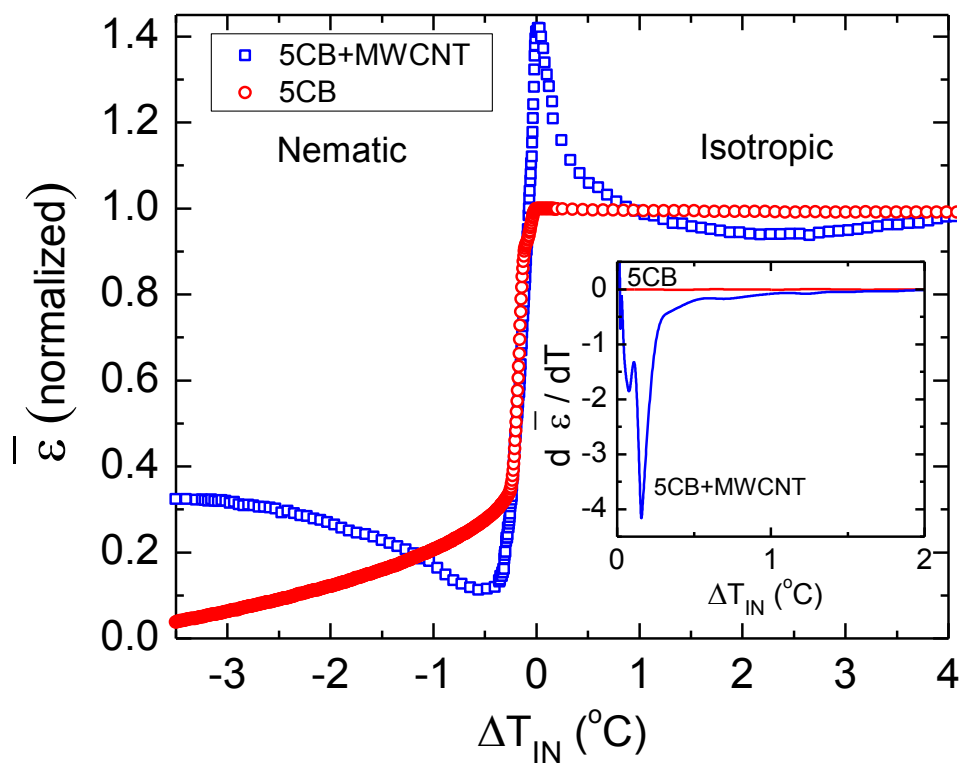

Figure 5.8: *Normalized average dielectric constant* $\bar{\varepsilon}$ *for 5CB and 5CB+MWCNT as a function of temperature shift,* $\Delta T_{IN} = T - T_{IN}$.

The value of $\bar{\varepsilon}$ for the composite mixture shows a dramatic change both in nematic and isotropic phases, shown in Fig. 5.8. The presence of CNTs increases the dielectric anisotropy locally in the system due to the anchoring energy. The larger the dielectric anisotropy the smaller the field is needed to make the system respond to it. The evolved wing of $\bar{\varepsilon}$ in the nematic phase ($\Delta T_{NI} < 0$) indicates that the LC+CNT system is more responsive to the low probing field than bulk 5CB; which is another evidence for ferroelectric-type behavior of 5CB+CNT. For this composite system, the curvature in $\bar{\varepsilon}$ and the nonzero value for $d\bar{\varepsilon}/dT$ in the isotropic phase ($\Delta T_{NI} > 0$) imply that the system does not reach a complete disorder state (order parameter, $S(T) \neq 0$), indicating the presence of *pseudo-nematic* domains discussed earlier.

5.4 Conclusions

We have demonstrated the dielectric hysteresis, relaxation response, and nematic to isotropic phase transition phenomena for a LC-CNT hybrid composite by probing its dielectric properties. The field annealing shows an electromechanical hysteresis of the director field in the composite system, indicating an increase in the elastic interaction in the nematic matrix due to the strong anchoring energy associated with the alignment mechanism. The dielectric relaxation dynamics reveal that incorporating CNTs in a nematic platform results in an improvement in relaxation decay time (for $E_{ac} > 80$ kV/m), decreasing rotational viscosity. The local anisotropic *pseudo-nematic* domains in the isotropic phase demonstrate a field-induced non-volatile memory effect. The dielectric constant as a function temperature represents *N–I* phase transition phenomena for the bulk and the composite. A strong temperature dependent dielectric constant for the LC+CNT system in the isotropic phase confirms the presence of *pseudo-nematic* domains. This versatile nano-scale electro-mechanical system might reveal interesting hysteresis effect in the high frequency regime due to their high frequency switching effect. Future work involves frequency dependent dielectric-hysteresis studies for different CNT concentrations in LC media for both the nematic and isotropic phases.

Reference:

[1] M. D. Lynch and D. L. Patrick, *Nano Letters* **2**, 1197 (2002)
[2] I. Dierking, G. Scalia and P. Morales, *J. Appl. Phys.* **97**, 044309 (2005)
[3] R. Basu and G. S. Iannacchione, *Appl. Phys. Lett.* **93**, 183105 (2008)
[4] In-Su Baik, S. Y. Jeon, S. H. Lee, K. A. Park, S. H. Jeong, K. H. An, and Y. H. Lee, *Appl. Phys. Lett.* **87**, 263110 (2005)

[5] P. V. Kamat, K. G. Thomas, S. Barazzouk, G. Girishkumar, K. Vinodgopal, and D. Meisel, *J. Am. Chem. Soc.* **126**, 10757 (2004)
[6] Joette M. Russell, Soojin Oh, Issac LaRue, Otto Zhou, and Edward T. Samulski, *Thin Solid Films* **509**, 53 (2006)
[7] J. Lagerwall, G. Scalia, M Haluska, U. Dettlaff-Weglikowska, S. Roth, F. Giesselmann, *Adv. Mater.* **19**, 359 (2007).
[8] R. Basu and G. S. Iannacchione, *Phys. Rev. E* **80**, 010701 (2009)
[9] K. A. Park, S. M. Lee, S. H. Lee, and Y. H. Lee, *J. Phys. Chem. C*, **111**, 1620 (2007)
[10] L. Onsager, *Ann. N.Y. Acad. Sci.*, **51**, 627 (1949)
[11] P. G. de Gennes and J. Prost, *The Physics of Liquid Crystals*, (Oxford University Press, 1974)
[12] P.P.A.M. van der Schoot, V. Popa-nita, S. Kralj, *J. Phys. Chem. B* **112**, 4512, (2008)
[13] Empty LC cells (*LC2-20.0, homogeneous anti-parallel rubbed with 1*^{o} pre-tilt) are commercially available from Instec Research Instrumentation Technology.
[14] S. Pilla, J. A. Hamida, and N. S. Sullivan, *Rev of Sci. Instrum.* **70**, 4055, (1999)
[15] S.C. Bera, S. Chattopadhyay, *Measurement* **33**, 3 (2003)
[16] M. C. Foote and A. C Anderson, *Rev of Sci. Instrum.* **58**, 130 (1987)
[17] R. Basu and G. S. Iannacchione, *J. Appl. Phys.* **104**, 114107 (2008)
[18] F. Kremer and A. Schonhals, *Broadband Dielectric Spectroscopy* (Springer, Berlin, 2003)
[19] R. Basu and G. Iannacchione, *Appl. Phys. Lett.* **92**, 052906 (2008)
[20] S. Y. Jeon, S. H. Shin, S. J. Jeong, S. H. Lee, S. H. Jeong, Y. H. Lee, H. C. Choi, and K. J. Kim, *Appl. Phys. Lett*. **90**, 121901 (2007).
[21] R. Basu and G. S. Iannacchione, *Appl. Phys. Lett.* **95**, 173113 (2009)
[22] G. V. Prakash, M. Kaczmarek, A. Dyadyusha, J. J. Baumberg, and G. D'Alessandro, *Opt. Express* **13**, 2201 (2005)
[23] J. A. Fagan, J. R. Simpson, B. J. Landi, L. Richter, I. Mandelbaum, J. Obrzut, V. Bajpai, R. Raffaelle, B. J. Bauer, A. R. Hight Walker, and E. K. Hobbie, *Phys. Rev. Lett.* **98**, 147402 (2007)
[24] J. Prakash, A. Choudhary, D. S. Mehta, and A. M. Biradar, *Phys. Rev. E* **80**, 012701 (2009)

CHAPTER 6

NEMATIC ANCHORING ON CARBON NANOTUBES

6.1 Introduction

A dilute suspension of carbon nanotubes (CNTs) in a nematic liquid crystal (LC) does not disturb the LC director. Due to a strong LC-CNT anchoring energy and structural symmetry matching, CNT long axis follows the director field, possessing enhanced dielectric anisotropy of the LC media. This strong anchoring energy stabilizes local *pseudo-nematic* domains, resulting in nonzero dielectric anisotropy in the isotropic phase. These anisotropic domains respond to external electric fields and show intrinsic frequency response. The presence of these domains makes the isotropic phase electric field-responsive, giving rise to a large dielectric hysteresis effect.

Nematic liquid crystals (LC) have gained great research interest in recent years for nano-templating purposes, imparting their orientational order onto dispersed nanomaterials [1,2,3,4,5,6,7]. Hybrid liquid crystal-carbon nanotube (CNT) systems increasingly rely on improving electro-optic properties of LCs [4], obtaining directed-self assembly of CNTs over macroscopic dimensions [1,2], and developing nano-electromechanical systems [3]. The CNT alignment mechanism is driven by the coupling of the unperturbed *director field* (average direction of LC molecules) to the anisotropic interfacial tension of the CNTs in the nematic LC matrix, as individual CNTs (not in bundle) are much thinner than the elastic penetration length [8]. So, a dilute suspension is stable because dispersed CNTs, without large agglomerates, does not perturb the director field significantly. Consequently, the suspended nanotubes share their intrinsic properties with the LC matrix, such as electrical conductivity [2], due to the alignment with the LC molecules. A dilute suspension of CNTs in an LC matrix is a unique assemblage of an anisotropic dispersion (CNTs) in an anisotropic media (LC), which makes it an important

and active area of research for realizing the LC-CNT interactions and the principles governing CNT-assembly through a nematic mediated platform. We observe that the presence of a small concentration of well-dispersed CNTs in an LC matrix produces enhanced dielectric anisotropy in the nematic phase and nonzero dielectric anisotropy in the isotropic phase. In this letter, we report the ac field-induced dielectric ($\bar{\varepsilon}$) response for multiwall carbon nanotubes (MWCNTs) dispersed in 4-cyano-4′-pentylbiphenyl (5CB) LC in both the nematic and isotropic phases.

The nematic phase shows dielectric anisotropy due to the anisotropic nature of the LC molecules where $\varepsilon_{\parallel}$ and $\varepsilon_{\perp}$ are the components parallel and perpendicular to the molecular long axis, respectively. For a positive dielectric anisotropic LC, $\varepsilon_{\parallel} > \varepsilon_{\perp}$, and so, the director field reorients parallel to an applied electric field. In a uniform homogeneously aligned parallel-plate cell configuration, the nematic director is aligned perpendicular to the applied electric field due to surface anchoring, but the director can reorient parallel to the applied field if the field magnitude is above some critical threshold. This is the essence of a Fréedericksz transition and an ac-capacitive measurement of the $\bar{\varepsilon}$ reveals $\varepsilon_{\perp}$ below and $\varepsilon_{\parallel}$ above this switching, the exact values depending on frequency.

6.2 Experiments

The hybrid LC-CNT mixture was prepared by dispersing 0.005 wt% of MWCNT sample (containing nanotubes < 8 nm in diameter and 0.5-2 μm in length) in 5CB ($T_{nematic\text{-}isotropic}$ = 35 ^{o}C) host via ultrasonication for 5 hours to reach mono-dispersion of CNTs. Soon after ultrasonication, the mixture was degassed under vacuum at 40°C for at least two hours. The mixture then was filled into a homogeneous LC cell (5 × 5 mm^2 indium tin oxide (ITO) coated area and 20 μm spacing [9]) by capillary action. Before performing any dielectric measurements, the CNT doped LC cell was studied under a cross polarized microscope. The micrographs revealed a uniform texture, like a pure LC cell, indicating a uniform nematic director field. There were no indications of phase separation or agglomerates at any temperature. Thus, at least on the length-scales probed by visible light, the structure of CNT-aggregates (if any) must be small enough that they don't perturb the director field due to their low concentration.

The dielectric ($\bar{\varepsilon}$) measurements, as a function of applied ac voltage, frequency, and temperature, were performed by the ac capacitance bridge technique [10,11,12] in the nematic and isotropic phases. The reason for applying the ac voltage (not dc) is to avoid the affect of ion migration on the dielectric measurements. The LC 5CB does not exhibit any tumbling mode [13] and MWCNTs show no space charge or dipole orientation dynamics [14] at the probing frequencies. Thus, the observed increase in $\bar{\varepsilon}$ as a function of applied ac voltage should be driven mainly by a mechanical rotation of the nematic director field.

6.3 Results and Interpretations

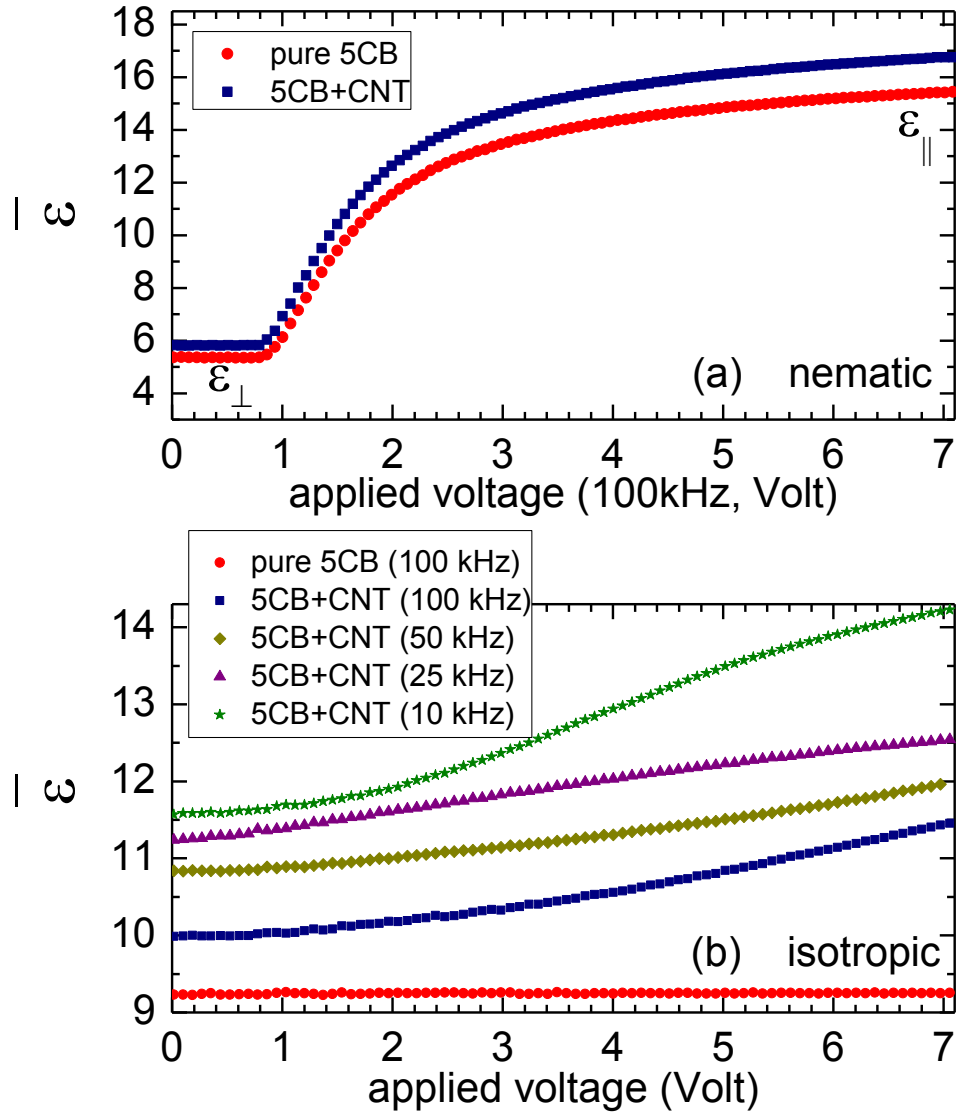

FIGURE 6.1: (a) *The average dielectric constant* $\bar{\varepsilon}$ *as a function of applied ac voltage for 5CB and 5CB+CNT in the nematic phase (T = 23°C);* **(b)** *The average dielectric constant* $\bar{\varepsilon}$ *as a function of applied ac voltage for 5CB and 5CB+CNT in the isotropic phase (T = 45°C).*

Figure 6.1 (a) shows the average dielectric constant ($\bar{\varepsilon}$) as a function of applied ac voltage for 5CB and 5CB+MWCNT sample in the nematic phase (T = 23° C). As seen in the Fig. 1, both the pure LC and the mixture undergo planner ($\varepsilon_{\perp}$) to homeotropic ($\varepsilon_{\parallel}$)

orientational transition, starting at around 0.9 V, saturating at around 7 V. The dielectric anisotropy ($\Delta\varepsilon = \varepsilon_{\parallel} - \varepsilon_{\perp}$) for pure 5CB is around +10 [15], as also observed experimentally ($\Delta\varepsilon_{LC} = +10.1$) in Fig. 6.1(a). The presence of CNTs in LC results in an increase in the dielectric anisotropy ($\Delta\varepsilon_{LC+CNT} = +11.1$), enhancing the order parameter, $S(T)$, in the nematic matrix. It is important to point out that this dramatic increase occurred due to the addition of only 0.005 wt% MWCNT sample. It has been experimentally shown that the isotropic to nematic phase transition temperature of a liquid crystal is enhanced by the incorporation of small amount of MWNT sample [16], indicating an improvement in the nematic order. A recent study shows that CNTs induce alignment on the nematic LC director field along their long axes due to LC-CNT anchoring effect [6]. Theoretical calculations predict that the strong interaction associated with the CNT alignment mechanism is mainly due to surface anchoring with a binding energy $U_{anchor} = -2$ eV for π–π stacking between CNT and LC molecules [4,17]. As the nanotubes used for this work are not ferroelectric in nature, the additional ordering effect must not be due to the electronic coupling of any permanent dipole moments with the LC dielectric anisotropy; which generally occurs in ferroelectric nanoparticle suspensions in the LCs [18]. Thus, the increase in $\Delta\varepsilon$ (hence, improvement in nematic order, as $\Delta\varepsilon \propto S(T)$ [19]) is attributed to the anchoring energy and anisotropic structure of CNTs. The reorientation threshold voltage V_{th} can be estimated by the expression for the Fréedericksz transition [19]: $V_{th} \propto \sqrt{K/\Delta\varepsilon}$; where K is the elastic constant for bent distortion. From Fig 6.1 (a), as $V_{th}^{LC} \simeq V_{th}^{LC+CNT}$, one can write, $\sqrt{K_{LC}/\Delta\varepsilon}_{LC} \simeq \sqrt{K_{LC+CNT}/\Delta\varepsilon}_{LC+CNT}$; which gives $K_{LC+CNT} \simeq 1.21K_{LC}$. The strong elastic interaction between CNTs and LC molecules due to surface anchoring may increase the elastic energy of the hybrid system and therefore can be attributed to the increase in K in the LC+CNT system.

As the dielectric constant of a material is determined by the structural arrangement and molecular polarizability, the dielectric spectra for 5CB and 5CB+CNT have been studied in the range $10^3 - 10^5$ Hz to probe any structural modification in hybrid 5CB+CNT system. The spectra, shown in Fig. 6.2, reveal significant difference in dielectric behavior between 5CB and 5CB+CNT, confirming a structural modification in the nematic phase due to the addition of a small amount of CNT sample.

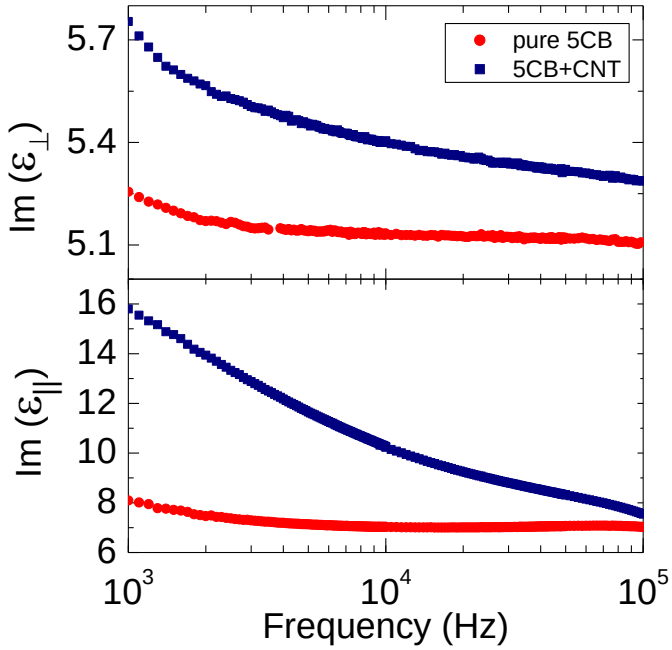

FIGURE 6.2: *Imaginary part of* $\varepsilon_{\perp}$ *(top panel) and* $\varepsilon_{//}$ *(bottom panel) for 5CB and 5CB+MWCNT in the nematic phase* ($T = 23^{o}C$).

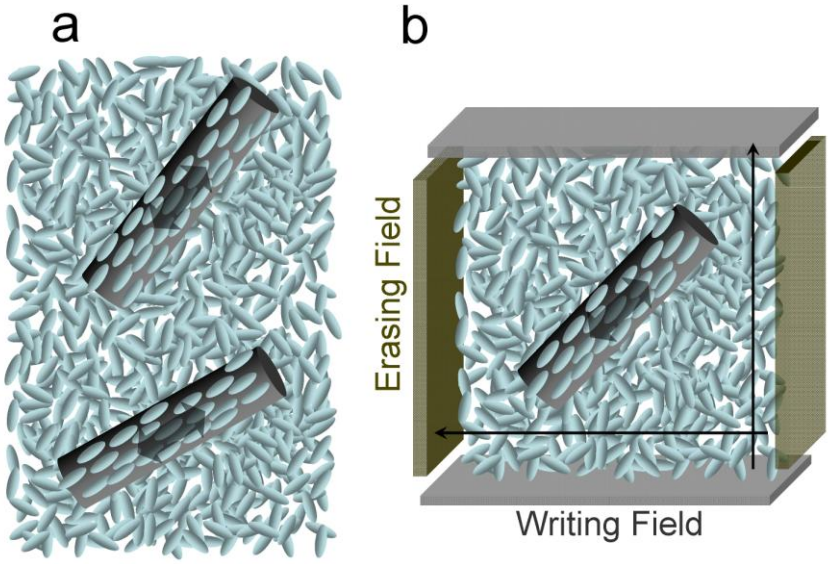

FIGURE 6.3: *Schematic diagrams;* **(a)** *presence of field-responsive anisotropic pseudo-nematic domains due to LC (ellipsoidal) –CNT (cylindrical) interaction in the isotropic media;* **(b)** *a model for a four-electrode LC cell for writing and erasing memory.*

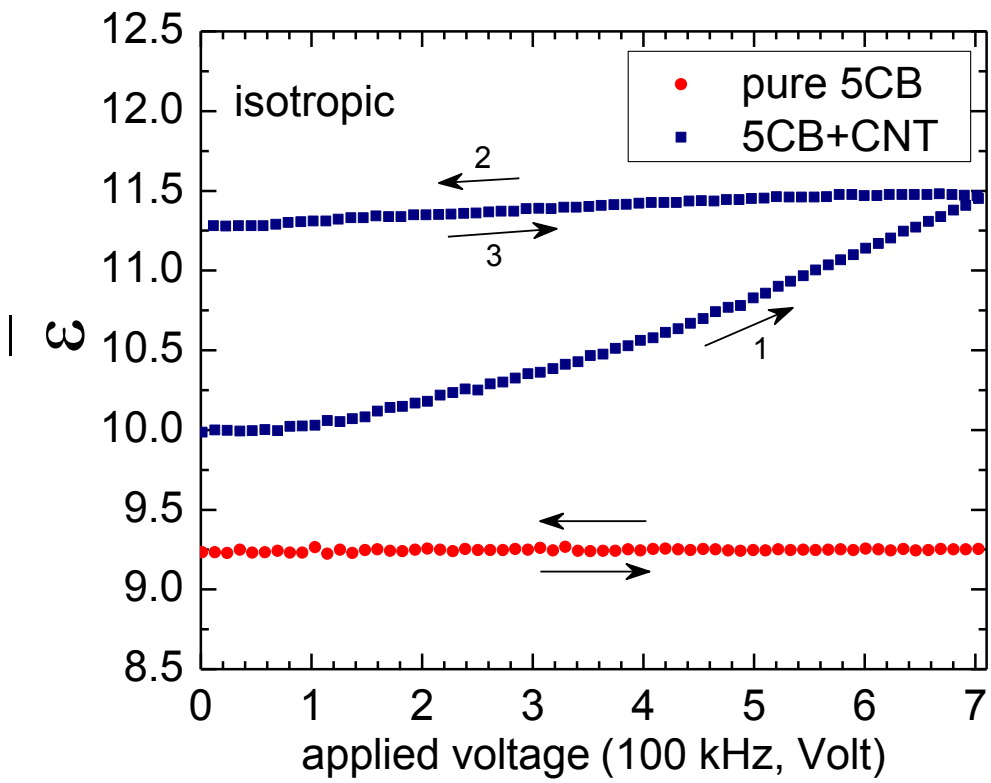

FIGURE 6.4: *Dielectric hysteresis for 5CB and 5CB+CNT in the isotropic phase. The arrows show the cycling direction of the applied ac voltage. The numbers with the arrows for the 5CB+CNT represent the step with the cycling direction.*

Due to the absence of elastic interactions in the isotropic phase, the LC molecules no longer maintain long range orientation order and act as an isotropic liquid. Isotropic phase of 5CB, as expected, does not respond to an external field, as also experimentally confirmed in Fig. 6.1(b). But, a dramatic change in the field-induced dielectric constant has been observed in the isotropic phase for the LC+CNT system. The composite system shows an increment in $\bar{\varepsilon}$ with increasing applied voltage, as shown in Fig 6.1(b). As stated earlier, the energy associated with LC-CNT anchoring mechanisms is $|U_{\text{anchor}}| = 2$ eV, which is much more than the thermal energy, $U_{\text{thermal}} \sim k_B T = 2.74 \times 10^{-2}$ eV, for the deep isotropic phase at $T = 45^{o}$C = 318 K. So, the thermal energy is not even close enough to eliminate the anchoring mechanisms in the deep isotropic phase. Due to this surface anchoring, the CNT induces local short-range orientation order of LC molecules surrounding the CNT having local director along the tube axis, which can be visualized as presence of isolated *pseudo-nematic* domains in an isotropic media, as schematically

shown in Fig. 6.3(a). As these local anisotropic *pseudo-nematic* domains have polarization, their *short-range director field* interact with external electric fields – hence, observed increase in $\bar{\varepsilon}$ with increasing applied voltage in the isotropic phase. These nanoscale anisotropic domains seem to have strong frequency response as the change in $\bar{\varepsilon}$ is different for different frequencies from 10 to 100 kHz in the same applied voltage range, observed in Fig. 6.1(b).

Dielectric hysteresis has been studied in the isotropic phase (T = 45°C) to understand the stability of these *pseudo-nematic* domains. See Fig. 6.4. The isotropic phase for pure 5CB does not show any hysteresis effect, as expected, as it does not respond to an external electric field. After reaching the maximum dielectric value at the highest applied field, $\bar{\varepsilon}$ for the composite system does not relax back to its original value cycling the field down to zero, showing a large dielectric hysteresis unlike the nematic phase. As there is no long range orientational order, there is no elastic interaction present in the isotropic LC media. As a result, when the field goes off, there is no restoring force to mechanically torque these domains back into the original orientation in the isotropic phase and the domains stay oriented. This indicates that CNTs, surrounded by few layers of LCs, stabilize nematic-like short-range order in the isotropic phase, giving rise to a ferroelectric type hysteresis. This is the essence of a non-volatile electro-mechanical memory effect. This memory may be erased by applying another field in the opposite direction of the first one in a four-electrode cell configuration as shown in Fig. 6.3(b). In that case the writing and erasing time can be in the order of the tumbling relaxation mode of the LC, which is 0.1 GHz [13] for 5CB. However, the time response would also depend on the distribution symmetry of the CNTs in the LC media.

The extracted dielectric anisotropy $\Delta\varepsilon$ for 5CB and 5CB+CNT is plotted as a function of temperature in Fig. 6.5. The composite system shows enhanced $\Delta\varepsilon$ in the nematic phase. As the order parameter [19] for the pure isotropic phase is zero, $\Delta\varepsilon$ for pure 5CB drops down to zero in the isotropic phase. The composite system shows a nonzero value of $\Delta\varepsilon$ [20], indicating the presence a net residual order in the isotropic phase. The value of $\Delta\varepsilon$ in the isotropic phase changes with increasing frequency in the frequency-range (10 – 100 kHz) studied.

In conclusion, we have observed that dispersing a low concentration of CNTs in a nematic LC, results in an improvement in the nematic ordering, showing enhanced $\Delta\varepsilon$. The presence of local anisotropic *pseudo-nematic* domains in the isotropic phase in the system causes an electro-mechanical hysteresis effects which could find potential applications in memory functions. Future work involves simultaneous dielectric and optical studies on size dependent CNT suspensions in LC media to investigate more on the anchoring effect in both the nematic and isotropic phases.

Reference

[1] M. D. Lynch and D. L. Patrick, *Nano Letters* **2**, 1197 (2002)

[2] I. Dierking, G. Scalia and P. Morales, *J. Appl. Phys.* **97**, 044309 (2005)

[3] R. Basu and G. S. Iannacchione, *Appl. Phys. Lett.* **93,** 183105 (2008)

[4] In-Su Baik, S. Y. Jeon, S. H. Lee, K. A. Park, S. H. Jeong, K. H. An, and Y. H. Lee, *Appl. Phys. Lett.* **87**, 263110 (2005)

[5] P. V. Kamat, K. G. Thomas, S. Barazzouk, G. Girishkumar, K. Vinodgopal, and D. Meisel, *J. Am. Chem. Soc.* **126**, 10757 (2004)

[6] J. M. Russell, S. Oh, I. LaRue, O. Zhou, and E. T. Samulski, *Thin Solid Films* **509**, 53 (2006)

[7] R. Basu and G. S. Iannacchione, *Phys. Rev. E* **80**, 010701 (2009).

[8] P. P. A. M. van der Schoot, V. Popa-nita, S. Kralj, *J. Phys. Chem. B* **112**, 4512, (2008)

[9] Empty LC cells (*LC2-20.0, homogeneous anti-parallel rubbed with 1° pre-tilt*) are commercially available from *Instec Research Instrumentation Technology.*

[10] S. Pilla, J. A. Hamida, and N. S. Sullivan, *Rev of Sci. Instrum.* **70**, 4055, (1999)

[11] M. C. Foote and A. C Anderson, *Rev of Sci. Instrum.* **58,** 130 (1987)

[12] R. Basu and G. S. Iannacchione, *J. Appl. Phys.* **104**, 114107 (2008).

[13] F. Kremer and A. Schonhals, *Broadband Dielectric Spectroscopy* (Springer, Berlin, 2003)

[14] R. Basu and G. Iannacchione, *Appl. Phys. Lett.* **92,** 052906 (2008)

[15] D. A. Dunmur, M.R. Manterfield, W.H. Miller and J.K. Dunleavy. *Mol. Cryst. Liq. Cryst.* **45**, 127 (1978)

[16] H. Duran, B. Gazdecki, A Yamashita, and T. Kyu, *Liquid Crystals* **32**, 815 (2005)

[17] K. A. Park, S. Mi Lee, S. Hee Lee, and Y. Hee Lee, *J. Phys. Chem. C* **111**, 1620 (2007)

[18] Y. Reznikov, O. Buchnev, O. Tereshchenko, V. Reshetnyak, A. Glushchenko, and John West, *Appl. Phys. Lett.* **82**, 1917 (2003)

[19] P. G. de Gennes and J. Prost, *The Physics of Liquid Crystals*, (Oxford University Press, 1974)

[20] $\Delta\varepsilon$ for the composite system in the isotropic phase is defined as ($\bar{\varepsilon}_{max} - \bar{\varepsilon}_{min}$), where $\bar{\varepsilon}_{max}$ and $\bar{\varepsilon}_{min}$ are determined from the ‘ $\bar{\varepsilon}$ *vs*. applied voltage’ graph [Fig. 6.1 (b)] at different temperatures above the nematic-isotropic transition temperature.

CHAPTER 7

ORIENTATIONAL COUPLING ENHANCEMENT IN CARBON NANOTUBE DISPERSED LIQUID CRYSTAL

7.1 Introduction

We present a detailed study of a dilute suspension of carbon nanotubes (CNTs) in a pentylcyanobiphenyl (5CB) liquid crystal (LC) by probing the dielectric properties as a function of applied ac voltage and frequency. In principle, to minimize the elastic distortion in the nematic matrix, the monodispersed CNTs follow the nematic director without disturbing the director field significantly. A strong anchoring energy due to π–π electron stacking between LC-CNT molecules results in an increase in the dielectric anisotropy for the hybrid system, indicating a significant enhancement in the orientational order parameter. The frequency dependent dielectric anisotropy for the composite system reveals the intrinsic frequency response of the LC-CNT anchoring mechanism. As a matter of consequence, the extracted value of splay elastic constant suggests that LC-CNT anchoring has an impact on the structural modification of the hybrid LC+CNT system. This strong anchoring energy stabilizes local *pseudo-nematic* domains, giving rise to a non-zero dielectric anisotropy in the isotropic phase that also shows an intrinsic frequency response.

Nematic liquid crystals (LC) have gained great research interest in recent years for transferring their orientational order onto dispersed nanomaterials [1,2,3,4,5,6,7]. Experiments have shown that a low concentration of carbon nanotubes (CNT) sample can be organized in a nematic matrix over macroscopic dimensions by dispersing them in LCs [1,2]. This hybrid LC-CNT represents a versatile composite system that has drawn a great deal of interest in fundamental and applied physics by exhibiting remarkable

physical phenomena, such as, improvement in electro-optic response of LCs [4], electromechanical memory effect [8,9], and superelongation of CNT-clusters in the nematic matrix [10]. A dilute suspension of CNTs in an LC platform is a unique assemblage of an anisotropic dispersion in an anisotropic media, which makes it an important and active area of research for realizing the LC-CNT interactions and the principles governing CNT-assembly through a nematic mediated platform. In general, the host particles introduce disorder in a nematic matrix, decreasing the nematic order parameter [11]. Here, we show that a dilute suspension of CNTs in a nematic LC results in a significant enhancement in the dielectric anisotropy of the system. Furthermore, the increment in the dielectric anisotropy strongly depends on the probing frequency of an applied ac field. As the dielectric anisotropy, $\Delta\varepsilon$ is proportional to the scalar order parameter S; an enhancement in the dielectric anisotropy indicates an improvement in the net orientational order of the LC. In this letter, we report the field-induced dielectric ($\bar{\varepsilon}$) response as a function of probing frequency (1 – 100 kHz) for multiwall carbon nanotubes (MWCNTs) dispersed in 4-cyano-4′-pentylbiphenyl (5CB) LC.

The nematic phase of 5CB LC shows dielectric anisotropy due to the anisotropic nature of the molecules where $\varepsilon_{\parallel}$ and $\varepsilon_{\perp}$ are the components parallel and perpendicular to the molecular long axis, respectively. 5CB being a positive dielectric anisotropic LC, $\varepsilon_{\parallel} > \varepsilon_{\perp}$, and so, the *director field* (average direction of LC molecules) reorients parallel to an applied electric field. In a uniform homogeneously aligned parallel-plate cell configuration, the nematic director is aligned perpendicular to the applied electric field due to surface anchoring, but the director can reorient parallel to the applied field if the field magnitude is above some critical threshold. This is the essence of a Fréedericksz transition and an ac-capacitive measurement of the $\bar{\varepsilon}$ reveals $\varepsilon_{\perp}$ below and $\varepsilon_{\parallel}$ above this switching, the exact values depending on frequency. Having very high aspect ratio, CNTs also exhibit dielectric anisotropy [12].

7.2 Experiments

The CNT alignment mechanism in an nematic matrix is driven by the coupling of the unperturbed director field to the anisotropic interfacial tension of the CNTs in the nematic LC matrix, as individual CNTs (not in bundle) are much thinner than the elastic penetration length [13]. Thus, a dilute concentration of CNTs in an LC is very important for this alignment process as monodispersion without any agglomerates is needed. The LC-CNT composite was prepared by dispersing 0.007 wt% of MWCNT sample in 5CB (nematic to isotropic transition at T_{NI} = 35°C) host. The MWCNT sample used for these experiments contains nanotubes < 8 nm in diameter and 0.5-2 μm in length. The mixture then was ultrasonicated for 6 - 8 hours to reach monodispersion of CNTs. Soon after ultrasonication, the mixture was degassed under a vacuum at 40°C for two hours. Homogeneous LC cells with 5 × 5 mm^2 indium tin oxide (ITO) coated area and 20 μm

spacing [14] were used for our dielectric studies. These cells were filled by capillary action with LC and CNT doped LC separately at an elevated temperature $T > 35^{o}$C. The typical amount of the LC or LC+CNT sample filled into the cell is around 0.5 mg. The cell spacing filters out any nanotube aggregates larger than the spacing dimension. Before performing any dielectric measurements, the CNT doped LC cell was studied under a cross polarized microscope. The optical micrographs revealed a uniform nematic texture, like a pure LC cell, indicating a uniform nematic director field. There were no indications of phase separation or agglomerates at any temperature. Thus, at least on the length-scales probed by visible light, the structure of CNT-aggregates (if any) must be small enough that they do not perturb the director field due to their low concentration and mono-dispersion.

The dielectric ($\bar{\varepsilon}$) measurements, as a function of applied ac voltage and frequency (1 – 100 kHz) were performed by the ac capacitance bridge technique [15,16,17]. The reason for applying the ac voltage (not dc) is to avoid the affect of ion migration on the dielectric measurements. The LC 5CB does not exhibit any tumbling mode [18] and MWCNTs show no space charge or dipole orientation dynamics [17,19] at the probing frequencies. Thus, the observed increase in $\bar{\varepsilon}$ as a function of applied ac voltage should be driven mainly by a mechanical rotation of the nematic director field.

7.3 Results, analysis, and conclusions

Figure 7.1(a) and (b) show the dielectric constant ($\bar{\varepsilon}$) as a function of applied ac voltage for 5CB and 5CB+MWCNT sample in the nematic phase ($T = 25^{o}$ C) at the two extreme probing frequencies 1 kHz and 100 kHz, respectively, in the frequency range studied. As seen in the Fig. 1, both the LC and the mixture undergo planner ($\varepsilon_{\perp}$) to homeotropic ($\varepsilon_{\parallel}$) orientational transition, as the applied voltage increases. The dielectric anisotropy ($\Delta\varepsilon = \varepsilon_{\parallel} - \varepsilon_{\perp}$) for pure 5CB is around +10 [20], as also experimentally observed $10.5 \geq \Delta\varepsilon_{LC} \geq 10.1$ in the probing frequency range 1 – 100 kHz, shown in Fig. 2(a). Figure 7.1 and 7.2(a) depict that the dilute concentration of CNTs in the LC results in a dramatic increase in the dielectric anisotropy of the system. At 1 kHz, $\Delta\varepsilon_{LC+CNT} = +13.8$, that gradually decreases to, $\Delta\varepsilon_{LC+CNT} = +11.2$ at 100 kHz. Everywhere in the frequency range studied, $\Delta\varepsilon_{LC+CNT} > \Delta\varepsilon_{LC}$. This indicates an improvement in the orientational order in the nematic matrix as $\Delta\varepsilon \propto S$ [21]. It is important to point out that this dramatic increase occurred due to the addition of only 0.007 wt% MWCNT sample to the LC.

The nanotubes used for this work are not ferroelectric in nature. Thus, an additional ordering effect observed must not be due to the electronic coupling of any permanent dipole moments with the LC dielectric anisotropy, that generally occurs in ferroelectric nanoparticle suspensions in the LCs [22]. A low concentration CNT-

suspension in an LC is stable because dispersed CNTs, without large agglomerates, does not disturb the director field significantly. Importantly, the suspended CNTs share their

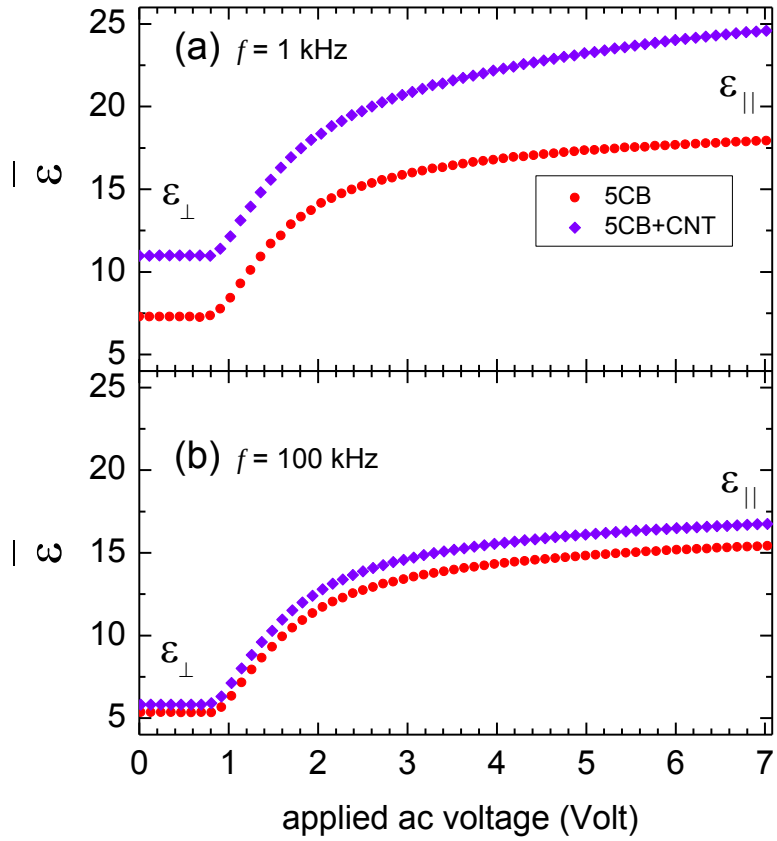

Figure 7.1: (a) *The dielectric constant* $\bar{\varepsilon}$ *as a function of applied ac voltage for 5CB and 5CB+CNT in the nematic phase (T = 25°C) at frequency 1 kHz;* $\Delta\varepsilon_{LC} = +10.5$ *and* $\Delta\varepsilon_{LC+CNT} = +13.8$*;* **(b)** *The dielectric constant* $\bar{\varepsilon}$ *as a function of applied ac voltage for 5CB and 5CB+CNT in the nematic phase (T = 25°C) at frequency 100 kHz;* $\Delta\varepsilon_{LC} = +10.1$ *and* $\Delta\varepsilon_{LC+CNT} = +11.2$*.*

intrinsic properties with the LC matrix, such as conductivity [2] or dielectric anisotropy in this case, due to the alignment with the LC molecules. The suspension, therefore, has been characterized by an effective dielectric anisotropy $\Delta\varepsilon_{LC+CNT}$, as if the CNTs acted as a molecular additive. As CNT concentration is very low (0.007 wt %), the CNT-CNT interaction is insignificant and, therefore, in the zero-order approximation,

$$\Delta\varepsilon_{LC+CNT} = \rho_{LC}\,\Delta\varepsilon_{LC} + \rho_{CNT}\,\Delta\varepsilon_{CNT}, \qquad (1)$$

where ρ_{LC} and ρ_{CNT} are volume fractions of LC and CNTs respectively in the mixture.

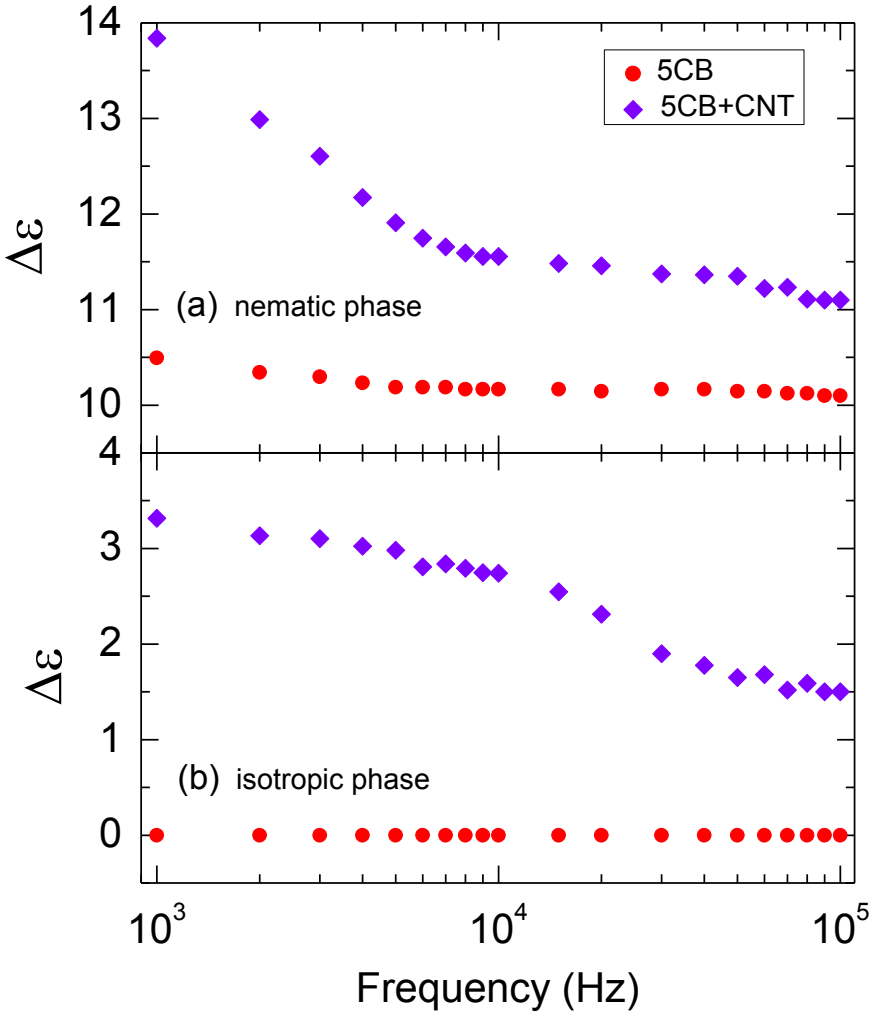

Figure 7.2: (a) *The dielectric anisotropy $\Delta\varepsilon$ as a function of frequency for 5CB and 5CB+CNT in the nematic phase* (T = 25°C); **(b)** *The dielectric anisotropy $\Delta\varepsilon$ as a function of frequency for 5CB and 5CB+CNT in isotropic phase* (T = 42°C).

Using ρ_{LC} = 0.99995, ρ_{CNT} = 5×10^{-5}, $\Delta\varepsilon_{LC}$(1 kHz) = 10.5, and $\Delta\varepsilon_{CNT} \approx 10^4$ [23], this formula gives $\Delta\varepsilon_{LC+CNT}$(1 kHz) = 10.999, that does not agree with the experimental value, $\Delta\varepsilon_{LC+CNT}$(1 kHz) = 13.8, indicating that only ρ_{CNT} and $\Delta\varepsilon_{CNT}$ are not responsible for the dramatic increase in $\Delta\varepsilon_{LC+CNT}$. Recent theoretical calculations predict that a strong interaction, mainly due to surface anchoring with a binding energy of about $U_{anchoring}$ = –2 eV for π–π electron stacking between LC-CNT molecules [4,24], is associated with the CNT alignment mechanism in the nematic state. In our model, this anchoring energy

induces local short-range orientation order of LC molecules surrounding the CNT-wall having *local director* along the tube axis, shown schematically in Fig 3. The mean

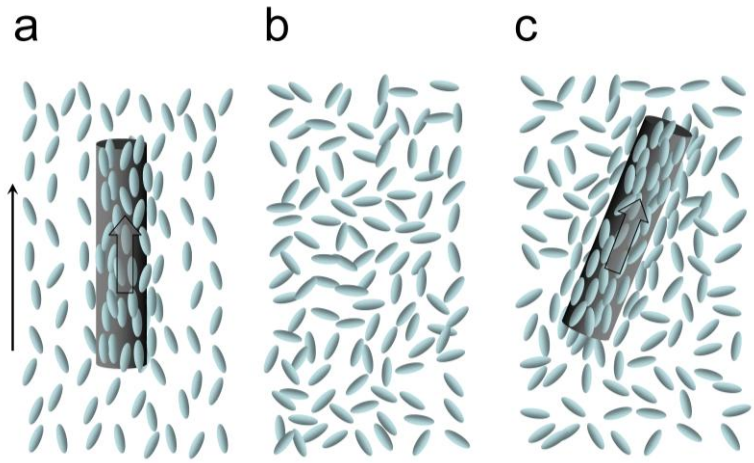

Figure 7.3: *Schematic diagrams;* **(a)** *the presence of a CNT (cylindrical) in an nematic LC media and formation of the local short range orientational order by LC molecules on the surface of the CNT due to the LC-CNT anchoring energy (π–π stacking). The thin arrow represents the long-range nematic director and the thick arrow on the CNT represents the short range local director;* **(b)** *the isotropic phase of LC;* ***(c)*** *the presence of a CNT (cylindrical) in an isotropic LC media and formation of the local short range orientational order by LC molecules.*

induced short-range orientation order increases the net polarizability of the system. In the nematic matrix a CNT long axis is coupled to the nematic director [1,2] and, so, the nematic state gains an additional orientational order for this anchoring energy due to the presence of CNTs. Thus, one can visualize the suspended CNTs in the nematic media as *local anchoring fields* along the nematic director that amplify the orientational order in the matrix. This enhancement in orientational order causes for an increase in $\Delta\varepsilon$ in the hybrid system. So, the formula for $\Delta\varepsilon_{LC+CNT}$ can be modified as,

$$\Delta\varepsilon_{LC+CNT} = \rho_{LC}\,\Delta\varepsilon_{LC} + \rho_{CNT}\,\Delta\varepsilon_{CNT} + \sum \Delta\varepsilon_{short\text{-}range}, \qquad (2)$$

where $\Delta\varepsilon_{short\text{-}range}$, the dielectric anisotropy of a local short-range domain, arises from LC-CNT interaction and, all the domains have cumulative effect on $\Delta\varepsilon_{LC+CNT}$. Simple calculation reveals that $\sum \Delta\varepsilon_{short\text{-}range}$ (= $\Delta\varepsilon_{LC+CNT} - \rho_{LC}\,\Delta\varepsilon_{LC} - \rho_{CNT}\,\Delta\varepsilon_{CNT}$ = 2.8) contributes as much as 20% to the total value of $\Delta\varepsilon_{LC+CNT}$. Additional measurements with

slightly lower CNT concentration (0.0045%) yielded lower value of $\Delta\varepsilon_{LC+CNT} = +13.1$, at 1 kHz. This indicates that more CNT-surface area leads more LC molecules to anchor the CNT-walls along the tube axis, possessing higher $\Delta\varepsilon$, enhancing the orientational order.

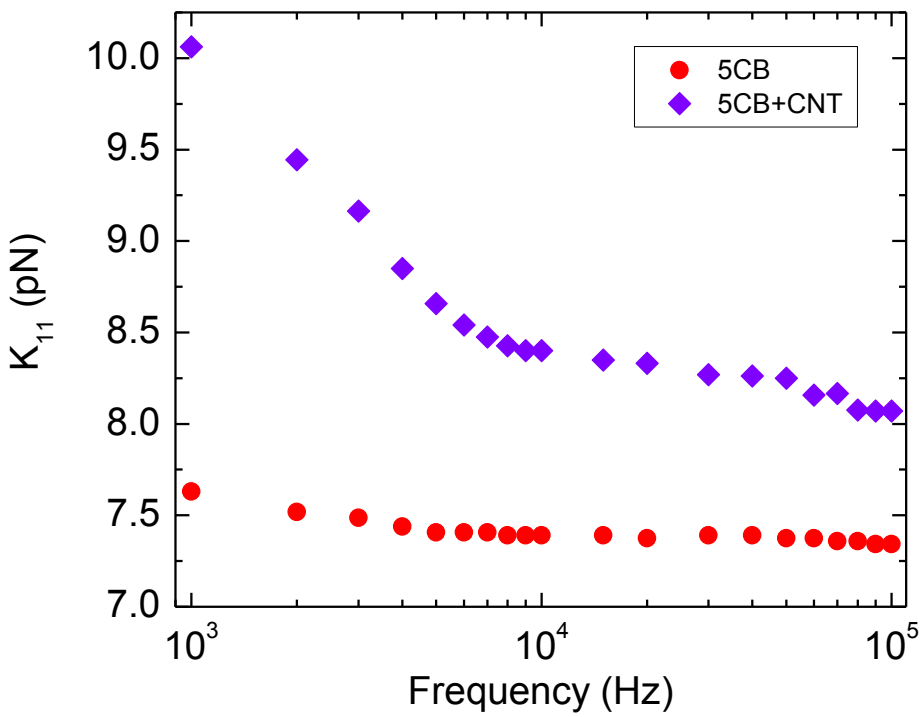

Figure 7.4: *The splay elastic constant K_{11} (in pico Newton) as a function of applied frequency for 5CB and 5CB+CNT in the nematic phase ($T = 25^oC$). K_{11} has been extracted from the formula $V_{th} = \pi\sqrt{(K_{11}/\varepsilon_o \Delta\varepsilon)}$.*

Figure 7.2(a) reveals the significant impact of the applied probing frequency on $\Delta\varepsilon$ for the hybrid LC-CNT system. A 4% increase (10.1 to 10.5) in the $\Delta\varepsilon$ for 5CB in the low frequency regime might be attributed to the ionic conduction/relaxation mechanism [25]. But, a 24% increase (11.2 to 13.8) in the $\Delta\varepsilon$ for the composite in the low frequency regime should not be caused only due to ionic conduction/relaxation mechanism as only 0.007 wt% CNTs were added to the LC. Also, some recent work shows that the presence of the CNTs reduces the free ion concentration in an LC media [4,26]. This suggests that the ions do not play a significant role in the dramatic increase in $\Delta\varepsilon$ for the composite system in the low frequency regime. It is possible that the anchoring mechanism by π–π electron stacking between LC-CNT molecules is affected by the applied probing frequency as the LC molecules have an intrinsic frequency response and, therefore,

$\Delta\varepsilon_{\text{short-range}}$ is a function of frequency. The dramatic increase in $\Delta\varepsilon_{\text{LC+CNT}}$ with decreasing frequency suggests that the anchoring mechanism favors the low frequency regime (1 – 10 kHz), showing the intrinsic frequency response of the *local directors* formed by LC-CNT anchoring.

The splay elastic constant K_{11} for the bent distortion for the LC and the hybrid system has been extracted from the well known formula,

$$V_{\text{th}} = \pi \sqrt{(K_{11} / \varepsilon_o \Delta\varepsilon)}, \tag{3}$$

where V_{th} is the reorientation threshold voltage for the Fréedericksz transition [21]. The estimated K_{11}, by using the observed experimental values of V_{th} and $\Delta\varepsilon$, is shown in the Fig. 7.4 as a function of the probing frequency. Clearly, $K_{11}^{\text{LC+CNT}} > K_{11}^{\text{LC}}$. It has been observed that V_{th} does not quite change with increasing frequency and, so, increasing $\Delta\varepsilon$ increases K_{11} with decreasing frequency for the hybrid system. The strong elastic interaction between LC-CNT due to the surface anchoring may increase the elastic energy of the hybrid system and therefore can be attributed to the increase in K_{11} in the LC+CNT system; which is essentially a structural modification in the nematic phase due to the addition of a small amount of CNTs. The dramatic increase in K_{11} for the hybrid system in the low frequency regime (same as $\Delta\varepsilon$) is attributed to the enhancement in the anchoring mechanism in that frequency range.

The LC-CNT anchoring mechanism becomes more prominent in the isotropic phase. Due to the absence of elastic interactions in the isotropic phase, the LC molecules no longer maintain long-range orientation order and act as an isotropic liquid. Isotropic phase of 5CB, as expected, shows $\Delta\varepsilon = 0$, confirming no long range orientational order; $S = 0$. See Fig. 7.2(b). But, a dramatic change in the field-induced dielectric constant has been observed in the isotropic phase for the hybrid system. The composite system shows an increment in $\bar{\varepsilon}$ with increasing applied voltage without saturating at the highest voltage applied. Also, no distinct V_{th} has been observed in the isotropic phase. So, the dielectric anisotropy in the isotropic phase for the LC+CNT system cannot be defined as $\Delta\varepsilon = \varepsilon_{\parallel} - \varepsilon_{\perp}$. Rather, the dielectric anisotropy for the composite system in the isotropic phase is defined as $\Delta\varepsilon = \bar{\varepsilon}_{\text{max}} - \bar{\varepsilon}_{\text{min}}$, where $\bar{\varepsilon}_{\text{max}}$ and $\bar{\varepsilon}_{\text{min}}$ are determined from an '$\bar{\varepsilon}$ vs. applied voltage' graph (not shown in this letter) at a temperature above T_{NI} = 35°C. The frequency dependence of $\Delta\varepsilon$ in the isotropic phase is shown in Fig. 7.2(b).

As stated earlier, the energy associated with LC-CNT anchoring mechanisms is $U_{\text{anchoring}} = -2$ eV. In the deep isotropic state at T = 42°C = 315 K, the thermal energy $U_{\text{thermal}} \sim k_B T = 2.71 \times 10^{-2}$ eV. So, the thermal energy is not even close enough to eliminate the anchoring mechanisms in the isotropic phase. Thus, local short-range orientation order of LC molecules surrounding the CNT due to the anchoring, discussed earlier, still exists in the isotropic media. This can be visualized as the presence of

isolated *pseudo-nematic* domains in an isotropic media, as schematically shown in Fig. 7.3(c). This indicates that in the isotropic phase CNTs, surrounded by few layers of LCs, stabilize nematic-like short-range order in the isotropic phase, giving rise to a non-zero order parameter. This *isotropic order parameter* would depend on the concentration and distribution symmetry of the CNTs in the LC media. As these local anisotropic *pseudo-nematic* domains have polarization, their *short-range director field* interact with external electric fields, resulting in a non-zero value of $\Delta\varepsilon$ in the isotropic phase. The intrinsic frequency response of the anchoring mechanism in the isotropic phase behaves in a very different way than it does in the nematic phase, clearly observed in Fig 7.2. However, the composite possesses higher anisotropy ($\Delta\varepsilon = 3.4$) at 1 kHz that gradually decreases ($\Delta\varepsilon = 1.5$) at 100 kHz, like the nematic state.

In conclusion, we have observed that a dilute suspension of CNTs in a nematic LC, results in a dramatic improvement in the nematic ordering, showing enhanced $\Delta\varepsilon$. Strong frequency dependence of the dielectric anisotropy suggests that the LC-CNT anchoring mechanism may be perturbed by the probing frequency of the applied field. However, more experimental and theoretical studies are needed to fully understand the frequency response of the anchoring mechanism. The presence of local anisotropic *pseudo-nematic* domains in the isotropic phase causes a net residual order in the hybrid system, exhibiting non-zero value of $\Delta\varepsilon$ that is also strongly influenced by the applied probing frequency. Future work involves light scattering studies on concentration dependent CNT suspensions in LC media to investigate more on the frequency dependent anchoring effect in both the nematic and isotropic phases.

Reference:

[1] M. D. Lynch and D. L. Patrick, *Nano Letters* **2**, 1197 (2002).
[2] I. Dierking, G. Scalia and P. Morales, *J. Appl. Phys.* **97**, 044309 (2005).
[3] R. Basu and G. Iannacchione, *Appl. Phys. Lett.* **93,** 183105 (2008).
[4] In-Su Baik, S. Y. Jeon, S. H. Lee, K. A. Park, S. H. Jeong, K. H. An, and Y. H. Lee, *Appl. Phys. Lett.* **87**, 263110 (2005).
[5] P. V. Kamat, K. G. Thomas, S. Barazzouk, G. Girishkumar, K. Vinodgopal, and D. Meisel; *J. Am. Chem. Soc.* **126**, 10757 (2004).
[6] J. M. Russell, S. Oh, I. LaRue, O. Zhou, and E. T. Samulski; *Thin Solid Films* **509**, 53 (2006).
[7] R. Basu and G. Iannacchione, *Phys. Rev. E* **80**, 010701 (2009).
[8] R. Basu and G. Iannacchione, *Appl. Phys. Lett.* **95**, 173113 (2009).
[9] R. Basu and G. Iannacchione, *J. Appl. Phys.* **106**, 124312 (2009).

[10] S. J. Jeong, K. Ah Park, S. H. Jeong, H. J. Jeong, K. H. An, C. W. Nah, D. Pribat, S. H. Lee, and Y. H. Lee, Sr, *Nano Letters* **7**, 2178 (2007).
[11] M. Caggioni, A. Roshi, S. Barjami, F. Mantegazza, G. S. Iannacchione, and T. Bellini; *Physical Review Letters* **93** (12), 127801 (2004).
[12] J. A. Fagan, J. R. Simpson, B. J. Landi, L. Richter, I. Mandelbaum, J. Obrzut, V. Bajpai, R. Raffaelle, B. J. Bauer, A. R. Hight Walker, and E. K. Hobbie, *Phys. Rev. Lett.*, **98**, 147402 (2007).
[13] P. P. A. M. van der Schoot, V. Popa-nita, S. Kralj, *J. Phys. Chem. B* **112**, 4512, (2008).
[14] Empty LC cells (*LC2-20.0, homogeneous anti-parallel rubbed with 1° pre-tilt*) are commercially available from *Instec Research Instrumentation Technology.*
[15] S. Pilla, J. A. Hamida, and N. S. Sullivan, *Rev of Sci. Instrum.* **70**, 4055, (1999).
[16] M. C. Foote and A. C Anderson, *Rev of Sci. Instrum.* **58,** 130 (1987).
[17] R. Basu and G. Iannacchione, *J. Appl. Phys.* **104**, 114107 (2008).
[18] F. Kremer and A. Schonhals, *Broadband Dielectric Spectroscopy* (Springer, Berlin, 2003).
[19] R. Basu and G. Iannacchione, *Appl. Phys. Lett.* **92,** 052906 (2008).
[20] D. A. Dunmur, M.R. Manterfield, W.H. Miller and J.K. Dunleavy; *Mol. Cryst. Liq. Cryst.* **45**, 127 (1978).
[21] P. G. de Gennes and J. Prost, *The Physics of Liquid Crystals*, (Oxford University Press, 1974).
[22] Y. Reznikov, O. Buchnev, O. Tereshchenko, V. Reshetnyak, A. Glushchenko, and J. West, *Appl. Phys. Lett.* **82**, 1917 (2003).
[23] S. Blatt, F. Hennrich, H. v. Lo1hneysen, M. M. Kappes, A. Vijayaraghavan, and R. Krupke, *Nano Letters* **7**, 1960 (2007).
[24] Kyung Ah Park, Seung Mi Lee, Seung Hee Lee, and Young Hee Lee, *J. Phys. Chem. C* **111**, 1620 (2007).
[25] G. G. Raju, *Dielectrics in Electric Fields* (Dekker, New York, 2003).
[26] J. Prakash, A. Choudhary, D. S. Mehta, and A. M. Biradar, *Phys. Rev. E* **80**, 012701 (2009).

CHAPTER 8

DIRECTED SELF-ASSEMBLY OF QUANTUM DOTS IN A NEMATIC LIQUID CRYSTAL

8.1 Introduction

Assembling quantum dots (QDs) into nanoscale configurations over macroscopic dimensions is an important goal to realizing their electro-optical potential. In this paper, we present a detailed study of a pentylcyanobiphenyl liquid crystal (LC) and a CdS QD colloidal dispersion by probing the dielectric property $\bar{\varepsilon}$ and relaxation as a function of an applied ac-electric field E_{ac}. In principle, dispersing QDs in a nematic LC medium can direct the dots to align in nearly one-dimensional chain-like structures along the nematic director and these assemblies of QDs can be directed by external electric fields. In a uniform planar aligned cell, the Fréedericksz switching of the LC+QDs appears as a two-step process with the same initial switching field as the bulk but with the final $\bar{\varepsilon}$ value larger than that for an aligned bulk LC. The relaxation of $\bar{\varepsilon}$ immediately following the removal of E_{ac} follows a single-exponential decay to its original value that is slower than the bulk but becomes progressively faster with increasing E_{ac}, eventually saturating. These results suggest that the arrangement of the QDs is mediated by the LC.

Controlled self-assembly of semiconductor Quantum Dots (QDs) holds great promise for numerous applications, such as next generation photonic devices, QD displays, biomedical imaging [1,2,3,4,5,6,7,8,9] and, perhaps, solid-state quantum computation. Electrochemical self-assembly of QDs on a chosen substrate is one of the most efficient techniques to form highly ordered QD-aggregates. However, this technique, like others, does not allow manipulating the QD-aggregates in a preferred direction after the completion of the self-assembly process. Recently, it has been demonstrated that nano-materials like nanotubes or nano-rods can be organized by

nematic *liquid crystals* (LCs) [10,11,12]. In this case, the anisotropic order of the LC imparts order onto the nano-size guest particles, along the *nematic director* (average orientational direction of the LC molecules) for example, due to the reduction of excluded volume [13]. Because the director can be aligned by external electric fields, the nanoscale assemblies of the QDs in the LC can be manipulated. Recent research shows that smectic LC environment allows QDs to achieve high spatial ordering into quasi-one-dimensional arrays along the director [14]. Understanding the interaction of nanoparticles with an LC and the principles governing their assembly through an LC mediated interactions is an important and active area of research.

The nematic phase shows dielectric anisotropy due to the anisotropic nature of the LC molecules where $\varepsilon_{\parallel}$ and $\varepsilon_{\perp}$ are the components parallel and perpendicular to the molecular long axis, respectively. For a positive dielectric anisotropic LC, $\varepsilon_{\parallel} > \varepsilon_{\perp}$, and so, reorients to align the molecular long axis (nematic director for the whole ensemble) parallel to an applied electric field. In a uniform homogeneously aligned parallel-plate cell configuration, the nematic director is aligned perpendicular to the applied electric field due to surface anchoring but the director can reorient parallel to E_{ac} if the field magnitude is above some critical threshold. This is the essence of a Fréedericksz transition and an ac-capacitive measurement of the $\bar{\varepsilon}$ will reveal $\varepsilon_{\perp}$ below and $\varepsilon_{\parallel}$ above this switching, the exact values depending on frequency. The dispersion of spherical particles having an isotropic $\bar{\varepsilon}$, such as CdS quantum dots, typically introduces random surfaces that disrupt the uniform nematic alignment. Thus, for such LC colloids, intermediate values of $\bar{\varepsilon}$ are observed but with a constant offset proportional to the amount of the spherical particles.

It has been shown that to minimize elastic distortions in the LC, micrometer size spherical particles tends to be distributed into cylindrically symmetric chain or strands along the global nematic director, which is essential a minimization of excluded volume [13,15]. However, it is not clear how this analysis would change, or remain valid, as the spherical particles diameter is reduced to nanometer scales, such as QDs.

In this paper, we report the dielectric constant $\bar{\varepsilon}$ and its relaxation as a function of the magnitude of an applied ac-electric field E_{ac} for a colloidal dispersion of cadmium sulfide (CdS) QDs in the nematic 4-cyano-4′-pentylbiphenyl (5CB), denoted LC+QD, inside a homogeneously aligned planar cell. With increasing E_{ac}, $\bar{\varepsilon}$ reveals a Fréedericksz reorientation transition for the LC+QD sample that initiates at the same E_{ac} as the bulk LC, but exhibits a second step at a higher E_{ac}, finally saturating at a value of $\bar{\varepsilon}$ larger than that for the bulk. For the relaxation study on switching E_{ac} off, the LC+QD system relaxes through a single-exponential decay back to a planar orientation, recovering the original value of $\bar{\varepsilon}$ prior to the application of E_{ac}. The relaxation time is larger for the LC+QD system than bulk 5CB but both saturate to a relaxation time above the same E_{ac}. We present a physical interpretation to explain these results that proposes

the QDs arranged in 'pearl-necklace' strands, held together by LC mediated interactions, that do not rotate as a single structure but re-assembles along the new orientation axis – hence, directed self-assembly.

8.2 Experiments

Our LC+QD sample consisted of a small amount (1 wt %) of CdS quantum dots (UV absorption peak: 361 nm and diameter- 2.3 nm in toluene solvent) [16] dispersed in 5CB (the isotropic to nematic transition at T_{IN} = 35°C). The LC+QD+solvent mixture was ultrasonicated for 5 hours to achieve a uniform dispersion. The mixture was then heated to just above T_{IN} to evaporate the toluene slowly followed by degassing under vacuum for 2 hours. The LC+QD mixture was then filled into an electro-optical cell (5 × 5 mm^2 indium tin oxide (ITO) coated area and 20 μm spacing) [17] by capillary action. The patterned-electrode-surface inside the LC cell imposes the uniform planar alignment to the nematic director. A homemade ac-capacitive dielectric spectrometer [18,19,20,21] was used to measure $\bar{\varepsilon}$ as a function of an applied ac-electric field E_{ac}, to avoid ion migration, as well as time following the removal of E_{ac}. All measurements were performed isothermally at T = 25 °C, deep in the nematic phase. An empty cell was also measured in order to extract the absolute $\bar{\varepsilon}$ value and an identical cell arrangement was used for pure bulk 5CB, and empty, in order to make quantitative comparisons to the 5CB+CdS sample.

After the 5CB+CdS sample was loaded into the cell, an external ac electric field pulse, E_{ac} (1 MHz of 30 sec duration) was applied across the cell at magnitudes ranging from 0 - 250 kV/m and $\bar{\varepsilon}$ measured. Following each measurement at a given E_{ac}, a relaxation study was performed by turning off the electric field (at t = 0 sec) and monitoring $\bar{\varepsilon}$ as a function of time. Once fully relaxed, the next higher value of E_{ac} was applied and the sequence repeated. Figure 8.1 shows the decay of $\bar{\varepsilon}(t)$ for each value of E_{ac} for the 5CB+QD sample. Figure 8.2 shows $\bar{\varepsilon}(t = 0^-)$, the value of $\bar{\varepsilon}$ just before E_{ac} is removed, for 5CB+QDs and bulk 5CB samples. Note that our dielectric measurements were performed using a probing field far below the reorientation threshold field and at frequency (100 kHz) far below that for E_{ac}.

8.3 Results, analysis, and conclusions

Field induced director orientation occurs when the torques, due to the external electric field, overcome the elastic interactions between LC molecules and, being embedded in the LC matrix, one-dimensional QD-chains coupled with the director follow the director reorientation. Soon after the field goes off, these restoring forces, between the planar surface state and LC director, drive the system (LC+QD-arrays) back to the original state. Figure 8.1 shows the average dielectric constant, $\bar{\varepsilon}$ (measured at 100 kHz)

as a function of time after E_{ac} was tuned off for the 5CB+CdS sample. In the nematic phase (T = 25° C), QD-arrays and LC molecules cooperatively relax back to the planar orientation after the field goes off. The field-saturated dielectric constant, $\bar{\varepsilon}_{max}$ ($\bar{\varepsilon}$ at t = 0, from Fig. 8.1) for each relaxation is plotted as a function of E_{ac} in Fig. 8.2a and is directly associated with the director orientation. The value of $\bar{\varepsilon}_{max}$ starts to increase

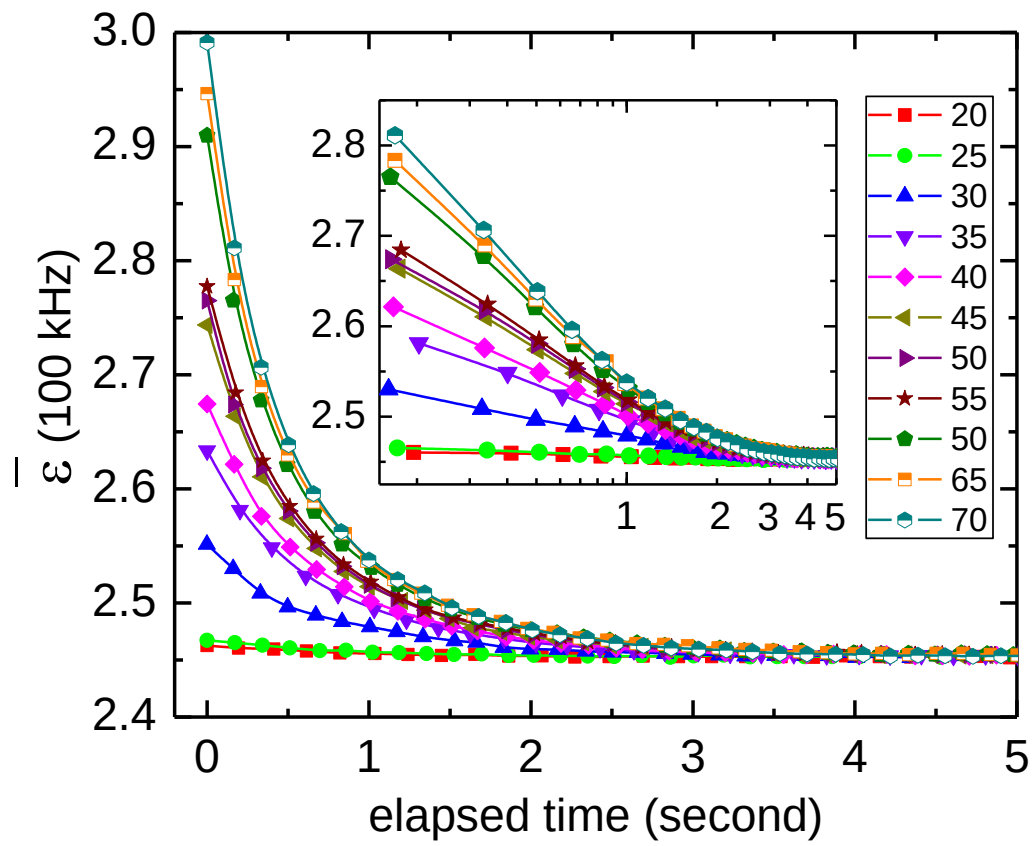

Figure 8.1: *Dynamic response of the average dielectric constant $\bar{\varepsilon}$ for the 5CB+CdS system in the nematic phase (T = 25°C) after E_{ac} = 0; the inset (same main graph axes) represents the same relaxation in log-time scale to show the single exponential decay. The legend represents the magnitude of E_{ac} (1 MHz) in kV/m.*

above E_{ac} = 20 kV/m for both pure 5CB and 5CB+CdS samples, confirming the director reorientation from planar to homeotropic. The saturation for $\bar{\varepsilon}_{max}$ above E_{ac} = 80 kV/m demonstrates the complete homeotropic alignment (tilt angle = 90°) of the LC director and the coupled QD-chains in the cell. Before the field-induced reorientation for the LC+QD system, one-dimensional QD-arrays, being perpendicular to the measuring field,

contribute their average $\varepsilon_{\perp}$ to the average dielectric constant of the system. Figure 8.2a shows that the average dielectric constant of the composite system increases by an amount $\Delta\varepsilon_1$ = 0.08. After the saturation point, when the system is fully reoriented parallel to the field, QD-arrays also show homeotropic alignment, contributing their average $\varepsilon_{\parallel}$ (> $\varepsilon_{\perp}$) to the system. The difference in $\bar{\varepsilon}_{max}$ between pure 5CB and 5CB+CdS after the saturation is given by $\Delta\varepsilon_2$ = 0.15 (87.5 % increase), shown in Fig. 8.2a. The significant dielectric difference $\Delta\varepsilon = \Delta\varepsilon_2 - \Delta\varepsilon_1$ = 0.07 due to the presence of only 1 wt% of QDs in LC media suggests that the spherical QDs form highly anisotropic structures along the director. This is consistent with the view that the anisotropic, cylindrically symmetric, nematic environment favors a cylindrically symmetric arrangement of the QDs, i.e. essentially one-dimensional QD-arrays or chains. If the QDs were to stay in the LC matrix without forming the arrays, one would expect $\Delta\varepsilon_1$ to be equal to $\Delta\varepsilon_2$. At each given field-induced director reorientation, QDs could form new chains keeping the average length and numbers of the chains roughly constant. At each magnitude of an applied electric field, the previously formed QD-chains could be deformed due to the nematic director coupling inducing mechanical torques. After completion of each director rotation, the QDs reassemble to construct new chains. The intermediate step found in $\bar{\varepsilon}_{max}$ (Fig. 8.2a) for 5CB+CdS system indicates that the presence of a small amount of QDs induces local random disorders in the nematic media. A strong enough E_{ac} allows the system to improve nematic ordering, compensating the disorder effect. This field-induced improved nematic order enhances the self-assembly of QDs, resulting in an increase in $\bar{\varepsilon}_{max}$ with further increasing E_{ac} above this intermediate step.

The same experiment was repeated in the isotropic phase (T = 45 ^{o} C). Due to the absence of the nematic mediated (elastic) interactions in the isotropic phase, it is expected that there should be no field induced director reorientation for pure 5CB in the isotropic phase, as confirmed in Fig. 8.2b. The value of $\bar{\varepsilon}_{max}$ of the 5CB+QD system in the isotropic phase does not change with increasing E_{ac}, indicating that the QDs are probably homogeneously distributed and do not form self-assembled arrays, see Fig. 8.2b. In addition, the dielectric constant of the CdS solution (2 mg/cc in toluene) under the same experimental condition does not depend on E_{ac}, confirming that the CdS nanocrystals in bulk solution are not field responsive to form anisotropic arrays.

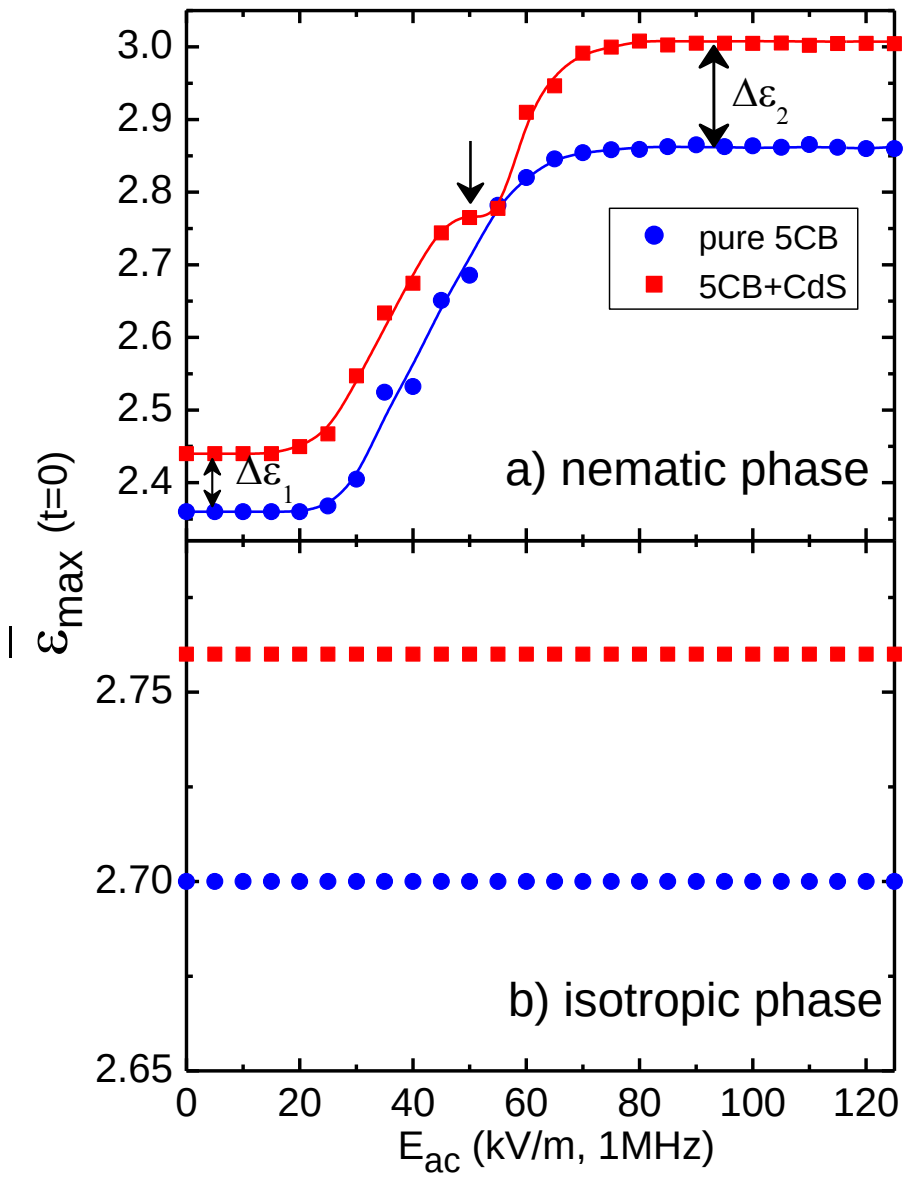

Figure 8.2: (a) *Field-saturated dielectric constant,* $\bar{\varepsilon}_{max}$ ($\bar{\varepsilon}$ *at t = 0) as a function* E_{ac} *for pure 5CB and 5CB+CdS in the nematic phase (T = 25°C). The downward arrow indicates the intermediate step for 5CB+CdS. Lines represent guide to the eye;* **(b)** *Field-saturated dielectric constant,* $\bar{\varepsilon}_{max}$ ($\bar{\varepsilon}$ *at t = 0) as a function* E_{ac} *for pure 5CB and 5CB+CdS in the isotropic phase (T = 45°C).*

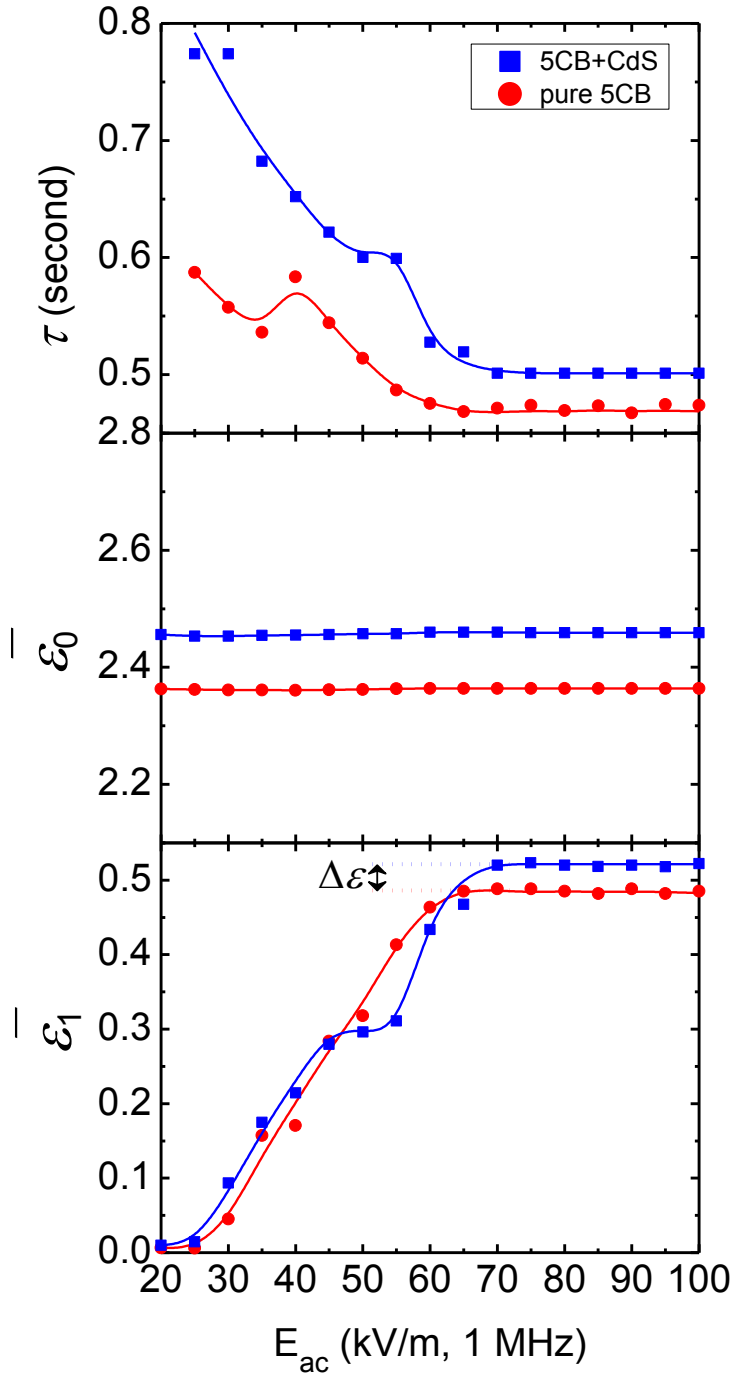

Figure 8.3: *Fitting parameters according to a single-exponential decay ($f(t) = \bar{\varepsilon}_1 e^{(-t/\tau)} + \bar{\varepsilon}_0$) function for pure 5CB and 5CB+CdS system. Lines represent guide to the eye.*

The relaxation dynamics of 5CB or the QDs cannot be separated from the dielectric relaxation in these studies, including at the intermediated step near E_{ac} = 50 kV/m. Only a single, exponential relaxation is observed as seen in Fig. 8.1, the semi-log inset in the Fig. 8.1. The dielectric relaxation curves for 5CB and 5CB+CdS composite were well fitted according to a single-exponential decay function $f(t) = \bar{\varepsilon}_1 e^{(-t/\tau)} + \bar{\varepsilon}_0$, with a typical regression coefficient of R = 0.9976. Here, τ is the relaxation decay time, $\bar{\varepsilon}_0$ is the average base dielectric constant, and $\bar{\varepsilon}_1$ is the field-induced average dielectric constant. Thus, the field-saturated average dielectric constant, $\bar{\varepsilon}_{max} = \bar{\varepsilon}_0 + \bar{\varepsilon}_1$. The values for the three fitting parameters, τ, $\bar{\varepsilon}_0$, and $\bar{\varepsilon}_1$ as a function of E_{ac} are shown in Fig. 8.3. The relaxation time for pure 5CB and 5CB+CdS decreases as E_{ac} increases and saturates at a higher field, which is consistent with the behaviors of $\bar{\varepsilon}_{max}$ shown in Fig. 8.2a. For E_{ac} larger than the saturation point, the composite system relaxes back slower than pure 5CB. It is possible that the presence of QD-arrays increases the mean viscosity and allows the system to relax slower but the low, fixed, concentration used seems unlikely without the self-assembled arrays having significant asymmetry. A cylindrically assembled array of QDs would affect the rotational viscosity more effectively and so more directly alter the dielectric relaxation. Additional measurements with the slightly larger dots (diameter 3.6 nm and 1.36 wt% in LC) yielded longer relaxation times (τ = 0.52 s), indicating that larger the anisotropy longer the relaxation dynamics. The fitting parameter, $\bar{\varepsilon}_1$, tracks the behavior of the observed $\bar{\varepsilon}_{max}$ for pure 5CB and 5CB+CdS, indicating self-consistency. The difference in $\bar{\varepsilon}_1$ between 5CB and 5CB+CdS after the saturation point is $\Delta\varepsilon = 0.0698$. See Figure 8.3. This value of Δε has been found to be very close to the value of $\Delta\varepsilon_2 - \Delta\varepsilon_1$ from Fig. 8a.

Optical cross-polarizing microscopy studies on the same sample of 5CB+QD was attempted. The micrographs reveal a uniform texture indicating a uniform nematic director field. No indicates of phase separation or large scale agglomerates were observed at any temperature. Thus, at least on the length-scales probed by visible light, the arrangements of the QD must be small structures, due to their low concentration, and uniformly distributed. More detailed optical and x-ray studies would be of great benefit to directly probe the local QD assemblies.

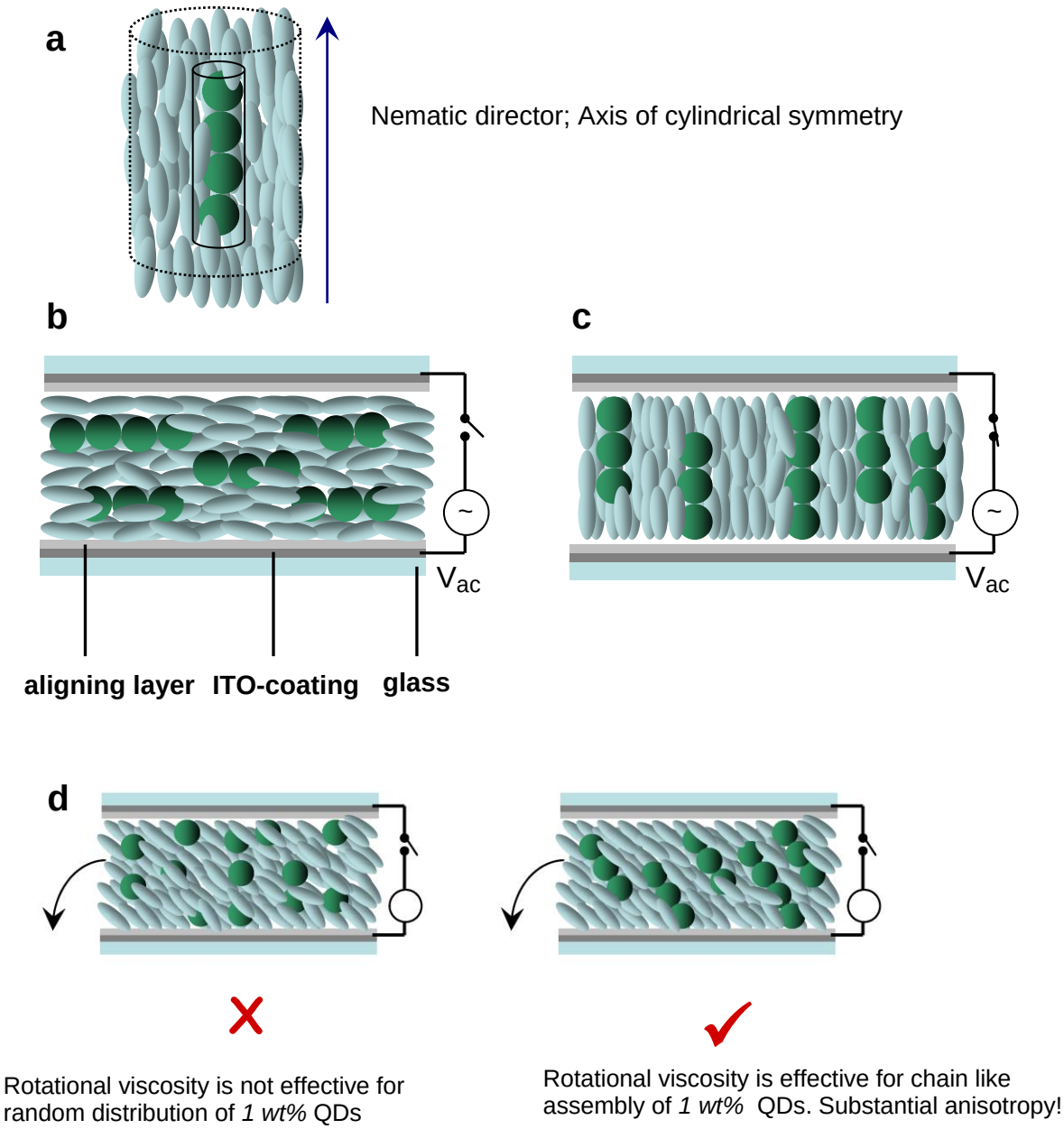

Figure 8.4: *Schematic diagrams;* **(a)** *Dotted cylinder shows the cylindrical symmetry of uniaxial nematic phase; the small cylinder shows the cylindrical confinement of self-assembled QDs aggregation;* **(b)** *Electrode-surface-induced homogeneous alignment of nematic LC molecules (ellipsoidal), and QD self-assembly (spherical) in the nematic matrix;* **(c)** *Electric field induced homeotropic alignment of nematic LC molecules, and homeotropically directed one-dimensional QD arrays.* **(d)** *Increasing rotational viscosity increases the relaxation time ($\tau_{LC+QD} > \tau_{LC}$) in LC+QD. Rotational viscosity arises due to viscous torques being exerted on the director during rotation*

A rough estimation of number of QD-chains and number of QDs in a chain can be made based on the following simple model. For the QD-chains, as explained earlier, the *homogeneous* configuration contributes $\varepsilon_{\|}$ and the *homeotropic* configuration contributes $\varepsilon_{\perp}$ to the average dielectric constant of the host system, $\Delta\varepsilon = \varepsilon_{\|} - \varepsilon_{\perp}$. Quantum dots were initially dispersed isotropically in toluene solvent. One can extract the average contribution, $\delta\varepsilon_0$, of QDs to the dielectric constant of any isotropic media once the average dielectric constants for the QD+toluene sample and pure toluene are known. If n is the number of QDs in a chain, then one can write $\Delta\varepsilon \cong n\ \delta\varepsilon_0 - \delta\varepsilon_0$ or, $n = (\Delta\varepsilon/\ \delta\varepsilon_0) - 1 \approx 2000$, using the dielectric values measured here. The total number of QDs in the 5CB+QD sample within the capacitive cell is known rough, $N \approx 70 \times 10^{12}$ and so, the total number of chains is approximately $m = n/N = 35 \times 10^9$. This is small compared to the total number of 5CB molecules, but their arrangement into LC+field aligned chains can significantly influence the measured dielectric constant. See Figure 8.4.

In summary, the dynamics of 5CB+CdS system has been probed by studying average dielectric response to understand the stability of this system. The results clearly demonstrate that the nematic phase imposes self-assembly on QDs to form one-dimensional arrays. An application of electric field can direct the axis of the self-aggregation in a preferred orientation direction, as illustrated in Fig. 4. This is consistent with the behavior in the isotropic phase being independent of E_{ac}, and the enhanced $\bar{\varepsilon}$ above E_{ac} = 50 kV/m, indicating that only the nematic phase of LC induces this self-assembly on CdS nanocrystals. This study opens up future theoretical and experimental studies to get precise information on structures of QD-arrays. Future work involves optoelectric studies of field-induced fluorescence spectra for different sizes of QDs in nematic LC media.

Reference:

[1] Xia Tong and Yue Zhao, *J. Am. Chem. Soc.* **129**, 6372 (2007)

[2] S-W Lee, C. Mao, C. E. Flynn, A. M. Belcher, Science **296**, 892 (2002).

[3] C. Jiang, S. Xu, D. Yang, F. Zhang and W. Wang, *Luminescence* **22**, 430 (2007).

[4] J. Zhao, J. A. Bardecker, A. M. Munro, M. S. Liu, Y. Niu, I-Kang Ding, J. Luo, B. Chen, A. K.-Y. Jen, and D. S. Ginger, *Nano Letters* **6**, 463 (2006).

[5] A. Balandin, K. L. Wang, N. Kouklin and S. Bandyopadhyay, *Appl. Phys. Lett.* **76**, 137 (2000).

[6] K. L. Wang and A. Balandin, in *Optics of Nanostructed Materials*, edited by V. A. Markel and T. F. George (Wiley, New York, 1999).

[7] S. Fafard, Z. R. Wasilewski, C. Ni Allen, D. Picard, P. G. Piva, and J. P. McCaffrey, *Superlattices Microstruct*. **25**, 87 (1999).

[8] W. Chen, A. G. Joly, J. O. Malm, J. O. Bovin, and S. Wang, *J. Phys.Chem. B* **107**, 6544 (2003).

[9] M. Tamborra, M. Striccoli, R. Comparelli, M. Curri, A. Petrella, A. Agostiano, *Nanotechnology* **15**, S240 (2004).

[10] Michael D. Lynch and David L. Patrick, *Nano Letters* **2**, 1197 (2002)

[11] I. Dierking, G. Scalia and P. Morales, *J. Appl. Phys.* **97**, 044309 (2005)

[12] R. Basu and G. S. Iannacchione, *Appl. Phys. Lett*. **93**, 183105 (2008)

[13] L. Onsager, *Ann. N.Y. Acad. Sci.* **51**, 627 (1949)

[14] Lian C. T. Shoute and David F. Kelley, *J. Phys. Chem. C* **111**, 10233 (2007).

[15] P. G. de Gennes and J. Prost, *The Physics of Liquid Crystals*, (Oxford University Press, 1974)

[16] CdS quantum dots (stabilized by oleic acid ligands) in toluene solvent (CS360-10) is commercially available from *Nanomaterials and Nanofabrication Laboratories* (*http://www.nn-labs.com*).

[17] Empty LC cells (*LC2-20.0, homogeneous anti-parallel rubbed with* 1° *pre-tilt*) are commercially available from *Instec Research Instrumentation Technology.*

[18] S. Pilla, J. A. Hamida, and N. S. Sullivan, *Rev of Sci. Instrum.* **70**, 4055, (1999)

[19] R. Basu and G. S. Iannacchione, *Appl. Phys. Lett.* **92**, 052906 (2008)

[20] M. C. Foote and A. C Anderson, *Rev of Sci. Instrum.* **58**, 130 (1987)

[21] R. Basu and G. S. Iannacchione, *J. Appl. Phys.* **104**, 114107 (2008)

CHAPTER 9

ISOTROPIC TO NEMATIC PHASE TRANSITION IN CARBON NANOTUBE DISPERSED LIQUID CRYSTAL

9.1 Introduction

A high-resolution dielectric and calorimetric study of the isotropic (*I*) to nematic (*N*) phase transition of carbon nanotube (CNT) dispersed liquid crystal (LC) functional composites as a function of CNT concentration has been discussed in this chapter. The evolution of the *I*-*N* phase transition, the temperature dependence of local nematic ordering formed by dispersed CNTs in the LC media and the transition enthalpy were coherently monitored. Anisotropic CNTs induce local deformation to the nematic director of LC and form lyotropic pseudo-nematic phase in the LC media. Results clearly indicate the dramatic impact of dispersed CNTs on both the isotropic and nematic phases of the composite.

Carbon nanotubes (CNTs) dispersed in a nematic liquid crystal (LC) represent a versatile functional composite that has gained interest in recent years for inducing parallel alignment of CNTs, improving electro-optic effect and switching behavior of LCs [1,2,3,4,5,6]. The LC+CNTs system is a unique assemblage of an anisotropic dispersion (CNTs) in an anisotropic media (LC), which makes it an attractive physical system to study the phase transition phenomena. At the isotropic (*I*) to nematic (*N*) transition, the orientational order can be described by a symmetric and traceless second rank tensor (Q_{ij}) which can be described by a scalar parameter S(*T*) on short length scale and on a longer length scale by a vector n called nematic director [7]. In particular, orientational coupling of LC and MWCNTs has an impact on both the nematic and isotropic phases of LC as well as on *I*-*N* transition. These can be probed by studying the dielectric behavior of the composite. Dielectric constant of an anisotropic material like LC is orientation dependent. A nematic LC confined between parallel plate electrodes maintains a constant

director, *n*, due to plate boundary conditions. Planar LC molecules, being perpendicular to the probing field, show smallest dielectric constant, $\varepsilon_{\perp}$; and homeotropically oriented (parallel to the probing field) LC molecules exhibit highest dielectric constant, $\varepsilon_{\parallel}$, assuming the LC is positive dielectric anisotropic. The dielectric anisotropy, $\Delta\varepsilon = (\varepsilon_{\parallel} - \varepsilon_{\perp})$, of LCs is one of the most important features to study their phase transitions. The average dielectric constant in a complete isotropic mixture is given by $\bar{\varepsilon} = (\varepsilon_{\parallel} + 2\varepsilon_{\perp})/3 = \varepsilon_{\text{iso}}$. In the uniaxial nematic phase the average dielectric constant can be written as $\bar{\varepsilon} = (a\ \varepsilon_{\parallel} + b\ \varepsilon_{\perp})$ which is lower than the extrapolated value of ε_{iso}. $\Delta\varepsilon$ depends on temperature and is proportional to the scalar order parameter, $S(T)$. Now, as the system reaches the complete disorder, i.e., isotropic liquid, the order parameter drops down to zero. This leads to the idea of having no temperature dependence of ε_{iso}.

9.2 Experimental procedure and sample preparation

In this paper, we present an experimental study of the nematic to isotropic phase transition in an LC+CNTs system for six different concentrations of multiwall carbon nanotubes (MWCNTs) in LC media, such as 0.05, 0.1, 0.15, 0.2, 0.25, and 0.3 wt %. Average dielectric constant ($\bar{\varepsilon}$) of such a system reveals information about local as well as long range nematic ordering. Calorimetric studies probe energy fluctuations of the phase transition character. Thus, a combined T-dependent dielectric and calorimetric investigation has been undertaken to study the *I-N* phase transition in LC+CNTs. This work reveals compelling evidence that nanotube aggregations create local and isolated short range orientation orders in the LC media which become prominent in the isotropic phase but does not cost any extra energy fluctuations for low CNT concentration.

For these experiments, the well characterized liquid crystal 4-cyano-4'-pentylbiphenyl (5CB) has been used as anisotropic host for MWCNTs. Pure 5CB (2 nm long and 0.5 nm wide, weakly polar molecule with M = 249.359 g/mol) has a weakly first-order isotropic to nematic phase transition at T^{0}_{IN} = 308K and strongly first order nematic to crystal transition at $T^{0}_{cr\text{-}N}$ = 295.5K. Six different concentrations of MWCNT sample (containing nanotubes 5 - 30 nm in diameter and 1-5 μm in length) in 5CB were prepared. After mixing each wt % of MWCNT sample with LC, the mixture was ultrasonicated for 5 hours. In general, nanotubes aggregate due to attractive mutual Van der Waals interactions but gentle ultrasonic agitations over a long period reduce tendency of bundling of nanotubes and effectively disperse and suspend them uniformly in a nematic LC matrix. Soon after ultrasonication, each mixture was degassed under vacuum at 40°C for at least two hours. In the LC+CNT system, helical surface anchoring of LC molecules to the CNT-wall enhances π-π stacking by maximizing the hexagon-hexagon interactions between this two species. See chapter 4, Fig. 4.1. Due to these interactions, self-assembled LC molecules impose alignment on suspended carbon nanotubes along the nematic director.

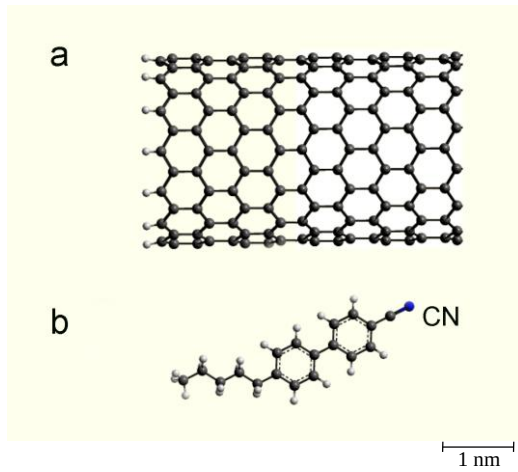

Figure 9.1: *Cartoons of* **(a)** *one carbon nanotube structure,* **(b)** *one 5CB liquid crystal molecule. The diagram of the MWCNT and 5CB are shown approximately to scale. Black spheres are carbon atoms and white spheres are hydrogen atoms.*

AC capacitance bridge technique, discussed in Chapter 1, has been used to measure $\bar{\varepsilon}$ as a function of temperature. A droplet of each mixture was sandwiched between parallel-plate capacitor configuration, 1 cm diameter and 100 cm thick, housed in a temperature controlled bath. Dielectric measurements were performed at very low probing field (5 kV/m) and at 100 kHz frequency. Comparison between the empty and sample filled capacitor allows for an absolute measurement of $\bar{\varepsilon}(T)$. Since low probing field strength does not disturb the director orientation, no director reorientation occurred. The samples that were used in dielectric study were used in this AC calorimetry [8,9] technique as well. The sample cell for calorimeter consists of an aluminum envelope of length ~ 15 mm, width ~ 8 mm and thickness ~ 0.5 mm with the three sides glued with super glue and was made using a cleaned sheet of aluminum. The aluminum was cleaned with water, ethanol and acetone using ultrasonic bath. Once the cell was dried thoroughly the desired amount of sample LC+CNTs was loaded into the cell and then a 120 Ω strain gauge heater and 1 MΩ carbon-flake thermistor were attached on its surfaces. The filled cell then was mounted in the high resolution AC calorimeter to study the phase transition behavior. In the ac mode oscillating power $P_{ac}\ exp(i\omega t)$ is applied to the cell resulting in the temperature oscillations with amplitude T_{ac} and a relative phase shift between T_{ac} and input power, $\varphi = \Phi + \pi/2$ where Φ is the absolute phase shift between T_{ac} and the input power. φ also provides the information regarding the order of the phase transition. With the definition of complex heat capacity, $C^* = P_{ac}/\omega T_{ac}$, the heat capacity at a heating frequency ω can be obtained. All calorimetric data presented here was taken at a heating

frequency of 31.25 mHz at a scanning rate of 1 K/hour. For all LC+CNTs samples each heating scan was followed by a cooling scan and experienced the same heating history.

9.3 Results

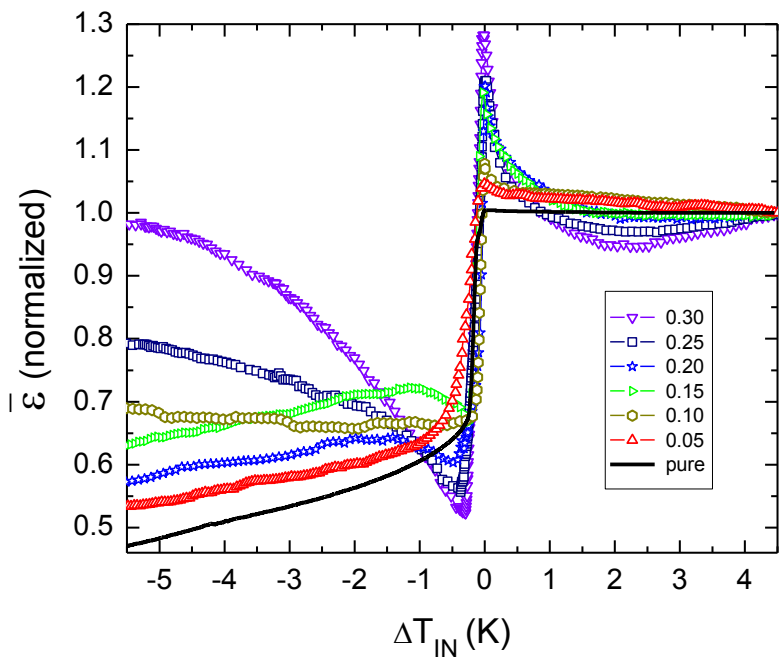

Figure 9.2: *Normalized average dielectric constant* $\bar{\varepsilon}$ *for pure 5CB and 5CB+MWCNTs as a function of temperature shift,* ΔT_{IN}*. The legend shows the concentrations of dispersed MWCNTs in weight % in 5CB. The absolutes values of* T_{IN} *for all concentrations are shown in Fig. 9.4a.*

The normalized $\bar{\varepsilon}$ for different concentrations of LC+CNTs are shown in Fig. 9.2 as a function of temperature shift ΔT_{IN}. The temperature shift is defined as $\Delta T_{IN} = T - T_{IN}$, where T_{IN} is the *I* to *N* transition temperature for each concentration. The transition temperature is defined as the temperature where $\bar{\varepsilon}$ shows the first discontinuity while entering the *N*+*I* phase coexistence region from isotropic phase and was determined from $\bar{\varepsilon}$ vs. *T* curves. Due to their high aspect ratio, CNTs also exhibit dielectric anisotropy and the value of average dielectric constant of aggregated CNTs is much larger than that of LCs. The addition of a very tiny amount of MWCNT sample causes large increment in dielectric constant for the LC+CNTs composites. To compare the dielectric behaviors properly for all the concentrations, the dielectric constants are normalized to the highest temperature (315 K) point studied. Bulk 5CB exhibits the classic temperature dependence of the dielectric constant, showing nematic to isotropic phase transition at T_{IN} = 308.1K, seen in Fig. 9.2 and Fig. 9.4a. Above the transition temperature the dielectric constant

flattens out in the isotropic phase and shows no temperature dependence at all ($\partial\varepsilon_{iso}/\partial T \neq f(T)$), indicating that, bulk 5CB reaches complete disorder state having order parameter, $S(T) = 0$.

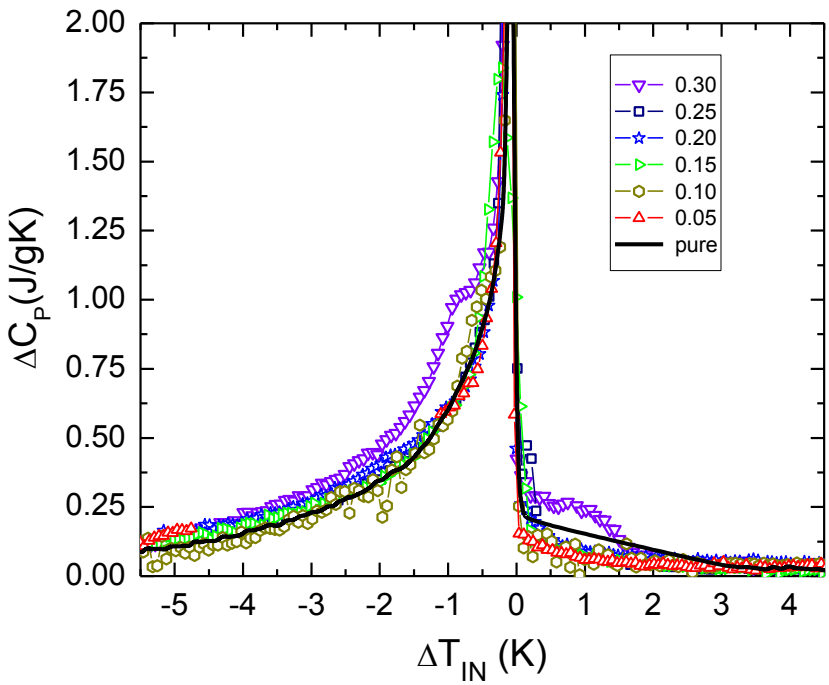

Figure 9.3: *Excess specific heat ΔC_p for pure 5CB and 5CB+MWCNTs as a function of temperature shift, ΔT_{IN}. The legend shows the concentrations of dispersed MWCNTs in weight % in 5CB. The absolutes values of T_{IN} for all concentrations are shown in Fig. 9.4a.*

I-N phase transition for pure 5CB has been found at T_{IN} = 307.8 K by using the AC calorimetry technique. The excess heat capacity, ΔC_p, associated with the phase transition can be determined by subtracting an appropriate background from total heat capacity over a wide temperature range. The resulting ΔC_p data for LC+CNTs samples studied are shown in Fig. 9.3 over a 10K temperature range window about ΔT_{IN}. The transition temperature is defined as the temperature of entering the *N+I* phase coexistence region from isotropic phase and was determined from C''_p vs. T curves. The excess heat capacity peaks are being shifted farther to zero of the temperature axis as the CNTs concentration increases, but the shifting does not have a fixed trend as also observed in dielectric results. The small shift on transition temperatures due to presence of CNTs is because of the large density differences between the liquid crystal and CNTs. The *I-N* transitions evolve in character. The nature of ΔC_p wings in Fig. 9.3 for *I-N* transitions are the same for all samples. The highest concentration (0.3 wt %) studied shows two extra

features at both sides of the transition. This is possibly due to the transition of pseudo-nematic phases of dispersed CNTs in LC media.

9.4 Discussions and conclusions

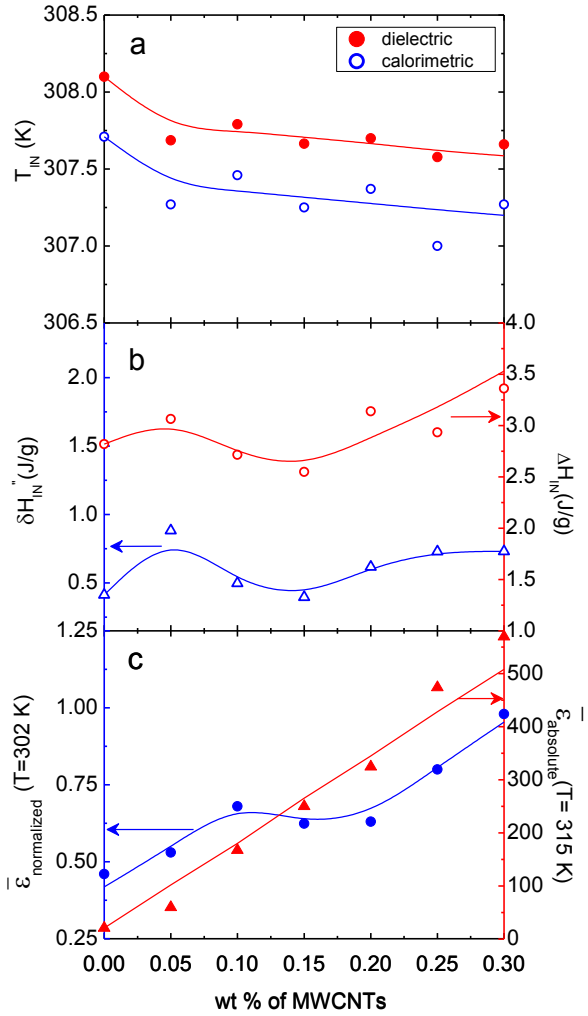

Figure 9.4: (a) *The transition temperature, T_{IN}, as a function of MWCNTs concentration and comparison between the two techniques used for the measurements*, **(b)** *AC- enthalpy (right) and imaginary enthalpy (left) as a function of MWCNTs concentration, for details see text,* **(c)** *The normalized dielectric constant, as a function of MWCNTs concentration at the starting temperature, 302 K (left) and absolute dielectric constant in the deep isotropic phase (315 K) as a function of MWCNTs concentration (right).*

Different weight concentrations of the 5CB+MWCNTs functional composites reveal a dramatic change in the dielectric behavior as well as in nematic to isotropic phase transition behaviors. Smaller amount of CNTs dispersed and suspended in nematic LC media is not frozen in the system; rather they diffuse in the nematic matrix due to the thermal fluctuation. This can be visualized as annealed random variables evolving with time. The nano dynamics of CNTs induce local deformation of LC nematic director. The higher the CNT concentration the larger local deformation occurs. Dielectric behaviors also provide information about the molecular arrangements in a particular system and the larger the $\Delta\varepsilon$ the smaller electric field is needed to make an anisotropic system respond to it. The value of $\Delta\varepsilon$ of aggregated CNTs is much higher than that of LCs. $\Delta\varepsilon$ increases locally in the LC+CNTs system in addition of CNTs. This makes the locally ordered domains, due to the presence of CNTs, more responsive to the probing field, hence the dramatic evolution in the nematic phase with different CNTs concentrations, clearly seen in Fig. 9.2. Fig. 6.4c shows the normalized $\bar{\varepsilon}$ at the starting temperature (302 K) as a function of concentration of CNTs. Clearly there is a crossover region from 0.1 to 0.2 wt %. Above the crossover region the locally ordered domains tend to align along the field and below that crossover region, the system is not that responsive to the low probing field. This explains the downward curvatures in the nematic phase for the higher concentrations observed in Fig. 9.2. Due to the elastic coupling and strong anchoring of LCs to nanotube-surfaces, both the species co-operatively create local short range orientation order. In addition to that, CNTs themselves form lyotropic nematic phase when they are dispersed in a fluid [10]. The curvatures in normalized $\bar{\varepsilon}$ in the isotropic phase for LC+CNTs seen in Fig. 9.2 are the evidence of presence of local pseudo-nematic order formed by CNTs in an isotropic liquid. The larger the CNT concentration the more curvature in $\bar{\varepsilon}$ occurs above T_{IN} confirming that the formed local order is lyotropic pseudo-nematic phase. It has been observed that at about 315 K the $\bar{\varepsilon}$ becomes independent of temperature for all concentrations, confirming that the thermal energy clears out the pseudo-nematic order and the system reaches complete isotropic state. The total enthalpy change associated with a first order phase transition is the sum of the pre-transitional enthalpy and latent heat. Due to partial phase conversion ($N \leftrightarrow I$) during a T_{ac} cycle, typical ΔC_p values obtained in two phase coexistence region are artificially high and frequency dependent. The procedure for calculating δH and ΔH is given in ref.11. An effective enthalpy change ΔH^*_{IN} which includes some of the latent heat contribution can be obtained by integrating observed ΔC_p peak. Here we performed a complete integration over the entire ΔC_p peak over a wide temperature range of around 300 K to 312 K for all 5CB+CNTs samples to get effective enthalpy change ΔH^*_{IN} associated with *I-N* transition. The integration of the imaginary part of heat capacity gives imaginary enthalpy, $\delta H''_{IN}$, which indicates the first order character of the transition or the dispersion of energy in the sample. As fixed frequency used for this work $\delta H''_{IN}$ is only approximately proportional to the transition latent heat even though it is the measure of

the dispersive part of the complex enthalpy. The proportionality constant is different for various CNT concentrations due to different values of the two phase conversion rate. The results of ΔH^*_{IN} and $\delta H''_{IN}$ as a function of CNT concentrations for all 5CB+CNTs samples are presented in Fig. 9.4b. Since ΔC_p values for the different concentration were different ac-enthalpy and imaginary enthalpy are also influenced by the CNT concentrations. ΔH^*_{IN} slightly increases with the increase in CNT concentration. The imaginary-enthalpy, $\delta H''_{IN}$ fluctuates slightly, but overall it also has the increasing trend with increase in CNT concentration. In ac-calorimetric technique the uncertainty in determining the enthalpy is typically 10%.

As demonstrated above, both dielectric and calorimetric measurements indicate that MWCNTs dispersed in 5CB create local lyotropic pseudo-nematic phase, but that does not change the net fluctuation of energy much during *I-N* transition. Evolving wings of normalized $\bar{\varepsilon}$ in the nematic phase in Fig. 9.2 indicate that local domains due to the presence of CNTs become more responsive to the probing field as CNT concentration increases in the system. A fixed trend in the curvature of $\bar{\varepsilon}$ in isotropic phase with increasing CNT concentration manifests the para-nematic phase formed by dispersed CNTs in an isotropic fluid. Calorimetric study conspicuously evidences that tiny amount of suspended CNTs in LC does not cause considerable enthalpy fluctuation about the *I-N* transition region. However, in the highest concentration (0.3 wt %), the pseudo-nematic phase formed by CNTs is strong enough and releases considerable amount of energy while melting, getting displayed in the ΔC_p vs. ΔT_{IN} graph. Additional electric field dependent experimental studies are planned to fully understand the character of field response of local domains in LC+CNT.

References

[1] Michael D. Lynch and David L. Patrick, *Nano Letters* **2**, 1197 (2002).

[2] I. Dierking, G. Scalia and P. Morales, *J. Appl. Phys.* **97**, 044309 (2005).

[3] I. Dierking, G. Scalia, P. Morales, and D. LeClere, *Adv. Mater.* (Weinheim, Ger.) **16** 865 (2004).

[4] In-Su Baik, S. Y. Jeon, S. H. Lee, K. A. Park, S. H. Jeong, K. H. An, and Y. H. Lee, *Appl. Phys. Lett.* **87**, 263110 (2005).

[5] P. V. Kamat, K. G. Thomas, S. Barazzouk, G. Girishkumar, K. Vinodgopal, and D. Meisel, *J. Am. Chem. Soc.* **126**, 10757 (2004).

[6] Joette M. Russell, Soojin Oh, Issac LaRue, Otto Zhou, and Edward T. Samulski, *Thin Solid Films* **509**, (2006).

[7] Kyung Ah Park, Seung Mi Lee, Seung Hee Lee, and Young Hee Lee, *J. Phys. Chem. C* **111**, 1620 (2007).

[8] P. F. Sullivan and G. Seidel, *Phys. Rev. E* **173**, 679 (1968).

[9] H. Yao and C. W. Garland, *Rev. Sci. Instrum*. **69**, 172 (1998).
[10] W. Song, I. A. Kinloch, and A. H. Windle, *Science* **302**, 1363 (2003).
[11] G. S. Iannacchione, C. W. Garland, J. T. mang, and T. P. Rieker, *Phys. Rev. E* **58**, 5966 (1998).

CHAPTER 10

GENERAL CONCLUSIONS AND FUTURE DIRECTIONS

10.1 Introduction

Self-assembly of nanomaterials over macroscopic dimensions and developing novel nano-electromechanical systems (NEMS) hold great promise for numerous nanotechnology applications. However, it has always been a great challenge to find a general route for controlled self-assembly of nanomaterials and generating electromechanical response at the nanoscale level. Our recent research indicates that the self-organized anisotropic nematic liquid crystals (LC) can be exploited for nanotemplating purposes to pattern carbon nanotubes (CNTs) and semiconductor quantum dots (QDs) over a macroscopic dimension. The pattern formed by the nanomaterials in an LC media can be controlled by applying external electric and magnetic fields, developing novel nano-electromechanical and nano-magnetomechanical systems. A part of my recent PhD work involves dielectric, calorimetric, and electro-optic studies of such LC-CNT and LC-QD soft nanocomposite systems.

Now, the goal and intellectual merits of my proposed activity are:

1. Using other experimental facilities (such as, X-ray scattering, Neutron scattering, High magnetic field application, Photoluminescence spectroscopy and many others) at to provide an unusually complete and coherent view of self-assembly phenomena of nanomaterials (CNTs and QDs) in liquid crystal matrix and nano-electromechanical as well as electro-optic response from these soft nanocomposite systems.

2. Extending my understanding of the dynamic response of the CNTs in the LC matrix at nanoscale level under application of high magnetic and electric fields.

3. Utilizing the rich orientational phase behavior of ferroelectric LCs to pattern other nanomaterials (such as silicon nano-wires, nano-rods) for developing nanoscale actuators.

4. Revealing the improvements in electrical, mechanical, and optical properties of LCs due to nanoparticle dispersions and their impact on LC display technology.

10.2 Back ground and summery of my work

Self-organizing nematic liquid crystals (LC) impart their orientational order onto dispersed carbon nanotubes (CNTs) and obtain CNT-self-assembly on a macroscopic dimension. The nanotubes-long axis, being coupled to the nematic director, enables orientational manipulation via the LC nematic reorientation. Electric field induced director rotation of a nematic LC+CNT system is of potential interest due to its possible application as a nano-electromechanical system. Electric field and temperature dependence of dielectric properties of an LC+CNT composite system have been investigated to understand the principles governing CNT-assembly mediated by the LC. (Ref. 1, 2, 3) In the LC+CNT nematic phase, the dielectric relaxation on removing the applied field follows a single exponential decay, exhibiting a faster decay response (important for LC Display technology) than the pure LC above a threshold field. Due to a strong LC-CNT anchoring energy and structural symmetry matching, CNT long axis follows the director field, possessing enhanced dielectric anisotropy of the LC media. This strong anchoring energy stabilizes local pseudo-nematic domains, resulting in nonzero dielectric anisotropy in the isotropic LC phase. These anisotropic domains respond to external electric fields and show intrinsic frequency response. The presence of these domains makes the isotropic phase electric field-responsive, giving rise to a large dielectric hysteresis effect. These polarized domains maintain local directors, and do not relax back to the original state on switching the field off, showing non-volatile electromechanical memory effect.

Assembling semiconductor QDs into nanoscale configurations over macroscopic dimensions is an important goal to realizing their electro-optical potential. A detailed study of an LC+QD system by probing the dielectric property and relaxation as a function of an applied electric field has been carried out to understand the QD self-assembly mechanism in LC (Ref. 4). Dispersing QDs in a nematic LC platform can direct the dots to align in nearly one-dimensional chain-like structures along the nematic director and these assemblies of QDs can be directed in a preferred direction by external electric fields. The studied dynamic response, on switching the field off, reveals insights on the field-induced self-assembly mechanism and the stability of the LC+QD system. These results suggest that the arrangement of the QDs is mediated by the LC.

10.3 My proposed research directions

Dielectric, calorimetric, and optical microscopic studies I have carried out so far to explore the LC-CNT and LC-QD systems. In addition to these experimental techniques used to study these soft-nanoscale systems, comprehensive studies of following experimental techniques on these systems would also reveal more detailed and important information about self-assembled structure formed by the nanomaterials in the liquid crystal media.

a. High magnetic field applications:

Recent research shows that under high magnetic field (20 T- 40 T) liquid crystal systems go through isotropic to nematic phase transition. So, it is important investigating the assembly processes of nanomaterials in LC matrix under external high magnetic field. This enables a new direction of research with a potential outcome of nano-magnetomechanical response. The response of the LC+CNT system under external magnetic field could find potential interest in developing future nano-magnetomechanical and magnetically-steered nanoscale memory storage devices. (As high magnetic field is needed to study these systems, collaborative work can be performed with the National High Magnetic Field Laboratory at Los Alamos.)

b. Photoluminescence spectroscopy:

Photoluminescence spectroscopy is a contactless, nondestructive method of probing the electronic structure of materials. Thus, as the assembled QDs behave differently from isolated QDs, the optical properties of QD-chains in an LC matrix can be studied by photoluminescence using high power laser source to explore their electro-optic potential.

c. Neutron scattering:

The simultaneous probing of structural geometry and the molecular dynamics is the great strength of the small angle neutron scattering (SANS) and the incoherent quasi-elastic neutron scattering (IQENS) methods. Thus, using these methods, these novel soft-nanocomposites (LC-CNT and LC-QD systems) can be explored even more by studying the distribution of CNTs in the LC matrix, the structural modification in the LC geometry due to LC-CNT anchoring energy, and the electric field induced structural (electromechanical) dynamics in an LC-CNT hybrid system.

1. Small angle neutron scattering (SANS): Neutron diffractions from isotopically labeled (hydrogenous and deuteriated) samples provides a technique to extend the structural information that can be determined by the scattering measurements. For the LC-CNT soft-nanocomposite this method can be held out, as it is possible to make small angle neutron scattering measurements on macroscopically aligned materials and, the structural information can be extracted

in the parallel and perpendicular direction to the applied fields. This SANS method can also be used to study the self-assembly phenomenon of the QDs in an LC platform, revealing more detailed information about self-assembled structures formed by the quantum dots.

2. Incoherent quasi-elastic neutron scattering (IQENS): Incoherent quasi-elastic neutron scattering (IQENS) is a very effective technique to study the diffusive molecular motions in liquid crystals. External field driven electromechanical rotational of the director field of an LC-CNT system reveals the information about intrinsic molecular dynamics which can be probed by high resolution IQENS. The individual dynamics of dispersed CNTs can also be probed by isotopic labeling. Thus, a concurrent probing of geometry and the time scale of electromechanical nano-scale dynamics of the LC-CNT system by using neutron scattering technique might reveal further novel phenomena which could bring potential interests into fundamental research as well as in applied areas.

d. X-ray scattering:

In addition to the experimental techniques used to study these soft-nanoscale systems, comprehensive studies of X-ray microscopy, small angle X-ray scattering, and advanced spectroscopy on these systems could also reveal more detailed information about self-assembled structure formed by the nanomaterials in liquid crystals. These are important issues to material science and contributes to the physics of nanoscale self assembly. The orientational order of CNTs in the LC matrix and the improvement in the nematic order due to LC-CNT anchoring mechanism can be obtained by static and dynamic X-ray studies, such percolation, gelation, and rigidity. Nanoscale confinements of the QDs over macroscopic dimensions and the structural manipulation via nematic platform can also be studied in more detail with glancing angle diffraction technique.

e. Smectic phase of LC:

The nematic phase of LCs has been exploited so far for imparting the orientational order onto nanomaterials. In addition to the orientation order, the smectic phase of LC has positional order. So, the smectic phase can also be exploited to transfer both orientational order and positional order onto nanomaterials, and high electric and magnetic fields can be applied to manipulate the orientation order of the nanomaterials. Previously applied experimental techniques along with the proposed techniques can be applied to investigate the nanomaterial distributions in the smectic phase.

10.4 Conclusions

In summary, my proposed research direction will reveal important and more detailed information about self-assembled structure of CNTs and QDs in nematic and

smectic LC. I believe that this research will lead to great improvement in understanding the fundamentals of self-assembly phenomena of nanomaterials in anisotropic hosts (like LC), as well as bring up potential applications, such as MEMS/NEMS and faster LC display response.

CHAPTER 11

JOURNAL ARTICLES

R. Basu and G. S. Iannacchione; "Nematic anchoring on carbon nanotubes"; *Applied Physics Letters* **95**, 173113 (2009).

- Selected for reprint for the *Virtual Journal of Nanoscale Science & Technology* **20** (19), 2009.

R. Basu and G. S. Iannacchione; "Dielectric hysteresis, relaxation dynamics, and non-volatile memory effect in carbon nanotube dispersed liquid crystal"; *Journal of Applied Physics* **106**, 124312 (2009).

- Selected for reprint for the *Virtual Journal of Nanoscale Science & Technology* **21** (2), 2009.

R. Basu and G. S. Iannacchione; "Evidence for directed self-assembly of quantum dots in a nematic liquid crystal"; *Physical Review E – Rapid Communications* **80**, 010701 (2009).

- Featured in InterNano*: NSF-National Nanomanufacturing Network News*; July 27, 2009.

R. Basu and G. S. Iannacchione; "Carbon nanotube dispersed liquid crystal – a nano electromechanical system"; *Applied Physics Letters* **93**, 183105 (2008).

- Selected for reprint for the *Virtual Journal of Nanoscale Science & Technology* **18** (20), 2008.

R. Basu and G. S. Iannacchione; "Dielectric response of multiwall carbon nanotubes as a function of applied ac-electric fields"; *Journal of Applied Physics* **104**, 114107 (2008).

- Selected for reprint for the *Virtual Journal of Nanoscale Science & Technology* **18** (25) 2008.

R. Basu and G. S. Iannacchione; "High-resolution dielectric spectroscopy and electric-field dependence of carbon allotropes including multi-wall and single-wall nanotubes"; *Applied Physics Letters* **92**, 052906 (2008).

- Selected for reprint for the *Virtual Journal of Nanoscale Science & Technology* **17** (7) 2008.

Pending:

R. Basu, K. P. Sigdel and G. S. Iannacchione; "Study of the isotropic to nematic phase transition in carbon nanotube dispersed liquid crystal composites" to be submitted to *Physical Review E-Rapid Communications*, (2009). Available in arXiv: http://arxiv.org/abs/0905.2779v1

High-resolution dielectric spectroscopy and electric-field dependence of carbon allotropes including multiwall and single-wall nanotubes

Rajratan Basu and Germano S. Iannacchione[a)]
Department of Physics, Worcester Polytechnic Institute, Worcester, Massachusetts 01609, USA

(Received 30 November 2007; accepted 21 January 2008; published online 7 February 2008)

High-resolution isothermal dielectric spectroscopy is reported as a function of frequency up to 10^5 Hz and electric field E_{rot} on four carbon allotropes; amorphous glass, diamond, multiwall nanotubes (MWNTs), and single-wall nanotubes (SWNTs). The diamond spectra are featureless while the glass, MWNT, and SWNT samples exhibit two modes. A common low-frequency mode, likely due to surface space charges, is observed at ~16 Hz that decreases in dispersion strength and increases in frequency linearly with increasing E_{rot}. A higher-frequency mode, different for each sample, is also observed having a dispersion strength and frequency independent of E_{rot}. © *2008 American Institute of Physics*. [DOI: 10.1063/1.2841826]

Carbon is an element of great technical importance and interest to industry and science. Pure carbon occurs as several different allotropes, or structures, that differ only in the arrangement of the atoms. Since their discovery in 1991,[1] carbon nanotubes (CNTs) have been studied extensively for their unique electrical, thermal, mechanical, and magnetic properties.[2–12] Recently, composites of CNT within ceramic metals such as alumina[13] or polymers such as polycarbonate[14] have been explored in order to improve their dielectric properties.

The complex dielectric constant $\varepsilon^* = \varepsilon' - i\varepsilon''$ of a material is determined by the molecular polarizability and structural arrangement. This is essentially a measure of a charge-free sample's response to an applied electric field. The real part of the dielectric constant $\varepsilon'(\omega)$ is associated with the storage of the electric field energy while the imaginary part $\varepsilon''(\omega)$ corresponds to the dissipation of energy through a relaxation process. Typically, relaxations below 100 Hz are due to normal conduction while those between 100 and 10^5 Hz are associated reorientation of permanent and/or induced molecular dipoles in the material. Molecular interactions play an important role in such relaxation processes. Changes in the structural arrangement of the molecules can also induce large changes in the dielectric spectra, leading to its use in the study of phase transitions.[15] Dielectric spectroscopy can provide detailed information on dynamic modes, such as segmental mobility of the molecules or vibrational modes of a solid.

In this paper, we use an ac-capacitance bridge technique[16] to measure the isothermal dielectric spectra from 1 to 10^5 Hz of four different carbon structures; amorphous glass, crystalline diamond, single-wall nanotubes (SWNTs), and multiwall nanotubes (MWNTs). In addition, the electric field dependence was probed by increasing the magnitude of the ac-electric field used in the capacitive measurement. The real and imaginary parts of the complex dielectric constant are determined from the in-phase and $(\pi/2)$ out-of-phase off-balance signal of the bridge. Because of the experimental arrangement, the actual magnitude of E_{rot} across the sample is not known (only the driving voltage was controlled). However, the factor by which E_{rot} increases is known if measured in units of that produced by the lowest voltage (denoted as E_{rot}^0 for applied 1 V), this normalized field is labeled $e_R = E_{rot}/E_{rot}^0$. The capacitive cell consists of a parallel-plate configuration, 1 cm across and 100 μm thick using a Kapton spacer, housed in a temperature controlled bath. Comparison between the empty and sample filled capacitors allows for an absolute measurement of $\varepsilon^*(\omega, e_R)$.

All carbon samples were of powder form. The glass sample consisted of spherical particles of 2–12 μm in diameter and 99.95% pure. The diamond sample was of natural monocrystalline form approximately 1 μm in size and 99.9% pure. These powders were obtained from Aldrich and used after degassing under vacuum at 100 °C. The MWNT sample contains nanotubes of 10–100 nm in diameter and 1–5 μm in length. The SWNT sample contains nanotubes ~1.3 nm in diameter and 0.5–50 μm in length. Both carbon nanotube samples were received from Sinha and used without further processing.

The same amount by mass of each sample was loaded into the capacitor cell. The orientation of CNTs was completely random as was the distribution of the diamond and amorphous powders, thus, only the average dielectric constant was determined. For consistency, the same thermal history was applied to each sample and all measurements reported here were performed at a fixed temperature of 328 K (55 °C) with a stability of ±0.005 °C. Temperature dependent experiments on all samples from 300 to 350 K reveal essentially identical spectra indicating that, at least, volatile impurities, which may have been adsorbed onto the carbon, do not play a significant role.

The dielectric spectra for the diamond powder sample reveal no features over the entire frequency range studied. An increase in ε' and ε'' is seen below 10 Hz and is attributed to the onset of normal static conduction. Given the static nature observed, a detailed electric field dependence study was not carried out on diamond. For powders of glass, MWNT, and SWNT carbon, the dielectric spectra exhibit two prominent features, clearly seen in Figs. 1–3, respectively. A low-frequency feature (denoted as mode 1), between 16 and 80 Hz and common to these three samples, is observed to decrease in dispersion strength (peak magnitude of ε'') and shifts to higher frequencies linearly with increasing e_R. The characteristics of mode 1 suggests that it is re-

[a)]Electronic mail: gsiannac@wpi.edu

 © 2008 American Institute of Physics
Downloaded 19 May 2008 to 130.215.36.230. Redistribution subject to AIP license or copyright; see http://apl.aip.org/apl/copyright.jsp

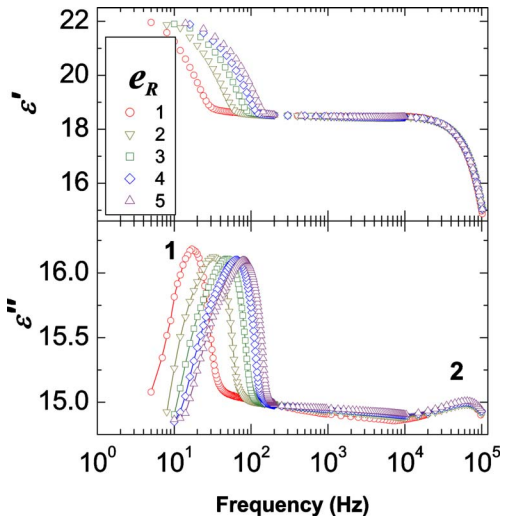

FIG. 1. (Color online) The electric field intensity dependence of $\varepsilon'(\omega)$ and $\varepsilon''(\omega)$ for the amorphous carbon sample. Upper panel legend lists the applied field factor e_R. In $\varepsilon''(\omega)$, the low-frequency mode is denoted by 1 while the high-frequency mode is denoted by 2.

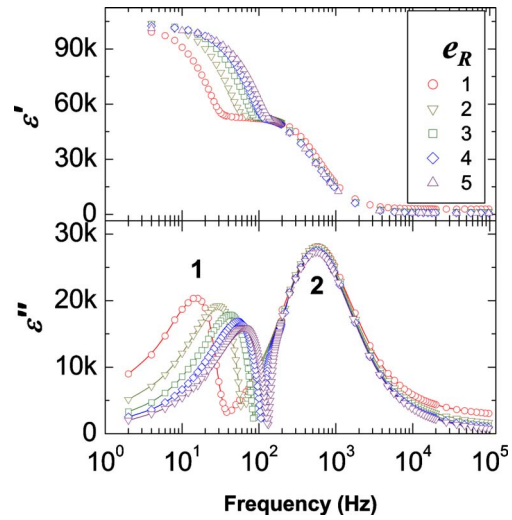

FIG. 3. (Color online) The electric field intensity dependence of $\varepsilon'(\omega)$ and $\varepsilon''(\omega)$ for the SWNT sample (in units of 1000). Upper panel legend lists the applied field factor e_R. For $\varepsilon''(\omega)$, the low-frequency mode is denoted by 1 and the high-frequency mode is denoted by 2.

lated to space charge polarization, which may involve several mechanisms of charge built up at the particle surface or electrode-sample interface.[17] Table I gives the result of a linear regression of the mode-1 peak frequency as a function of e_R.

A higher-frequency feature (mode 2) is observed for the glass, MWNT, and SWNT samples whose peak frequencies occur at 63, 1.9, and 0.6 KHz, respectively, independent of e_R. In addition, the magnitude of the mode-2 dispersion peak is also independent of e_R and exhibits markedly different appearance for the glass than for either of the nanotube samples. The behavior of this mode is consistent with orientational polarization of molecular permanent and/or induced dipoles in the different samples.

To further illuminate the nature of the observed spectra, a "Cole–Cole" construction[18,19] is performed for the glass, MWNT, and SWNT samples. In making this construction, the complex dielectric constant is written as, $\varepsilon^* = \varepsilon_\infty + \Delta\varepsilon(1+i\omega\tau)^{-\beta} - \alpha i(\sigma_0/\omega\varepsilon_{\text{vac}})$ where $\Delta\varepsilon = \varepsilon_\infty - \varepsilon_0$ is the dielectric strength. Here, ε_∞ is the dielectric constant of the material at infinite frequency, ε_0 is the static dielectric constant, ω is the frequency, τ is the relaxation time constant, and β is the fitting factor (where normally $0<\beta<1$). The last term describes electronic conduction where α is the conduction factor, σ_0 is the static conductivity, and ε_{vac} is the vacuum permittivity. For $\alpha=0$, i.e., negligible conduction, this relation yields the Cole–Davidson form[20] while setting $\beta=\alpha=1$ results in the Debye dispersion relation with a static conductivity.[21,22] For $\beta=1$ and $\alpha=0$, a plot of the same scaled units of $\varepsilon''(\omega)$ versus $\varepsilon'(\omega)$ (a Cole–Cole plot) would reveal a semicircle for a single well-defined relaxation process whose diameter is $\Delta\varepsilon$. However, dc conductivity, resulting in a divergence of $\varepsilon''(\omega\to 0)$ or a distribution of relaxation times ($\beta<1$), will lead to distortions of the semicircle.[23,24] Figure 4 shows a Cole–Cole plot for the glass, MWNT, and SWNT carbon samples at the same e_R revealing two well-separated features for each sample. Clearly, Fig. 4 indicates that mode 2 for the glass sample does not represent a typical relaxation process while mode 2 for the MWNT and SWNT samples are similar to each other, though at different frequencies, and represent a single, well-defined, relaxation process.

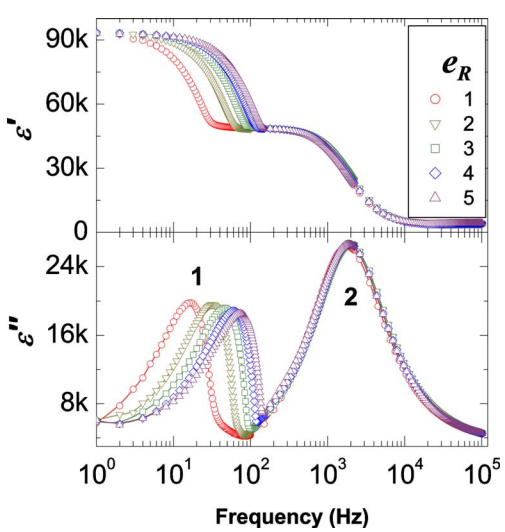

FIG. 2. (Color online) The electric field intensity dependence of $\varepsilon'(\omega)$ and $\varepsilon''(\omega)$ for the MWNT sample (in units of 1000). Upper panel legend lists the applied field factor e_R. For $\varepsilon''(\omega)$, the low-frequency mode is denoted by 1 and the high-frequency mode is denoted by 2.

In summary, the local molecular structures of carbon allotropes have a strong effect on their dielectric spectra of up to 10^5 Hz. Given the static and featureless spectra for

TABLE I. Results of a linear fit to the mode-1 peak frequency f_1 as a function of electric field e_R. The slope m and intercept b (in the appropriate units) are given along with the regression coefficient R and the square-root of χ^2 per point. Note that all fits contain the same number of points ($N=5$) and so, the R and $\sqrt{(\chi^2/N)}$ can be quantitatively compared among each set.

Quantity	m (Hz)	b (Hz)	R	$\sqrt{(\chi^2/N)}$ (Hz)
f_1 (AG)	15.8 ± 0.1	0.8 ± 0.4	0.999 92	0.282
f_1 (MWNT)	14.2 ± 0.2	2.6 ± 0.7	0.999 63	0.548
f_1 (SWNT)	12.4 ± 0.6	3.6 ± 2.0	0.996 36	1.483

Downloaded 19 May 2008 to 130.215.36.230. Redistribution subject to AIP license or copyright; see http://apl.aip.org/apl/copyright.jsp

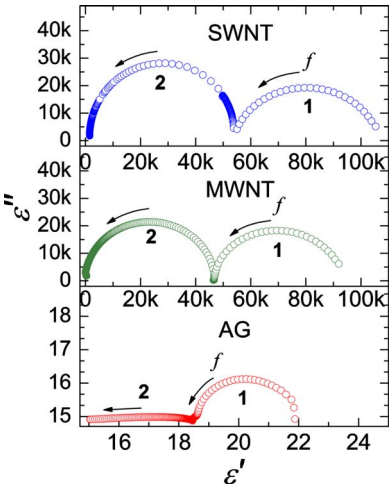

FIG. 4. (Color online) Cole–Cole plots of $\varepsilon''(\omega)$ vs $\varepsilon'(\omega)$ for the SWNT (top), MWNT (middle), and amorphous glass AG (bottom) carbon samples at $e_R=2$. Note that the upper two panels are in units of 1000. The arrows indicate the direction of increasing frequency and the labels denote the mode.

the diamond sample under identical experimental conditions, the two features in the spectra of the other carbon powders are intrinsic to their particular form and nature. For the glass, MWNT, and SWNT samples, the ac-electric field e_R plays an important role in linearly changing the peak position of mode 1 but does not affect the higher frequency mode 2. All samples are powders of comparable grain size but the diamond is an insulator while the glass is a conductor and the MWNT and SWNT are potential conductors depending on their chirality, which is not precisely known in our samples but highly likely. Thus, mode 1 is consistent with the buildup of space charges within the sample+cell, presumably at the grain/nanotube surfaces.

The mode 2 observed for the MWNT and SWNT appears as a single well-defined relaxation process, possibly due to orientational dynamics of permanent and/or induced dipoles in the graphene layers. The mode observed in the glass sample at similar frequencies is of a different character and likely related to the amorphous powder containing a range of distorted carbon structures, some of which are similar to nanotubes. The higher frequency of mode 2 in the MWNT compared to that in SWNT may be due to the "capacitorlike" structure of the multiple graphene walls and so, coupling of the polarization between layers. Coupling of polarization between the curved layers in MWNT would enhance dissipation and so, shifts this mode to higher frequencies. These results clearly indicate that the local structure plays a crucial role for mode 2 while mode 1 appears to be dictated by surfaces and the conducting nature of the samples. Additional experimental studies are planned but theoretical efforts are needed to fully understand the physics of these relaxation mechanisms.

[1]S. Iijima, Nature (London) **354**, 56 (1991).
[2]P. Poncharal, Z. L. Wang, D. Ugarate, and W. A. de Heer, Science **283**, 1513 (1999).
[3]J. W. Mintmire, B. I. Dunlap, and C. T. White, Appl. Phys. Lett. **68**, 631 (1992).
[4]L. Wang and Z.-M. Dang, Appl. Phys. Lett. **87**, 042903 (2005).
[5]Y. Xu, Y. Zhang, and E. Suhir, J. Appl. Phys. **100**, 074302 (2006).
[6]G. L. Zhao, D. Bagayoko, and L. Yang, J. Appl. Phys. **99**, 114311 (2006).
[7]S. Sinha, S. Barjami, G. Iannacchione, A. Schwab, and G. Muench, J. Nanopart. Res. **7**, 651 (2005).
[8]M. Han and L. Deng, Appl. Phys. Lett. **90**, 011101 (2007).
[9]X. Guo, D. Yu, Y. Gaol, Q. Li, W. Wan, and Z. Gao, *Proceedings of the 1st IEEE International Conference on Nano/Micro Engineered and Molecular Systems*, Zhuhai, China (IEEE, New York, 2006).
[10]O. Stephan, D. Taverna, M. Kociak, K. Suenaga, L. Henrard, and C. Colliex, Phys. Rev. B **66**, 155422 (2002).
[11]A. Madarhri, G. Pecastings, F. Carmona, and M. E. Achour, J. Microwave Optoelect. **6**, 36 (2007).
[12]Y. Sato, M. Terauchi, Y. Saito, and R. Saito, J. Electron Microsc. **55**, 137 (2006).
[13]K. Ahmad, W. Pan, and S.-L. Shi, Appl. Phys. Lett. **89**, 133122 (2006).
[14]P. Pötschke, S. M. Dudkin, and I. Alig, Polymer **44**, 5023 (2003).
[15]J. Leys, G. Sinha, C. Glorieux, and J. Thoen, Phys. Rev. E **71**, 051709 (2005).
[16]S. Pilla, J. A. Hamida, and N. S. Sullivan, Rev. Sci. Instrum. **70**, 4055 (1999).
[17]G. G. Raju, *Dielectrics in Electric Fields* (Dekker, New York, 2003).
[18]K. S. Cole and R. H. Cole, J. Chem. Phys. **9**, 341 (1941); **10**, 98 (1942).
[19]Y.-Z. Wei and S. Sridhar, J. Chem. Phys. **99**, 3119 (1993).
[20]D. W. Davidson and R. H. Cole, J. Chem. Phys. **19**, 1484 (1951).
[21]Y. Wei and S. Sridhar, J. Chem. Phys. **92**, 923 (1990).
[22]Y. Wei, P. Chiana, and S. Sridhar, J. Chem. Phys. **96**, 4569 (1992).
[23]*Relaxation Phenomena*, edited by W. Haase and S. Wrobel (Springer, Berlin, 2003).
[24]F. Kremer and A. Schonhals, *Broadband Dielectric Spectroscopy* (Springer, Berlin, 2003).

Downloaded 19 May 2008 to 130.215.36.230. Redistribution subject to AIP license or copyright; see http://apl.aip.org/apl/copyright.jsp

Carbon nanotube dispersed liquid crystal: A nano electromechanical system

Rajratan Basu and Germano S. Iannacchione[a)]
Order-Disorder Phenomena Laboratory, Department of Physics, Worcester Polytechnic Institute, Worcester, Massachusetts 01609, USA

(Received 12 September 2008; accepted 1 October 2008; published online 4 November 2008)

Electric field induced director orientation of a nematic liquid crystal (LC)+carbon nanotube (CNT) system reveals insights on switching behavior for this anisotropic composite. Once the field goes off, the LC+CNT system relaxes back to the original orientation through a mechanical rotation, revealing the intrinsic dynamics. LC molecules and CNTs cooperatively form local *pseudonematic* domains in the isotropic phase due to strong LC-CNT interactions. These field-responsive anisotropic domains do not relax back to the original orientation on switching of the field off, which could find potential applications in memory devices. © *2008 American Institute of Physics*.
[DOI: 10.1063/1.3005590]

Carbon nanotubes (CNTs) dispersed nematic liquid crystal (LC) represents a versatile functional composite that has gained interest in recent years for inducing parallel alignment of CNTs and improving electro-optic effect of LCs.[1–6] This LC+CNT system is a unique assemblage of an anisotropic dispersion (CNTs) in an anisotropic media (LC). This makes it an attractive anisotropic physical system to study the electric field induced switching behavior and nanodynamic response of LC and CNTs. After a field induced *director* (average direction of LC molecules) orientation of the nematic LC+CNT system,[1–3] the LC molecules, as well as the CNTs dynamically reorient back into their original orientation on turning the electric field off, revealing the intrinsic dynamics. However, the reorientation and relaxation mechanisms of CNTs are strongly influenced by the surrounding LC media, such as nematic phase or isotropic phase. In this letter, we report the dynamic response of the average dielectric constant ($\bar{\varepsilon}$) for multiwall CNTs (MWCNTs) dispersed in 4-cyano-4′-pentylbiphenyl (5CB) LC as a function of applied ac-field in both the nematic and isotropic phases.

Both the LC and CNTs systems show dielectric anisotropy due to their structural anisotropy. For a positive dielectric anisotropic system, planar configured molecules being perpendicular to the measuring field show smallest dielectric constant $\varepsilon=\varepsilon_{\perp}$. When the director rotates, the dielectric constant increases until the system is homeotropically aligned (parallel to the measuring field) and the dielectric constant reaches its largest value $\varepsilon_{\parallel}$. However, the values of $\varepsilon_{\perp}$ and $\varepsilon_{\parallel}$ depend on the frequency of the measuring field.

A small amount (0.005 wt %) of MWCNT sample (containing nanotubes <8 nm in diameter and 0.5–2 μm in length) was dispersed in 5CB ($T_{\text{nematic-isotropic}}=35\ ^{\circ}\text{C}$) and the mixture was ultrasonicated for 5 h to reduce the bundling tendency of CNTs. Strong interaction with a binding energy of about −2 eV between LC-CNT (Refs. 4 and 7) makes the long axes of CNTs follow the nematic LC director.[1–3] After ultrasonication, the mixture was filled into a cell (5 $\times$5 mm^2 indium tin oxide coated area and 20 μm spacing) by capillary action, housed in a temperature controlled bath. Surface treatment inside the LC cell imposes the planar alignment to the nematic director. Empty LC cells[8] were measured first in order to extract the absolute $\bar{\varepsilon}$ The relax-

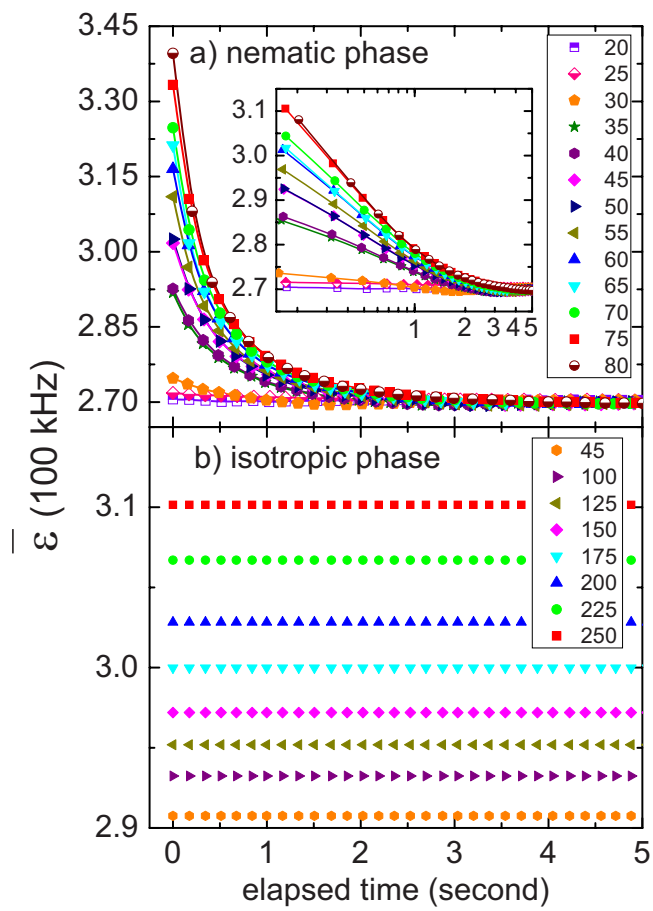

FIG. 1. (Color online) (a) Dynamic response of the average dielectric constant $\bar{\varepsilon}$ for the LC+CNT system in the nematic phase ($T=20\ ^{\circ}\text{C}$) after $E_{ac}=0$. The inset (same main graph axes) represents the same relaxation in log-time scale to show the single exponential decay. Lines represent the fitting according to a single exponential decay function, see text for details. (b) Dynamic response of the average dielectric constant $\bar{\varepsilon}$ for LC+CNT system in the isotropic phase ($T=45\ ^{\circ}\text{C}$) after $E_{ac}=0$. The legends in both the panels represent the magnitude of E_{ac} (kV/m, 1 MHz).

[a)]Electronic address: gsiannac@wpi.edu.

 © 2008 American Institute of Physics

Downloaded 04 Nov 2008 to 130.215.169.7. Redistribution subject to ASCE license or copyright; see http://apl.aip.org/apl/copyright.jsp

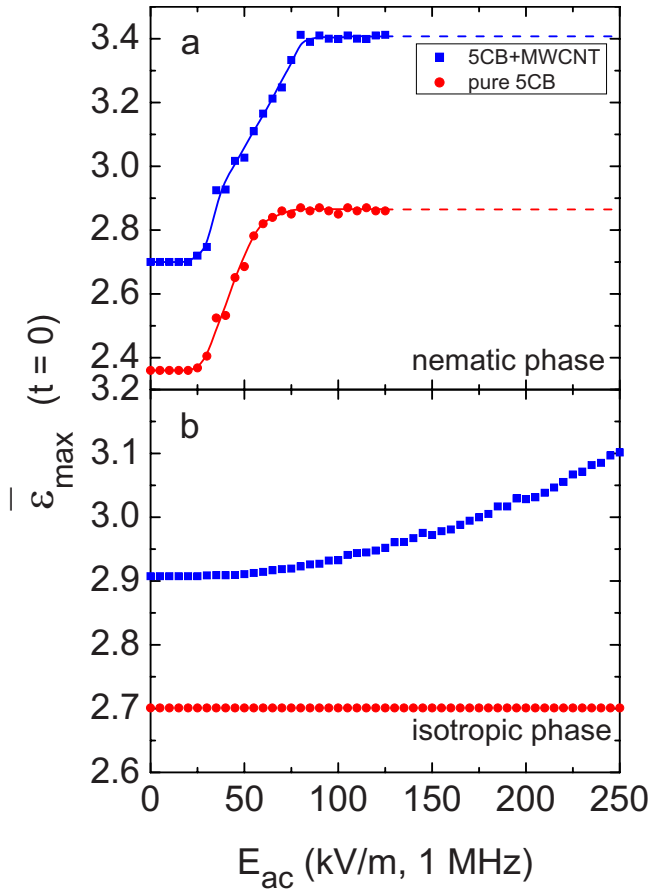

FIG. 2. (Color online) (a) Field-saturated dielectric constant $\bar{\varepsilon}_{max}$ ($\bar{\varepsilon}$ at t =0) as a function E_{ac} in the nematic phase (T=20 °C). Lines represent guide to the eye. (b) Field-saturated dielectric constant $\bar{\varepsilon}_{max}$ ($\bar{\varepsilon}$ at t=0) as a function E_{ac} in the isotropic phase (T=45 °C).

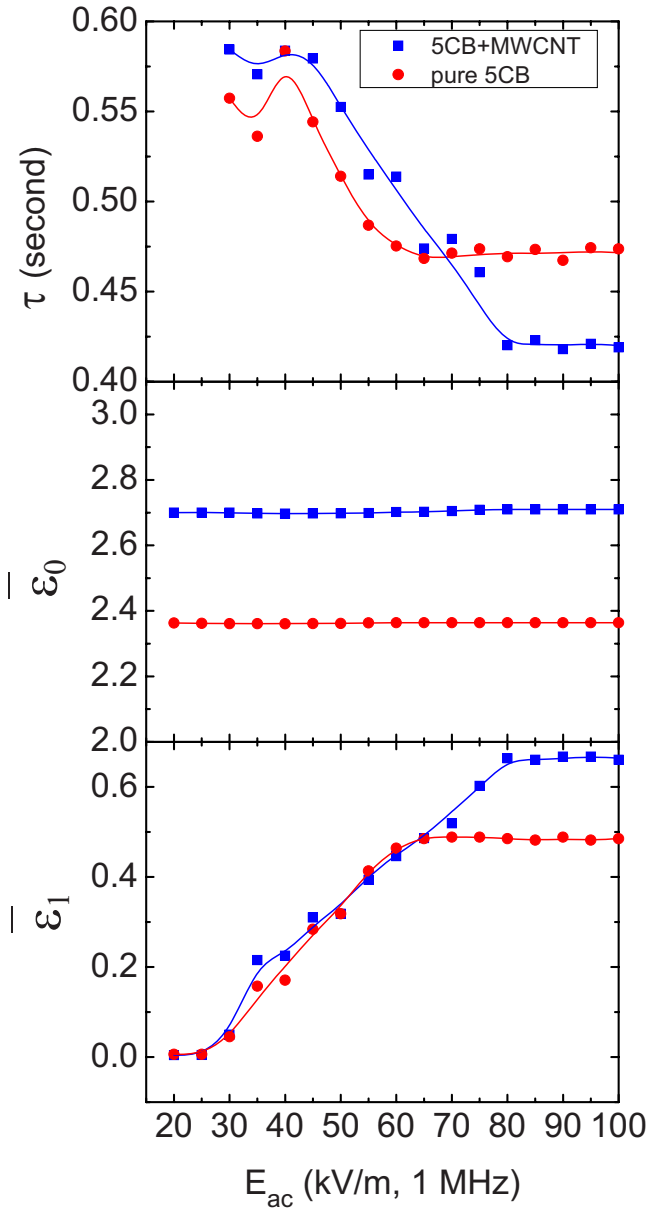

FIG. 3. (Color online) Fitting parameters according to a single-exponential decay $[f(t)=\bar{\varepsilon}_1 e^{(-t/\tau)}+\bar{\varepsilon}_0]$ function for pure 5CB and 5CB+MWCNT system. Lines represent guide to the eye.

ation dynamics also depend on cell configuration; for comparisons, the same type of cells was used for both pure 5CB and 5CB+MWCNT.

After the LC+CNT sample was loaded into the cell, an external ac electric field pulse, E_{ac} (1 MHz) of 30 s duration was applied across the cell at magnitudes ranging from 0 to 250 kV/m. The reason for applying the ac field (not dc) is to avoid the affect of ion migration on the dielectric relaxation measurements. Once E_{ac} was turned off (at t=0 s), isothermal average dielectric ($\bar{\varepsilon}$) measurements were carried in the nematic (T=20 °C) and isotropic (T=45 °C) phases as a function of time, see Fig. 1. The dielectric measurements were performed by the ac capacitance bridge technique,[9–11] operating with a probing field far below the reorientation threshold field and at 100 kHz frequency. The LC 5CB does not exhibit any tumbling mode[12] and MWCNTs show no space charge or dipole orientation dynamics at this probing frequency.[13] Thus, the observed dynamics should be driven mainly by a mechanical relaxation mechanism of the director after E_{ac} is switched off.

Figure 1 shows the average complex dielectric constant, $\bar{\varepsilon}$ (100 kHz) as a function of time after E_{ac} was tuned off for 5CB+MWCNT sample. In the nematic phase (T=20 °C), CNTs and LC molecules cooperatively relax back to the planar orientation after the field goes off, clearly seen in Fig. 1(a). Field induced director orientation occurs when the torques, due to the external electric field, overcome the elastic interactions between LC molecules and, through surface coupling, the CNT long axis follows the director orientation. Soon after the field goes off, these restoring forces between the planar surface state and LC director drive the system back to the original orientation through a mechanical rotation. The field-saturated dielectric constant $\bar{\varepsilon}_{max}$ [$\bar{\varepsilon}$ at t=0, from Fig. 1(a)] for each relaxation is plotted as a function of E_{ac} in Fig. 2(a) and is directly associated with the director orientation. The value of $\bar{\varepsilon}_{max}$ starts to increase above E_{ac} =20 kV/m for both pure 5CB and 5CB+MWCNT samples, confirming the director reorientation from planar to homeotropic, but $\bar{\varepsilon}_{max}$ saturates at a higher field for the composite sample than pure 5CB, see Fig. 2(a). This is probably due to the higher aspect ratio of CNTs that require higher fields to fully reorient.

A dramatic change in the field induced orientation mechanism has been observed in the isotropic phase (T =45 °C). Due to the absence of elastic interactions in the isotropic phase, the LC molecules no longer form long range

Downloaded 04 Nov 2008 to 130.215.169.7. Redistribution subject to ASCE license or copyright; see http://apl.aip.org/apl/copyright.jsp

orientation order. So, it is expected to have no field induced director reorientation for pure 5CB, as also experimentally observed in Fig. 2(b). However, the composite shows an increment in $\bar{\varepsilon}$ on application of electric field which does not relax back over time on switching the field off, as seen in Fig. 1(b). Even though there are no long-range nematic interactions in the isotropic phase, the coupling between LC-CNT (Ref. 4 and 7) still exists. Due to this coupling, the CNT induces local short-range orientation order of LC surrounding the CNT, which can be visualized as presence of isolated pseudonematic domains in an isotropic media. These local anisotropic pseudonematic domains are also field responsive and can be reoriented on application of E_{ac}. However, after the field goes off, there is no restoring force in the isotropic LC media to mechanically torque these domains back into the original orientation. Figure 2(b) depicts that in the isotropic phase there is no sharp threshold field to start the reorientation and $\bar{\varepsilon}_{max}$ does not seem to saturate in the field range studied. The field induced reorientations of these anisotropic domains can only be erased by slowly cooling the system down to the nematic phase and then heating it up again to the isotropic phase.

Dielectric relaxation curves for 5CB and 5CB +MWCNT composite were fitted according to a single exponential decay function $f(t)=\bar{\varepsilon}_1 e^{(-t/\tau)}+\bar{\varepsilon}_0$ with a typical regression coefficient of $R=0.9996$. Here, τ is the relaxation decay time and $\bar{\varepsilon}_1+\bar{\varepsilon}_0=\bar{\varepsilon}_{max}$. The inset in Fig. 1(a) shows the linear dependency of $\bar{\varepsilon}$ at small t with logarithmic time scale. The values for the three fitting parameters τ, $\bar{\varepsilon}_0$, and $\bar{\varepsilon}_1$ as a function of E_{ac} are shown in Fig. 3. Generally, the relaxation time decreases as E_{ac} increases and, for the composite, saturates at a higher field than that of pure 5CB, which is consistent with the behaviors of $\bar{\varepsilon}_{max}$ shown in Fig. 2(a). For E_{ac} larger than the saturation point, the composite system relaxes back faster than pure 5CB, as seen in Fig. 3. It is possible that the dispersed CNTs attract ions present in the LC media,[4] which may influence this result. The presence of ions would slow down the elastic-force driven mechanical relaxation of the nematic domains. The presence of CNTs would lower the free ion concentration and allow the composite system relax faster. If true, this could be an interesting application for image stabilization in LC displays.

In summary, the nanodynamics of LC+CNT system has been studied to understand the stability of these systems. In the nematic phase, the composite system results in an improvement in relaxation decay time for larger E_{ac}, which might be an application for LC display technology. The presence of local anisotropic pseudonematic domains in the isotropic phase in the system demonstrates a promising field induced storage memory device application. This versatile nanoscale electromechanical system might reveal interesting individual molecular dynamics of LC and CNTs in high frequency gigahertz dielectric measurements. Future work involves field-induced frequency dependent dielectric studies for different CNT concentrations in LC media for both the nematic and isotropic phases.

[1] M. D. Lynch and D. L. Patrick, Nano Lett. **2**, 1197 (2002).
[2] I. Dierking, G. Scalia, and P. Morales, J. Appl. Phys. **97**, 044309 (2005).
[3] I. Dierking, G. Scalia, P. Morales, and D. LeClere, Adv. Mater. (Weinheim, Ger.) **16**, 865 (2004).
[4] I.-S. Baik, S. Y. Jeon, S. H. Lee, K. A. Park, S. H. Jeong, K. H. An, and Y. H. Lee, Appl. Phys. Lett. **87**, 263110 (2005).
[5] P. V. Kamat, K. G. Thomas, S. Barazzouk, G. Girishkumar, K. Vinodgopal, and D. Meisel, J. Am. Chem. Soc. **126**, 10757 (2004).
[6] J. M. Russell, S. Oh, I. LaRue, O. Zhou, and E. T. Samulski, Thin Solid Films **509**, 53 (2006).
[7] K. A. Park, S. M. Lee, S. H. Lee, and Y. H. Lee, J. Phys. Chem. C **111**, 1620 (2007).
[8] Empty LC cells (LC2-20.0, homogeneous antiparallel rubbed with 1° pretilt) are commercially available from Instec Research Instrumentation Technology.
[9] S. Pilla, J. A. Hamida, and N. S. Sullivan, Rev. Sci. Instrum. **70**, 4055 (1999).
[10] S. C. Bera and S. Chattopadhyay, Measurement **33**, 3 (2003).
[11] M. C. Foote and A. C. Anderson, Rev. Sci. Instrum. **58**, 130 (1987).
[12] F. Kremer and A. Schonhals, *Broadband Dielectric Spectroscopy* (Springer, Berlin, 2003).
[13] R. Basu and G. Iannacchione, Appl. Phys. Lett. **92**, 052906 (2008).

Downloaded 04 Nov 2008 to 130.215.169.7. Redistribution subject to ASCE license or copyright; see http://apl.aip.org/apl/copyright.jsp

Dielectric response of multiwalled carbon nanotubes as a function of applied ac-electric fields

Rajratan Basu and Germano S. Iannacchione[a)]
Department of Physics, Order-Disorder Phenomena Laboratory, Worcester Polytechnic Institute, Worcester, Massachusetts 01609, USA

(Received 18 July 2008; accepted 19 October 2008; published online 5 December 2008)

The complex dielectric constant (ε^*) is reported for multiwalled carbon nanotubes (MWCNTs) up to 10^5 Hz as a function of ac-electric field amplitudes E_{rot} (in phase and same frequency as the measurement) and E_{ac} (different phase and fixed frequency with respect to the measurement). A slow relaxation process (mode 1) is observed, which shifts to higher frequency with increasing E_{rot} but is independent of E_{ac}. A fast relaxation process (mode 2) is also observed, which is independent of E_{rot} but shifts to higher frequency with increasing E_{ac} (opposite to that of mode 1). An ac-conductivity analysis of MWCNT reveals insights on how E_{rot} and E_{ac} influence the dissipation.
© *2008 American Institute of Physics*. [DOI: 10.1063/1.3035963]

I. INTRODUCTION

One-dimensional carbon nanotubes (CNTs) have been of intense research interest due to their unique atomic and electronic structures (Ref. 1). In addition to their extraordinary thermal, mechanical, and magnetic properties,[2–12] their unique electrical character makes them potentially useful materials for use in nanoelectronic devices.[13–17] The dielectric storage and loss properties are of special interest to researchers and engineers as these two parameters, among others, provide insight to CNTs and their suitability for electronic applications.

In recent years, a CNT dispersion in an anisotropic liquid media (such as a liquid crystal) has gained interest for inducing parallel alignment of CNTs and ac-field induced orientation manipulation for use as switches at the nanoscale level.[18–20] In these kinds of applications, it is important to know the dynamic dielectric modes of CNTs as well as their behavior under an applied ac-electric field. Dielectric spectroscopy of CNTs can reveal insights on those dynamic modes of potential interests as a function of ac field intensity.

Aggregated CNTs show unique dielectric spectra,[21] and the relaxation mechanisms are found to be distorted upon application of electric fields. However, the experimental application of an external ac-electric field can be complicated. For example, the probing field $E_{rot}(\omega)$ in an ac-capacitive measurement is in phase and at the same frequency ω as the measurement of the complex dielectric constant $\varepsilon^*(\omega)=\varepsilon' - i\varepsilon''$. Thus, in the complex *rotating frame* of the measurement, E_{rot} can be considered a "static" field. Conversely, the applied ac-electric field may be at a fixed frequency ω' with respect to the ac-capacitive measurement frequency ω, i.e., $\omega'=\text{const}>\omega$. The field $E_{ac}(\omega')$ is an oscillating field in the complex rotating frame of the measurement. Figure 1 illustrates the phasor diagram of these two electric fields.

In this paper, the focus is to understand the dielectric response of CNTs with respect to applied ac-electric fields. The dielectric storage $\varepsilon'(\omega)$ and the loss $\varepsilon''(\omega)$ of a multiwalled CNT (MWCNT) sample are reported as a function of amplitude of both $E_{rot}(\omega)$ and $E_{ac}(\omega'=203\text{ kHz})$ over the frequency range of $1\leq\omega\leq10^5$ Hz. The results demonstrate how E_{ac} and E_{rot} polarize the curved graphene layers in the MWCNT sample. The dielectric spectra reveal two relaxation modes: a slow mode below 100 Hz that is likely attributed to space-charge polarization at the electrode-nanotube interface and a fast mode in the kilohertz range that is discussed in terms of reorientation polarization of permanent and/or induced electric dipoles.

Following this introduction, a description of the ac-capacitive bridge technique, materials, and sample preparation are given in Sec. II. Dielectric spectra results as a function of applied ac-electric field amplitude are presented in Sec. III, followed by discussions and conclusions in Sec. IV, where a simple physical model is introduced to interpret the fast relaxation mode.

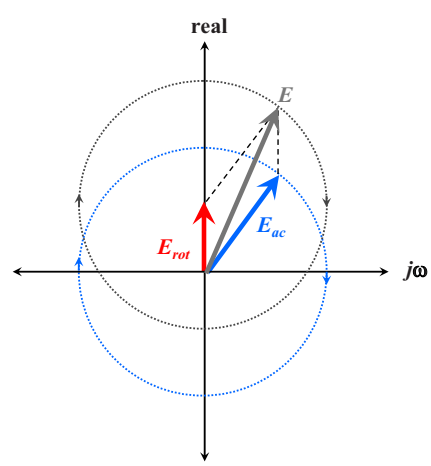

FIG. 1. (Color online) The ac-electric fields E_{rot} and E_{ac} in the *complex rotating frame* of the dielectric measurement. The field E_{rot}, along the real axis, is in phase and at the same frequency as the measurement, hence static in complex rotating frame. Being at a different frequency than the measurement, E_{ac} acts as an ac field in the complex rotating frame. The field E is the resultant field and, at any time, the sample experiences the real component.

[a)]Electronic mail: gsiannac@wpi.edu.

 © 2008 American Institute of Physics

Downloaded 05 Dec 2008 to 130.215.36.61. Redistribution subject to AIP license or copyright; see http://jap.aip.org/jap/copyright.jsp

II. EXPERIMENTAL PROCEDURES

A. ac-capacitance bridge technique

A homebuilt ac-capacitance bridge technique,[22–24] operating with a probing field $E_{\mathrm{rot}}(\omega)$, is used to measure $\varepsilon'(\omega)$ and $\varepsilon''(\omega)$ as a function of frequency and magnitude of E_{rot} and E_{ac}. The capacitive cell consists of a parallel-plate configuration, 1 cm across with a 100 μm gap using a Kapton spacer, housed in a temperature controlled bath. The real and imaginary parts of the complex dielectric constant are determined from the in-phase and $(\pi/2)$ out-of-phase off-balance signals of the bridge. Comparison between the empty capacitor and sample filled capacitor allows for an absolute measurement of $\varepsilon^*(\omega, E_{\mathrm{rot}}, E_{\mathrm{ac}})$. The probing ac-field $E_{\mathrm{rot}}(\omega)$ is applied across the sample through the capacitive bridge and is adjusted by increasing the probing voltage. Because of this technique, the actual magnitude of E_{rot} across the sample is not known (only the driving voltage across the bridge was controlled). However, the factor that E_{rot} increases is known if measured in units of that produced by the lowest voltage (denoted as E_{rot}^0 for a 1 V amplitude applied probing voltage), this factor is labeled $\boldsymbol{e}_R = E_{\mathrm{rot}}/E_{\mathrm{rot}}^0$. To apply and vary the $E_{\mathrm{ac}}(\omega')$ field, a second signal generator, independent of the capacitance bridge, is applied directly across the parallel capacitor plates parallel to the bridge. The presence of E_{ac} can be visualized as making the measurement of $\varepsilon^*(\omega)$ constant in the presence of an ac bias field that is independent of the measurement technique. The frequency of E_{ac} is a constant 203 kHz that is well above the maximum frequency range (100 kHz) of the lock-in amplifier used to detect the off-balance signal and so avoids interference. For consistency, the magnitude of E_{ac} is also labeled $\boldsymbol{e}_{\mathrm{ac}} = E_{\mathrm{ac}}/E_{\mathrm{ac}}^0$, where E_{ac}^0 is that produced using 1 V amplitude output. The quantities $\boldsymbol{e}_R$ and $\boldsymbol{e}_{\mathrm{ac}}$ are the factors that the actual electric field magnitudes increase from their lowest to higher values.

B. Materials and sample preparation

The MWCNT sample, received from Sinha, was used without further processing other than drying under vacuum prior to loading into the spectrometer. The MWCNT sample used is polydisperse containing nanotubes 10–100 nm in diameter and 1–5 μm in length. Approximately 80 vol % of the capacitive cell was occupied by the MWCNT. The sample was filled into the capacitive cell by drop-cast evaporation; thus the orientation of the nanotubes is random between the plates. The measurements reported here are of the *average* complex dielectric constant $\varepsilon^*(\omega) = (\varepsilon_{\parallel} + 2\varepsilon_{\perp})/3$, where $\varepsilon_{\parallel}$ and $\varepsilon_{\perp}$ are the complex dielectric constants parallel and perpendicular to the nanotube long axis, respectively.

III. RESULTS

The dielectric spectra of the MWCNT sample exhibit two well-distinguished dynamic modes in the frequency range studied, as shown in Fig. 2. The slow mode occurring between 20 and 100 Hz is likely due to space charge polarization at the electrode-nanotube interface (denoted mode 1), and the faster mode occurring between 1.5 and 12 kHz is likely due to orientational polarization of permanent and/or induced dipoles (denoted mode 2) either of the nanotubes themselves or within the multiple graphene layers. Mode 1 is strongly coupled to E_{rot}, while mode 2 is independent of E_{rot} (see Fig. 2). The spectra reveal the opposite behavior with the application of E_{ac}. Here, the relaxation frequency increases while the strength (peak height of ε'' for mode 2, $\Delta\varepsilon_2''$) decreases for mode 2 as E_{ac} increases, while mode 1 is independent of E_{ac}.

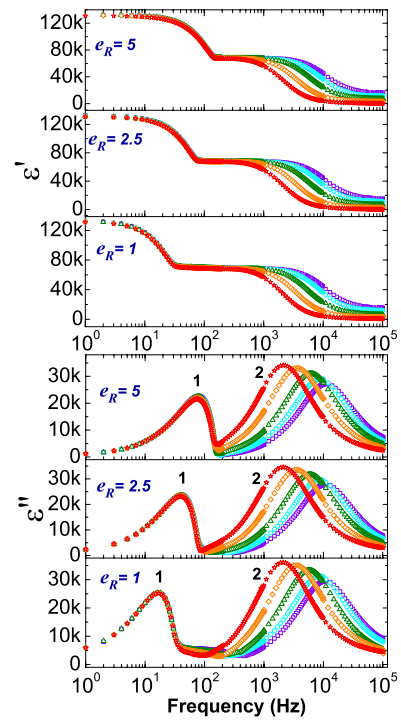

FIG. 2. (Color online) The frequency and E_{ac} (shown by field factor $\boldsymbol{e}_{\mathrm{ac}}$: star=1, diamond=2, triangle=3, circle=4, and square=5) dependence of dielectric storage ε' (top panel) and loss ε'' (bottom panel) of MWCNT sample for three values of E_{rot} (or $\boldsymbol{e}_R$).

Since mode 1 is likely to originate from space charge polarization, it may involve several mechanisms of space charge accumulation at the electrode-nanotube interface. However, all such processes for powder dielectric samples generally occur at low frequency, typically below 100 Hz,[25] and depend strongly on the surface conductivity of the sample and the cell.[21] Note that the probing field E_{rot} is static in the rotating frame and so represents an effective dc field that couples strongly to charge conduction. This should cause the relaxation frequency of mode 1 to shift as a function of $\boldsymbol{e}_R$ but is independent of $\boldsymbol{e}_{\mathrm{ac}}$, as observed in Fig. 2. Figure 3(a) shows the relaxation frequency of mode 1 (f_1) increasing linearly for $0 \le \boldsymbol{e}_R < 3$. For $\boldsymbol{e}_R > 3$, f_1 appears to begin saturating, reaching approximately $f_1^{\max} \sim 75$ Hz for $\boldsymbol{e}_R > 5$. The observed behavior of f_1 is consistent with conduction of finite space charges built up at the electrode-nanotube (and perhaps nanotube-nanotube) interfaces. To strengthen this interpretation, f_1 extrapolates to zero as $\boldsymbol{e}_R = 0$, further indicating that mode 1 is associated with a charge conduction mechanism that vanishes as the field strength goes to zero.

It is expected that the magnitude of the probing field in an ac-capacitance bridge method (E_{rot}) should not affect the orientational relaxation of permanent or induced

Downloaded 05 Dec 2008 to 130.215.36.61. Redistribution subject to AIP license or copyright; see http://jap.aip.org/jap/copyright.jsp

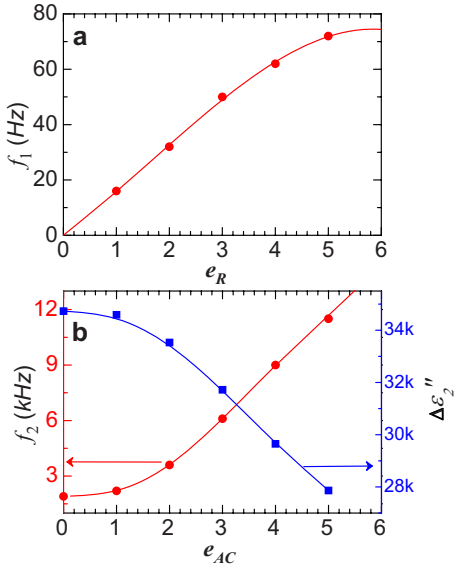

FIG. 3. (Color online) (a) Relaxation frequency of mode 1 (f_1) as a function of E_{rot} (or e_R). Note the initial linear dependence with zero intercept and the apparent saturation for $e_R > 5$. (b) Relaxation frequency of mode 2 (f_2) and dispersion strength ($\Delta\varepsilon''_2$, peak magnitude of ε'') of mode 2 as a function of E_{ac} (or e_{ac}) for $e_R = 1$.

dipoles.[22,26–28] Thus, it is expected that the faster mode 2, being associated with a dipole relaxation process, should be independent of E_{rot}, as seen in Fig. 2 for constant e_{ac}. Figure 3(b) reveals that above a threshold ($e_{ac} \approx 1$ where both E_{rot} and E_{ac} are approximately of equal magnitude), f_2 increases linearly while the strength $\Delta\varepsilon''_2$ decreases linearly with increasing E_{ac}.

IV. DISCUSSIONS AND CONCLUSIONS

The observed behavior of mode 2 with respect to E_{ac} may be interpreted by the following simple model, which suggests a unique relaxation mechanism. The multiple graphene layers of a MWCNT can be visualized as an effective capacitor (C) between the layers in series with an effective resistor (R) of the carbon wall. The applied field E_{ac} generates a voltage difference $V = E_{ac}d$ between successive graphene layers in an MWCNT, where d is the average distance between graphene layers. The natural frequency of a single layer element of this analogous RC circuit is given by $\omega_0 = 2\pi f_2 = 1/RC$. The equivalent effective capacitor C for multiple graphene walls is approximately given by $C = (V/Q + V/Q + \cdots n\text{th layer})^{-1} = Q/(nV)$, where n is the number of walls and Q is the charge on the each curved graphene layer. Substituting gives $\omega_0 = Vn/RQ = E_{ac}(dn/RQ)$, a linear dependence of ω_0 with increasing E_{ac} (once E_{ac} is sufficiently above the effect of E_{rot}) with all other factors being constant for a given sample. This simple model appears to describe well the observed amplitude dependence of the relaxation frequency of mode 2.

To further illuminate the observed dielectric spectra, an ac-conductivity analysis was conducted. The ac conductivity is related to the dielectric properties by $\sigma_{ac} = \omega\varepsilon''\varepsilon_0$ (Ref. 29) and represents the sum contributions from all dissipative mechanisms. Figure 4 shows the MWCNT sample ac-conductivity frequency dependence and reveals the two

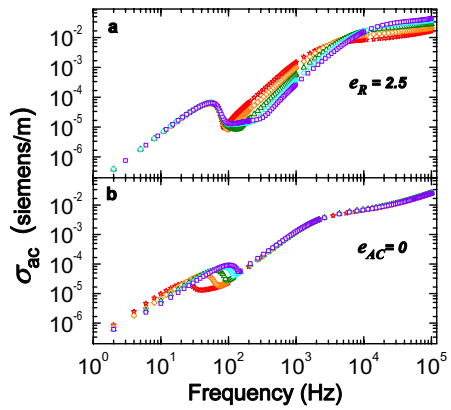

FIG. 4. (Color online) The dielectric ac conductivity σ_{ac} of MWCNT sample as a function of frequency. (a) For constant e_R and varying e_{ac}: star=1, diamond=2, triangle=3, circle=4, and square=5. (b) For constant e_{ac} and varying e_R: star=1, diamond=2, triangle=3, circle=4, and square =5.

modes seen in the original dielectric spectra. The slow and fast modes are observed with a $\sigma_{ac}(\omega)$ for mode 1 typical of charge conduction, while that for mode 2 reminiscent of that for induced polarization (perhaps, as discussed above, related to that between the graphene layers within a nanotube). For frequencies at or above 50 kHz, σ_{ac} exhibits a slow increase above the plateau associated with mode 2, which may be a signature of the mode observed by Ahmad *et al.*[12] at $\sim 10^7$ Hz for the highest volume concentration of MWCNT in alumina.

Finally, a Debye relaxation analysis has been performed on the observed dielectric spectra. A Debye relaxation can be expressed as

$$\varepsilon^* = \left(\varepsilon_\infty + \frac{\Delta\varepsilon}{1 + (\omega\tau)^2}\right) - i\left(\frac{\Delta\varepsilon\omega\tau}{1 + (\omega\tau)^2}\right),$$

where τ is the relaxation time constant and $\Delta\varepsilon = \varepsilon_0 - \varepsilon_\infty$ is the dielectric relaxation strength (the difference between the static and infinite frequency dielectric constants) for a single relaxation process. Figure 5 shows such a fit and indicates that mode 2 is quite consistent with this form without any additional fitting factor. This confirms that mode 2 is related to a polarization process where charge migration does not

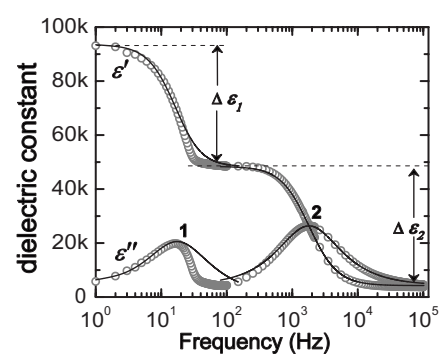

FIG. 5. The dielectric spectrum of the MWCNT sample for $e_R = 1$ and $e_{ac} = 0$; open circles are the data and the solid lines are fits to a Debye relaxation form. Modes 1 and 2 are labeled in the figure, where $\Delta\varepsilon_1$ and $\Delta\varepsilon_2$ are the real dielectric strengths, respectively.

Downloaded 05 Dec 2008 to 130.215.36.61. Redistribution subject to AIP license or copyright; see http://jap.aip.org/jap/copyright.jsp

play an important role. Clearly, mode 1 is asymmetric and not a Debye relaxation.

In summary, these results clearly reveal that this nanoscale system can be perturbed by applying ac-electric fields in two different ways: E_{rot} and E_{ac}. The observed electric field dependence of the spectra reveals the polarization mechanism within the graphene layers of MWCNT. A simple theoretical model can explain the observed frequency shift of mode 2 with E_{ac}: capacitor-resistor-like structure of the multiple graphene walls. This model accounts for the coupling of the polarization between multiple graphene layers in MWCNT. The extracted dielectric ac conductivity increases by four orders of magnitude for increasing frequencies up to 100 kHz and suggests a way to tune the suitable value of conductivity of a MWCNT for a given application.

[1]S. Iijima, Nature (London) **354**, 56 (1991).
[2]P. Poncharal, Z. L. Wang, D. Ugarate, and W. A. de Heer, Science **283**, 1513 (1999).
[3]L. Wang and Z.-M. Dang, Appl. Phys. Lett. **87**, 042903 (2005).
[4]Y. Xu, Y. Zhang, and E. Suhir, J. Appl. Phys. **100**, 074302 (2006).
[5]G. L. Zhao, D. Bagayoko, and L. Yang, J. Appl. Phys. **99**, 114311 (2006).
[6]S. Sinha, S. Barjami, G. Iannacchione, A. Schwab, and G. Muench, J. Nanopart. Res. **7**, 651 (2005).
[7]X. Guo, D. Yu, Y. Gaol, Q. Li, W. Wan, and Z. Gao, *Proceedings of the First IEEE International Conference on Nano/Micro Engineered and Molecular Systems*, Zhuhai, China (IEEE, New York, 2006).
[8]O. Stephan, D. Taverna, M. Kociak, K. Suenaga, L. Henrard, and C. Colliex, Phys. Rev. B **66**, 155422 (2002).
[9]A. Madarhri, G. Pecastings, F. Carmona, and M. E. Achour, Journal of Microwaves and Optoelectronics **6**, 36 (2007).
[10]Y. Sato, M. Terauchi, Y. Saito, and R. Saito, J. Electron Microsc. **55**, 137 (2006).
[11]P. Pötschke, S. M. Dudkin, and I. Alig, Polymer **44**, 5023 (2003).
[12]K. Ahmad, W. Pan, and S.-L. Shi, Appl. Phys. Lett. **89**, 133122 (2006).
[13]E. T. Thostenson, Z. Ren, and T.-W. Chou, Compos. Sci. Technol. **61**, 1899 (2001).
[14]R. H. Baughman, A. A. Zakhidov, and W. A. de Heer, Science **297**, 787 (2002).
[15]P. G. Collins and P. Avouris, Sci. Am. **283**, 38 (2000).
[16]A. Javey, Q. Wang, A. Urai, Y. Li, and H. Dai, Nano Lett. **2**, 929 (2002).
[17]R. Martel, T. Schmidt, H. R. Shea, T. Hertel, and P. Avouris, Appl. Phys. Lett. **73**, 2447 (1998).
[18]M. D. Lynch and D. L. Patrick, Nano Lett. **2**, 1197 (2002).
[19]I. Dierking, G. Scalia, and P. Morales, J. Appl. Phys. **97**, 044309 (2005).
[20]S. J. Jeong, K. A. Park, S. H. Jeong, H. J. Jeong, K. H. An, C. W. Nah, D. Pribat, S. H. Lee, and Y. H. Lee, Sr., Nano Lett. **7**, 2178 (2007).
[21]R. Basu and G. Iannacchione, Appl. Phys. Lett. **92**, 052906 (2008).
[22]S. Pilla, J. A. Hamida, and N. S. Sullivan, Rev. Sci. Instrum. **70**, 4055 (1999).
[23]S. C. Bera and S. Chattopadhyay, Measurement **33**, 3 (2003).
[24]M. C. Foote and A. C. Anderson, Rev. Sci. Instrum. **58**, 130 (1987).
[25]G. G. Raju, *Dielectrics in Electric Fields* (Dekker, New York, 2003).
[26]*Relaxation Phenomena*, edited by W. Haase and S. Wrobel (Springer, New York, 2003).
[27]F. Kremer and A. Schonhals, *Broadband Dielectric Spectroscopy* (Springer, New York, 2003).
[28]N. E. Hill, W. E. Vaughan, A. H. Price, and M. Davies, *Dielectric Properties and Molecular Behavior* (Van Nostrand Reinhold Co., London, 1969).
[29]*Dielectric Materials and Applications*, edited by A. R. Von Hippel (Chapman and Hall, London, 1954).

Downloaded 05 Dec 2008 to 130.215.36.61. Redistribution subject to AIP license or copyright; see http://jap.aip.org/jap/copyright.jsp

PHYSICAL REVIEW E **80**, 010701(R) (2009)

Evidence for directed self-assembly of quantum dots in a nematic liquid crystal

Rajratan Basu and Germano S. Iannacchione*
Order-Disorder Phenomena Laboratory, Department of Physics, Worcester Polytechnic Institute, Worcester, Massachusetts 01609, USA
(Received 27 January 2009; published 22 July 2009)

Assembling quantum dots (QDs) into nanoscale configurations over macroscopic dimensions is an important goal to realizing their electro-optical potential. In this Rapid Communication, we present a detailed study of a pentylcyanobiphenyl liquid crystal (LC) and a CdS QD colloidal dispersion by probing the dielectric property $\bar{\varepsilon}$ and relaxation as a function of an applied ac electric field E_{ac}. In principle, dispersing QDs in a nematic LC medium can direct the dots to align in nearly one-dimensional chainlike structures along the nematic director and these assemblies of QDs can be directed by external electric fields. In a uniform planar aligned cell, the Fréedericksz switching of the LC+QDs appears as a two-step process with the same initial switching field as the bulk but with the final $\bar{\varepsilon}$ value larger than that for an aligned bulk LC. The relaxation of $\bar{\varepsilon}$ immediately following the removal of E_{ac} follows a single-exponential decay to its original value that is slower than the bulk but becomes progressively faster with increasing E_{ac}, eventually saturating. These results suggest that the arrangement of the QDs is mediated by the LC.

DOI: 10.1103/PhysRevE.80.010701 PACS number(s): 77.84.Nh, 73.21.La

Controlled self-assembly of semiconductor quantum dots (QDs) holds great promise for numerous applications, such as next generation photonic devices, QD displays, biomedical imaging [1–9], and, perhaps, solid-state quantum computation. Electrochemical self-assembly of QDs on a chosen substrate is one of the most efficient techniques to form highly ordered QD aggregates. However, this technique, such as others, does not allow manipulating the QD aggregates in a preferred direction after the completion of the self-assembly process. Recently, it has been demonstrated that nanomaterials such as nanotubes or nanorods can be organized by nematic *liquid crystals* (LCs) [10–12]. In this case, the anisotropic order of the LC imparts order onto the nanosize guest particles, along the *nematic director* (average orientational direction of the LC molecules), for example, due to the reduction in excluded volume [13]. Because the director can be aligned by external electric fields, the nanoscale assemblies of the QDs in the LC can be manipulated. Recent research shows that smectic LC environment allows QDs to achieve high spatial ordering into quasi-one-dimensional arrays along the director [14]. Understanding the interaction of nanoparticles with an LC and the principles governing their assembly through an LC mediated interactions is an important and active area of research.

The nematic phase shows dielectric anisotropy due to the anisotropic nature of the LC molecules where $\varepsilon_{\parallel}$ and $\varepsilon_{\perp}$ are the components parallel and perpendicular to the molecular long axis, respectively. For a positive dielectric anisotropic LC, $\varepsilon_{\parallel} > \varepsilon_{\perp}$ and so reorients to align the molecular long axis (nematic director for the whole ensemble) parallel to an applied electric field. In a uniform homogeneously aligned parallel-plate cell configuration, the nematic director is aligned perpendicular to the applied electric field due to surface anchoring but the director can reorient parallel to E_{ac} if the field magnitude is above some critical threshold. This is the essence of a Fréedericksz transition and an ac capacitive measurement of the $\bar{\varepsilon}$ will reveal $\varepsilon_{\perp}$ below and $\varepsilon_{\parallel}$ above this switching, the exact values depending on frequency. The dispersion of spherical particles having an isotropic $\bar{\varepsilon}$, such as CdS quantum dots, typically introduces random surfaces that disrupt the uniform nematic alignment. Thus, for such LC colloids, intermediate values of $\bar{\varepsilon}$ are observed but with a constant offset proportional to the amount of the spherical particles.

It has been shown that to minimize elastic distortions in the LC, micrometer size spherical particles tends to be distributed into cylindrically symmetric chain or strands along the global nematic director, which is essential a minimization of excluded volume [13,15]. However, it is not clear how this analysis would change or remain valid as the spherical particles diameter is reduced to nanometer scales, such as QDs.

In this Rapid Communication, we report the dielectric constant $\bar{\varepsilon}$ and its relaxation as a function of the magnitude of an applied ac electric field E_{ac} for a colloidal dispersion of cadmium sulfide (CdS) QDs in the nematic 4-cyano-4′-pentylbiphenyl (5CB), denoted as LC+QD, inside a homogeneously aligned planar cell. With increasing E_{ac}, $\bar{\varepsilon}$ reveals a Fréedericksz reorientation transition for the LC+QD sample that initiates at the same E_{ac} as the bulk LC but exhibits a second step at a higher E_{ac}, finally saturating at a value of $\bar{\varepsilon}$ larger than that for the bulk. For the relaxation study on switching E_{ac} off, the LC+QD system relaxes through a single-exponential decay back to a planar orientation, recovering the original value of $\bar{\varepsilon}$ prior to the application of E_{ac}. The relaxation time is larger for the LC+QD system than bulk 5CB but both saturate to a relaxation time above the same E_{ac}. We present a physical interpretation to explain these results that proposes the QDs arranged in "pearl-necklace" strands, held together by LC mediated interactions, that do not rotate as a single structure but reassembles along the new orientation axis—hence, directed self-assembly.

Our LC+QD sample consisted of a small amount (1 wt %) of CdS quantum dots (UV absorption peak: 361 nm and diameter of 2.3 nm in toluene solvent) [16] dispersed

*gsiannac@wpi.edu

 ©2009 The American Physical Society

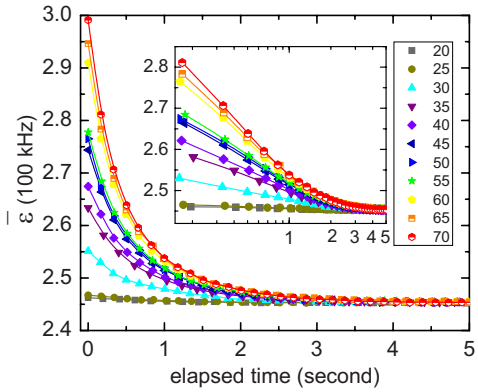

FIG. 1. (Color online) Dynamic response of the average dielectric constant $\bar{\varepsilon}$ for the 5CB+CdS system in the nematic phase (T =25 °C) after E_{ac}=0. The inset (same main graph axes) represents the same relaxation in logarithmic time scale to show the single exponential decay. The lines represent the fitting according to a single exponential decay function, see text for details. The legend represents the magnitude of E_{ac} (1 MHz) in kV/m.

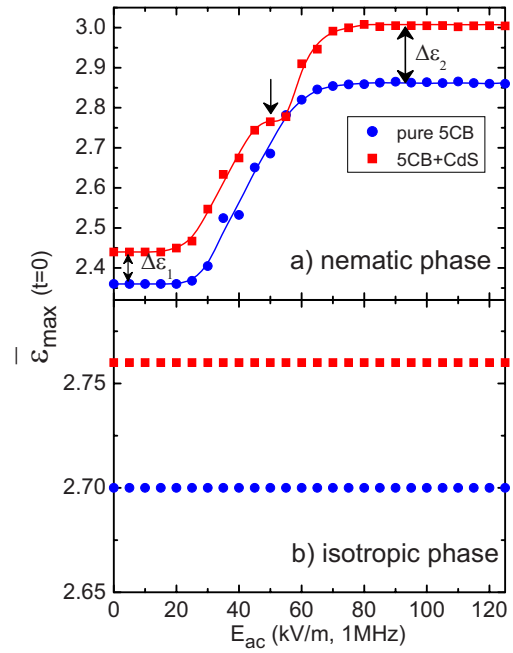

FIG. 2. (Color online) (a) Field-saturated dielectric constant, $\bar{\varepsilon}_{max}$ ($\bar{\varepsilon}$ at t=0) as a function E_{ac} for pure 5CB and 5CB+CdS in the nematic phase (T=25 °C). The downward arrow indicates the intermediate step for 5CB+CdS. Lines represent guide to the eyes; (b) Field-saturated dielectric constant, $\bar{\varepsilon}_{max}$ ($\bar{\varepsilon}$ at t=0) as a function E_{ac} for pure 5CB and 5CB+CdS in the isotropic phase (T=45 °C)

in 5CB (the isotropic to nematic transition at T_{IN}=35 °C). The LC+QD+solvent mixture was ultrasonicated for 5 h to achieve a uniform dispersion. The mixture was then heated to just above T_{IN} to evaporate the toluene slowly followed by degassing under vacuum for 2 h. The LC+QD mixture was then filled into an electro-optical cell [5×5 mm^2 indium tin oxide (ITO) coated area and 20 μm spacing] [17] by capillary action. The patterned-electrode surface inside the LC cell imposes the uniform planar alignment to the nematic director. A homemade ac capacitive dielectric spectrometer [18–21] was used to measure $\bar{\varepsilon}$ as a function of an applied ac electric field E_{ac}, to avoid ion migration, as well as time following the removal of E_{ac}. All measurements were performed isothermally at T=25 °C, deep in the nematic phase. An empty cell was also measured in order to extract the absolute $\bar{\varepsilon}$ value, and an identical cell arrangement was used for pure bulk 5CB and empty in order to make quantitative comparisons to the 5CB+CdS sample.

After the 5CB+CdS sample was loaded into the cell, an external ac electric field pulse, E_{ac} (1 MHz of 30 s duration) was applied across the cell at magnitudes ranging from 0–250 kV/m and $\bar{\varepsilon}$ measured. Following each measurement at a given E_{ac}, a relaxation study was performed by turning off the electric field (at t=0 s) and monitoring $\bar{\varepsilon}$ as a function of time. Once fully relaxed, the next higher value of E_{ac} was applied and the sequence repeated. Figure 1 shows the decay of $\bar{\varepsilon}$ (t) for each value of E_{ac} for the 5CB+QD sample. Figure 2 shows $\bar{\varepsilon}$ (t=0$^-$), the value of $\bar{\varepsilon}$ just before E_{ac} is removed for 5CB+QDs and bulk 5CB samples. Note that our dielectric measurements were performed using a probing field far below the reorientation threshold field and at frequency (100 kHz) far below that for E_{ac}.

Field-induced director orientation occurs when the torques due to the external electric field overcome the elastic interactions between LC molecules, and being embedded in the LC matrix, one-dimensional QD chains coupled with the director follow the director reorientation. Soon after the field goes off, these restoring forces, between the planar surface state and LC director, drive the system (LC+QD arrays) back to the original state. Figure 1 shows the average dielectric constant, $\bar{\varepsilon}$ (measured at 100 kHz) as a function of time after E_{ac} was tuned off for the 5CB+CdS sample. In the nematic phase (T=25 °C), QD arrays and LC molecules cooperatively relax back to the planar orientation after the field goes off. The field-saturated dielectric constant, $\bar{\varepsilon}_{max}$ ($\bar{\varepsilon}$ at t =0, from Fig. 1) for each relaxation is plotted as a function of E_{ac} in Fig. 2(a) and is directly associated with the director orientation. The value of $\bar{\varepsilon}_{max}$ starts to increase above E_{ac} =20 kV/m for both pure 5CB and 5CB+CdS samples, confirming the director reorientation from planar to homeotropic. The saturation for $\bar{\varepsilon}_{max}$ above E_{ac}=80 kV/m demonstrates the complete homeotropic alignment (tilt angle=90°) of the LC director and the coupled QD chains in the cell. Before the field-induced reorientation for the LC+QD system, one-dimensional QD arrays, being perpendicular to the measuring field, contribute their average $\varepsilon_{\perp}$ to the average dielectric constant of the system. Figure 2(a) shows that the average dielectric constant of the composite system increases by an amount $\Delta\varepsilon_1$=0.08. After the saturation point, when the system is fully reoriented parallel to the field, QD arrays also show homeotropic alignment, contributing their average $\varepsilon_{\parallel}$ ($>\varepsilon_{\perp}$) to the system. The difference in $\bar{\varepsilon}_{max}$ between pure 5CB and 5CB+CdS after the saturation is given by $\Delta\varepsilon_2$ =0.15 (87.5% increase), shown in Fig. 2(a). The significant dielectric difference $\Delta\varepsilon=\Delta\varepsilon_2-\Delta\varepsilon_1$=0.07 due to the presence of only 1 wt % of QDs in LC media suggests that the spherical QDs form highly anisotropic structures along the director. This is consistent with the view that the anisotropic cylindri-

cally symmetric nematic environment favors a cylindrically symmetric arrangement of the QDs, i.e., essentially one-dimensional QD arrays or chains. If the QDs were to stay in the LC matrix without forming the arrays, one would expect $\Delta\varepsilon_1$ to be equal to $\Delta\varepsilon_2$. At each given field-induced director reorientation, QDs could form new chains keeping the average length and numbers of the chains roughly constant. At each magnitude of an applied electric field, the previously formed QD chains could be deformed due to the nematic director coupling inducing mechanical torques. After completion of each director rotation, the QDs reassemble to construct new chains. The intermediate step found in $\bar{\varepsilon}_{max}$ [Fig. 2(a)] for 5CB+CdS system indicates that the presence of a small amount of QDs induces local random disorders in the nematic media. A strong enough E_{ac} allows the system to improve nematic ordering, compensating the disorder effect. This field-induced improved nematic order enhances the self-assembly of QDs, resulting in an increase in $\bar{\varepsilon}_{max}$ with further increasing E_{ac} above this intermediate step.

The same experiment was repeated in the isotropic phase (T=45 °C). Due to the absence of the nematic mediated (elastic) interactions in the isotropic phase, it is expected that there should be no field-induced director reorientation for pure 5CB in the isotropic phase as confirmed in Fig. 2(b). The value of $\bar{\varepsilon}_{max}$ of the 5CB+QD system in the isotropic phase does not change with increasing E_{ac}, indicating that the QDs are probably homogeneously distributed and do not form self-assembled arrays, see Fig. 2(b). In addition, the dielectric constant of the CdS solution (2 mg/cc in toluene) under the same experimental condition does not depend on E_{ac}, confirming that the CdS nanocrystals in bulk solution are not field responsive to form anisotropic arrays.

The relaxation dynamics of 5CB or the QDs cannot be separated from the dielectric relaxation in these studies, including at the intermediated step near E_{ac}=50 kV/m. Only a single exponential relaxation is observed as seen in Fig. 1, the semilogarithmic inset in Fig. 1. The dielectric relaxation curves for 5CB and 5CB+CdS composite were well fitted according to a single-exponential decay function $f(t) = \bar{\varepsilon}_1 e^{(-t/\tau)} + \bar{\varepsilon}_0$, with a typical regression coefficient of R =0.9976. Here, τ is the relaxation decay time, $\bar{\varepsilon}_0$ is the average base dielectric constant, and $\bar{\varepsilon}_1$ is the field-induced average dielectric constant. Thus, the field-saturated average dielectric constant, $\bar{\varepsilon}_{max} = \bar{\varepsilon}_0 + \bar{\varepsilon}_1$. The values for the three fitting parameters, τ, $\bar{\varepsilon}_0$, and $\bar{\varepsilon}_1$ as a function of E_{ac} are shown in Fig. 3. The relaxation time for pure 5CB and 5CB+CdS decreases as E_{ac} increases and saturates at a higher field, which is consistent with the behaviors of $\bar{\varepsilon}_{max}$ shown in Fig. 2(a). For E_{ac} larger than the saturation point, the composite system relaxes back slower than pure 5CB. It is possible that the presence of QD-arrays increases the mean viscosity and allows the system to relax slower but the low fixed concentration used seems unlikely without the self-assembled arrays having significant asymmetry. A cylindrically assembled array of QDs would affect the rotational viscosity more effectively and so more directly alter the dielectric relaxation. Additional measurements with the slightly larger dots (diameter 3.6 nm and 1.36 wt % in LC) yielded longer relaxation times (τ=0.52 s), indication that larger the anisotropy longer the relaxation dynamics. The fitting parameter, $\bar{\varepsilon}_1$, tracks the

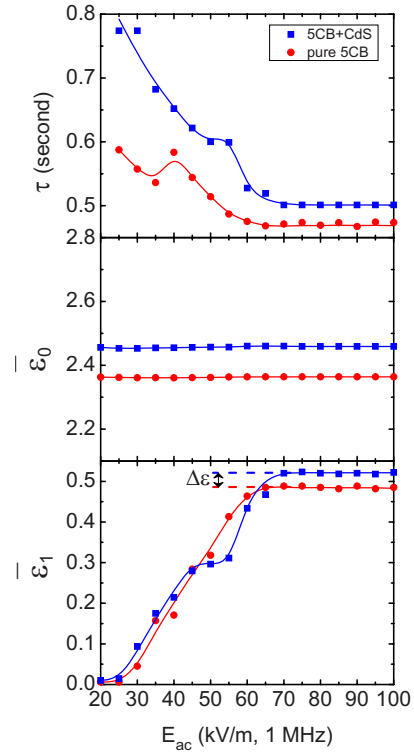

FIG. 3. (Color online) Fitting parameters according to a single-exponential decay ($f(t) = \bar{\varepsilon}_1 e^{(-t/\tau)} + \bar{\varepsilon}_0$) function for pure 5CB and 5CB+CdS system. Lines represent guide to the eyes.

behavior of the observed $\bar{\varepsilon}_{max}$ for pure 5CB and 5CB+CdS, indicating self-consistency. The difference in $\bar{\varepsilon}_1$ between 5CB and 5CB+CdS after the saturation point is $\Delta\varepsilon$ =0.0698. See Fig. 3. This value of $\Delta\varepsilon$ has been found to be very close to the value of $\Delta\varepsilon_2 - \Delta\varepsilon_1$ from Fig. 2(a).

Optical cross-polarizing microscopy studies on the same

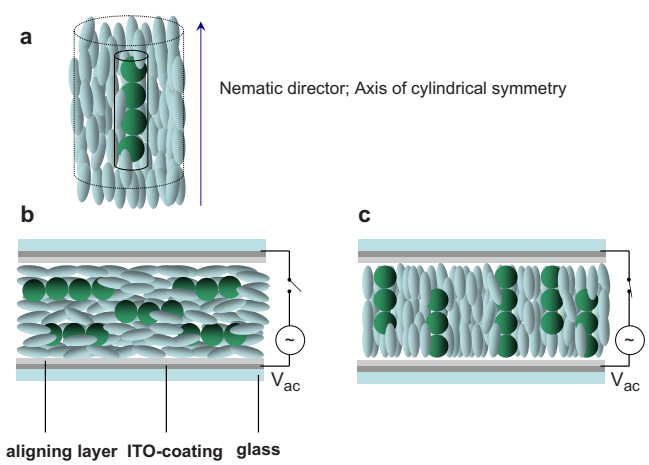

FIG. 4. (Color online) Schematic diagrams; (a) dotted cylinder shows the cylindrical symmetry of uniaxial nematic phase; the small cylinder shows the cylindrical confinement of self-assembled QDs aggregation; (b) electrode-surface-induced homogeneous alignment of nematic LC molecules (ellipsoidal), and QD self-assembly (spherical) in the nematic matrix; (c) electric field-induced homeotropic alignment of nematic LC molecules, and homeotropically directed one-dimensional QD arrays.

sample of 5CB+QD was attempted. The micrographs reveal a uniform texture indicating a uniform nematic director field. No indicates of phase separation or large scale agglomerates were observed at any temperature. Thus, at least on the length scales probed by visible light, the arrangements of the QD must be small structures due to their low concentration and uniformly distributed. More detailed optical and x-ray studies would be of great benefit to directly probe the local QD assemblies.

A rough estimation of number of QD chains and number of QDs in a chain can be made based on the following simple model. For the QD chains, as explained earlier, the *homogeneous* configuration contributes $\varepsilon_{\parallel}$ and the *homeotropic* configuration contributes $\varepsilon_{\perp}$ to the average dielectric constant of the host system, $\Delta\varepsilon=\varepsilon_{\parallel}-\varepsilon_{\perp}$. Quantum dots were initially dispersed isotropically in toluene solvent. One can extract the average contribution, $\delta\varepsilon_0$, of QDs to the dielectric constant of any isotropic media once the average dielectric constants for the QD+toluene sample and pure toluene are known. If n is the number of QDs in a chain, then one can write $\Delta\varepsilon \cong n\delta\varepsilon_0 - \delta\varepsilon_0$ or $n=(\Delta\varepsilon/\delta\varepsilon_0)-1\approx 2000$ using the dielectric values measured here. The total number of QDs in the 5CB+QD sample within the capacitive cell is known to be roughly $N\approx 70\times 10^{12}$, and so the total number of chains is approximately $m=n/N=35\times 10^9$. This is small compared to the total number of 5CB molecules, but their arrangement into LC+field aligned chains can significantly influence the measured dielectric constant. See Fig. 4.

In summary, the dynamics of 5CB+CdS system has been probed by studying average dielectric response to understand the stability of this system. The results clearly demonstrate that the nematic phase imposes self-assembly on QDs to form one-dimensional arrays. An application of electric field can direct the axis of the self-aggregation in a preferred orientation direction as illustrated in Fig. 4. This is consistent with the behavior in the isotropic phase being independent of E_{ac}, and the enhanced $\bar{\varepsilon}$ above $E_{ac}=50$ kV/m, indicating that only the nematic phase of LC induces this self-assembly on CdS nanocrystals. This Rapid Communication opens up future theoretical and experimental studies to get precise information on structures of QD arrays. Future work involves optoelectric studies of field-induced fluorescence spectra for different sizes of QDs in nematic LC media.

[1] X. Tong and Y. Zhao, J. Am. Chem. Soc. **129**, 6372 (2007).
[2] S.-W. Lee, C. Mao, C. E. Flynn, and A. M. Belcher, Science **296**, 892 (2002).
[3] C. Jiang, S. Xu, D. Yang, F. Zhang, and W. Wang, J. Biolumin. Chemilumin. **22**, 430 (2007).
[4] J. Zhao, J. A. Bardecker, A. M. Munro, M. S. Liu, Y. Niu, I-K. Ding, J. Luo, B. Chen, A. K.-Y. Jen, and D. S. Ginger, Nano Lett. **6**, 463 (2006).
[5] A. Balandin, K. L. Wang, N. Kouklin, and S. Bandyopadhyay, Appl. Phys. Lett. **76**, 137 (2000).
[6] K. L. Wang and A. Balandin, in *Optics of Nanostructed Materials*, edited by V. A. Markel and T. F. George (Wiley, New York, 1999).
[7] S. Fafard, Z. R. Wasilewski, C. Ni Allen, D. Picard, P. G. Piva, and J. P. McCaffrey, Superlattices Microstruct. **25**, 87 (1999).
[8] W. Chen, A. G. Joly, J. O. Malm, J. O. Bovin, and S. Wang, J. Phys. Chem. B **107**, 6544 (2003).
[9] M. Tamborra, M. Striccoli, R. Comparelli, M. Curri, A. Petrella, and A. Agostiano, Nanotechnology **15**, S240 (2004).
[10] M. D. Lynch and D. L. Patrick, Nano Lett. **2**, 1197 (2002).
[11] I. Dierking, G. Scalia, and P. Morales, J. Appl. Phys. **97**, 044309 (2005).
[12] R. Basu and G. Iannacchione, Appl. Phys. Lett. **93**, 183105 (2008).
[13] L. Onsager, Ann. N. Y. Acad. Sci. **51**, 627 (1949).
[14] L. C. T. Shoute and D. F. Kelley, J. Phys. Chem. C **111**, 10233 (2007).
[15] P. G. de Gennes and J. Prost, *The Physics of Liquid Crystals* (Oxford University Press, New York, 1974).
[16] CdS quantum dots (stabilized by oleic acid ligands) in toluene solvent (CS360–10) is commercially available from Nanomaterials and Nanofabrication Laboratories (http://www.nn-labs.com).
[17] Empty LC cells (LC2-20.0, homogeneous antiparallel rubbed with 1° pre-tilt) are commercially available from Instec Research Instrumentation Technology.
[18] S. Pilla, J. A. Hamida, and N. S. Sullivan, Rev. Sci. Instrum. **70**, 4055 (1999).
[19] R. Basu and G. Iannacchione, Appl. Phys. Lett. **92**, 052906 (2008).
[20] M. C. Foote and A. C. Anderson, Rev. Sci. Instrum. **58**, 130 (1987).
[21] R. Basu and G. Iannacchione, J. Appl. Phys. **104**, 114107 (2008).

Nematic anchoring on carbon nanotubes

Rajratan Basu[a)] and Germano S. Iannacchione[b)]
Department of Physics, Order-Disorder Phenomena Laboratory, Worcester Polytechnic Institute, Worcester, Massachusetts 01609, USA

(Received 5 August 2009; accepted 7 October 2009; published online 29 October 2009)

A dilute suspension of carbon nanotubes (CNTs) in a nematic liquid crystal (LC) does not disturb the LC director. Due to a strong LC-CNT anchoring energy and structural symmetry matching, CNT long axis follows the director field, possessing enhanced dielectric anisotropy of the LC media. This strong anchoring energy stabilizes local *pseudonematic* domains, resulting in nonzero dielectric anisotropy in the isotropic phase. These anisotropic domains respond to external electric fields and show intrinsic frequency response. The presence of these domains makes the isotropic phase electric field-responsive, giving rise to a large dielectric hysteresis effect. © *2009 American Institute of Physics*. [doi:10.1063/1.3256013]

Nematic liquid crystals (LCs) have gained great research interest in recent years for nanotemplating purposes, imparting their orientational order onto dispersed nanomaterials.[1–7] Hybrid liquid crystal-carbon nanotube (CNT) systems increasingly rely on improving electro-optic properties of LCs,[4] obtaining directed-self assembly of CNTs over macroscopic dimensions,[1,2] and developing nanoelectromechanical systems.[3] The CNT alignment mechanism is driven by the coupling of the unperturbed *director field* (average direction of LC molecules) to the anisotropic interfacial tension of the CNTs in the nematic LC matrix, as individual CNTs (not in bundle) are much thinner than the elastic penetration length.[8] So, a dilute suspension is stable because dispersed CNTs, without large agglomerates, does not perturb the director field significantly. Consequently, the suspended nanotubes share their intrinsic properties with the LC matrix, such as electrical conductivity,[2] due to the alignment with the LC molecules. A dilute suspension of CNTs in an LC matrix is a unique assemblage of an anisotropic dispersion (CNTs) in an anisotropic media (LC), which makes it an important and active area of research for realizing the LC-CNT interactions and the principles governing CNT-assembly through a nematic mediated platform. We observe that the presence of a small concentration of well-dispersed CNTs in an LC matrix produces enhanced dielectric anisotropy in the nematic phase and nonzero dielectric anisotropy in the isotropic phase. In this letter, we report the ac field-induced dielectric ($\bar{\varepsilon}$) response for multiwall carbon nanotubes (MWCNTs) dispersed in 4-cyano-4′-pentylbiphenyl (5CB) LC in both the nematic and isotropic phases.

The nematic phase shows dielectric anisotropy due to the anisotropic nature of the LC molecules where $\varepsilon_{\parallel}$ and $\varepsilon_{\perp}$ are the components parallel and perpendicular to the molecular long axis, respectively. For a positive dielectric anisotropic LC, $\varepsilon_{\parallel} > \varepsilon_{\perp}$, and so, the director field reorients parallel to an applied electric field. In a uniform homogeneously aligned parallel-plate cell configuration, the nematic director is aligned perpendicular to the applied electric field due to surface anchoring, but the director can reorient parallel to the applied field if the field magnitude is above some critical threshold. This is the essence of a Fréedericksz transition and an ac-capacitive measurement of the $\bar{\varepsilon}$ reveals $\varepsilon_{\perp}$ below and $\varepsilon_{\parallel}$ above this switching, the exact values depending on frequency.

The hybrid LC-CNT mixture was prepared by dispersing 0.005 wt % of MWCNT sample (containing nanotubes <8 nm in diameter and 0.5–2 μm in length) in 5CB ($T_{\text{nematic-isotropic}}$=35 °C) host via ultrasonication for 5 h to reach monodispersion of CNTs. Soon after ultrasonication, the mixture was degassed under vacuum at 40 °C for at least two hours. The mixture then was filled into a homogeneous LC cell (5×5 mm^2 indium tin oxide (ITO) coated area and 20 μm spacing[9]) by capillary action. Before performing any dielectric measurements, the CNT doped LC cell was studied under a cross polarized microscope. The micrographs revealed a uniform texture, like a pure LC cell, indicating a uniform nematic director field. There were no indications of phase separation or agglomerates at any temperature. Thus, at least on the length-scales probed by visible light, the structure of CNT-aggregates (if any) must be small enough that they don't perturb the director field due to their low concentration.

The dielectric ($\bar{\varepsilon}$) measurements, as a function of applied ac voltage, frequency, and temperature, were performed by the ac capacitance bridge technique[10–12] in the nematic and isotropic phases. The reason for applying the ac voltage (not dc) is to avoid the affect of ion migration on the dielectric measurements. The LC 5CB does not exhibit any tumbling mode[13] and MWCNTs show no space charge or dipole orientation dynamics[14] at the probing frequencies. Thus, the observed increase in $\bar{\varepsilon}$ as a function of applied ac voltage should be driven mainly by a mechanical rotation of the nematic director field.

Figure 1(a) shows the average dielectric constant ($\bar{\varepsilon}$) as a function of applied ac voltage for 5CB and 5CB+MWCNT sample in the nematic phase (T=23 °C). As seen in the Fig. 1, both the pure LC and the mixture undergo planner ($\varepsilon_{\perp}$) to homeotropic ($\varepsilon_{\parallel}$) orientational transition, starting at around 0.9 V, saturating at around 7 V. The dielectric anisotropy ($\Delta\varepsilon=\varepsilon_{\parallel}-\varepsilon_{\perp}$) for pure 5CB is around +10,[15] as also observed experimentally ($\Delta\varepsilon_{\text{LC}}$=+10.1) in Fig. 1(a). The presence of CNTs in LC results in an increase in the dielectric anisotropy ($\Delta\varepsilon_{\text{LC+CNT}}$=+11.1), enhancing the order parameter, $S(T)$, in

[a)]Electronic mail: basu@wpi.edu.
[b)]Electronic mail: gsiannac@wpi.edu.

 © 2009 American Institute of Physics

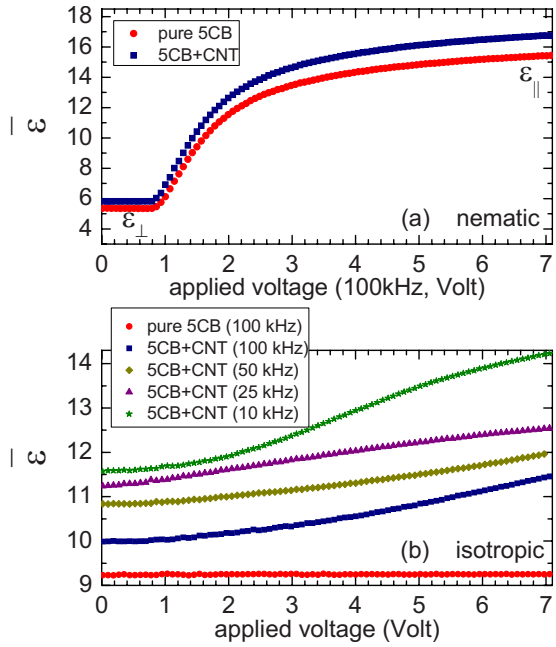

FIG. 1. (Color online) (a) The average dielectric constant $\bar{\varepsilon}$ as a function of applied ac voltage for 5CB and 5CB+CNT in the nematic phase (T=23 °C); (b) The average dielectric constant $\bar{\varepsilon}$ as a function of applied ac voltage for 5CB and 5CB+CNT in the isotropic phase (T=45 °C).

the nematic matrix. It is important to point out that this dramatic increase occurred due to the addition of only 0.005 wt % MWCNT sample. It has been experimentally shown that the isotropic to nematic phase transition temperature of a liquid crystal is enhanced by the incorporation of small amount of MWNT sample,[16] indicating an improvement in the nematic order. A recent study shows that CNTs induce alignment on the nematic LC director field along their long axes due to LC-CNT anchoring effect.[6] Theoretical calculations predict that the strong interaction associated with the CNT alignment mechanism is mainly due to surface anchoring with a binding energy $U_{\text{anchor}}=-2$ eV for π-π stacking between CNT and LC molecules.[4,17] As the nanotubes used for this work are not ferroelectric in nature, the additional ordering effect must not be due to the electronic coupling of any permanent dipole moments with the LC dielectric anisotropy; which generally occurs in ferroelectric nanoparticle suspensions in the LCs.[18] Thus, the increase in $\Delta\varepsilon$ [hence, improvement in nematic order, as $\Delta\varepsilon \propto S(T)$ (Ref. 19)] is attributed to the anchoring energy and anisotropic structure of CNTs. The reorientation threshold voltage V_{th} can be estimated by the expression for the Fréedericksz transition:[19] $V_{\text{th}} \propto \sqrt{K/\Delta\varepsilon}$; where K is the elastic constant for bent distortion. From Fig. 1(a), as $V_{\text{th}}^{\text{LC}} \simeq V_{\text{th}}^{\text{LC+CNT}}$, one can write, $\sqrt{K_{\text{LC}}/\Delta\varepsilon_{\text{LC}}} \simeq \sqrt{K_{\text{LC+CNT}}/\Delta\varepsilon_{\text{LC+CNT}}}$; which gives $K_{\text{LC+CNT}} \simeq 1.21 K_{\text{LC}}$. The strong elastic interaction between CNTs and LC molecules due to surface anchoring may increase the elastic energy of the hybrid system and therefore can be attributed to the increase in K in the LC+CNT system.

As the dielectric constant of a material is determined by the structural arrangement and molecular polarizability, the dielectric spectra for 5CB and 5CB+CNT have been studied in the range 10^3–10^5 Hz to probe any structural modification in hybrid 5CB+CNT system. The spectra, shown in Fig. 2, reveal significant difference in dielectric behavior between 5CB and 5CB+CNT, confirming a structural modification in

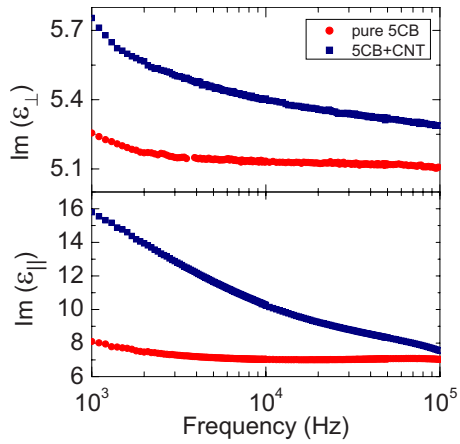

FIG. 2. (Color online) Imaginary part of $\varepsilon_{\perp}$ (top panel) and $\varepsilon_{\parallel}$ (bottom panel) for 5CB and 5CB+MWCNT in the nematic phase (T=23 °C).

the nematic phase due to the addition of a small amount of CNT sample.

Due to the absence of elastic interactions in the isotropic phase, the LC molecules no longer maintain long range orientation order and act as an isotropic liquid. Isotropic phase of 5CB, as expected, does not respond to an external field, as also experimentally confirmed in Fig. 1(b). But, a dramatic change in the field-induced dielectric constant has been observed in the isotropic phase for the LC+CNT system. The composite system shows an increment in $\bar{\varepsilon}$ with increasing applied voltage, as shown in Fig. 1(b). As stated earlier, the energy associated with LC-CNT anchoring mechanisms is $|U_{\text{anchor}}|=2$ eV, which is much more than the thermal energy, $U_{\text{thermal}} \sim k_B T = 2.74 \times 10^{-2}$ eV, for the deep isotropic phase at T=45 °C=318 K. So, the thermal energy is not even close enough to eliminate the anchoring mechanisms in the deep isotropic phase. Due to this surface anchoring, the CNT induces local short-range orientation order of LC molecules surrounding the CNT having local director along the tube axis, which can be visualized as presence of isolated *pseudonematic* domains in an isotropic media, as schematically shown in Fig. 3(a). As these local anisotropic pseudonematic domains have polarization, their *short-range director field* interact with external electric fields—hence, observed increase in $\bar{\varepsilon}$ with increasing applied voltage in the

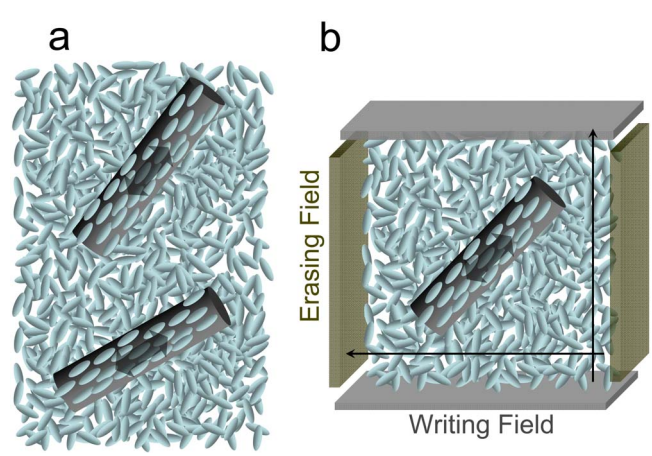

FIG. 3. (Color online) Schematic diagrams; (a) presence of field-responsive anisotropic pseudonematic domains due to LC (ellipsoidal)–CNT (cylindrical) interaction in the isotropic media; (b) a model for a four-electrode LC cell for writing and erasing memory.

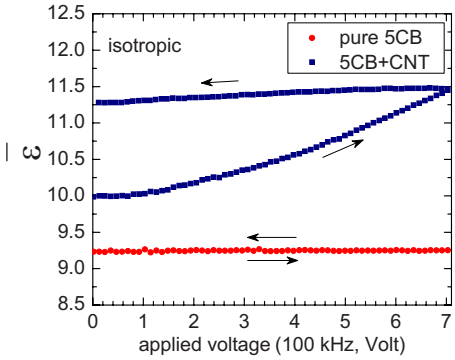

FIG. 4. (Color online) Dielectric hysteresis for 5CB and 5CB+CNT. The arrows show the cycling direction of the applied ac voltage.

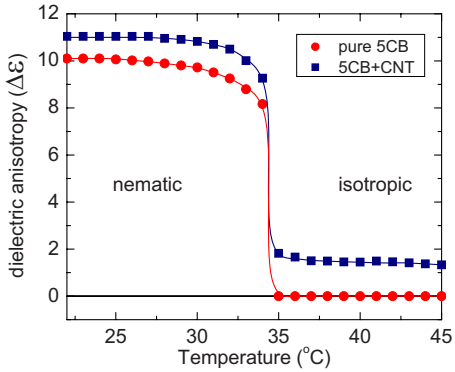

FIG. 5. (Color online) Dielectric anisotropy as a function of temperature for 5CB and 5CB+CNT. Lines represent guide to the eye.

isotropic phase. These nanoscale anisotropic domains seem to have strong frequency response as the change in $\bar{\varepsilon}$ is different for different frequencies from 10 to 100 kHz in the same applied voltage range, observed in Fig. 1(b).

Dielectric hysteresis has been studied in the isotropic phase (T=45 °C) to understand the stability of these pseudonematic domains, see Fig. 4. The isotropic phase for pure 5CB does not show any hysteresis effect, as expected, as it does not respond to an external electric field. After reaching the maximum dielectric value at the highest applied field, $\bar{\varepsilon}$ for the composite system does not relax back to its original value cycling the field down to zero, showing a large dielectric hysteresis unlike the nematic phase. As there is no long range orientational order, there is no elastic interaction present in the isotropic LC media. As a result, when the field goes off, there is no restoring force to mechanically torque these domains back into the original orientation in the isotropic phase and the domains stay oriented. This indicates that CNTs, surrounded by few layers of LCs, stabilize nematiclike short-range order in the isotropic phase, giving rise to a ferroelectric type hysteresis. This is the essence of a nonvolatile electromechanical memory effect. This memory may be erased by applying another field in the opposite direction of the first one in a four-electrode cell configuration as shown in Fig. 3(b). In that case the writing and erasing time can be in the order of the tumbling relaxation mode of the LC, which is 0.1 GHz (Ref. 13) for 5CB. However, the time response would also depend on the distribution symmetry of the CNTs in the LC media.

The extracted dielectric anisotropy $\Delta\varepsilon$ for 5CB and 5CB+CNT is plotted as a function of temperature in Fig. 5. The composite system shows enhanced $\Delta\varepsilon$ in the nematic phase. As the order parameter[19] for the pure isotropic phase is zero, $\Delta\varepsilon$ for pure 5CB drops down to zero in the isotropic phase. The composite system shows a nonzero value of $\Delta\varepsilon$ (Ref. 20) indicating the presence a net residual order in the isotropic phase. The value of $\Delta\varepsilon$ in the isotropic phase changes with increasing frequency in the frequency range (10–100 kHz) studied.

In conclusion, we have observed that dispersing a low concentration of CNTs in a nematic LC, results in an improvement in the nematic ordering, showing enhanced $\Delta\varepsilon$. The presence of local anisotropic pseudonematic domains in the isotropic phase in the system causes an electromechanical hysteresis effects which could find potential applications in memory functions. Future work involves simultaneous dielectric and optical studies on size dependent CNT suspensions in LC media to investigate more on the anchoring effect in both the nematic and isotropic phases.

[1] M. D. Lynch and D. L. Patrick, Nano Lett. **2**, 1197 (2002).
[2] I. Dierking, G. Scalia, and P. Morales, J. Appl. Phys. **97**, 044309 (2005).
[3] R. Basu and G. Iannacchione, Appl. Phys. Lett. **93**, 183105 (2008).
[4] I. S. Baik, S. Y. Jeon, S. H. Lee, K. A. Park, S. H. Jeong, K. H. An, and Y. H. Lee, Appl. Phys. Lett. **87**, 263110 (2005).
[5] P. V. Kamat, K. G. Thomas, S. Barazzouk, G. Girishkumar, K. Vinodgopal, and D. Meisel, J. Am. Chem. Soc. **126**, 10757 (2004).
[6] J. M. Russell, S. Oh, I. LaRue, O. Zhou, and E. T. Samulski, Thin Solid Films **509**, 53 (2006).
[7] R. Basu and G. Iannacchione, Phys. Rev. E **80**, 010701 (2009).
[8] P. P. A. M. van der Schoot, V. Popa-nita, and S. Kralj, J. Phys. Chem. B **112**, 4512 (2008).
[9] Empty LC cells (LC2-20.0, homogeneous anti-parallel rubbed with 1° pretilt) are commercially available from Instec Research Instrumentation Technology.
[10] S. Pilla, J. A. Hamida, and N. S. Sullivan, Rev. Sci. Instrum. **70**, 4055 (1999).
[11] M. C. Foote and A. C. Anderson, Rev. Sci. Instrum. **58**, 130 (1987).
[12] R. Basu and G. Iannacchione, J. Appl. Phys. **104**, 114107 (2008).
[13] F. Kremer and A. Schonhals, *Broadband Dielectric Spectroscopy* (Springer, Berlin, 2003).
[14] R. Basu and G. Iannacchione, Appl. Phys. Lett. **92**, 052906 (2008).
[15] D. A. Dunmur, M. R. Manterfield, W. H. Miller, and J. K. Dunleavy, Mol. Cryst. Liq. Cryst. (Phila. Pa.) **45**, 127 (1978).
[16] H. Duran, B. Gazdecki, A. Yamashita, and T. Kyu, Liq. Cryst. **32**, 815 (2005).
[17] K. A. Park, S. Mi Lee, S. Hee Lee, and Y. Hee Lee, J. Phys. Chem. C **111**, 1620 (2007).
[18] Y. Reznikov, O. Buchnev, O. Tereshchenko, V. Reshetnyak, A. Glushchenko, and J. West, Appl. Phys. Lett. **82**, 1917 (2003).
[19] P. G. de Gennes and J. Prost, *The Physics of Liquid Crystals* (Oxford University Press, New York, 1974).
[20] $\Delta\varepsilon$ for the composite system in the isotropic phase is defined as ($\bar{\varepsilon}_{max} - \bar{\varepsilon}_{min}$), where $\bar{\varepsilon}_{max}$ and $\bar{\varepsilon}_{min}$ are determined from the "$\bar{\varepsilon}$ versus applied voltage" graph [Fig. 1(b)] at different temperatures above the nematic-isotropic transition temperature.

Dielectric hysteresis, relaxation dynamics, and nonvolatile memory effect in carbon nanotube dispersed liquid crystal

Rajratan Basu[a)] and Germano S. Iannacchione[b)]
Department of Physics, Order-Disorder Phenomena Laboratory, Worcester Polytechnic Institute, Worcester, Massachusetts 01609, USA

(Received 7 May 2009; accepted 12 November 2009; published online 23 December 2009)

Self-organizing nematic liquid crystals (LCs) impart their orientational order onto dispersed carbon nanotubes (CNTs) and obtain CNT-self-assembly on a macroscopic dimension. The nanotube-long axis, being coupled to the nematic director, enables orientational manipulation via the LC nematic reorientation. Electric-field-induced director rotation of a nematic LC+CNT system is of potential interest due to its possible application as a nanoelectromechanical system. Electric field and temperature dependence of dielectric properties of a LC+CNT composite system have been investigated to understand the principles governing CNT assembly mediated by the LC. In the LC+CNT nematic phase, the dielectric relaxation on removing the applied field follows a single-exponential decay, exhibiting a faster decay response than the pure LC above a threshold field. The observed dielectric behaviors on field cycling in the nematic phase for the composite indicates an electromechanical hysteresis effect of the director field due to the LC-CNT anchoring mechanism. Observations in the isotropic phase coherently combine to confirm the presence of anisotropic *pseudonematic* domains stabilized by the LC-CNT anchoring energy. These polarized domains maintain local directors and respond to external fields, but do not relax back to the original state on switching the field off, showing nonvolatile memory effect. © *2009 American Institute of Physics*. [doi:10.1063/1.3272080]

I. INTRODUCTION

Self-organizing nematic liquid crystal (LC) has gained interest in recent years for transferring orientational order onto suspended nanoparticles.[1–8] It has been demonstrated that inside a nematic LC matrix, the long axes of carbon nanotubes (CNTs) orient parallel to the *director field* (average direction of LC molecules) with an orientational order parameter S between 0.6 and 0.9,[1,2,7] while bulk nematic LCs themselves have orientational order of $S \approx 0.6$. Recent theoretical work shows that a strong interaction, mainly due to surface anchoring with a binding energy of about -2 eV for π-π stacking between LC-CNT,[4,9] is associated with the CNT alignment mechanism in the nematic state. It has also been known theoretically for some time that the distribution of orientations of the nanosize anisotropic guest particles in an anisotropic and ordered solution is along the symmetry axis of the solution.[10] An anisotropic nematic LC shows cylindrical symmetry along the director field.[10,11] Thus, the anchoring energy favors the dispersed CNT long axis parallel to the director field, minimizing the elastic distortion of the nematic matrix, which is essential a minimization of excluded volume.[10] This is shown schematically in Fig. 1.

As the CNTs are much thinner than the elastic penetration length, the alignment is driven by the coupling of the unperturbed director field to the anisotropic interfacial tension of the CNTs in the nematic LC matrix.[12] Thus, the concentration of CNTs in LC is a very important parameter for this alignment process as monodispersion without any agglomerates is needed. The dilute suspensions are stable because well dispersed CNTs individually (not in bundles) do not perturb the director field significantly. Consequently, the nanotubes share their intrinsic properties with the LC matrix, such as electrical conductivity[2] due to the alignment with the LC molecules. Thus, comprehensive understanding of the interaction of CNTs with a LC and the principles governing their self-assembly through LC mediated interactions is an important and active area of research. Exploiting the nematic LC for nanotemplating purposes and controlling the director by applying fields make the LC+CNT mixture an attractive anisotropic physical system to study the Fréedericksz switching through an electromechanical response at the nanoscale level. After a field-induced director rotation of the nematic in a LC+CNT (Refs. 1–3) contained in a planar LC cell,[13] the LC molecules, as well as the CNTs, dynamically reorient

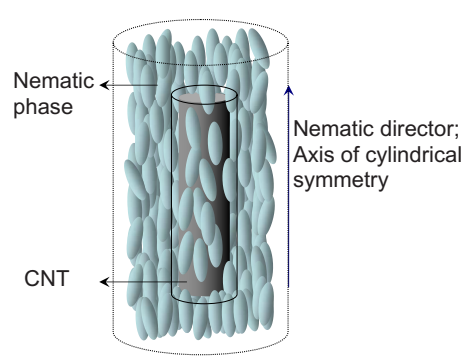

FIG. 1. (Color online) Schematic of symmetry matching; the dotted cylinder shows the cylindrical symmetry of uniaxial nematic phase; the small cylinder shows the cylindrical confinement of a CNT.

[a)]Electronic mail: basu@wpi.edu.
[b)]Electronic mail: gsiannac@wpi.edu.

 © 2009 American Institute of Physics

Author complimentary copy. Redistribution subject to AIP license or copyright, see http://jap.aip.org/jap/copyright.jsp

back into their original orientation on the immediate removal of the electric field, exhibiting the intrinsic relaxation dynamics. The LC media, such as nematic phase or isotropic phase, strongly influence the reorientation and relaxation mechanisms of the CNTs.

In this paper, we report the dynamic response, the hysteresis effect, and the temperature dependence of the dielectric constant ($\bar{\varepsilon}$) for multiwalled carbon nanotubes (MWCNTs) dispersed in 4-cyano-4′-pentylbiphenyl (5CB) LC in both the nematic and isotropic phases. The nematic phase shows dielectric anisotropy due to the anisotropic nature of the LC molecules where $\varepsilon_{\parallel}$ and $\varepsilon_{\perp}$ are the components parallel and perpendicular to the molecular long axis, respectively. For a positive dielectric anisotropic LC, $\varepsilon_{\parallel} > \varepsilon_{\perp}$, and so, the director field reorients parallel to an applied electric field. In a uniform homogeneously aligned parallel-plate cell configuration, the nematic director is aligned perpendicular to the applied electric field due to surface anchoring, but the director can reorient parallel to the field if the field magnitude is above some critical threshold. This is the essence of a Fréedericksz transition, and an ac-capacitance measurement of the $\bar{\varepsilon}$ will reveal $\varepsilon_{\perp}$ below and $\varepsilon_{\parallel}$ above this switching, the exact values depending on frequency. Having a very high aspect ratio, CNTs also exhibit dielectric anisotropy.

Following this introduction, a description of the materials, sample preparation, and ac-capacitance bridge technique are given in Sec. II. Dielectric hysteresis, dynamic response of $\bar{\varepsilon}$, and temperature dependence of $\bar{\varepsilon}$ are presented in Sec. III, followed by conclusions in Sec. IV.

II. EXPERIMENTAL PROCEDURES

A. Materials and sample preparation

The MWCNT sample used for this experiment contains nanotubes <8 nm in diameter and 0.5–2 μm in length with purity of 95%, purchased from Nanostructured and Amorphous Materials, Inc. The well characterized LC 5CB used for this experiments has a nematic to isotropic phase transition at temperature $T_{NI}=35$ °C. A small amount (0.005 wt %) of MWCNT sample was dispersed in 5CB, and the mixture was ultrasonicated for 5 h to reduce the bundling tendency of CNTs. Soon after ultrasonication, the mixture was degassed under vacuum at 40 °C for at least 2 h. The mixture then was filled into a homogeneous LC cell (5×5 mm^2 indium tin oxide coated area and 20 μm spacing) by capillary action, housed in a temperature controlled bath. The typical amount of the LC filled into the cell is around 0.5 mg. The cell spacing filters out any nanotube aggregates larger than the spacing dimension. Surface treatment inside the LC cell induces the planar alignment to the nematic director.[13] Empty LC cells were measured separately first in order to extract the $\bar{\varepsilon}$. The relaxation dynamics also depend on cell configuration; for comparisons, the same type of cells was used for both pure 5CB and 5CB+MWCNT.

B. ac-capacitance bridge technique and dielectric spectrometer

The dielectric measurements were performed by the ac-capacitance bridge technique,[14–16] operating with a probing field E at 100 kHz frequency. Comparison between the empty capacitance (C_o) and sample filled cell capacitance (C_s) allows for a relative measurement of dielectric constant $\bar{\varepsilon}(=C_s/C_o)$ with respect to the empty cell. The probing field E (100 kHz), in a capacitive measurement, is in phase and at the same frequency as the measurement of the complex dielectric constant $\bar{\varepsilon}$ (100 kHz). Thus, in the complex *rotating frame* of the measurement, the probing field E (100 kHz) can be considered a "static" field.[17] After the sample was freshly loaded into the cell, dielectric hysteresis experiments were performed by cycling the E (100 kHz) field magnitude ranging from $25 \leftrightarrow 250$ kV/m and monitoring $\bar{\varepsilon}(E)$. The field annealing treatment trains the sample to improve the nematic ordering controlling any defects in the nematic matrix. Temperature annealing was also performed by heating the system to isotropic phase and then cooling it down to the nematic phase, but no thermal hysteresis was observed.

After the completion of field and temperature annealing, an external ac electric field pulse E_{ac} (1 MHz) of 30 s duration was applied across the cell at magnitudes ranging from 0 to 250 kV/m. The field E_{ac} (1 MHz) is independent of the capacitance bridge and measurement technique. The reason for applying the ac field (not dc) is to avoid the effect of ion migration or ionic conduction on the dielectric relaxation measurements. Once E_{ac} was turned off (at $t=0$ s), isothermal average dielectric $\bar{\varepsilon}(t)$ measurements were carried in the nematic ($T=25$ °C) and isotropic ($T=37$ °C) phases as a function of time. The magnitude of the probing field E (5 kV/m, 100 kHz) was kept far below the Fréedericksz reorientation threshold field during this measurement. The LC 5CB does not exhibit any tumbling relaxation mode[18] and MWCNTs show no space charge or dipole orientation dynamics at this probing frequency, 100 kHz.[16,19] Therefore, the observed dielectric relaxation is caused mainly by a mechanical relaxation mechanism of the director on turning E_{ac} off. The temperature dependence of $\bar{\varepsilon}$ was studied in order to understand the behavior of nematic and isotropic phases of the LC in the presence of CNTs. The temperature dependence of $\bar{\varepsilon}$ provides information about the isotropic to nematic phase transition and the structural changes due to the anchoring energy arising from the presence of CNTs.

III. RESULTS AND DISCUSSIONS

A. Dielectric hysteresis in the nematic phase

Figure 2(a) depicts the dielectric hysteresis effects for 5CB and 5CB+MWCNT in the nematic phase ($T=25$ °C). The area under the hysteresis loop, which is proportional to the energy lost during the cycle, is shown in Fig. 2(b). The hysteresis area for bulk 5CB decreases by a considerable amount after the first cycle and then remains constant for the rest of the number of cycles performed. A vivid change in the dielectric hysteresis has been observed for the composite system. The first cycle shows the highest amount of hysteresis loss, which gradually decreases through the second and third

Author complimentary copy. Redistribution subject to AIP license or copyright, see http://jap.aip.org/jap/copyright.jsp

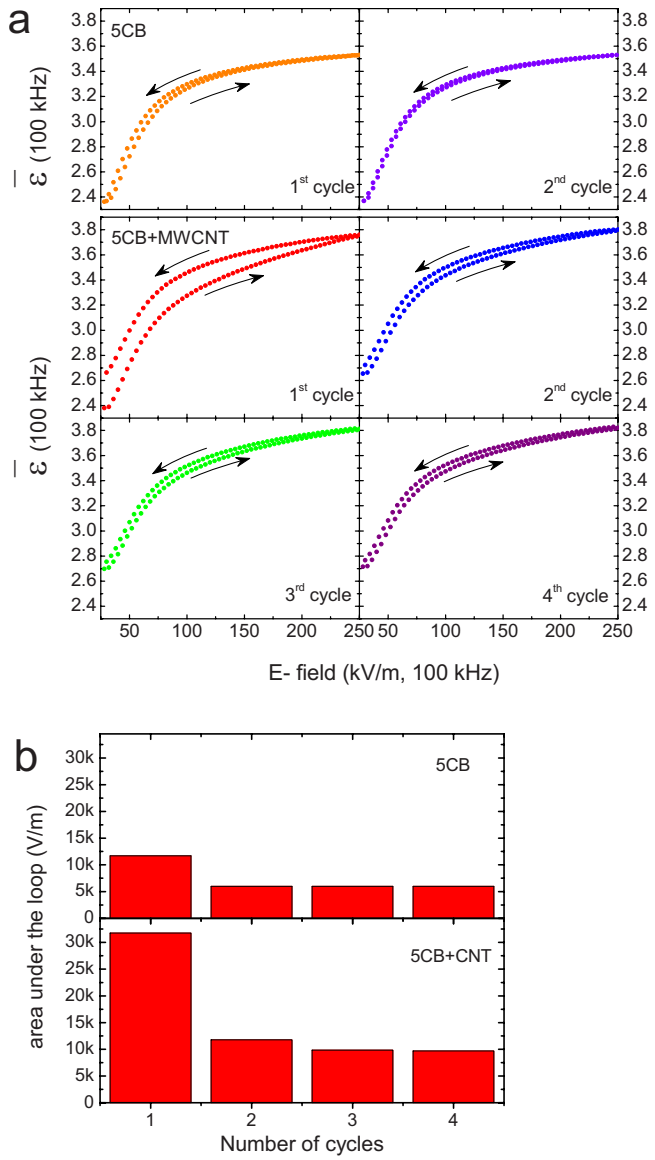

FIG. 2. (Color online) (a) Field annealing hysteresis cycles, $\bar{\varepsilon}$ vs E, for 5CB (top two panels) and 5CB+MWCNT (bottom four panels) in the nematic phase (T=25 °C). (b) The area under the hysteresis loops as a function number of cycles for 5CB and 5CB+MWCNT.

cycles, reaching saturation at the fourth cycle. After the fourth cycle the hysteresis area remains the same throughout the rest of the number of annealing cycles performed. It is important to note that this dramatic change is observed due to the presence of only 0.005 wt % of MWCNTs in the nematic LC media. As an ac field is used for this annealing process, ion migration or ionic conduction has no contribution to the dielectric behavior observed, and so, the hysteresis effects observed are not caused by the residual dc effect.

The structural changes due to the application of an ac field in the LC-CNT nematic matrix result in the observed *electromechanical* hysteresis of the director field. The LC-CNT anchoring energy increases the elastic constant for bent distortion in the nematic phase, increasing the elastic energy in the LC molecules.[20,21] The increase in the elastic constant for bent distortion leads the director field to follow different paths during field cycling up and down, hence the observed electromechanical hysteresis in the LC-CNT hybrid system.

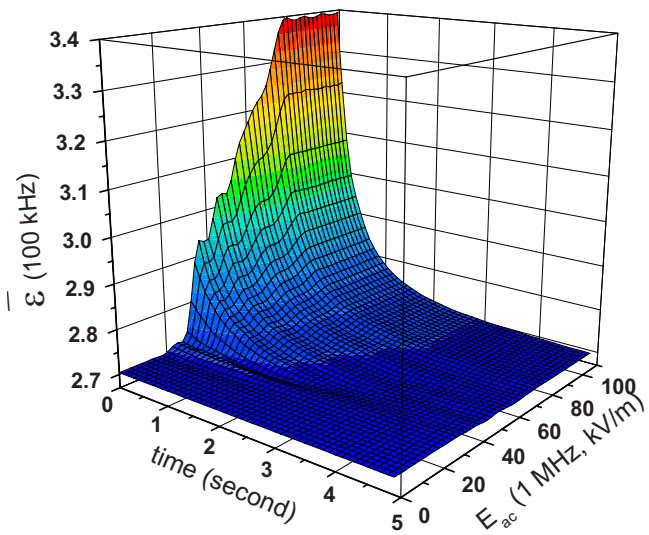

FIG. 3. (Color online) Dynamic response of the average dielectric constant $\bar{\varepsilon}$ for 5CB+MWCNT as a function of *time* and E_{ac} (1 MHz) in the nematic phase (T=25 °C) after E_{ac} goes off.

The hysteresis area has been found to be increasing with increasing CNT concentration. Also, the multiple field annealing controls LC defects[22] and perhaps results in a reduction in the defects in the matrix inside the cell, hence, decreasing the hysteresis area with increasing cycle number for the first few cycles.

B. Relaxation dynamics of $\bar{\varepsilon}$ in the nematic phase

The planar rubbing direction on the surface of the electrodes inside the LC cell acts as an anchoring field that induces homogeneous alignment on the first few LC layers touching the top and bottom electrodes. Then, the elastic interaction between the LC molecules makes the homogeneous alignment propagate through the whole media, obtaining a planar director profile inside the cell. Being embedded in the nematic matrix CNT long axis also follows the planar director field. Electric-field-induced director reorientation occurs when the torques, due to the external electric field, overcome the elastic interactions between LC molecules, and, through surface coupling, the CNT long axis follows the director rotation. Soon after the field goes off, these restoring forces, between the planar surface state and the LC director, drive the system back to the planar configuration through a mechanical rotation.

The dielectric constant $\bar{\varepsilon}$ as a function of time and E_{ac}, after switching E_{ac} off for the 5CB+MWCNT sample in the nematic phase (T=25 °C), is shown in Fig. 3. The relaxation of $\bar{\varepsilon}$ follows a single-exponential decay, reaching its original value. The field-saturated dielectric constant $\bar{\varepsilon}_{max}$ ($\bar{\varepsilon}$ at t=0, from Fig. 3) for each relaxation is plotted as a function of E_{ac} in Fig. 4 and is directly associated with the director profile. The value of $\bar{\varepsilon}_{max}$ starts to increase above E_{ac}=20 kV/m for both pure LC and LC+CNT samples, confirming the director reorientation from planar to homeotropic, but $\bar{\varepsilon}_{max}$ saturates at a higher field for the composite sample than pure 5CB; see Fig. 4. This is probably due to the higher aspect ratio of CNTs that require higher fields to fully reorient. As men-

Author complimentary copy. Redistribution subject to AIP license or copyright, see http://jap.aip.org/jap/copyright.jsp

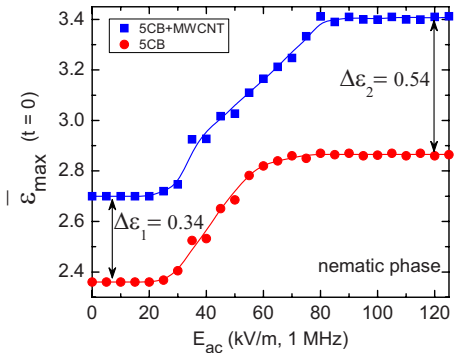

FIG. 4. (Color online) Field-saturated dielectric constant, $\bar{\varepsilon}_{max}$ ($\bar{\varepsilon}$ at $t=0$) as a function of E_{ac} for 5CB and 5CB+MWCNT in the nematic phase ($T=25$ °C). The lines represent a guide to the eyes.

tioned earlier, because of having a very high aspect ratio, CNTs also exhibit dielectric anisotropy[23] and contribute their $\varepsilon_\perp$ or $\varepsilon_\parallel$ to the system depending on a particular orientation. For the homogeneous director profile ($E_{ac}<20$ kV/m in Fig. 4), individual CNTs being perpendicular to the measuring field contribute their average $\varepsilon_\perp$ to the average dielectric constant of the system. Figure 4 shows that the average dielectric constant of the composite system increases by an amount $\Delta\varepsilon_1=0.34$. After the saturation point, when the system is fully reoriented parallel to the field, dispersed CNTs also show homeotropic alignment, contributing their average $\varepsilon_\parallel$ ($>\varepsilon_\perp$) to the system. Above the saturation ($E_{ac}>80$ kV/m) point, the dielectric increment is given by $\Delta\varepsilon_2=0.54$. The significant dielectric difference $\Delta\varepsilon=\Delta\varepsilon_2-\Delta\varepsilon_1=0.2$ due to the presence of only 0.005 wt % CNTs in LC media confirms that the dispersed CNTs follow the field-induced director rotation. If the CNTs were to stay in the LC matrix in random orientation without following the nematic director, one would expect $\Delta\varepsilon_1$ to be equal to $\Delta\varepsilon_2$. Thus, parallelly organized CNTs in the nematic matrix can be rotated (between 0° and 90°) mechanically by switching E_{ac} on and off, obtaining directed self-assembly of suspended CNTs. This directed self-assembled system can be used as a nanoelectromechanical system and a micro-/nanoswitch exploiting the high electrical conductivity of CNTs along the long axis. It is important to point out that the E_{ac} driven director rotation is a much faster response than the relaxation response (decay) on switching E_{ac} off. On switching E_{ac} on and off this system acts as a *nano-oscillator* governing two different characteristic frequencies.

Dielectric relaxation curves for 5CB and 5CB+MWCNT were fitted according to a single-exponential decay function $f(t)=\bar{\varepsilon}_1 e^{(-t/\tau)}+\bar{\varepsilon}_0$ with a typical regression coefficient of $R=0.9996$. Here, τ is the relaxation decay time, $\bar{\varepsilon}_0$ is the average base dielectric constant, and $\bar{\varepsilon}_1$ is the field-induced average dielectric constant. Thus, the field-saturated average dielectric constant $\bar{\varepsilon}_{max}=\bar{\varepsilon}_0+\bar{\varepsilon}_1$. Figure 5(a) shows the linear dependency of $\bar{\varepsilon}$ with a logarithmic time scale. The values for the three fitting parameters, $\bar{\varepsilon}_1$, τ, and $\bar{\varepsilon}_0$ as a function of E_{ac}, are shown in Figs. 5(b)–5(d), respectively. It is obtained from Fig. 5(b) that the difference in field-induced average dielectric constant $\bar{\varepsilon}_1$ between 5CB and 5CB+MWCNT after the saturation point is $\Delta\varepsilon=0.19$. As expected, this value of $\Delta\varepsilon$ has been found to be very close to the value of $\Delta\varepsilon_2-\Delta\varepsilon_1$ from Fig. 4. It is observed that the relaxation time decreases as E_{ac} increases, and, for the composite, saturates at a higher field than that of pure 5CB. This is consistent with the behaviors of $\bar{\varepsilon}_{max}$ shown in Fig. 4. Figure 5(c) depicts that the composite system for E_{ac} larger than the saturation point ($E_{ac}>80$ kV/m) relaxes back faster than pure 5CB. Possibly, dispersed CNTs attract free ions present in the LC media.[4] The presence of ions would slow down the elastic-force driven mechanical relaxation of the nematic domains. The presence of CNTs would lower the free ion concentration allowing the composite system to relax considerably faster. The reduction in the free ion concentration results in a decrease in the rotational viscosity of the

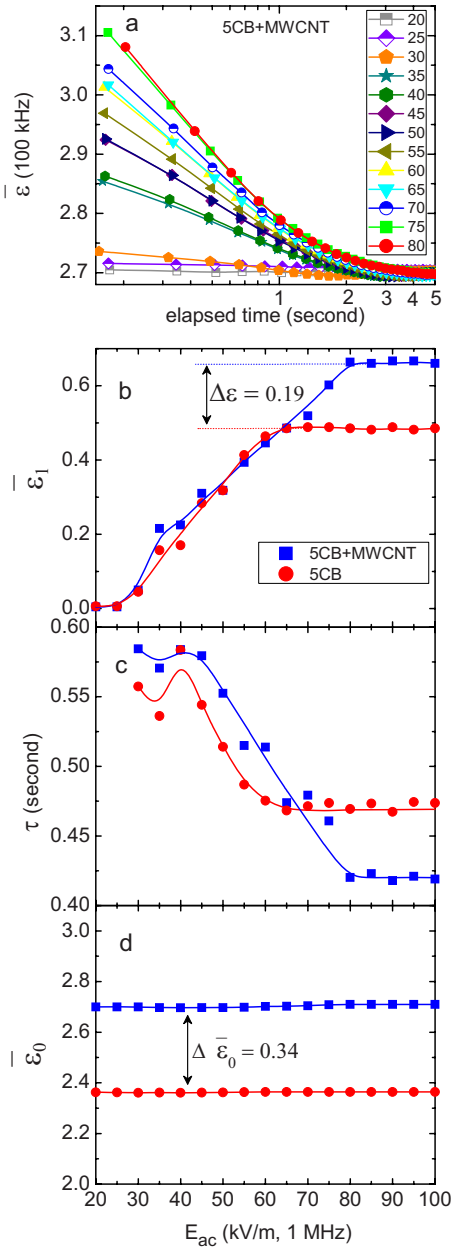

FIG. 5. (Color online) (a) Relaxation dynamic response of $\bar{\varepsilon}$ in a logarithmic time scale. The legend represents the magnitude of E_{ac} (1 MHz) in kV/m; [(b)–(d)] fitting parameters according to a single-exponential decay [$f(t)=\bar{\varepsilon}_1 e^{(-t/\tau)}+\bar{\varepsilon}_0$] function for 5CB and 5CB+MWCNT system. The lines represent a guide to the eyes.

Author complimentary copy. Redistribution subject to AIP license or copyright, see http://jap.aip.org/jap/copyright.jsp

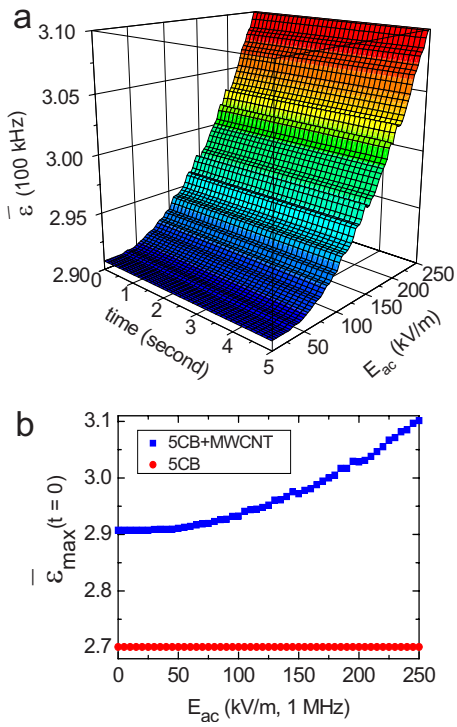

FIG. 6. (Color online) (a) Dynamic response of the average dielectric constant $\bar{\varepsilon}$ for 5CB+MWCNT as a function of time and E_{ac} (1 MHz) in the isotropic phase (T=37 °C) after E_{ac} goes off; (b) field-saturated dielectric constant, $\bar{\varepsilon}_{max}$ ($\bar{\varepsilon}$ at t=0) as a function of E_{ac} for 5CB and 5CB+MWCNT in the isotropic phase (T=37 °C). The lines represent a guide to the eyes.

nematic media. Thus the improvement in the relaxation time is attributed to the decrease in rotational viscosity.[24] The average base dielectric constant $\bar{\varepsilon}_0$, shown in Fig. 5(d), does not depend on E_{ac}. Also, as expected, the increment in average base dielectric constant $\Delta\bar{\varepsilon}_0$ is found to be equal to $\Delta\varepsilon_1$ from Fig. 4, indicating self-consistency.

C. Relaxation dynamics of $\bar{\varepsilon}$ in the isotropic phase

The same experiment was repeated in the isotropic phase (T=37 °C) to study the relaxation dynamics. A dramatic change in the field-induced orientation mechanism has been observed in this phase; see Fig. 6(a). Due to the absence of elastic interactions in the isotropic phase, the LC molecules no longer maintain a long-range orientation order and act as an isotropic liquid. The isotropic phase, as expected, does not respond to an external field, as also experimentally confirmed in Fig. 6(b). But, the composite shows an increment in $\bar{\varepsilon}$ on application of electric field. Interestingly, $\bar{\varepsilon}$ does not relax back over time on switching the field off, as observed in Fig. 6(a). The data of $\bar{\varepsilon}$ versus time were recorded for a few hours [not shown in Fig. 6(a)] and no decays in $\bar{\varepsilon}$ were observed during that period. This suggests that the hybrid system goes through some permanent structural changes each time on application of E_{ac}.

Even though there are no long-range nematic interactions in the isotropic phase, the interaction (surface anchoring) between the LC and CNT surfaces[4,7] still exists. Due to this coupling, the CNT induces a local short-range orientation order of LC molecules surrounding the CNT. The presence of a few layers of LC molecules on CNT walls can be

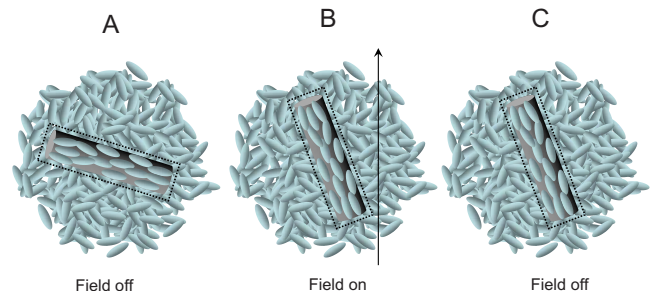

FIG. 7. (Color online) Schematic of the presence of field-responsive anisotropic pseudonematic domains in the isotropic media. The dashed rectangles represent the LC-CNT pseudonematic domains.

visualized as the presence of isolated *pseudonematic* domains[21] in an isotropic media as described in Fig. 7. These local anisotropic *pseudonematic* domains have polarization and they interact with external electric fields. Thus, these field-responsive domains can be rotated on application of E_{ac} without disturbing the isotropic media. But, after the field goes off, there is no restoring force in the isotropic LC media to mechanically torque these domains back into the original state. Therefore, each time higher E_{ac} is applied, the system goes through some permanent local structural changes, exhibiting a nonvolatile memory effect; thus, $\bar{\varepsilon}$ shown in Fig. 6(a) does not decay over time. It is important to note that it is a structural memory on application of E_{ac}. Figure 6(b) displays that there is no sharp threshold field to start the reorientation in the isotropic phase and $\bar{\varepsilon}_{max}$ does not seem to saturate in the field range studied. The field-induced reorientations of these anisotropic domains can only be erased by slowly cooling the system down to the nematic phase and then heating it up again to the isotropic phase.

D. Temperature dependence of $\bar{\varepsilon}$ in the nematic and isotropic phases

For a temperature dependent study a different cell was used in order to maintain temperature stabilization of the sample inside the cell. A droplet of each sample was sandwiched between parallel-plate capacitor configurations, 1 cm diameter and 100 μm spacing, housed in a temperature controlled bath. Dielectric measurements were performed at a very low probing field (5 kV/m) and at 100 kHz frequency. The normalized $\bar{\varepsilon}$ for 5CB and 5CB+MWCNT are shown in Fig. 8 as a function of temperature shift ΔT_{NI}. The temperature shift is defined as $\Delta T_{NI}=T-T_{NI}$, where T_{NI} is the nematic (N) to isotropic (I) transition temperature for each sample. The transition temperature is defined as the temperature where $\bar{\varepsilon}$ shows the first discontinuity while entering the $N+I$ phase coexistence region from isotropic phase and was determined from $\bar{\varepsilon}$ versus T graphs. For 5CB T_{NI}=35.1 °C and for 5CB+MWCNT T_{NI}=34.67 °C. To compare the dielectric behaviors properly for 5CB and 5CB+MWCNT, the dielectric constants are normalized to the highest temperature (42 °C) point studied. The bulk 5CB exhibits the classic temperature dependence of the dielectric constant. Above the transition temperature ($\Delta T_{NI}>0$) the dielectric constant $\bar{\varepsilon}$ for 5CB flattens out in the isotropic phase and shows no temperature dependence at all. This indicates that the bulk 5CB,

Author complimentary copy. Redistribution subject to AIP license or copyright, see http://jap.aip.org/jap/copyright.jsp

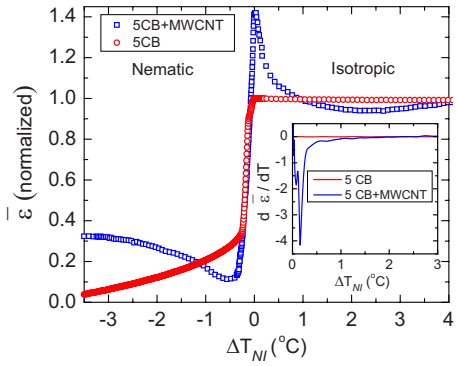

FIG. 8. (Color online) Normalized average dielectric constant $\bar{\varepsilon}$ for 5CB and 5CB+MWCNT as a function of temperature shift $\Delta T_{NI}=T-T_{NI}$.

for $\Delta T_{NI}>0$, reaches a complete disorder state having an order parameter $S(T)=0$. The inset in Fig. 8 presents the extracted $d\bar{\varepsilon}/dT$ in the isotropic temperature range. This shows that $d\bar{\varepsilon}/dT=0$ for 5CB in the isotropic phase, further indicating the complete isotropic phase of 5CB above the transition temperature.

The value of $\bar{\varepsilon}$ for the composite mixture shows a dramatic change both in nematic and isotropic phases, as shown in Fig. 8. The presence of CNTs increases the dielectric anisotropy locally in the system due to the anchoring energy. The larger the dielectric anisotropy, the smaller the field is needed to make the system respond to it. The evolved wing of $\bar{\varepsilon}$ in the nematic phase ($\Delta T_{NI}<0$) indicates that the LC+CNT system is more responsive to the low probing field than bulk 5CB, which is another evidence for a ferroelectric-type behavior of 5CB+CNT. For this composite system, the curvature in $\bar{\varepsilon}$ and the nonzero value for $d\bar{\varepsilon}/dT$ in the isotropic phase ($\Delta T_{NI}>0$) imply that the system does not reach a complete disorder state [order parameter, $S(T)\neq 0$], indicating the presence of pseudonematic domains discussed earlier.

IV. CONCLUSIONS

We have demonstrated the dielectric hysteresis, relaxation response, and nematic to isotropic phase transition phenomena for a LC-CNT hybrid composite by probing its dielectric properties. The field annealing shows an electromechanical hysteresis of the director field in the composite system, indicating an increase in the elastic interaction in the nematic matrix due to the strong anchoring energy associated with the alignment mechanism. The dielectric relaxation dynamics reveal that incorporating CNTs in a nematic platform results in an improvement in relaxation decay time (for $E_{ac}>80$ kV/m), decreasing rotational viscosity. The local anisotropic pseudonematic domains in the isotropic phase demonstrate a field-induced nonvolatile memory effect. The dielectric constant as a function temperature represents $N-I$ phase transition phenomena for the bulk and the composite. A strong temperature dependent dielectric constant for the LC+CNT system in the isotropic phase confirms the presence of pseudonematic domains. This versatile nanoscale electromechanical system might reveal an interesting hysteresis effect in the high frequency regime due to their high frequency switching effect. Future work involves frequency dependent dielectric hysteresis studies for different CNT concentrations in LC media for both the nematic and isotropic phases.

ACKNOWLEDGMENTS

The authors are grateful to Professor Rafael Garcia for useful discussions. This work was supported by the Department of Physics, WPI.

[1]M. D. Lynch and D. L. Patrick, Nano Lett. **2**, 1197 (2002).
[2]I. Dierking, G. Scalia, and P. Morales, J. Appl. Phys. **97**, 044309 (2005).
[3]R. Basu and G. Iannacchione, Appl. Phys. Lett. **93**, 183105 (2008).
[4]I.-S. Baik, S. Y. Jeon, S. H. Lee, K. A. Park, S. H. Jeong, K. H. An, and Y. H. Lee, Appl. Phys. Lett. **87**, 263110 (2005).
[5]P. V. Kamat, K. G. Thomas, S. Barazzouk, G. Girishkumar, K. Vinodgopal, and D. Meisel, J. Am. Chem. Soc. **126**, 10757 (2004).
[6]J. M. Russell, S. Oh, I. LaRue, O. Zhou, and E. T. Samulski, Thin Solid Films **509**, 53 (2006).
[7]J. Lagerwall, G. Scalia, M. Haluska, U. Dettlaff-Weglikowska, S. Roth, and F. Giesselmann, Adv. Mater. **19**, 359 (2007).
[8]R. Basu and G. Iannacchione, Phys. Rev. E **80**, 010701 (2009).
[9]K. A. Park, S. M. Lee, S. H. Lee, and Y. H. Lee, J. Phys. Chem. C **111**, 1620 (2007).
[10]L. Onsager, Ann. N.Y. Acad. Sci. **51**, 627 (1949).
[11]P. G. de Gennes and J. Prost, *The Physics of Liquid Crystals* (Oxford University Press, Oxford, 1974).
[12]P. van der Schoot, V. Popa-Nita, and S. Kralj, J. Phys. Chem. B **112**, 4512 (2008).
[13]Empty LC cells (LC2-20.0, homogeneous antiparallel rubbed with 1° pretilt) are commercially available from Instec Research Instrumentation Technology.
[14]S. Pilla, J. A. Hamida, and N. S. Sullivan, Rev. Sci. Instrum. **70**, 4055 (1999).
[15]S. C. Bera and S. Chattopadhyay, Measurement **33**, 3 (2003).
[16]M. C. Foote and A. C. Anderson, Rev. Sci. Instrum. **58**, 130 (1987).
[17]R. Basu and G. Iannacchione, J. Appl. Phys. **104**, 114107 (2008).
[18]F. Kremer and A. Schonhals, *Broadband Dielectric Spectroscopy* (Springer, Berlin, 2003).
[19]R. Basu and G. Iannacchione, Appl. Phys. Lett. **92**, 052906 (2008).
[20]S. Y. Jeon, S. H. Shin, S. J. Jeong, S. H. Lee, S. H. Jeong, Y. H. Lee, H. C. Choi, and K. J. Kim, Appl. Phys. Lett. **90**, 121901 (2007).
[21]R. Basu and G. Iannacchione, Appl. Phys. Lett. **95**, 173113 (2009).
[22]G. V. Prakash, M. Kaczmarek, A. Dyadyusha, J. J. Baumberg, and G. D'Alessandro, Opt. Express **13**, 2201 (2005).
[23]J. A. Fagan, J. R. Simpson, B. J. Landi, L. Richter, I. Mandelbaum, J. Obrzut, V. Bajpai, R. Raffaelle, B. J. Bauer, A. R. Hight Walker, and E. K. Hobbie, Phys. Rev. Lett. **98**, 147402 (2007).
[24]J. Prakash, A. Choudhary, D. S. Mehta, and A. M. Biradar, Phys. Rev. E **80**, 012701 (2009).

Author complimentary copy. Redistribution subject to AIP license or copyright, see http://jap.aip.org/jap/copyright.jsp